NASA
Technical
Paper
2365

January 1985

Effect of Aerodynamic and Angle-of-Attack Uncertainties on the May 1979 Entry Flight Control System of the Space Shuttle From Mach 8 to 1.5

Howard W. Stone and
Richard W. Powell

NASA

NASA Technical Paper 2365

1985

Effect of Aerodynamic and Angle-of-Attack Uncertainties on the May 1979 Entry Flight Control System of the Space Shuttle From Mach 8 to 1.5

Howard W. Stone and
Richard W. Powell

Langley Research Center
Hampton, Virginia

National Aeronautics
and Space Administration

Scientific and Technical Information Branch

Contents

Summary

A six-degree-of freedom simulation analysis has been performed for the Space Shuttle Orbiter during entry from Mach 8 to Mach 1.5 with realistic off-nominal conditions by using the flight control system defined by the Shuttle contractor in May 1979. The off-nominal conditions included the following: (1) aerodynamic uncertainties in extrapolating from wind-tunnel-derived characteristics to full-scale flight characteristics, (2) uncertainties in the estimates of the reaction-control-system interaction with the Orbiter aerodynamics, (3) an error in deriving the angle of attack from onboard instrumentation, (4) the failure of two of the four reaction-control-system thrusters on each side (design specification), and (5) a lateral center-of-gravity offset coupled with vehicle and flow asymmetries.

With combinations of the above off-nominal conditions, the flight control system performed satisfactorily with a few exceptions. The cases that did not exhibit satisfactory performance displayed the following main weaknesses. Unacceptable performance was exhibited at low-hypersonic speeds for a few cases when errors in deriving the angle of attack from the onboard instrumentation were modeled. Between Mach 5 and Mach 2, the Orbiter was unable to maintain lateral trim for some cases. Also for some cases, the Orbiter exhibited limit-cycle tendencies or residual roll oscillations between Mach 3 and Mach 1. Several system modifications were identified through this analysis to help alleviate these problems. These modifications involved suggested piloting techniques and changes in gains and switching times in the flight control system.

Introduction

The Space Shuttle Orbiter has the capability to enter the Earth's atmosphere, glide up to 1100 n.mi. cross range, and land horizontally on a prepared runway. A closed-loop entry guidance system has been developed to provide the necessary commands for either an automatic flight control system or a pilot-operated, augmented flight control system. A general description of the Space Shuttle configuration and mission is given in reference 1, and the Orbiter avionics are described in reference 2.

The initial flights of the Space Shuttle were designed to verify the vehicle flight worthiness. The first flight was designed to demonstrate the safe ascent and return of the Orbiter and crew for conservative flight conditions. The vehicle was launched from the John F. Kennedy Space Center into a 120-n.mi. circular orbit inclined 38°. After approximately 20 orbits, a deorbit maneuver occurred, which was followed by the entry and landing at the Dryden Flight Research Facility of the Ames Research Center. A further description of this flight is presented in reference 3.

The NASA Langley Research Center performed evaluations of the guidance and flight control system as it evolved for the first mission. These evaluations were performed to cover system uncertainties thoroughly, identify weaknesses, and suggest appropriate modifications to maximize mission safety. The purpose of the analysis reported herein was to evaluate the ability of the flight control system specified by the prime Shuttle contractor in May 1979 to withstand uncertainties. This control system evolved from the system analyzed in reference 4 and has several modifications to the roll and yaw channels. These system modifications were a result of changing requirements and weaknesses found in the study reported in reference 4 and other simulation testing.

The analysis of the flight control system was performed with the aid of six-degree-of-freedom simulation with man-in-the-loop capability. (See ref. 5.) The flight regime studied was from a Mach number of approximately 8 and an altitude of 150 000 ft down to Mach 1.5, which occurs at an altitude of approximately 63 000 ft. This 360-sec segment of the entry represents the period during which the Orbiter performs some of its most extreme maneuvers, the aerodynamic parameters are undergoing significant changes as the vehicle decelerates from hypersonic to low-supersonic velocities, and the angle of attack is lowered from 34° to 9°. These simulation studies considered the center of gravity to be located at 66.7 percent of the body reference length with a lateral center-of-gravity offset of 0.7 in. toward the right wing. In addition, two of the four yaw thrusters on each side were assumed to be inoperable (off). The design specification calls for the Space Shuttle Orbiter to be able to fly safely with this condition. To these were added the aerodynamic uncertainties (ref. 6) that are intended to encompass any differences that might occur between the wind-tunnel data base and actual flight values. These uncertainties are based on the scatter in the wind-tunnel data and historical comparisons of flight and wind-tunnel data for various aircraft and lifting-body configurations.

Uncertainties in RCS/aerodynamic interaction effects were also evaluated in this study. These RCS uncertainties represent twice the standard deviation in the wind-tunnel data scatter, as explained in reference 7. In addition to uncertainties, projected navigation-system errors in deriving angle of attack from onboard instrumentation were included in the simulations. Since the Orbiter has no method of directly measuring angle of attack until the velocity has been reduced to Mach 2.5, this error was introduced to account for winds and navigation platform errors.

Following the study reported in reference 4, the roll and yaw channels of the flight control system were modified to further decrease the sensitivity to aerodynamic uncertainties and errors. The study described herein is similar to the study reported in reference 4, except that the control laws have been modified. The aerodynamic uncertainties and angle-of-attack error have been applied to the baseline entry trajectory for the first mission in this study. In this report, the Orbiter guidance and control systems are described, the test simulation system is briefly described, and the test conditions are defined. Then the simulation response results

are presented with and without the uncertainties, and control-system modifications to handle any system weaknesses are suggested and tested.

Symbols

All coefficients and vehicle rates are in the body-axis system. Computer symbols are shown in parentheses.

b	reference wing span, ft
C_l	rolling-moment coefficient, Rolling moment/$q_\infty Sb$
C_{l_β}	effective-dihedral parameter, $\partial C_l/\partial\beta$, deg^{-1}
$C_{l_{\delta a}}$	rolling-moment coefficient due to aileron deflection, $\partial C_l/\partial\delta_a$, deg^{-1}
$C_{l_{\delta r}}$	rolling-moment coefficient due to rudder deflection, $\partial C_l/\partial\delta_r$, deg^{-1}
C_m	pitching-moment coefficient, Pitching moment/$q_\infty Sc$
C_n	yawing-moment coefficient, Yawing moment/$q_\infty Sb$
C_{n_β}	directional-stability parameter, $\partial C_n/\partial\beta$, deg^{-1}
$(C_{n_\beta})_{dyn}$	dynamic-stability parameter, $C_{n_\beta}\cos\alpha - (I_Z/I_X)C_{l_\beta}\sin\alpha$, deg^{-1}
$C_{n_{\delta a}}$	yawing-moment coefficient due to aileron deflection, $\partial C_n/\partial\delta_a$, deg^{-1}
$C_{n_{\delta r}}$	yawing-moment coefficient due to rudder deflection, $\partial C_n/\partial\delta_r$, deg^{-1}
C_Y	side-force coefficient, Side force/$q_\infty S$
C_{Y_β}	side-force coefficient due to sideslip angle, deg^{-1}
$C_{Y_{\delta r}}$	side-force coefficient due to rudder deflection, $\partial C_Y/\partial\delta_r$, deg^{-1}
c	mean aerodynamic chord, ft
GPFBAY	gain to schedule high gain on side-acceleration feedback, g units/(deg/sec)
GRAY	gain to convert filtered lateral-acceleration error to yaw-rate command, (deg/sec)/g unit
g	acceleration due to gravity, 32.152 ft/sec^2
h	altitude, ft
I_{sp}	specific impulse, sec
I_X	moment of inertia about body roll axis, slug-ft^2
I_Y	moment of inertia about body pitch axis, slug-ft^2
I_Z	moment of inertia about body yaw axis, slug-ft^2
I_{XY}	product of inertia in body XY-plane, slug-ft^2
I_{XZ}	product of inertia in body XZ-plane, slug-ft^2
I_{YZ}	product of inertia in body YZ-plane, slug-ft^2
LCDP	lateral control departure parameter, $C_{n_\beta}C_{l_{\delta a}} - C_{l_\beta}C_{n_{\delta a}}$
M	Mach number
N_Y	side acceleration, g units
p (P)	roll rate about body axis, deg/sec
q_∞	free-stream dynamic pressure, psf
r	yaw rate about body axis, deg/sec
r' (RPRIME)	$= r - (180g\sin\phi\cos\theta)/\pi V_R$, deg/sec
S	reference area, ft^2
V_R	relative velocity of Earth, ft/sec

α (ALPHA)	angle of attack, deg
α_c (ALPHAC)	commanded angle of attack, deg
β (BETA)	sideslip angle, deg
ΔC_l	increment in rolling-moment coefficient due to vehicle and flow asymmetries
ΔC_n	increment in yawing-moment coefficient due to vehicle and flow asymmetries
δ_a (DELA)	aileron-deflection angle, (Left elevon angle — Right elevon angle)/2, deg
$\delta_{a,\text{trim}}$	aileron deflection required for directional trim calculated by control system, deg
δ_{BF} (DELBF)	body-flap-deflection angle (positive down), deg
δ_e (DELE)	elevator-deflection angle (positive down), (Left elevon angle + Right elevon angle)/2, deg
δ_r (DELR)	rudder-deflection angle (positive trailing edge left), deg
δ_{SB} (DELSB)	speed-brake-deflection angle, deg
θ	pitch angle about body axis, deg
ϕ (PHI)	roll angle about body axis, deg
ϕ_c (PHICM)	commanded roll angle, deg

Abbreviations:

RCS	reaction control system
TAEM	terminal-area-energy management
(YAWJET)	number of yaw RCS thrusters firing (positive for right side thrusters)

Description of Space Shuttle Orbiter

The physical characteristics of the Orbiter are summarized in table I. The longitudinal center of gravity is located at 66.7 percent of the body reference length measured from the nose. A sketch of the Orbiter and its control effectors (control surfaces and RCS thrusters) is shown in figure 1. The first entry is depicted on a world map in figure 2, and figure 3 shows the time history of selected nominal trajectory parameters.

Guidance System

The guidance system has separate algorithms for the three different guidance regimes: entry, terminal-area-energy management, and autoland. The entry guidance is designed to take the Orbiter from the atmospheric interface at an altitude of 400 000 ft down to the initiation of the terminal-area-energy-management (TAEM) phase, which occurs at an altitude of approximately 85 000 ft at Mach 2.5. At an altitude of approximately 10 000 ft, the autoland guidance is engaged and directs the Orbiter until touchdown. During entry, the angle of attack follows a preselected schedule, whereas roll angle is modulated to control both down range and cross range. Additional information on the guidance algorithm can be obtained in reference 8.

Flight Control System

The flight control system specified in May 1979 converts either guidance-system commands or pilot-control commands into aerodynamic-control-surface deflections and reaction-control-system (RCS) thruster firings. It also takes rate gyro and accelerometer feedbacks and provides stability, damping, and turn coordination outputs to these effectors. The aerodynamic control surfaces depicted in figure 1 include elevons (which are used as ailerons and elevators), a rudder with speed-brake capability, and a body flap for longitudinal trim. The RCS thrusters are used to supplement control about the roll, pitch, and yaw axes. The roll and pitch thrusters are used only during the early portion of the entry at low dynamic pressures. The yaw RCS thrusters are used down to Mach 1. The thrust level per thruster used in this study was 870 lb, and the I_{sp} was 289 sec.

The flight control system has several system changes throughout the trajectory. These changes depend upon the

guidance algorithm and the relative effectiveness of the various control effectors. From the entry interface to the TAEM interface, in the automatic mode, the control system nulls angle-of-attack errors by using the pitch thrusters (until dynamic pressure increases to 20 psf) and the elevons. From the TAEM interface to landing, in the automatic mode, a normal acceleration error is nulled by the elevons. In the manual mode, the control system converts stick deflections to rate commands. The body flap is a trim device used to maintain the average elevon deflection (elevator) near a preselected elevon profile. Since the elevons are also used as ailerons, the aileron characteristics are a function of the elevator deflection, and thus this preselected elevon profile is designed to help insure the proper aileron characteristics. The elevon and body-flap time histories for the nominal entry are shown in figure 4. The speed brake follows a schedule down to Mach 0.9, after which it follows a guidance-system command. Between Mach 10 and 0.9, the speed brake is used to provide a pitch-up moment to aid in longitudinal trim. Below Mach 0.9, the speed brake is used to control dynamic pressure. The nominal speed-brake time history is also shown in figure 4. A detailed description of the longitudinal, speed-brake, and body-flap channels is presented in appendix B of reference 5.

Control about the lateral-directional axes for a dynamic pressure less than 2 psf is achieved with roll and yaw RCS thrusters only. As the dynamic pressure increases, the ailerons are added for control, and at a dynamic pressure of 10 psf, the roll thrusters are turned off. From initial entry into the atmosphere to about Mach 1.5, the control system operates in a "spacecraft mode," where the roll-rate command is directed to the yaw channel to produce a yaw rate and a small sideslip angle β. This β generates a rolling moment because of the positive effective dihedral of the Orbiter. In this mode, the ailerons are used for turn coordination and directional trim.

The spacecraft mode was chosen for two reasons. First, the aerodynamics for this flight regime of the Orbiter are such that the vehicle exhibits roll-reversal characteristics; that is, if the ailerons are used to roll the vehicle with no yaw input from any other surface or RCS, the vehicle will start to roll in the desired direction and then roll in the opposite direction. The rudder is ineffective at flight conditions above Mach 4, and thus, the RCS system would be required to provide much of the maneuver coordination. Second, to roll about the velocity vector at high values of α requires a large yawing moment about the body axis. Below Mach 1.5, the control system switches to a more conventional aircraft mode, in which ailerons are used for roll control and the rudder is used for turn coordination. Between Mach 3 and 1.5, the flight control system is a blend between those two control modes. The roll and yaw channels of the flight control system are described in more detail in the appendix.

The May 1979 flight control system was a modified version of the May 1978 blended system described in reference 4. The May 1978 system was modified because of weaknesses found in the simulation testing, such as those reported in reference 4, and system requirement changes. The changes to the 1978 system were as follows. The side-acceleration feedback gain to the yaw channel was reduced by 60 percent, and the feedback was retained down to subsonic speeds in both the roll and yaw channels. The forward-loop gains in both the aileron and yaw channels were changed. The rudder was activated at a lower Mach number (3.5 instead 4.5), and the cross feed to the aileron trim was retained to a lower Mach number (2.1 as compared with 4.0). Fourth-order bending filters were added to both channels while the yaw thrusters are active, and the minimum number of yaw thrusters allowed to fire was increased from one to two with appropriate changes in the deadband. Also, the rudder trim integrator gain was reduced, and the trim limit was significantly reduced.

Description of Simulation

The reentry flight dynamics simulator (RFDS) used for this study is a nonlinear, six-degree-of-freedom, interactive digital computer program with man-in-the-loop capability developed by the Langley Research Center. The cockpit is not a replica of the Space Shuttle Orbiter cockpit, but it does have the instrumentation and controls necessary for engineering investigations. The vehicle response was recorded on time-history charts. A more complete simulation description is available in reference 5. A static aeroelastic model has been incorporated in the simulation and is described in appendix B of reference 4.

Test Conditions

The off-nominal conditions considered in this evaluation involved aerodynamics, RCS/aerodynamic interactions, vehicle asymmetries, errors in the navigation-system-derived angle of attack, and yaw RCS thruster failures. The Space Shuttle design specification requires that the Orbiter be able to fly safely with two of the four yaw thrusters on each side inoperable (off). Because of this requirement, most of the runs in this study had such a failure.

The nominal and off-nominal aerodynamics used in this study were obtained from reference 9. The off-nominal values were estimated 3σ envelopes of possible variations between wind-tunnel-derived characteristics and full-scale flight characteristics. Because a normal distribution was assumed, the variations could be either added to or subtracted from the nominal aerodynamics. The aerodynamic data base consisted of the six force and moment coefficients for the airframe with undeflected controls. These coefficients are functions of Mach number, angle of attack, and sideslip angle. To these are added the force and moment contribution of the control surfaces (functions of Mach

number and angle of attack). The elevons (when used as an elevator), the body flap, and the speed brake are all considered to have nonlinear aerodynamic increments which are functions of Mach number, angle of attack, and surface position. Both the aileron and rudder have linear aerodynamics that are a function of Mach number and angle of attack, with the aileron aerodynamics also being a function of the average elevon position. The off-nominal aerodynamics are a function of Mach number.

All possible lateral-directional combinations involving moments generated by the bare airframe and the aileron were considered in this study. Table II shows the nomenclature used in the discussion of the results to describe these 16 cases of off-nominal conditions. Examination of the aerodynamic data of reference 9 revealed that the rudder derivatives $C_{l_{\delta r}}$, $C_{Y_{\delta r}}$, and $C_{n_{\delta r}}$ are approximately linearly dependent; therefore, they were varied together. In addition, none of the rudder derivatives were allowed to differ in sign from the nominal. Figure 4 of reference 10 shows the range of off-nominal lateral-directional stability and the aileron and rudder control effectiveness. The curves were generated by assuming that the angle of attack was exactly the value commanded by the guidance algorithm and that the elevator position was the desired position used by the body-flap-control logic. The aileron is used for directional trim, as shown in the appendix of the present paper. This requirement places a great deal of dependence on $C_{n_{\delta a}}$. Reference 10 indicates that because of the uncertainty in the data, $C_{n_{\delta a}}$ could switch signs below Mach 5.5, and the magnitude could vary greatly above Mach 5.5. Thus, the control system should show a high sensitivity to uncertainties in $C_{n_{\delta a}}$. This sensitivity is confirmed in the discussion of the results that follow.

Since the flight control system has a side-acceleration feedback, the magnitude of C_{Y_β} should have an effect on the system response. Thus, for some select cases, C_{Y_β} uncertainties were examined.

Reference 9 also presents the longitudinal aerodynamic characteristics. Longitudinal uncertainties, as was shown in reference 11, did not impact the control of the Orbiter unless (1) the vehicle no longer can be trimmed, or (2) the elevator must move to a position that adversely affects the aileron characteristics. This control system uses the body flap to maintain the proper elevator position; thus, no effects of pitching-moment variation would be expected until the body flap was forced to its limit and the elevator had to move from its desired position. This occurs in the Mach 5 to 3 flight regime, and thus uncertainties in pitching moment were applied to some select cases in this flight regime.

Four combinations of RCS/aerodynamic interaction uncertainties were considered in this study, as shown in table III. Since the yaw jets are the only thrusters operating in the flight regime of interest in this study, only uncertainties in the interaction because of yaw jet thrusting were considered. The primary effects were the yawing moment and rolling moment because of the yaw jets firing, and all positive and negative combinations for these moments were examined. The pitching moment that results from the yaw jets was considered to be correlated with the rolling moment. Figures 4 and 6 of reference 7 show the uncertainties in the rolling and yawing moments that were used in the present study.

Vehicle asymmetries because of manufacturing uncertainty and flow asymmetries have been estimated and were included in the modeling of the system. The values were given in coefficient form and are $\Delta C_l = 0.0005$ and $\Delta C_n = -0.0005$. Also, a lateral center-of-gravity offset of 0.7 in. was included to account for manufacturing and payload-loading uncertainties.

Because angle of attack is not measured directly during a portion of the entry investigated in this study, it must be derived from the navigation-system onboard inertial platform data. When error sources such as platform drift and winds are considered, angle of attack can be in error by as much as $\pm 4°$. Since the flight control system (see appendix) uses angle of attack extensively, the system should be sensitive to this potential error in sensed α.

Discussion of Results

In order to evaluate the off-nominal effects on the flying qualities of the Space Shuttle Orbiter with the May 1979 flight control system, a test maneuver was devised to represent the maneuvering required during the entry phase. As noted earlier, the Orbiter flies a preselected angle-of-attack schedule and modulates the commanded roll angle ϕ_c to control both down range and cross range. The test maneuver consisted of maintaining the initial ϕ for a short period of time, rolling 60° at maximum roll rate, and then rolling back 55°. The commanded angle of attack α_c was generated by the guidance algorithm. The test maneuver was initiated at Mach numbers of 7.9, 7.0, 6.1, 4.6, and 3.8 along the entry profile, and the response of the Orbiter was examined. Unless otherwise noted, all cases were flown with the automatic control system (that is, no pilot inputs) and with only two yaw jets operable on each side.

System Performance Results at Hypersonic Speeds

The test cases were initiated at Mach numbers of 7.9, 7.0, and 6.1. The 16 off-nominal aerodynamic cases shown in table II did not reveal any significant problem at Mach 7.9. Some cases did require large aileron deflections, and large sideslip angles occurred when RCS aerodynamic uncertainties were added. Also, some cases exhibited slight overshoot and oscillatory tendencies when α errors were introduced. Because all these problems became more severe as the Mach number decreased, the presentation of the time-history results will be limited to the Mach 7 and 6.1 cases.

The system performance with off-nominal aerodynamics initiated at Mach 7.0 and Mach 6.1 was generally good. Three cases required about 50 percent more RCS fuel than the nominal case, but there was little evidence that the

aerodynamics were other than nominal. For cases where the navigation-derived angle of attack was low and the vehicle was flying higher than the system indicated by 4° (indicated-α error low), the system performance was good. However, when the vehicle was actually flying lower than the system-indicated α (navigation-derived angle of attack high, indicated-α error high), the effect of off-nominal aerodynamics was quite evident. Several cases displayed overshoot and oscillatory tendencies in response to the roll-reverse-roll command at Mach 7 and Mach 6.1. Cases 11 and 15 were the worst cases. Figure 5 shows the time-history response for cases 11 and 15 at Mach 7 (indicated-α error of 4° high) and case 11 at Mach 6.1 (indicated-α error of 3° high). These cases shown have marginal or unacceptable bank-angle control. Case 11 with an indicated-α error of 4° high at Mach 6.1 diverged, and control was completely lost. The improper turn coordination due to the erroneous α used in the flight control system produced large yawing moments and sideslip angles ($\beta > 1°$) resulting in larger rolling rates ($p > 5$ deg/sec) than the system was designed to produce in these off-nominal aerodynamics cases. Reduced $(C_{n\beta})_{dyn}$ along with higher than expected roll control effectiveness, which occurs for cases 11 and 15, appears to degrade the ability of the system to control roll rate and results in large sideslip angles ($\beta > 1°$). Decreasing the yaw-control authority, such as by applying the RCS uncertainty set 2, resulted in unacceptable performance (see fig. 6) for an indicated-α error of 2° high. An indicated-α error of 2.5° high resulted in loss of control at Mach 6.1 for case 11.

The sensitivity to α errors had been a problem in a previous flight-control-system design. (See ref. 10.) This was corrected by adding a side-force feedback to the yaw channel to maintain tighter control of β. The side-force feedback exists in the present system design, but the gain, GPFBAY, has a value of 0.2 in this Mach range, where it had a value of 0.5 previously. (See appendix, fig. A2.)

Using a value of 0.5 for GPFBAY eliminated the sensitivity to α errors for nominal RCS/aerodynamic interactions (fig. 7). Without the RCS uncertainties, the system had enough control power to tighten the sideslip control and remove the overshoot and oscillatory tendency, as shown in figure 7(a). Case 11 with an indicated-α error of 4° high performs satisfactorily at Mach 6.1. Figure 7(b) shows the performance results for case 11 with RCS uncertainty set 2 for an indicated-α error of 2.5° high and with GPFBAY = 0.5. The vehicle has a significant roll-angle overshoot and a damped oscillation. A GPFBAY value of 0.7 reduced the overshoot slightly, but it did not reduce the oscillatory tendency. Another gain in the side-force feedback circuit is GRAY. This gain has a value of 10 except from Mach 4 to 1.5, where the value is 12.5. Increasing GRAY to 12.5 at Mach 6 reduced the overshoot and oscillatory tendency of case 11, as is shown in figure 7(c). Although the response performance was more acceptable, the RCS fuel consumption was high. Approximately 300 lb of RCS fuel were consumed in this 120-sec run.

System Performance Results at High-Supersonic Speeds

Runs initiated at Mach 4.6 with nominal rudder effectiveness but with the off-nominal aerodynamics for cases 1 through 16 given in table II exhibited little effect due to the off-nominal aerodynamics. The cases with a positive uncertainty in $C_{n_{\delta a}}$ required approximately 40 percent more RCS fuel because $\delta_{a,trim}$ changed rapidly in this speed range, and large δ_a values were required. This was also true for cases initialized at Mach 3.8.

When the off-nominal aerodynamics were combined with an indicated-α error that was 4° low (i.e., vehicle flying higher than system indicated by 4°), the system performance was generally satisfactory. The erroneous turn coordination signal in the aileron channel because of the α error resulted in roll rates that were lower than the system design. Figure 8 shows the time-history results for cases 3 and 14 with increased rudder effectiveness for runs initialized at Mach 4.6. Spikes in δ_r, δ_a, p, and β occurred when the rudder was activated, and a residual p oscillation occurred after the maneuver was completed for case 3. This characteristic was observed to be more severe in previous system designs and was found to be a result of the relatively high gain of the rudder compared with the aileron. (See ref. 10.) When RCS/aerodynamic uncertainty sets 1 and 3 were included (the roll due to the yaw jets was decreased), the spikes at rudder activation worsened. (See fig. 9.) RCS uncertainty sets 2 and 4 improved the situation. Decreasing the α error to 0° reduced the β spike and eliminated the δ_r spike, but the oscillatory tendencies remained. This is shown in figures 10(a) and (b) along with the time history for a run with nominal aerodynamics and indicated-α error of 4° low included (fig. 10(c)). Notice that the δ_r and β spikes are still quite large. The error signal to the rudder and yaw jets is a function of α and will be biased as a result of the α error.

When an indicated-α error 4° high occurred (vehicle flying 4° lower than system indicated), numerous cases exhibited poor system response. In general, the behavior was either a roll-angle overshoot and oscillatory tendency or a lack of yaw-control authority due to $C_{n_{\delta a}}$ approaching zero or becoming positive as Mach number and α decreased. Both of the problems were magnified by putting a positive uncertainty on the side force due to β (C_{Y_β}). Since C_{Y_β} is nominally negative, this uncertainty reduces N_Y, the force input to the side-force accelerometer, and thereby reduces the effective N_Y feedback used in the control system. The cases where $C_{n_{\delta a}}$ was approaching zero were also adversely affected by a negative uncertainty in the pitching moment. This drove the body flap to the upper limit and forced the elevons to move up also. This caused $C_{n_{\delta a}}$ to increase and in some cases to become positive. Since the system assumes $C_{n_{\delta a}}$ is negative until Mach 2.1 is reached, the control authority in yaw was degraded because of the pitch uncertainty. With these uncertainties and the

RCS/aerodynamic interaction uncertainties included, cases 3 and 11 exhibited the overshoot and oscillatory tendency and diverged, as was shown at the higher speeds. An example (case 11) is shown in figure 11(a). The modification to the N_Y feedback discussed previously (GPFBAY = 0.5) corrected the problem up to an indicated-α error of 3° high, as is shown in figure 11(b).

The cases where the $C_{n_{\delta a}}$ uncertainty was applied in the positive direction usually resulted in large δ_a and β values for trim below Mach 5. Therefore, to provide realistic test conditions on the simulator, the cases were initialized at Mach 6.1 and run with the nominal guidance commands for 240 sec to approximately Mach 1.8. Cases 6 and 8 are shown in figure 12 as examples with an indicated-α error 4° high. In both of these cases, δ_a is close to the −3° limit for the trim integrator, and considerable yaw jet firing is required to maintain control. The lateral trim function is governed by the lateral control departure parameter (LCDP), LCDP = $C_{n_\beta} C_{l_{\delta a}} - C_{l_\beta} C_{n_{\delta a}}$, as explained in reference 12. In both of these cases, $C_{n_{\delta a}}$ became positive around Mach 5, and the LCDP changed sign just below Mach 5. LCDP changing sign indicates that the $\delta_{a,\text{trim}}$ logic will drive the aileron in the wrong direction. Thus, although the aileron was deflected to the limit (assuming $C_{n_{\delta a}}$ was negative), actually below Mach 5 a yawing moment was being generated by the aileron that tended to move the vehicle out of trim. The time history of RPRIME (r' = Actual yawing rate − Computed yawing rate required for a coordinated turn) indicated that the multiple jet firings were sufficient to keep RPRIME very close to zero. When the rudder was activated at Mach 3.5, it was driven by the same signal that fired the yaw jets. The rudder, therefore, deflected to help keep RPRIME near zero. Unfortunately, the rudder is a very weak control device at this relatively high Mach number and angle of attack. Therefore, in both of these cases nearly 900 lb of RCS fuel were expended in the 240-sec run.

Adding RCS/aerodynamic interaction uncertainties to cases 6 and 8 resulted in loss of control for indicated-α errors of 2.5° high and greater. These cases, 6 and 8, are shown in figures 13(a) and 13(b), respectively. The roll-off occurred when the two jets plus the rudder were unable to keep RPRIME near zero. There appears to be an upsetting pulse to the system when the rudder was activated. The error signal to the yaw channel was sufficient to have two jets firing, and thus the rudder moved rapidly to about −7°. However, the rudder produced an adverse rolling moment, which had to be balanced by changes in β and δ_a. Figure 13(c) shows that four jets can hold the system up to an indicated-α error of 4° high; however, over 1,200 lb of RCS fuel were expended in flying through this 240-sec portion of the entry. If the pilot can be made aware of what is happening, he can use the roll panel beep trim switch located on the panel in front of the pilot to remove the aileron trim deflection and thus remove the undesirable yawing moment.

Case 16 was also initialized at Mach 6.1 and allowed to fly on the nominal guidance commands for 240 sec. With an indicated-α error of 4° high, this case diverged when the rudder was activated. (See fig. 14(a).) In this case, β became very large, but δ_a did not go to the trim limit. The value of $C_{n_{\delta a}}$ became positive around Mach 5, but LCDP did not change sign until close to Mach 4 because of the increased $C_{l_{\delta a}}$. The value of β became so large that C_{l_β} counteracted $C_{l_{\delta a}}$. When the rudder was activated, it produced a rolling moment in the same direction as the rolling moment of the aileron, and these rolling moments apparently overpowered the rolling moment due to β. This case did not diverge with an indicated-α error of 3° high, but the vehicle was unable to maneuver until Mach 2.5 was reached. With the addition of RCS/aerodynamic uncertainties, the vehicle diverged with an indicated-α error of 3° high with two yaw jets and also diverged with an indicated-α error of 4° high with four yaw jets. (See figs. 14(b) and (c).) The RCS uncertainty set 2 resulted in the worst case, a rolling moment which is out of coordination with the yawing moment. This divergence can be prevented by aggressive use of the roll panel beep trim switch, as for case 6. When the aileron was driven by the roll panel beep trim switch in the direction to remove the aileron deflection and cause β to move nearly a degree in the opposite direction, control could be maintained.

System Performance Results at Low-Supersonic Speeds

To make sure the initialization did not affect the results in the Mach 2.5 and below flight regime, the runs were started at Mach 3.8 and flown down to Mach 2.5 by using the guidance system roll-angle and angle-of-attack commands. At the TAEM interface (Mach 2.5), the control system was commanded to hold a roll angle of 15°. Four seconds later, it was commanded to either pitch up or down by using a programmed manual pitch input to simulate the high- or low-angle-of-attack conditions. Since the air data system becomes operational at Mach 2.5, no indicated-α errors were simulated. In general, the cases tested with pitch commands under the control of the guidance system exhibited satisfactory response, except that some cases had a rather asymmetric roll-rate time history. This was particularly true for cases with reduced rudder effectiveness. Again, the system lateral-trim function uses the aileron down to Mach 2.1 and assumes that $C_{n_{\delta a}}$ is negative. When $C_{n_{\delta a}}$ became zero or positive, the yaw jets and rudder had to counteract out-of-trim moments, which reduced control authority in one direction. This occurs somewhere below Mach 5, depending upon α, δ_e, and off-nominal aerodynamic case selected. Use of the roll panel beep trim switch to remove the aileron trim can relieve this problem. One of the worst cases with decreased rudder effectiveness was case 8. The time histories for this case are shown in figure 15. Since a negative uncertainty in the pitching moment (C_m) forces the elevon up and causes $C_{n_{\delta a}}$ to be more

positive, the case shown has the negative C_m uncertainty. In figure 15(a), the maximum roll rate (magnitude) was about 10 deg/sec. The saw-tooth appearance of p, δ_r, and δ_a is a result of the positive yaw jet firings required to counteract the negative yawing moment due to the aileron. Figures 15(b) and (c) show the results with side force due to β (C_{Y_β}) uncertainties. Since C_{Y_β} is nominally negative, a positive uncertainty reduced C_{Y_β} and thereby reduced the N_Y feedback to the control system. Figure 15(b) shows the results with the positive uncertainty in C_{Y_β}, and it appears to have the least asymmetric p of the three cases shown. However, this particular case consumed by far the most RCS fuel, 220 lb in the 120-sec run. The sideslip angle β reached almost 3° at one point during this run.

The cases tested with increased rudder effectiveness, guidance-system-controlled α, and nominal RCS all performed the maneuver satisfactorily. However, cases 9 and 10 exhibited strong limit-cycle tendencies beginning at approximately Mach 3 with both two and four jets operating. The time histories for these cases are shown in figure 16. These runs were initiated at Mach 4.6 and continued for 240 sec to approximately Mach 1. Case 10 was the worst case. Below Mach 1.9 (not shown), any stick input would excite the limit cycle, which would continue to Mach 1, where the yaw jets were turned off. Over 400 lb of RCS fuel were consumed with four jets operating. This limit-cycle tendency was not a function of the C_m or $C_{Y\beta}$ uncertainties. The limit cycling occurred even when the $C_{n\delta a}$ and $C_{l\delta a}$ uncertainties were reduced to zero. When the increased rudder effectiveness uncertainties were reduced by one-half, the limit cycling would start but then die out. Reducing the rudder forward-loop gain to 600 appeared to have little effect on the limit-cycle tendency, and increasing the N_Y feedback gain GPFBAY to 0.5 made a slight improvement. There was no apparent difference between cases with aeroelastic model in or out.

When RCS uncertainties were included in this flight regime, several cases exhibited degraded flying qualities. The cases with decreased rudder effectiveness are presented in figure 17. Case 3 exhibited an undesirable roll response, particularly during the second roll-command segment, and a slight overshoot and oscillation occurred, as was discussed earlier. (See fig. 17(a).) Large rudder inputs were required to control the overshoot. Case 6, shown in figure 17(b), completed the maneuver satisfactorily; however, the aileron was on the trim limit the entire run, and 328 lb of RCS fuel were consumed in 120 sec. The pilot can relieve this problem by using the roll panel trim switch. Case 8, shown in figure 17(c), has a severe roll-rate asymmetry problem, as does case 16, shown in figure 17(e). Case 8 with RCS uncertainty set 2 consumed the same amount of RCS fuel as with RCS uncertainty set 1, but it appears to have slightly better performance. (Compare figs. 17(c) and (d).)

The cases with the worst performance with RCS uncertainties and increased rudder effectiveness included are presented in figure 18. Figure 18(a) shows that the increased rudder effectiveness has a marked effect on case 3. The maneuver exhibits undesirable roll response during both roll-command segments, and there is a residual p oscillation. Case 7, shown in figure 18(b), has a similar problem. Cases 9 and 10, presented in figures 18(c) and (d), exhibit the limit-cycle tendency.

To obtain the lower angle-of-attack data, the pitch-down maneuver was initiated at Mach 2.5. The lower angle of attack resulted in dynamic pressures that were somewhat higher than the nominal, reaching over 300 psf by the end of the 120-sec run. Also, to keep the angle of attack from drifting up, several stick inputs which resulted in significant elevon activity were required. Several of the worst cases are shown in figure 19.

Case 3 with RCS uncertainty set 1 has an undesirable roll response, as is shown in figure 19(a). Cases 6, 8, and 16 all exhibited severe roll-rate asymmetry and a lack of control authority (roll divergence in some cases), as is shown in figures 19(b), (c), (d), (e), and (g). Some of the figures show that the system began to recover when the aileron trim was terminated at Mach 2.1 at approximately 110 sec. In each of these cases, $C_{n_{\delta a}}$ was positive throughout the run, and when the roll panel beep trim switch was used to remove the aileron trim deflection, the divergence was avoided. Also, the dynamic pressure was 240 psf or less for these cases when the divergence began.

Figure 19(f) shows the time-history results for case 11 with RCS uncertainty set 1 and four yaw RCS jets operating. This case completed the commanded roll maneuver satisfactorily but then diverged. It appears that the jets and rudder were simply unable to hold the β. Notice the time scale and Mach number initialization change. This divergence was just beginning to occur at 120 sec when the initialization was at Mach 3.8. This divergence was a definite function of the dynamic pressure (q_∞), and it required q_∞ values greater than 350 psf to occur. This divergence also occurred for case 11 without RCS uncertainties and with two yaw jets failed and for several other cases.

Since cases 6, 8, and 16 exhibited a lack of control authority because of the aileron trim being retained to Mach 2.1, some control-system modifications were studied. The aileron trim switch was changed to Mach 2.7, and the rudder trim limit was increased from 4° to 7°. The resulting system performance is presented in figure 20 for cases 3, 6, 8, and 16. Case 3 (shown in fig. 20(a)) still displays undesirable roll response but does not appear to be worsened by the modifications. Cases 6, 8, and 16 all show the effects of the roll-rate asymmetry problem and were not able to respond to the Mach 2.5 manuever, but none diverged.

Runs to simulate high-angle-of-attack conditions were accomplished by pitching the vehicle up slightly at Mach 2.5 and holding α around 15° for the duration of the 240-sec runs, as shown in figure 21. The Mach number at the end of the run was about 1.0, and the dynamic pressure decreased, reaching 100 psf at about 185 sec. Case 3, shown in figure 21(a), displays the undesirable roll response shown previously. This case also shows a strong oscillatory tendency after the maneuver and some limit cycling. Cases 9, 10, and 16 (see figs. 21(b), (c), and (d)) have the limit-cycle tendency shown in other runs, and case 16 has the asymmetric roll-rate problem.

Conclusions and Recommendations

With combinations of aerodynamic uncertainties, reaction-control-system aerodynamic/interaction uncertainties, errors in the navigation-system-derived angle of attack, failure of two yaw reaction-control thrusters on each side, and lateral control-of-gravity offset, the flight control system specified by the contractor in May 1979 performed satisfactorily with a few exceptions. The cases that did not exhibit satisfactory performance displayed the following weaknesses. At low-hypersonic speeds, unacceptable control performance was exhibited by a few cases with indicated-angle-of-attack errors. Increasing two gains in the side-force feedback to the yaw channel significantly improved the system capability to tolerate indicated-angle-of-attack errors. Some cases were unable to hold lateral trim in the Mach 5 to 2 flight regime. Aggressive use of the roll panel beep trim switch by the pilot will be required if these off-nominal conditions are encountered. At the lower supersonic speeds, the trim problem can be relieved by moving the aileron trim termination condition from Mach 2.1 to 2.7 and by increasing the rudder trim integrator limit from 4° to 7°. Also, some cases exhibited limit-cycle tendencies or residual roll oscillations from Mach 3 to 1. These system modifications were part of a flight-control-system redesign in July 1980.

Langley Research Center
National Aeronautics and Space Administration
Hampton, VA 23665
September 4, 1984

Appendix

Roll and Yaw Channels of Flight Control System

The flight control system described in references 4 and 5 was revised to solve the problems discussed in reference 4. The revised roll and yaw channels are described in this appendix.

Symbols and Abbreviations

AL	approach and landing guidance
AUTO	autopilot control mode
BANKERR	control-system roll-angle error, deg
COSTHE	cosine of pitch angle
CSS	pilot command mode
DAM	roll-rotation hand-controller command, deg
DAMAX	roll-stick-command limit, deg
DAMS	shaped roll-stick command, deg
DNY	stability-axis yaw rate due to side acceleration, deg/sec
DRM	rudder-pedal command, deg
DRMS	shaped rudder-pedal command, deg
DRRC	yaw-rate error, deg/sec
ENTRY	entry guidance
FLATURN	flat-turn regime
GALR	scheduled gain to blend yaw jet/aileron control and aileron/rudder control
GDA	gain to convert roll-rate error into aileron command, deg/(deg/sec)
GDRC	gain to convert yaw-rate error to rudder-deflection command, deg/(deg/sec)
GLIN	linear coefficient in roll-stick shaping, deg/deg
GNY	gain to convert rudder-pedal command to side-acceleration command, g units/deg
GPAY	gain to scale lateral acceleration
GPFBAY	gain to schedule high gain on side-acceleration feedback, g units/(deg/sec)
GPPHI	gain to convert roll-angle error to roll-rate command, (deg/sec)/deg
GRAY	gain to convert filtered lateral-acceleration error to yaw-rate command, (deg/sec)/g unit
GRH	gain to scale yaw-rate error
GRRHC	gain to convert roll-stick command to rate command, (deg/sec)/deg
GTRA	gain to scale rudder trim integrator
g	acceleration due to gravity, 32.152 ft/sec^2
KGDA	scheduled gain to obtain GDA, (deg/(deg/sec))/psf
MACH	Mach number
NY	side-acceleration feedback, g units
P	sensed roll rate, deg/sec
PAR	coefficient of squared term in roll-stick shaping, deg/deg^2
PC	commanded roll rate, deg/sec
PCLIM	roll-rate-command limit, deg/sec
PCOR	= P + (RTDG)(TANP)(SINTHE)/V, deg/sec
PFB	turn coordination roll-rate error, deg/sec
PHICM	guidance-system roll-angle command, deg
PHIDG	sensed roll angle, deg
PTEM	side-acceleration feedback gain, deg/sec
QB	dynamic pressure, psf
R	sensed yaw rate, deg/sec
RCS	reaction control system
RP	= R − (RTDG)(SINPHI)(COSTHE)/V, deg/sec

RTDG	= 57.3g, deg-ft/sec^2
SINPHI	sine of roll angle
SINTHE	sine of pitch angle
TAEM	terminal-area-energy-management guidance
TANP	tangent of roll angle
TAS	true airspeed
TF	flight control fast-cycle time, 0.04 sec
TS	flight control slow-cycle time, 0.160 sec
V	airspeed, ft/sec
z	z transform variable
α	angle of attack, deg
β	angle of sideslip, deg

Description of System

Diagrams of the roll and yaw channels are presented in figures A1 and A2. The system was designed to minimize the time required to complete the flight control calculations in the onboard digital computers. This was accomplished by operating various elements of the control laws at the minimum acceptable frequency; thus, a variation in computational frequency existed among the various signal paths of the flight control system. The frequency is indicated on the block diagrams either in the figure legend or by the dashed boxes around the control-system signal paths.

Computational frequency differences between the guidance system and flight control system resulted in a requirement to smooth the signals at the interface. This was accomplished by the SMOOTHER logic, which is shown as a block in figure A1. Lateral-trim logic switching required a signal-fading logic indicated by the block FADER in figure A1. The SMOOTHER logic and FADER logic are described in detail in appendix B of reference 5.

Roll channel. The aileron command and roll RCS command control laws are presented in figure A1. Figure A1 shows how either the roll-stick command (DAM) or the roll-angle-guidance command (PHICM), depending on pilot selection in the cockpit, is converted to roll-rate command (PC). This command signal was directed to the yaw channel (fig. A2) and to the aileron and roll RCS jet commands, as is shown in figure A1.

The Orbiter enters the Earth's atmosphere at about $\alpha = 40°$, holds this α until the Mach number decreases to about 13, then begins a slow transition in α, and reaches an α of 13° at approximately Mach 2.5. At the higher angles of attack, the stability-axis roll rate was obtained by using the yaw thrusters to produce a body-axis yawing rate and allowing the relatively large effective dihedral to generate the body-axis rolling rate. The aileron was used as a coordinating controller in maneuvering.

The gain 1 - GALR (fig. A1) was very small at the higher Mach numbers because of the scheduled gain GALR, and thus, only a small percentage of the roll rate commanded was directed to the roll thrusters and aileron. At the lower Mach numbers, this gain was 1.0, and the commanded roll rate was directed entirely to the ailerons. Thus, the scheduled gain GALR was the mechanism by which the flight control system was blended from one type of system to another. Note, the roll jets were disengaged at a dynamic pressure of 10 psf.

Cross feed between the yaw channel and the roll channel, DRRC, was used to generate the aileron trim signal above Mach 4. (See fig. A1.) The pilot has access to a roll panel beep trim switch, which directly drives the aileron trim integrator, as shown in figure A1. Below Mach 2.1, lateral trim was handled by the rudder forward-loop integration. The 40-sec FADER was triggered at this Mach 2.1 switch to minimize the transient.

Yaw channel. The rudder and yaw RCS command diagams are presented in figure A2. Below Mach 3.5, the rudder was active, and commands could be input through the rudder pedals (DRM) (fig. A2). The system was designed, however, for the yaw channel to operate without requiring manual inputs through the rudder pedals. At the higher angles of attack, the stability-axis roll-rate command (PC) was used to generate a yaw-rate error (DRRC) (fig. A2). At the lower angles of attack, the yaw-rate-feedback (RP) is the predominant feedback signal for the desired turn coordination.

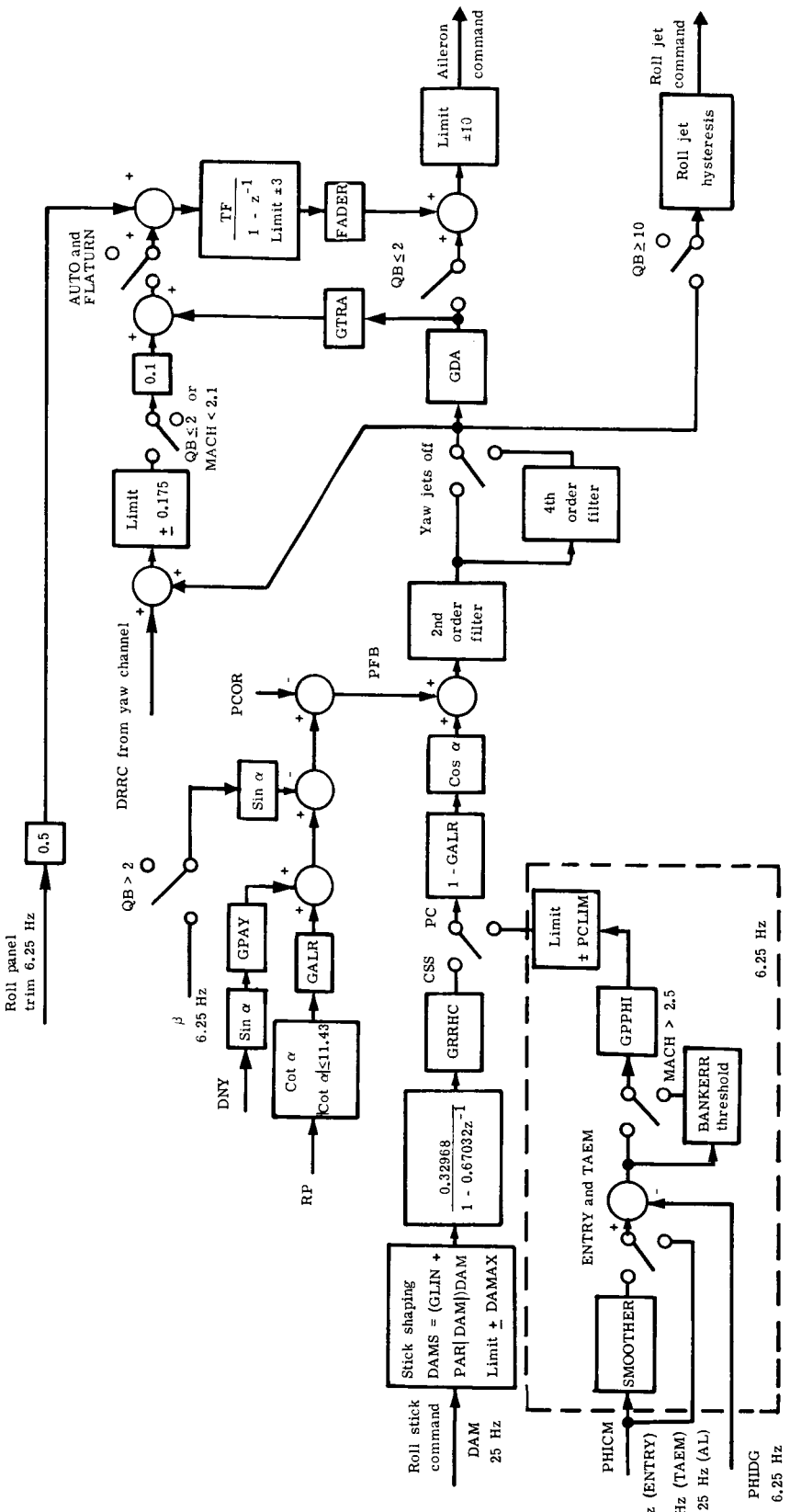

(a) Block diagram. Frequency = 25 Hz unless otherwise noted.

Figure A1. Roll channel.

$$GDA = \frac{KGDA}{QB + 10}, \quad 0.1 \leq GDA \leq 8$$

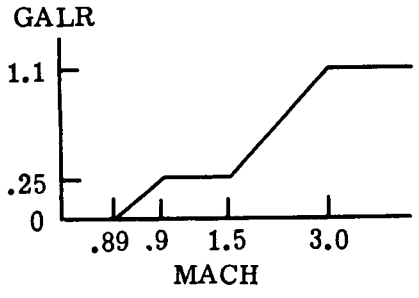

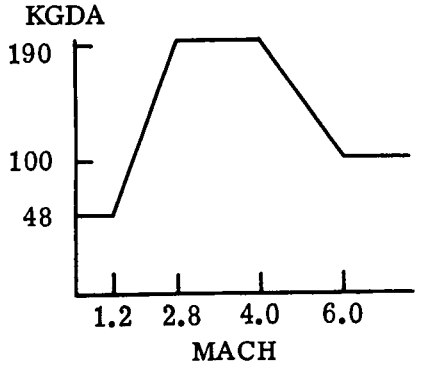

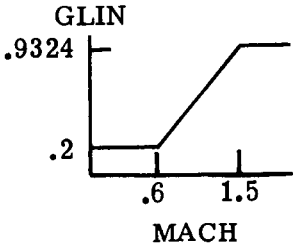

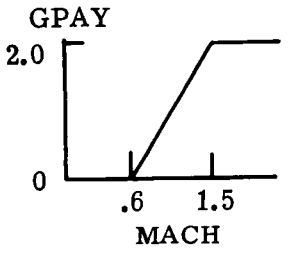

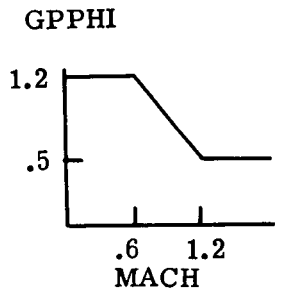

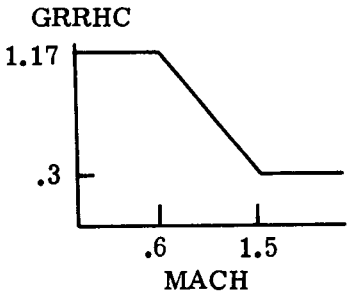

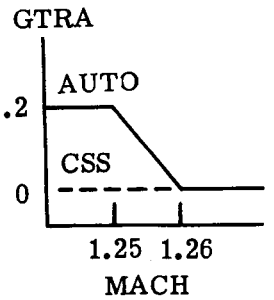

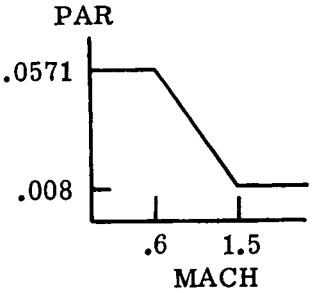

(b) Gain schedules.
Figure A1. Continued.

BANKERR Threshold

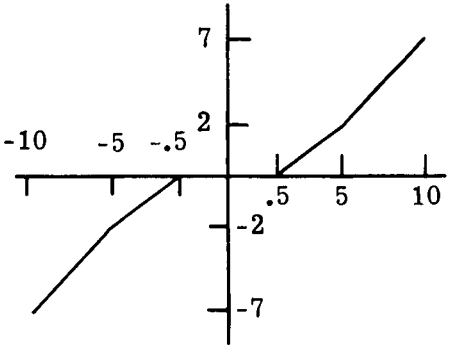

DAMAX

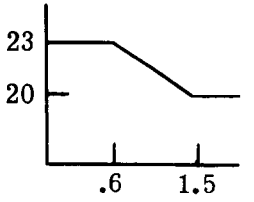

PCLIM

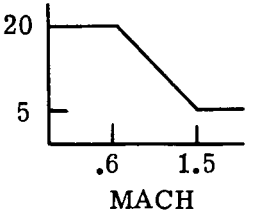

Roll jet hysteresis

No. of jets

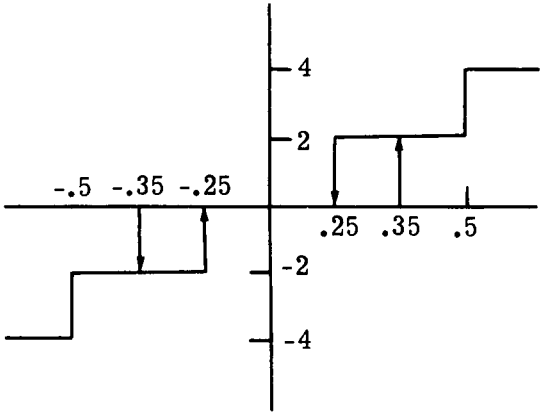

Second-order filter

$$\frac{0.51558 - 0.0470063z^{-1} + 0.137522z^{-2}}{1 - 0.643921z^{-1} + 0.250017z^{-2}}$$

Fourth-order filter (sequential second-order filters)

$$\frac{0.469695 - 0.295307z^{-1} + 0.247485z^{-2}}{1 - 1.09522z^{-1} + 0.517095z^{-2}} \qquad \frac{0.601143 + 1.20229z^{-1} + 0.601143z^{-2}}{1 + 1.08577z^{-1} + 0.318804z^{-2}}$$

(c) Limits and filters.

Figure A1. Concluded.

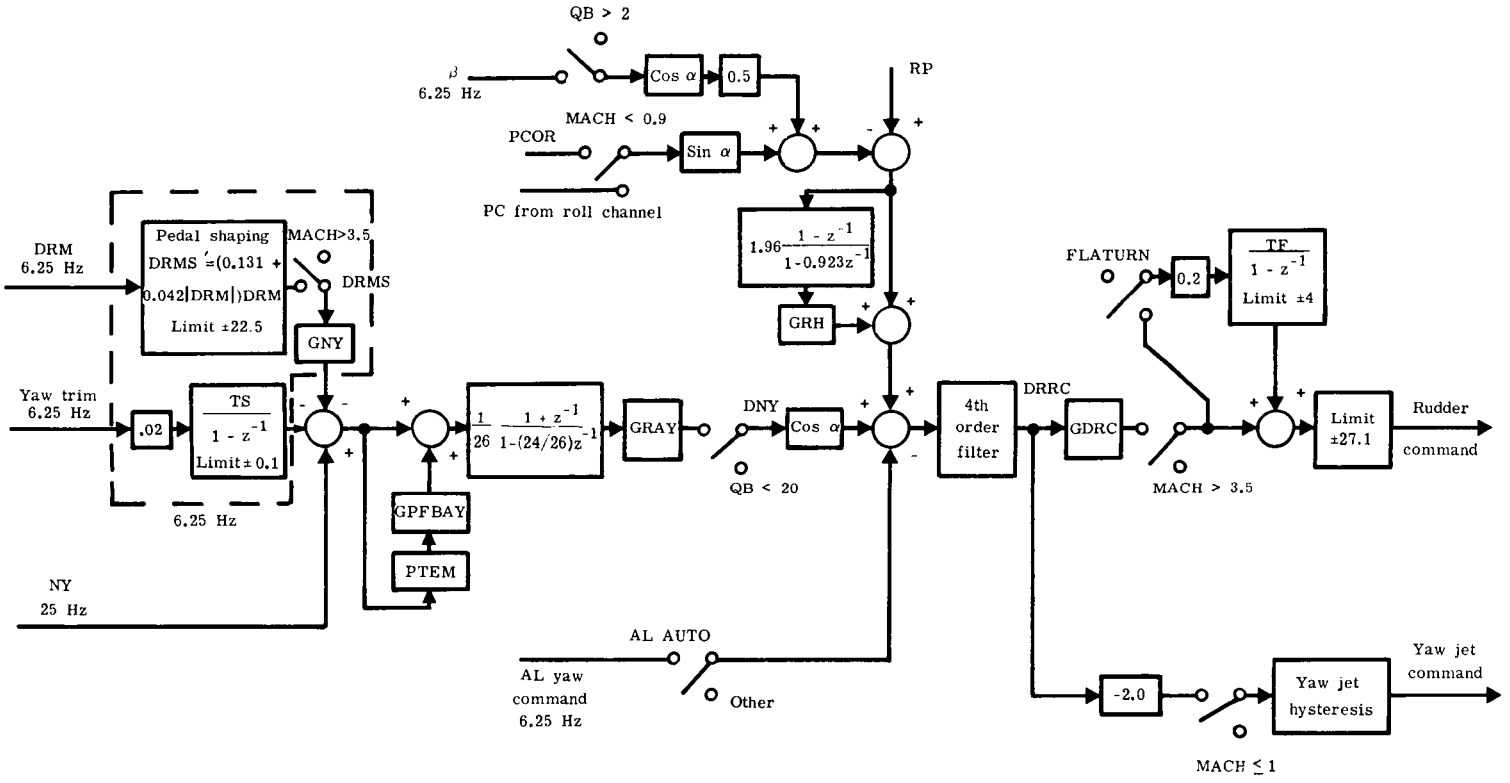

(a) Block diagram. Frequency = 25 Hz unless otherwise noted.

Figure A2. Yaw channel.

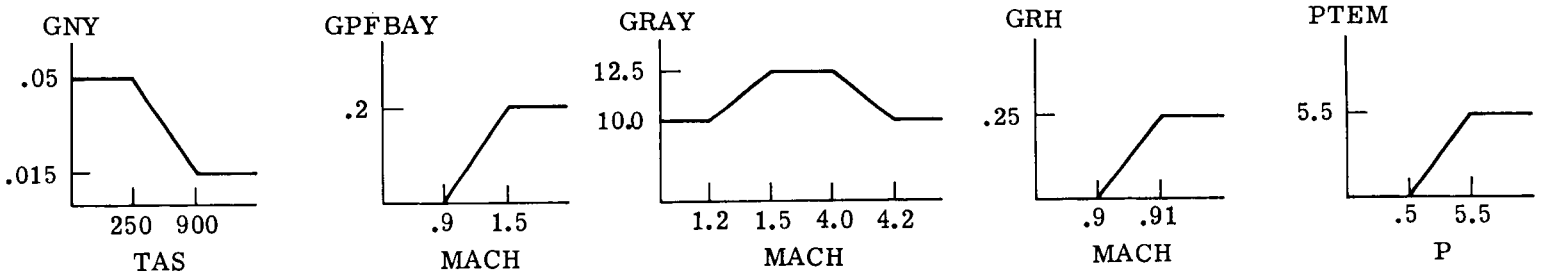

GDRC

$$GDRC = \frac{750}{QB + 10}, \qquad 1.2 < GDRC < 15$$

Fourth-order filter (sequential second-order filters)

$$\frac{0.276344 - 0.31236z^{-1} + 0.267492z^{-2}}{1 - 1.28541z^{-1} + 0.516834z^{-2}}$$

$$\frac{0.244425 + 0.48885z^{-1} + 0.244425z^{-2}}{1 - 0.473567z^{-1} + 0.451268z^{-2}}$$

Yaw jet hysteresis

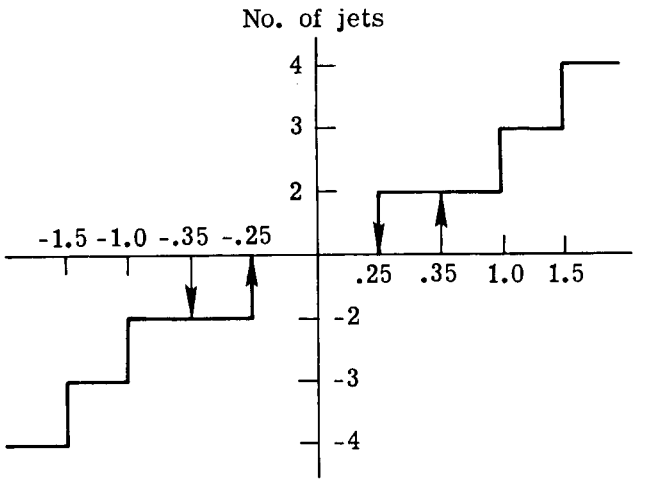

(b) Gains, filters, and hysteresis.

Figure A2. Concluded.

References

1. *Space Shuttle.* NASA SP-407, 1976.

2. Carrier, L.M.; and Minor, R.G.: Space Shuttle Orbiter Avionics. *A Collection of Technical Papers—AIAA 2nd Digital Avionics Systems Conference,* Nov. 1977, pp. 146–156. (Available as AIAA Paper 77-1501.)

3. Brand, Vance D.: Return to Earth in the Space Shuttle. 1977 Report to the Aerospace Profession, *Tech. Rev.,* vol. 13, no. 4, Soc. Exp. Test Pilots, c.1978, pp. 223–231.

4. Stone, Howard W.; and Powell, Richard W.: *Effect of Aerodynamic and Angle-of-Attack Uncertainties on the Blended Entry Flight Control System of the Space Shuttle From Mach 10 to 2.5.* NASA TP-2283, 1984.

5. Rowell, Lawrence F.; Powell, Richard W.; and Stone, Howard W., Jr.: *Development of the Reentry Flight Dynamics Simulator for Evaluation of Space Shuttle Orbiter Entry Systems.* NASA TP-1700, 1980.

6. Young, James C.; and Underwood, Jimmy M.: The Development of Aerodynamic Uncertainties for the Space Shuttle Orbiter. *A Collection of Technical Papers—12th Aerodynamic Testing Conference,* Mar. 1982, pp. 9–14. (Available as AIAA-82-0563.)

7. Kanipe, David B.: Plume/Flowfield Jet Interaction Effects on the Space Shuttle Orbiter During Entry. AIAA-82-1319, Aug. 1982.

8. Harpold, Jon C.; and Gavert, Donald E.: Atmospheric Guidance Techniques and Performance. *A Collection of Technical Papers—AIAA Guidance and Control Conference,* Aug. 1982, pp. 531–537. (Available as AIAA-82-1600.)

9. *Aerodynamic Design Data Book. Volume 1: Orbiter Vehicle.* NASA CR-160386, 1978.

10. Powell, Richard W.; and Stone, Howard W.: *Analysis of the Space Shuttle Orbiter Entry Dynamics From Mach 10 to Mach 2.5 With the November 1976 Flight Control System.* NASA TP-1667, 1980.

11. Stone, Howard W.; and Powell, Richard W.: *Entry Dynamics of Space Shuttle Orbiter With Longitudinal Stability and Control Uncertainties at Supersonic and Hypersonic Speeds.* NASA TP-1084, 1977.

12. Gamble, J.D.; and Young, J.C.: The Development and Application of Aerodynamic Uncertainties in the Design of the Entry Trajectory and Flight Control System of the Space Shuttle Orbiter. AIAA-82-1335, Aug. 1982.

TABLE I. PHYSICAL CHARACTERISTICS OF SPACE

SHUTTLE ORBITER DURING ENTRY

Mass properties:	
Weight, lb	189 844.0
Moments of inertia:	
I_X, slug-ft^2	846 379.4
I_Y, slug-ft^2	6 594 353.0
I_Z, slug-ft^2	6 854 100.9
I_{XY}, slug-ft^2	14 251.2
I_{XZ}, slug-ft^2	−171 380.4
I_{YZ}, slug-ft^2	532.8
Wing:	
Reference area, ft^2	2 690
Chord, ft	39.57
Span, ft	78.057
Elevon:	
Reference area, ft^2	206.57
Chord, ft	7.46
Deflection range, deg	−35 to 20
Rudder and speed brake:	
Reference area, ft^2	97.84
Chord, ft	6.07
Rudder deflection, deg	±27.1
Speed-brake deflection range, deg	0 to 98.6
Body flap:	
Reference area, ft^2	135.75
Chord, ft	6.75
Deflection range, deg	−11.7 to 22.5

TABLE II. OFF-NOMINAL AERODYNAMIC VARIATIONS[a]

Case	$C_{n\beta}$	$C_{l\beta}$	$C_{n\delta a}$	$C_{l\delta a}$
1	−	−	−	−
2	+	−	−	−
3	−	+	−	−
4	+	+	−	−
5	−	−	+	−
6	+	−	+	−
7	−	+	+	−
8	+	+	+	−
9	−	−	−	+
10	+	−	−	+
11	−	+	−	+
12	+	+	−	+
13	−	−	+	+
14	+	−	+	+
15	−	+	+	+
16	+	+	+	+

Rudder Effectiveness	$C_{Y_{\delta r}}$	$C_{n\delta r}$	$C_{l\delta r}$
Increased effectiveness	+	−	+
Decreased effectiveness	−	+	−

[a] A plus sign (+) indicates that aerodynamic variation is added to the nominal coefficient. A minus sign (−) indicates that aerodynamic variation is subtracted from the nominal coefficient.

TABLE III. OFF-NOMINAL RCS/AERODYNAMIC INTERFERENCE UNCERTAINTY SETS[a]

Set	Pitch due to yaw	Roll due to yaw	Yaw due to yaw
1	−	−	−
2	+	+	−
3	−	−	+
4	+	+	+

[a] A plus sign (+) indicates that aerodynamic variation is added to the nominal coefficient. A minus sign (−) indicates that aerodynamic variation is subtracted from the nominal coefficient.

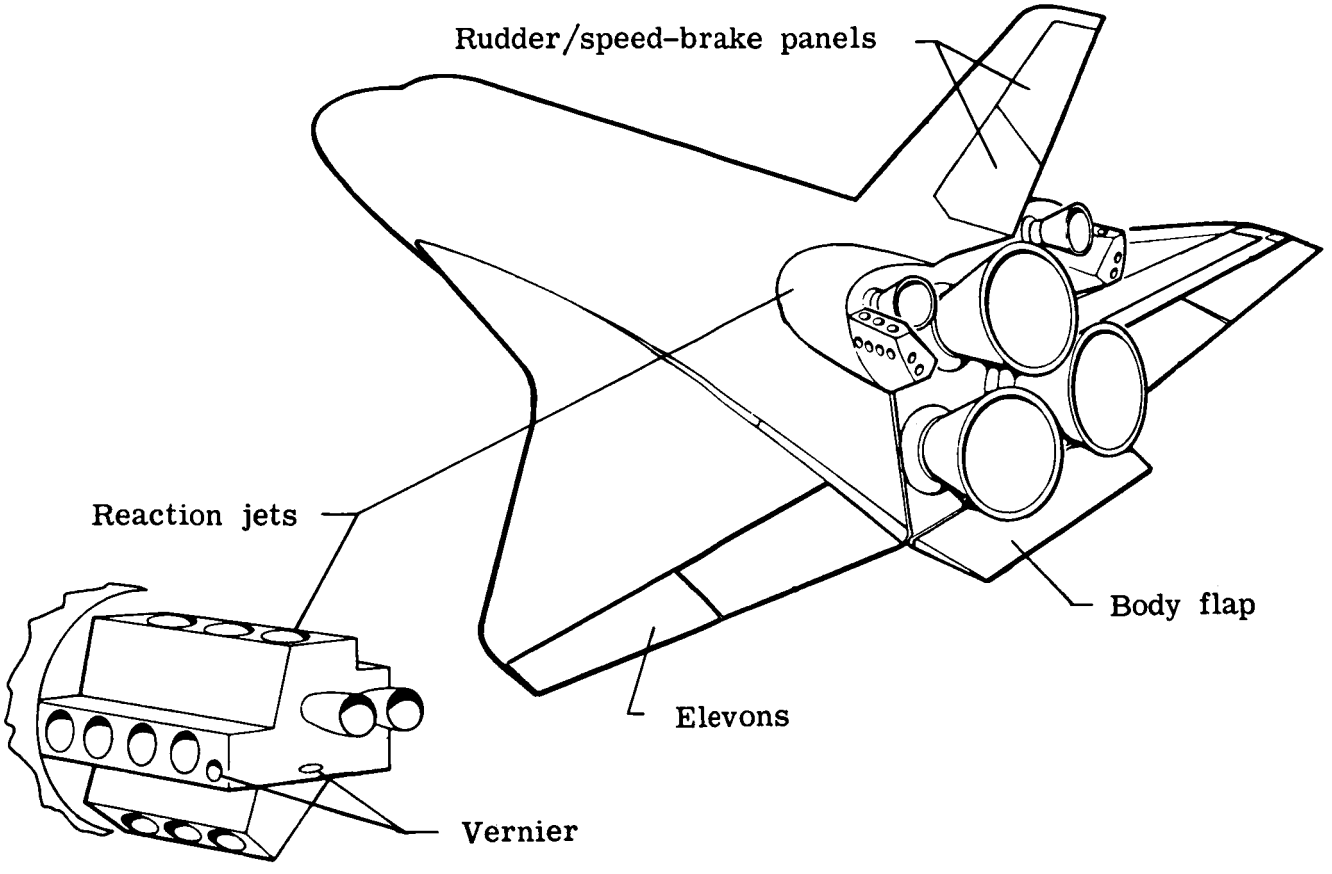

Figure 1. Sketch of Space Shuttle Orbiter.

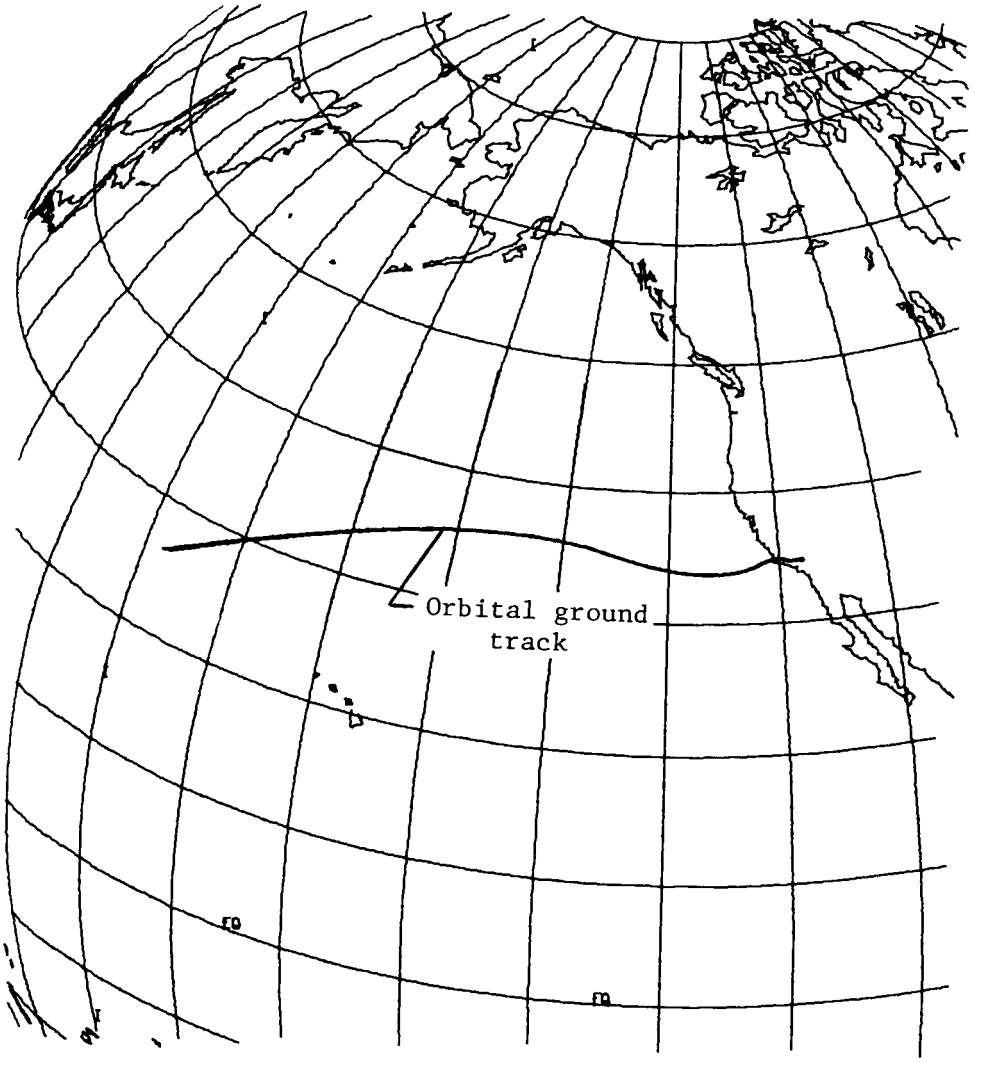

Figure 2. Entry trajectory of Space Shuttle Orbiter on first flight.

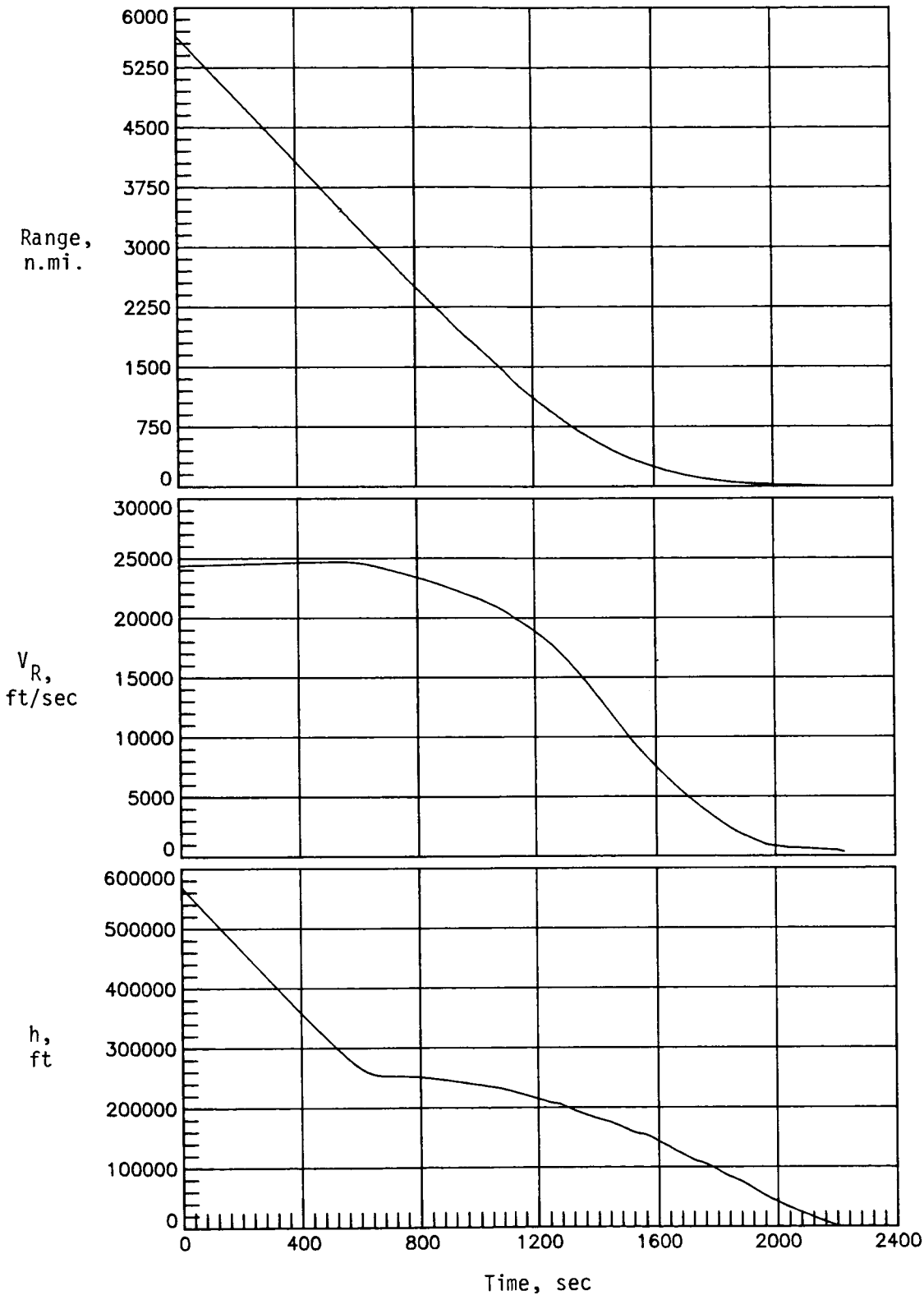

Figure 3. Nominal entry trajectory parameters of Space Shuttle Orbiter on first flight.

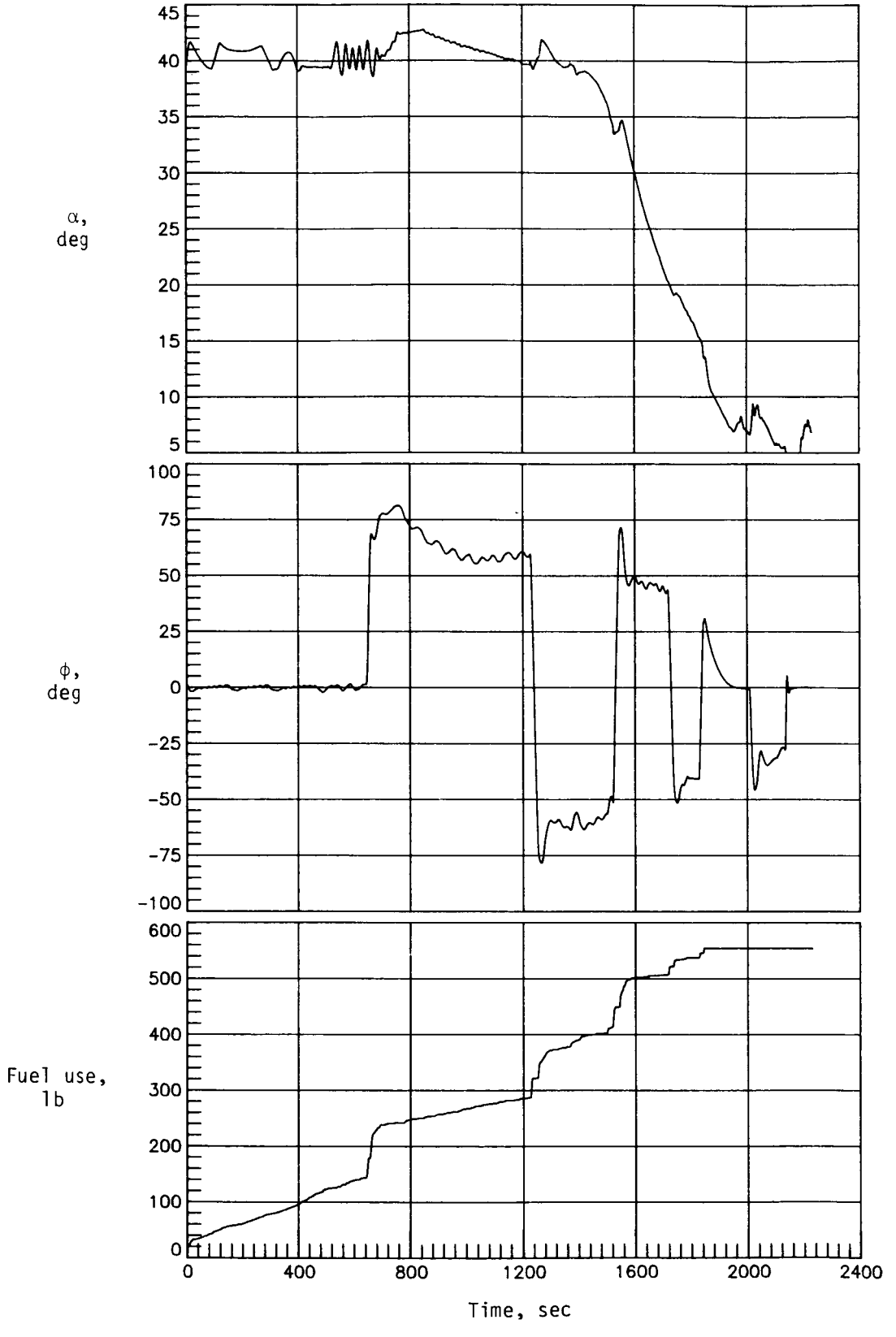

Figure 3. Concluded.

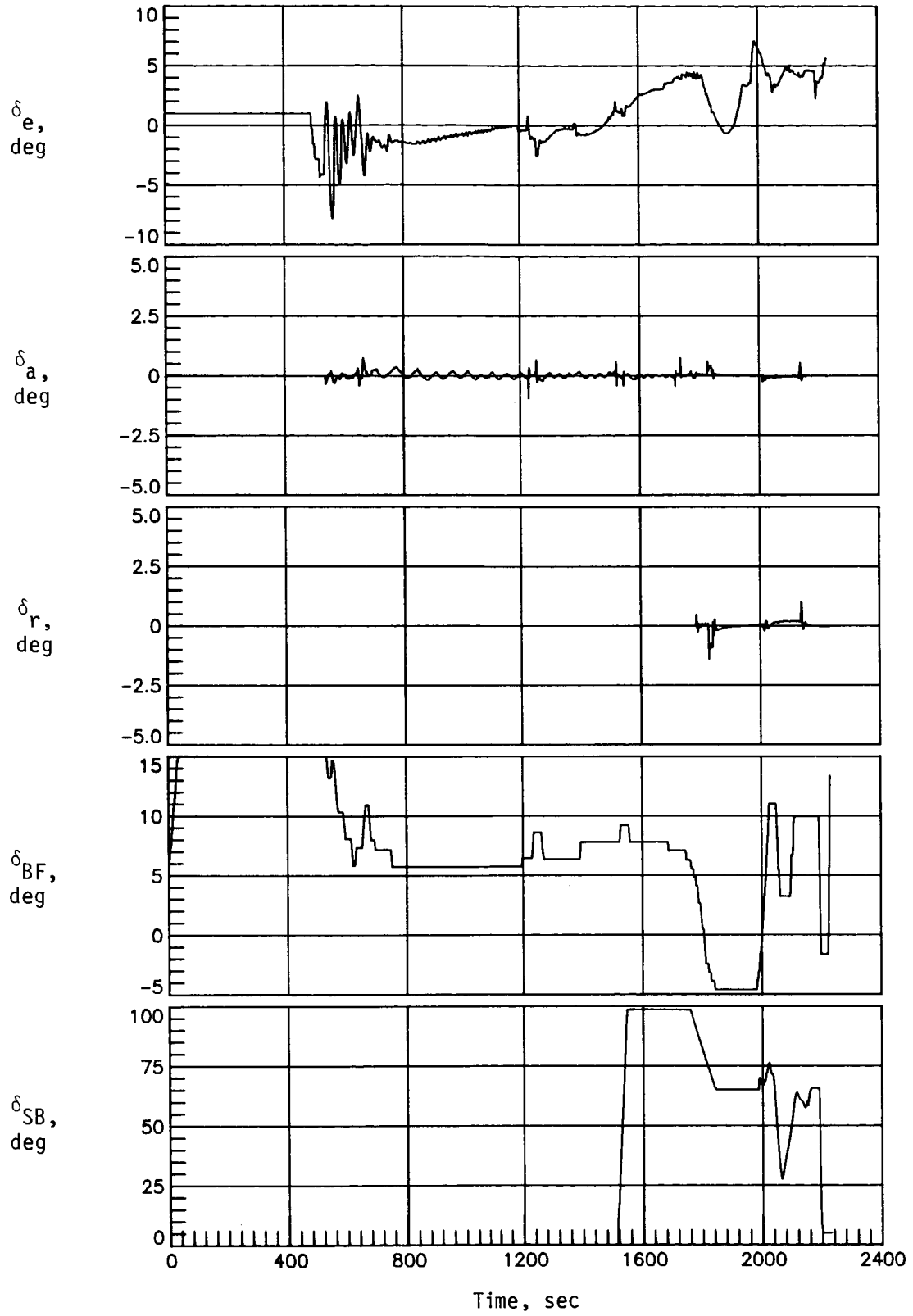

Figure 4. Space Shuttle Orbiter nominal controls history.

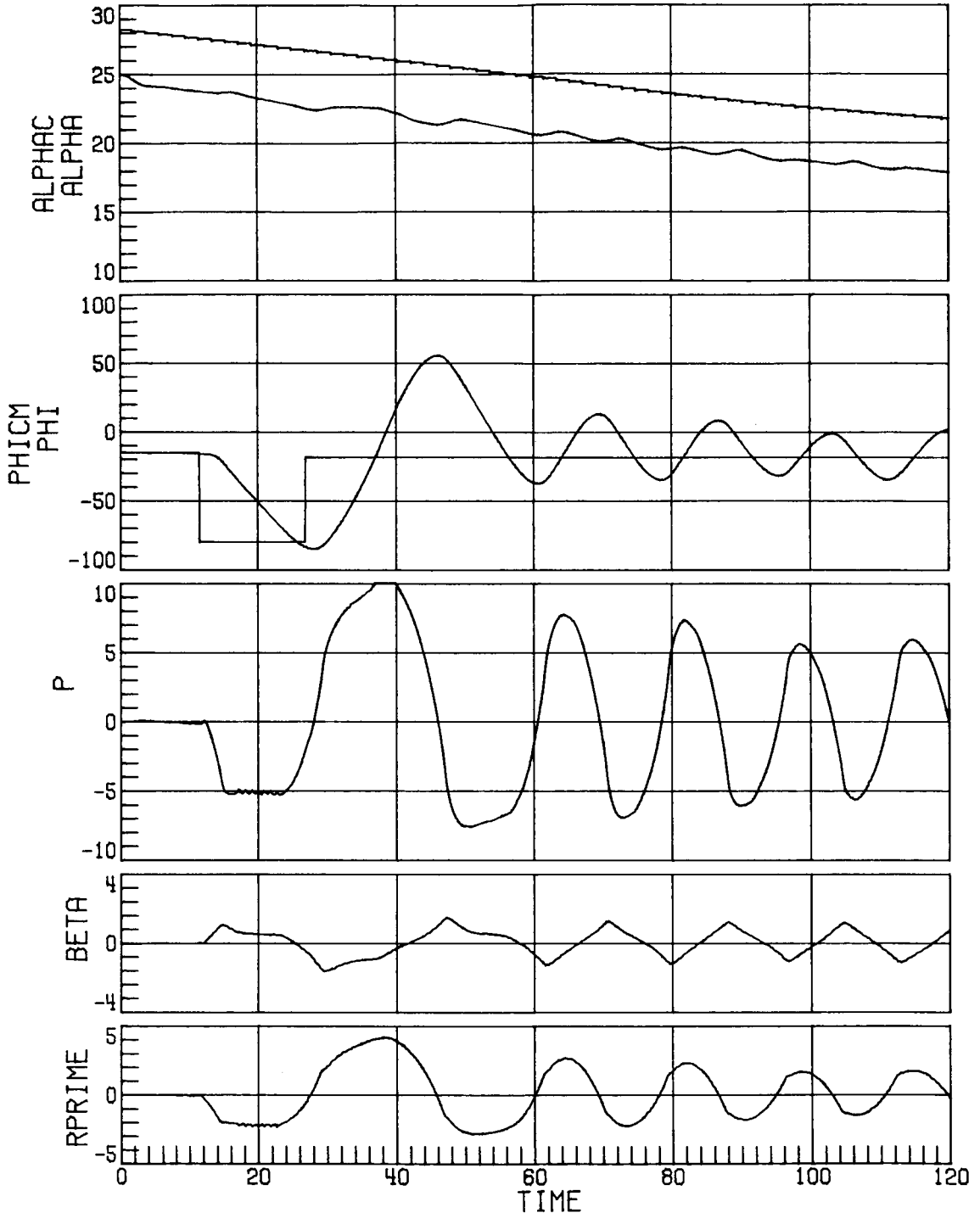

(a) Case 11; Mach 7; indicated α 4° high.

Figure 5. Time-history response. Time in seconds.

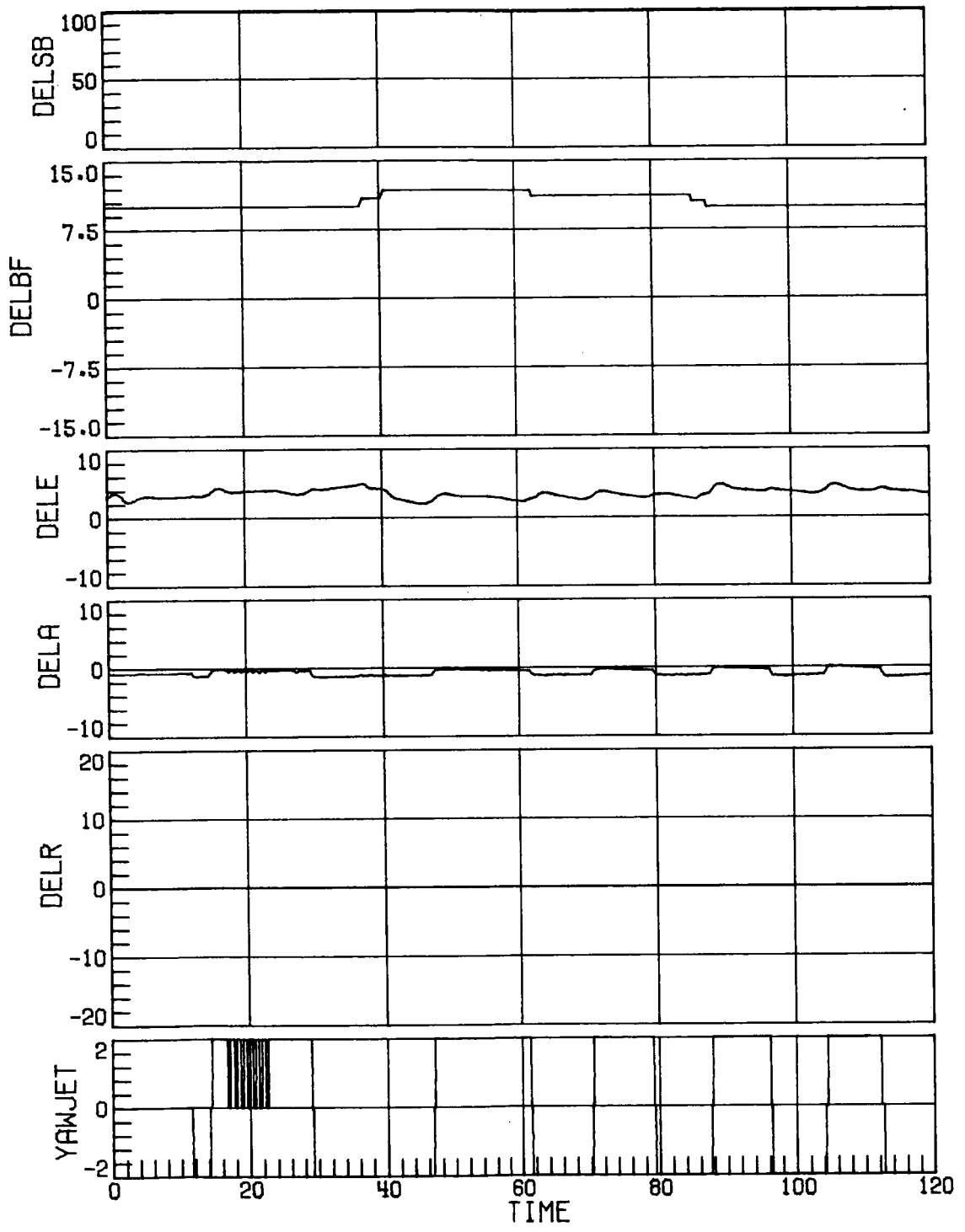

(a) Concluded.
Figure 5. Continued.

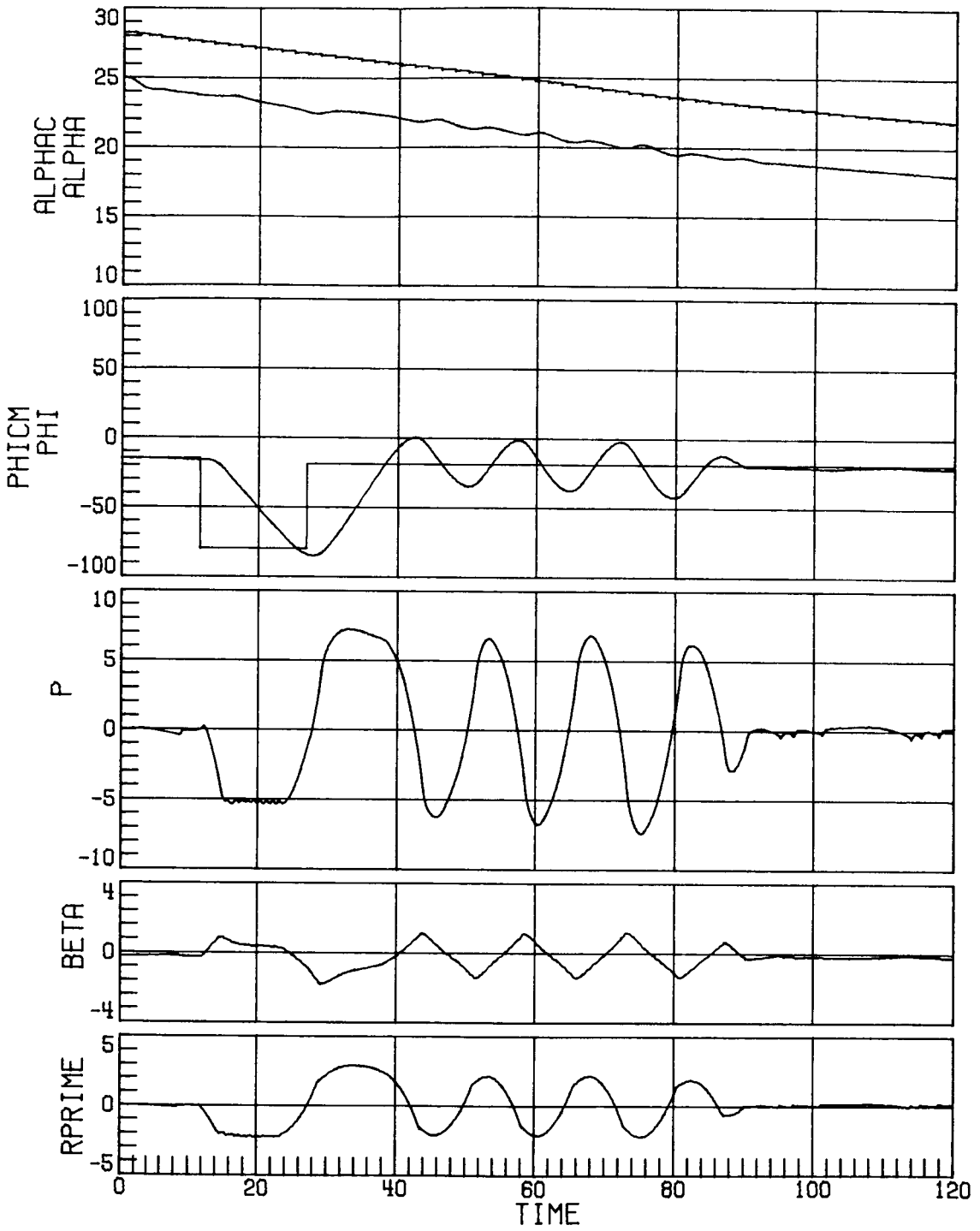

(b) Case 15; Mach 7; indicated α 4° high.
Figure 5. Continued.

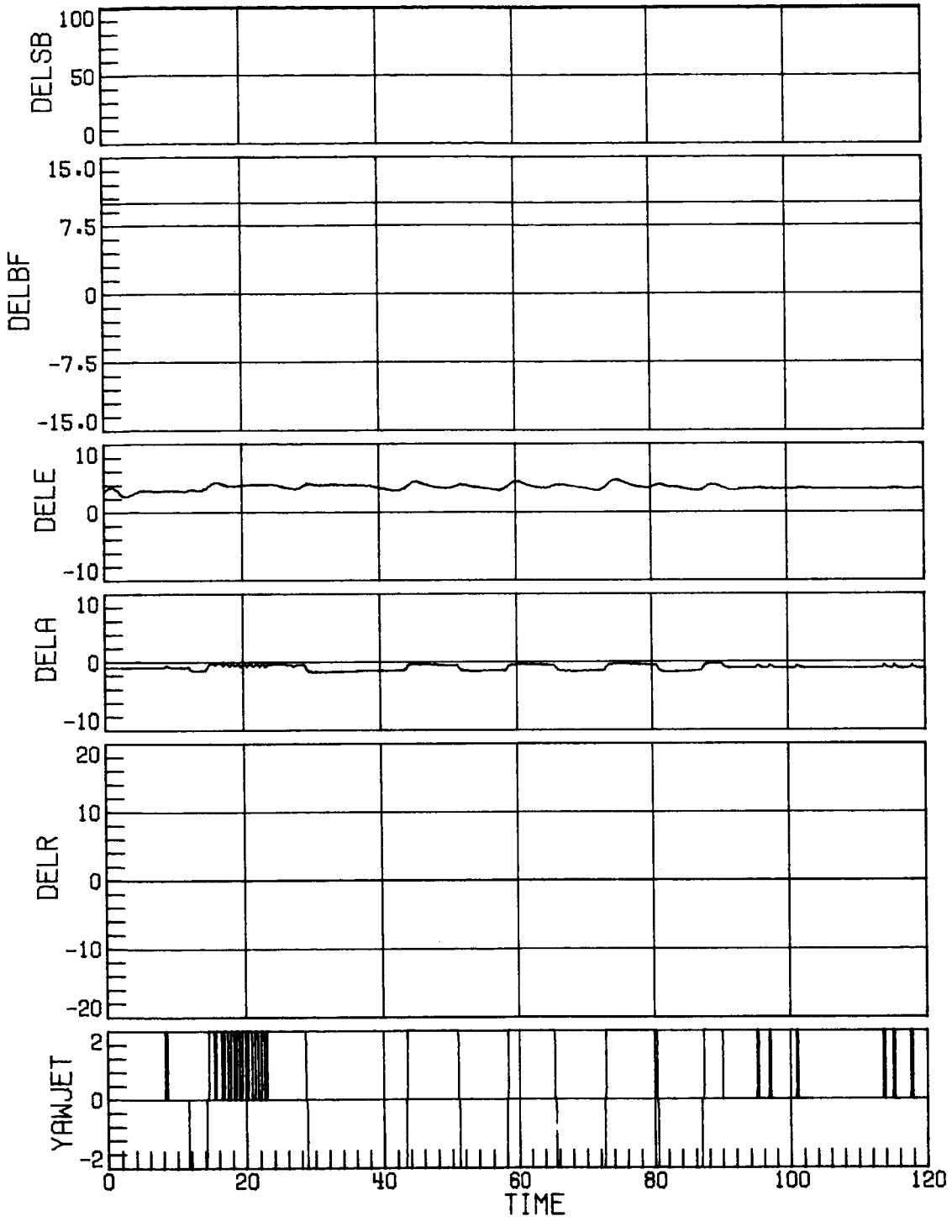

(b) Concluded.
Figure 5. Continued.

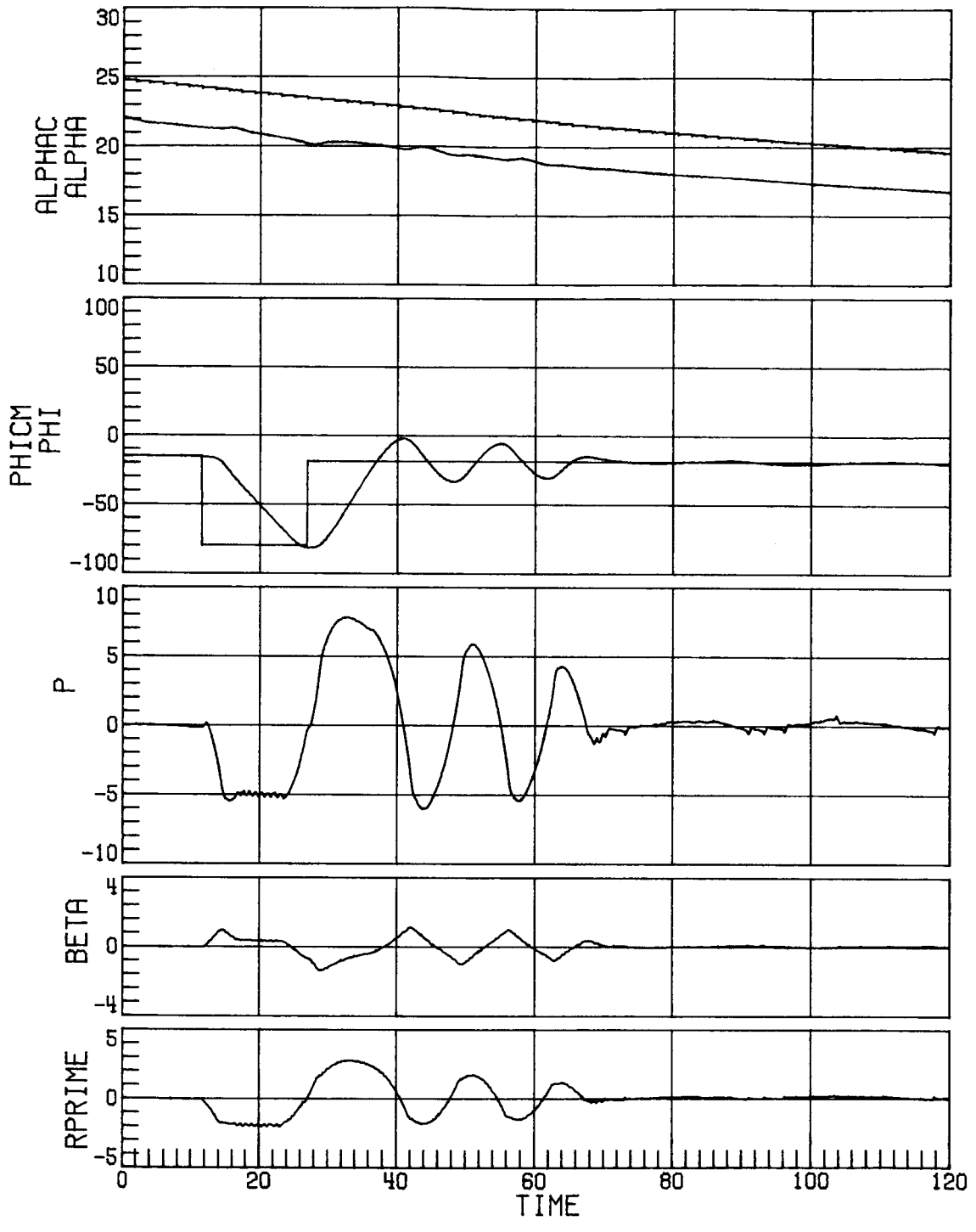

(c) Case 11; Mach 6.1; indicated α 3° high.
Figure 5. Continued.

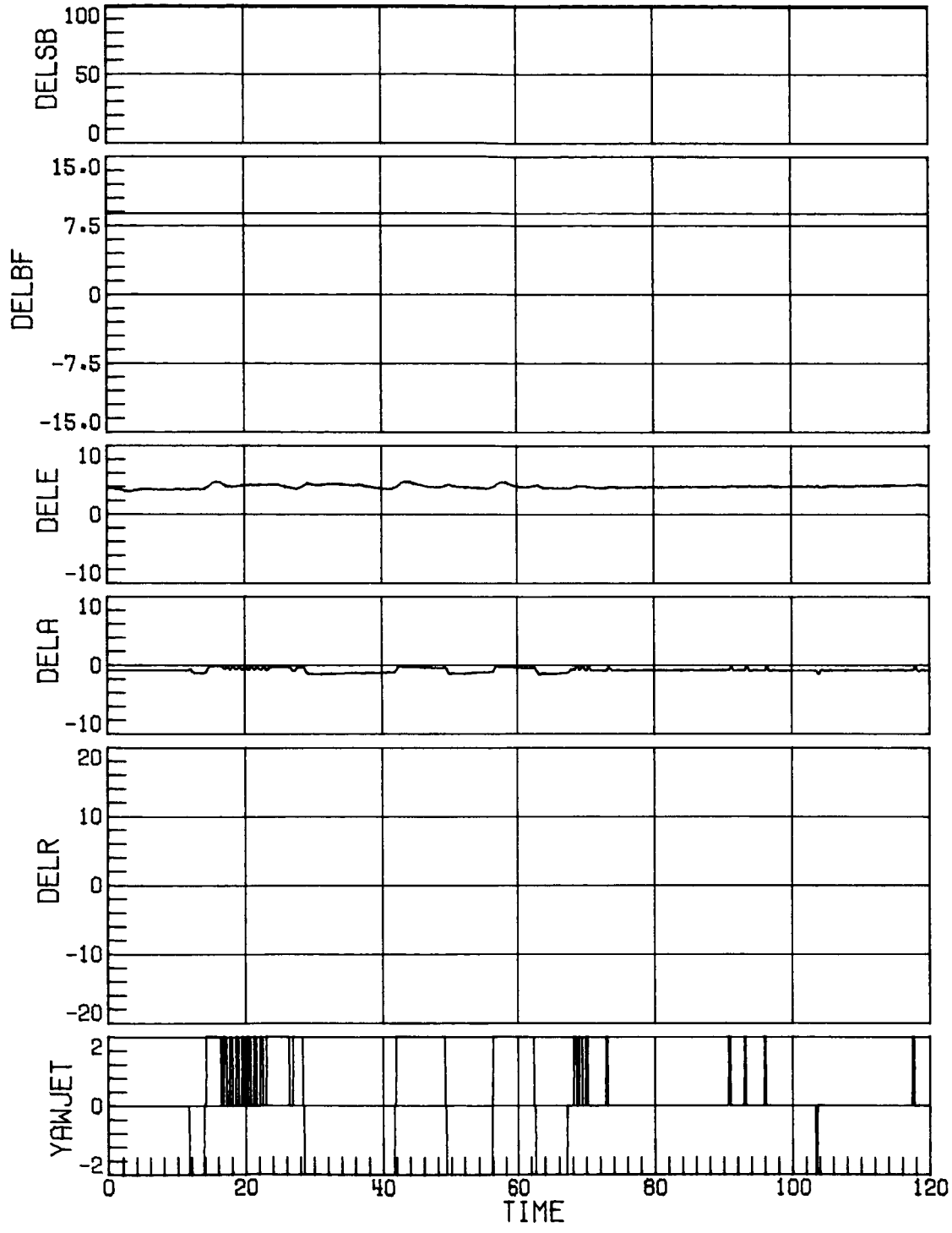

(c) Concluded.
Figure 5. Concluded.

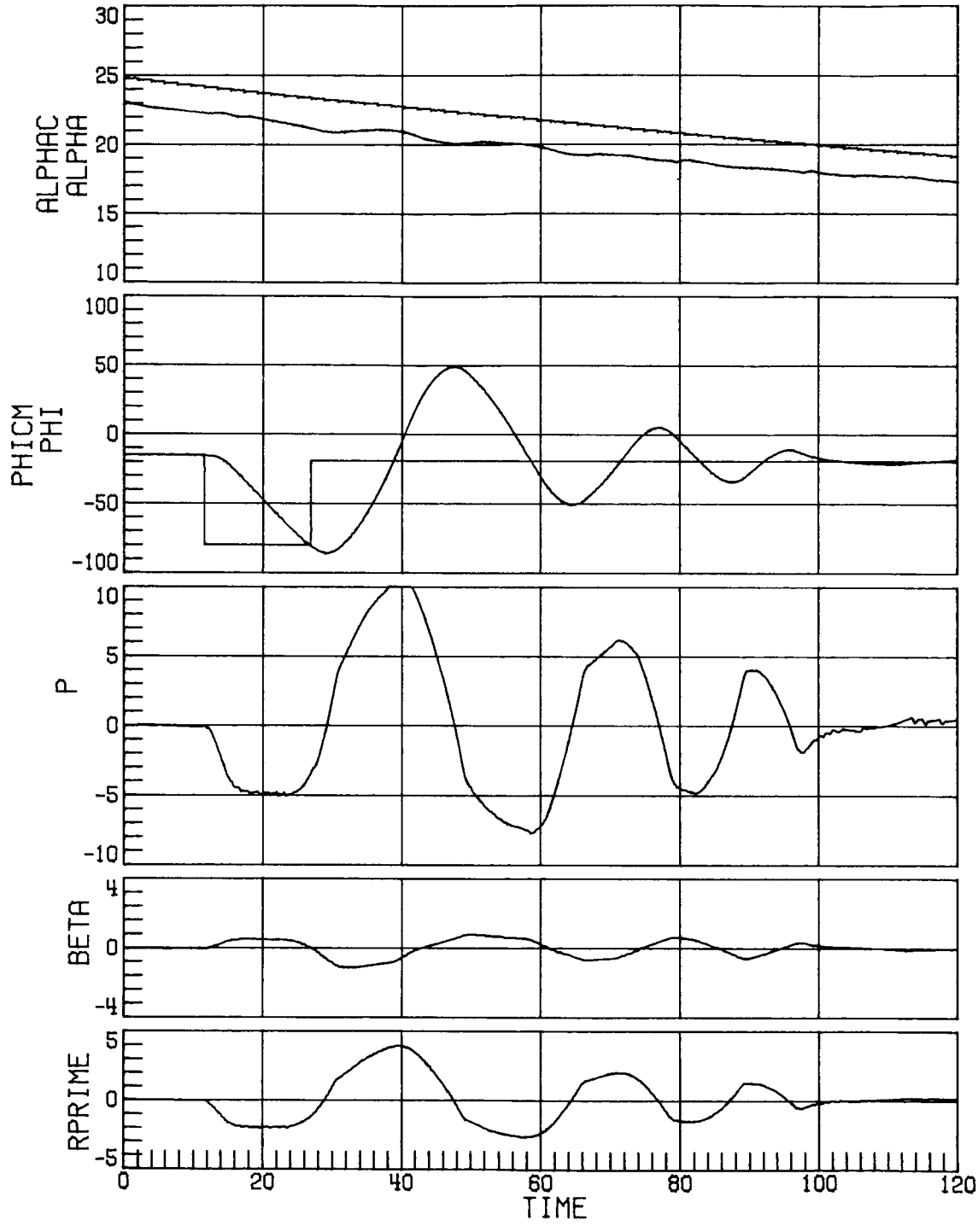

Figure 6. Time-history response for case 11 at Mach 6.1 with RCS uncertainty set 2 and indicated α 2° high. Time in seconds.

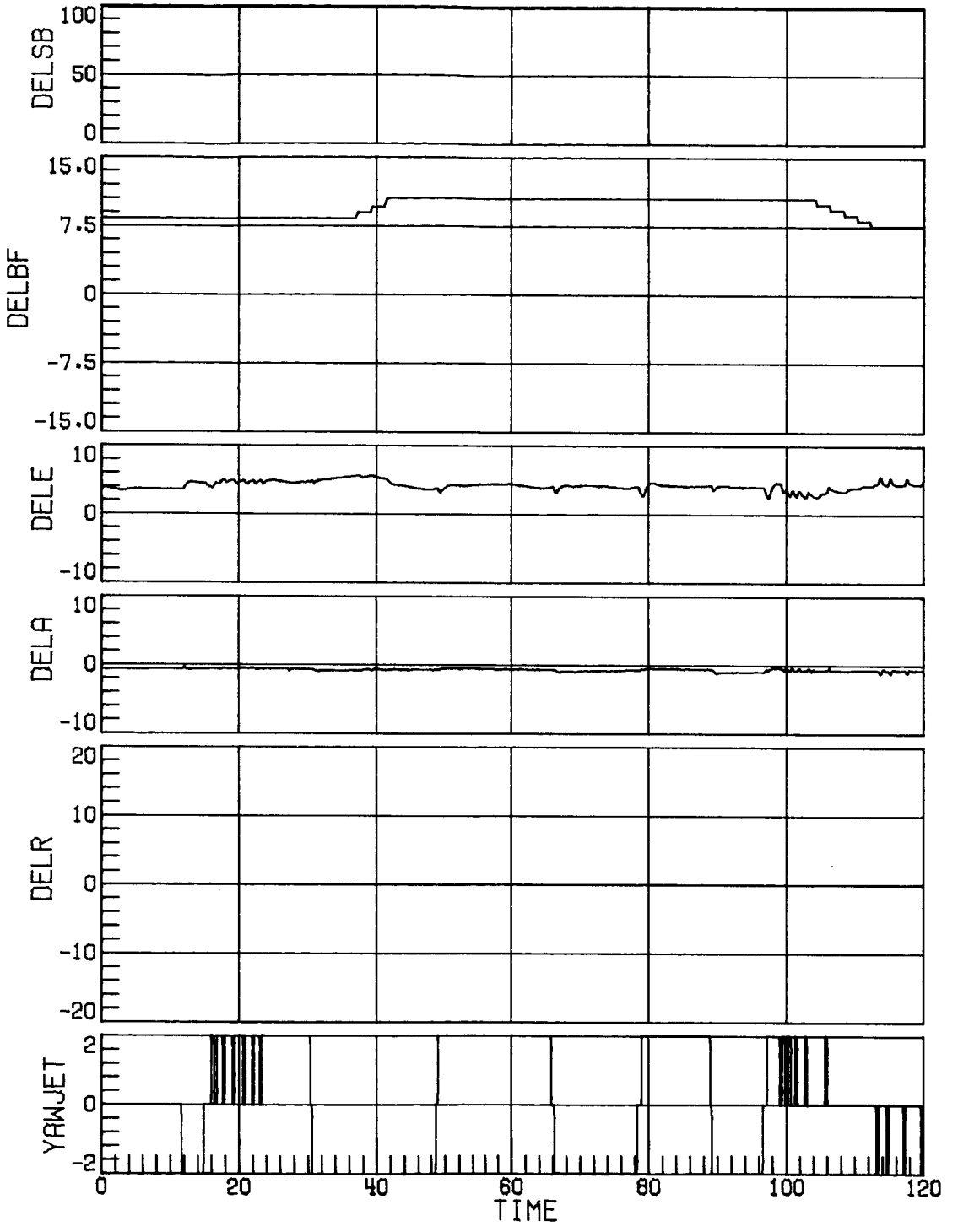

Figure 6. Concluded.

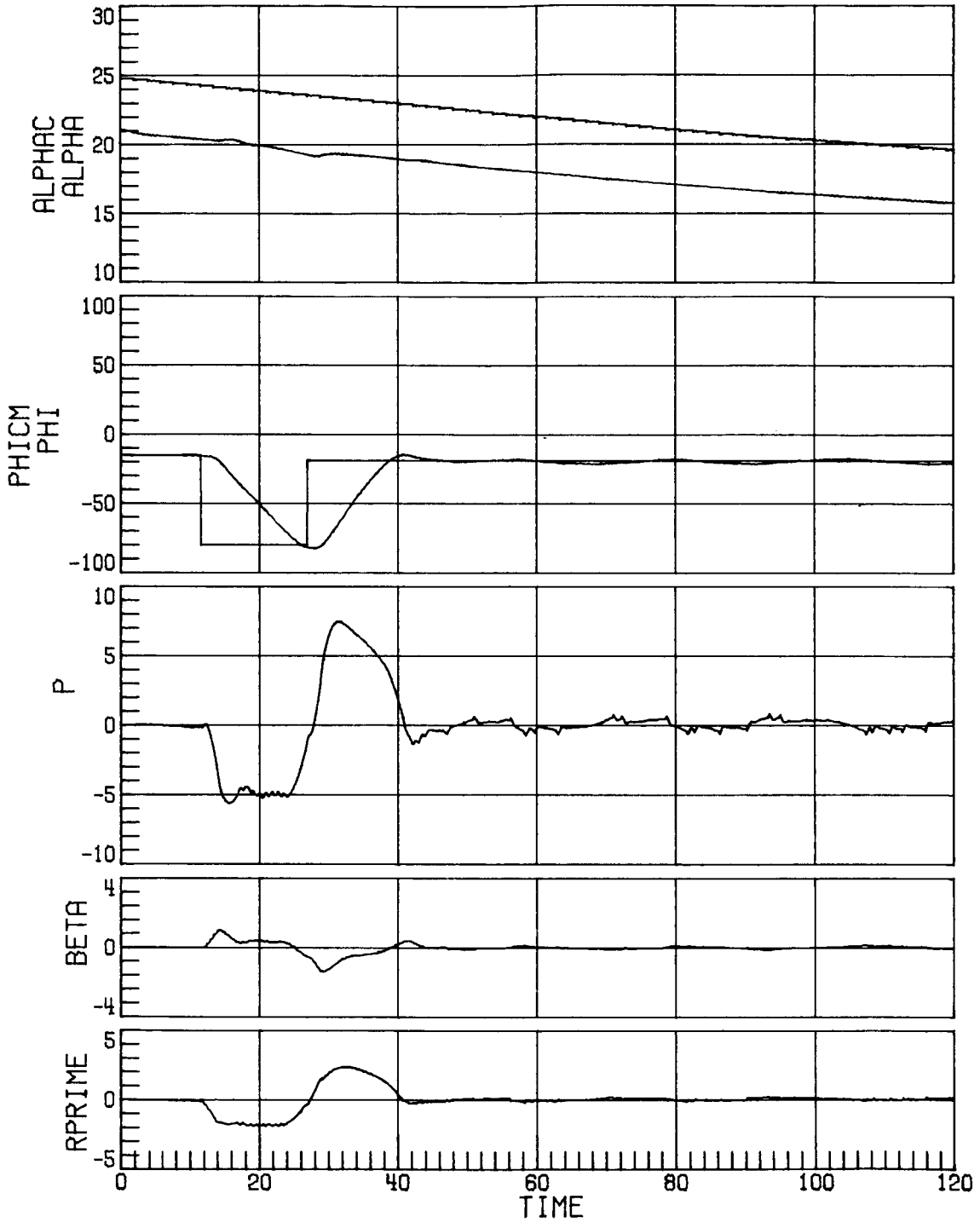

(a) Indicated α 4° high; without RCS uncertainties.

Figure 7. Time-history response at Mach 6.1 for case 11 with side-force feedback gain GPFBAY = 0.5. Time in seconds.

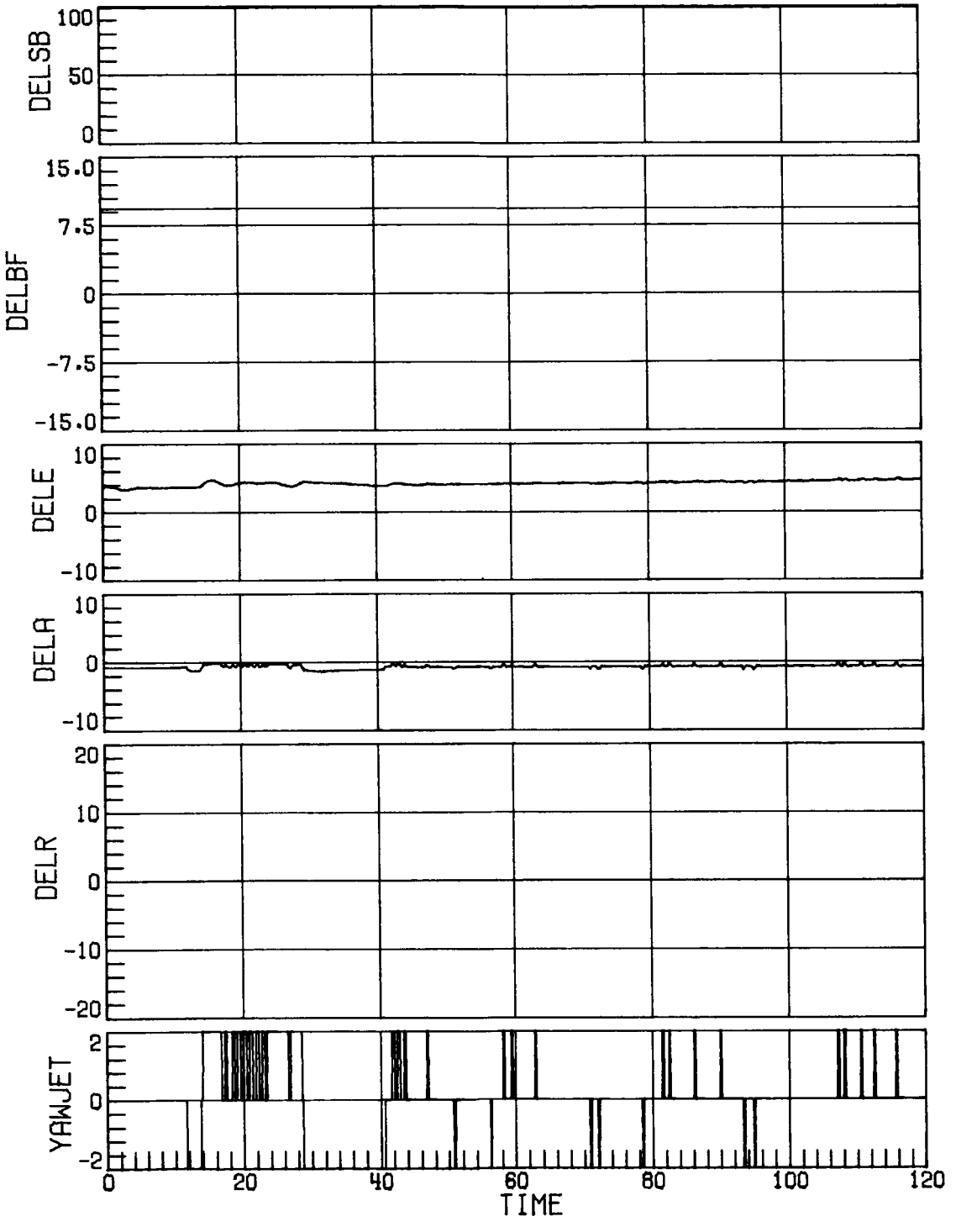

(a) Concluded.
Figure 7. Continued.

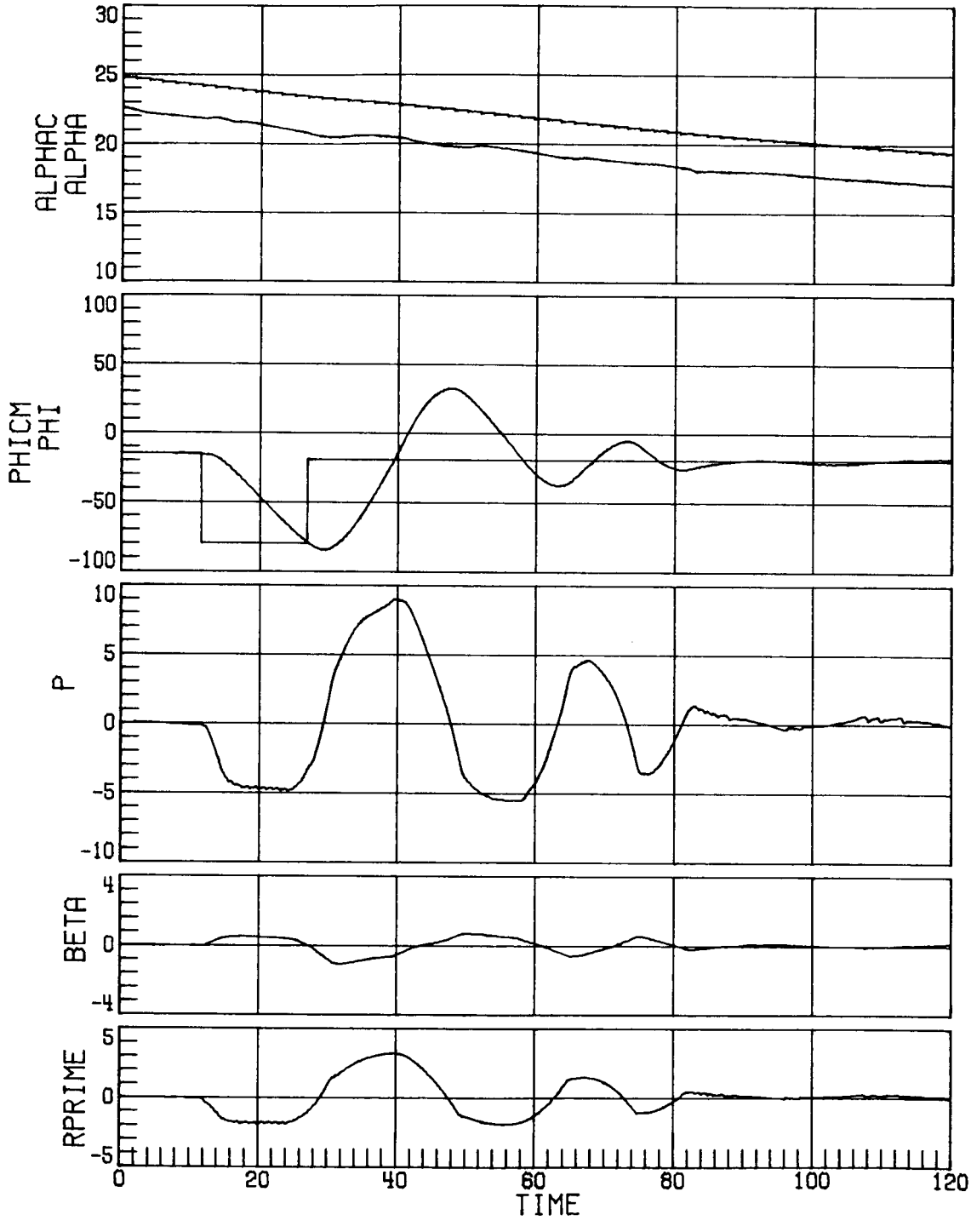

(b) Indicated α 2.5° high; RCS uncertainty set 2.
Figure 7. Continued.

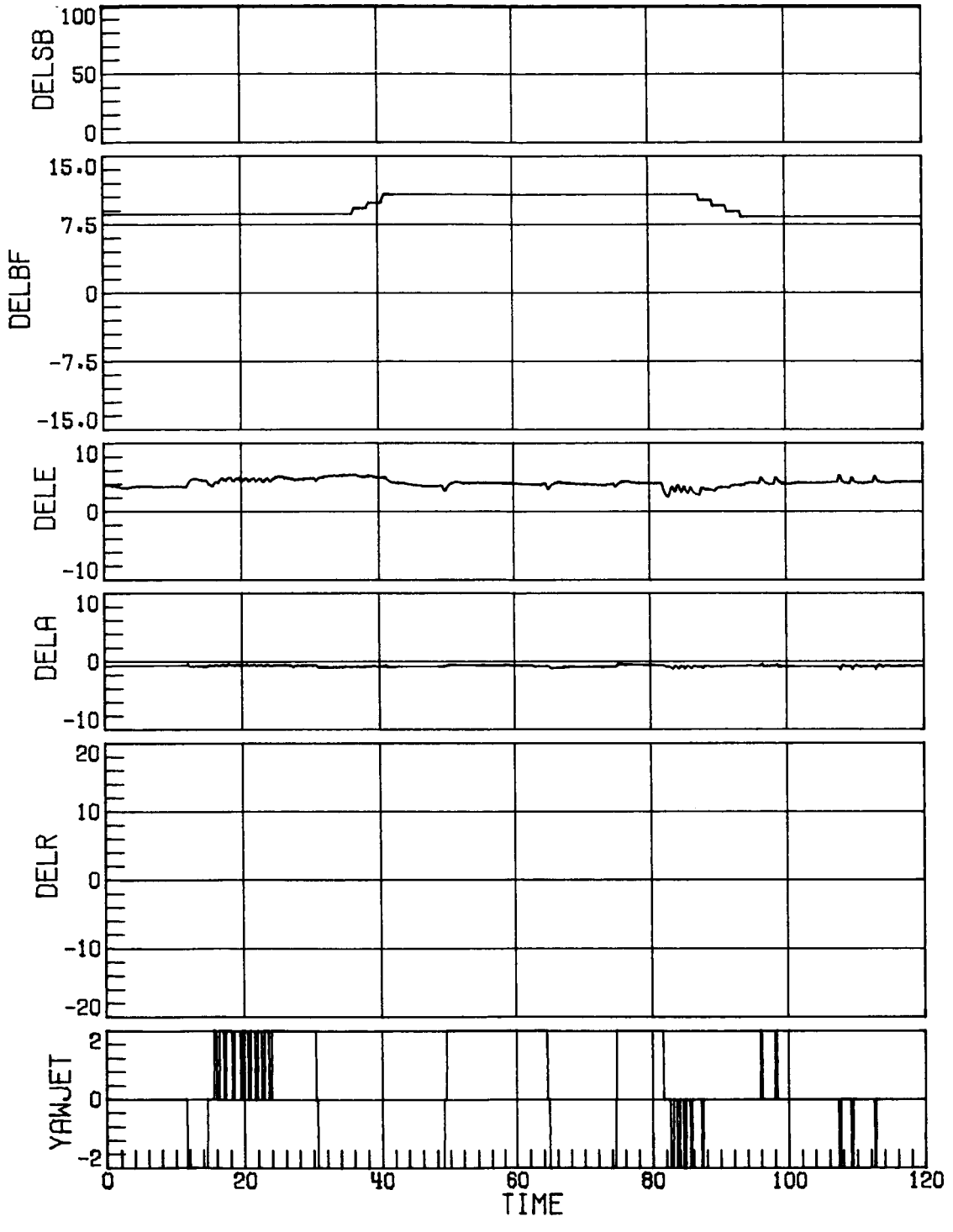

(b) Concluded.
Figure 7. Continued.

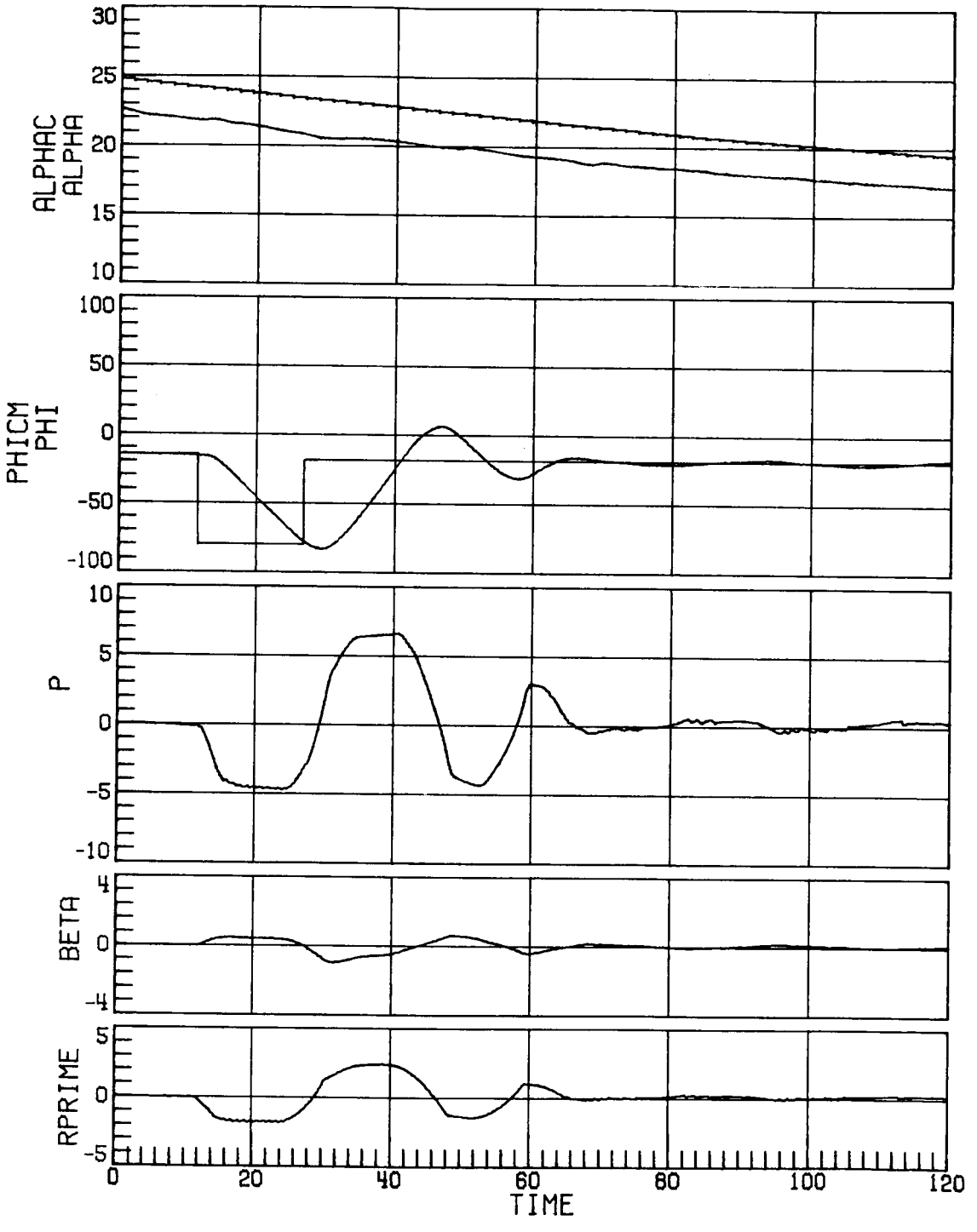

(c) Indicated α 2.5° high; RCS uncertainty set 2; GRAY = 12.5.
Figure 7. Continued.

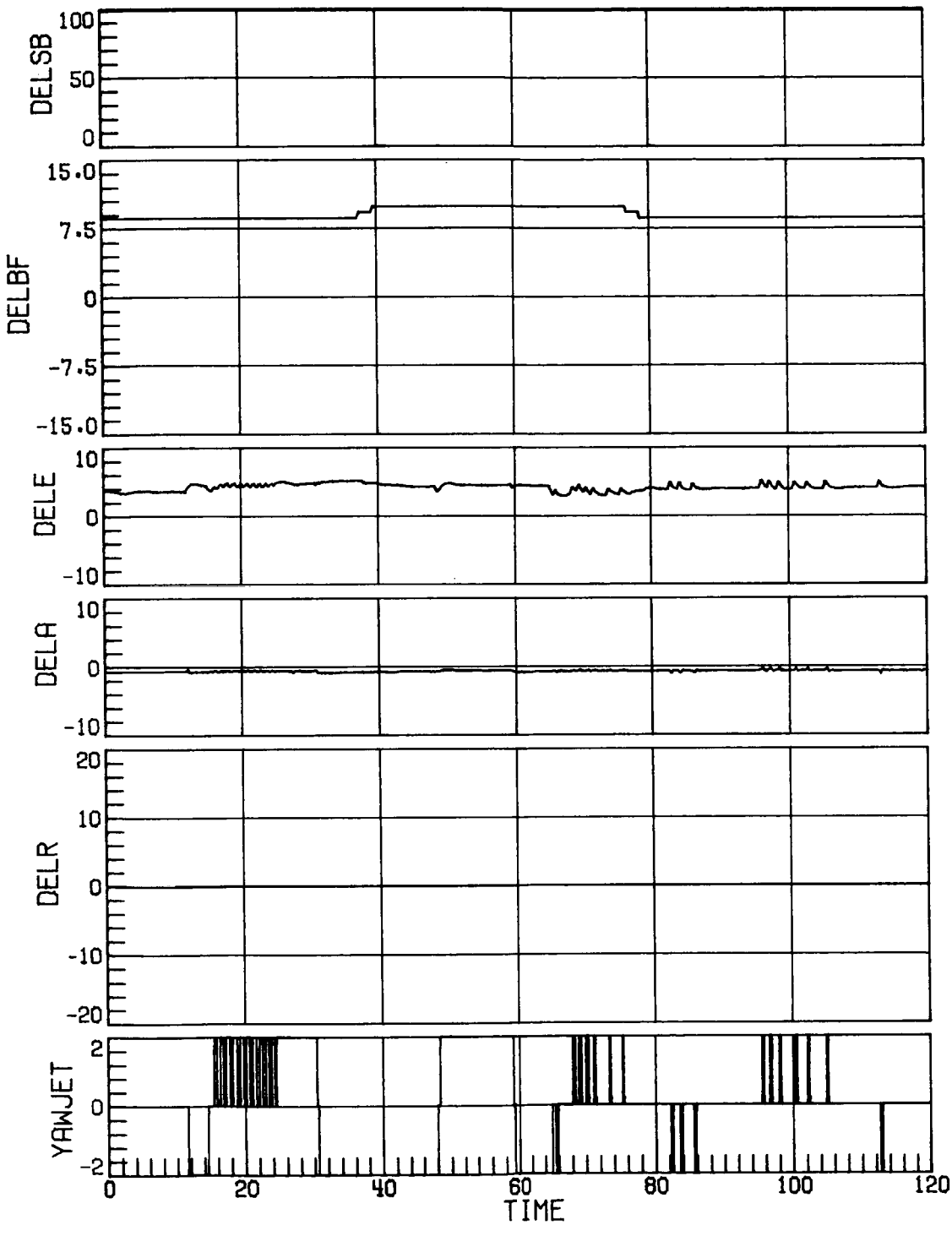

(c) Concluded.
Figure 7. Concluded.

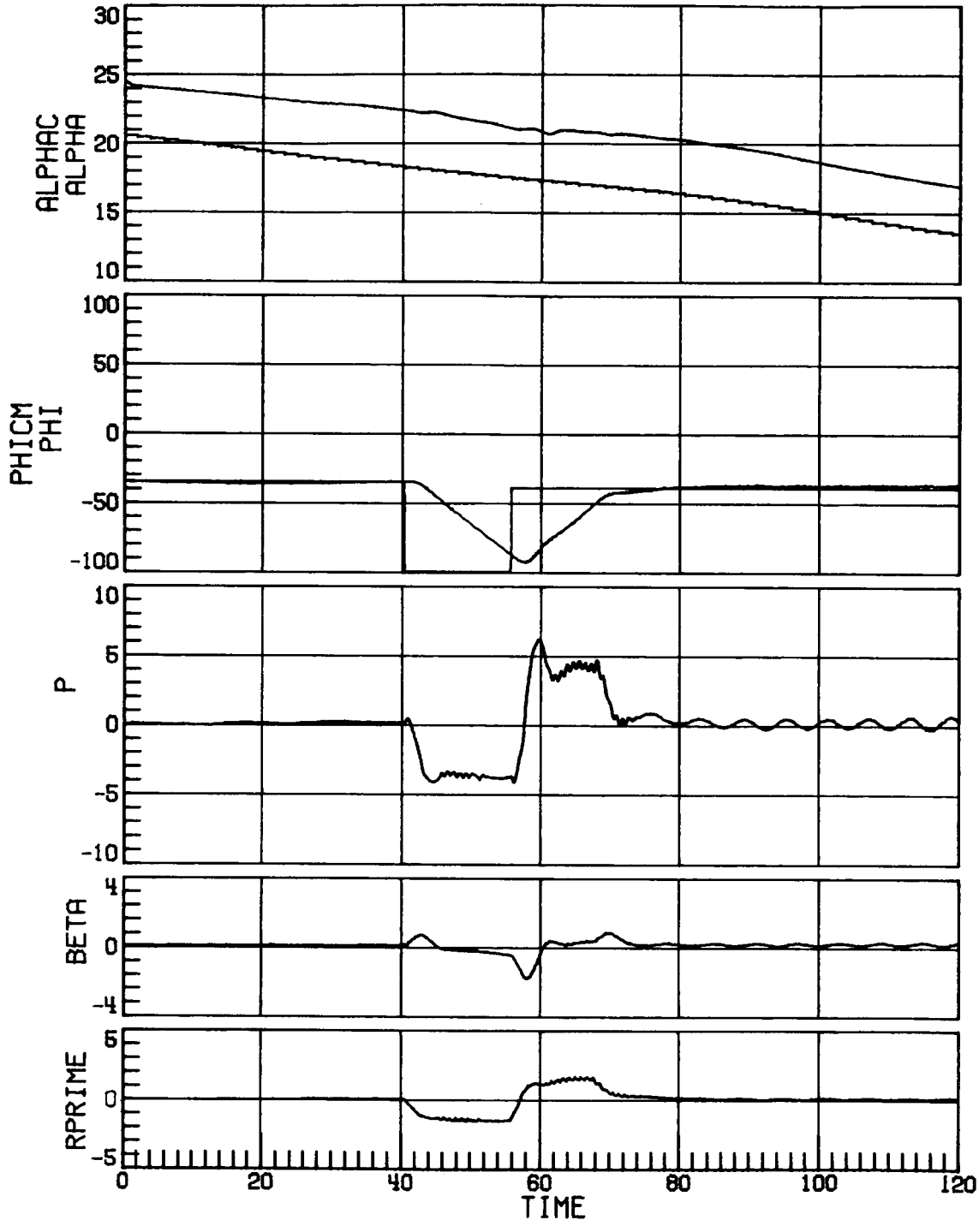

Figure 8. Time-history response at Mach 4.6, indicated δ 4° low, and increased rudder effectiveness. Time in seconds.

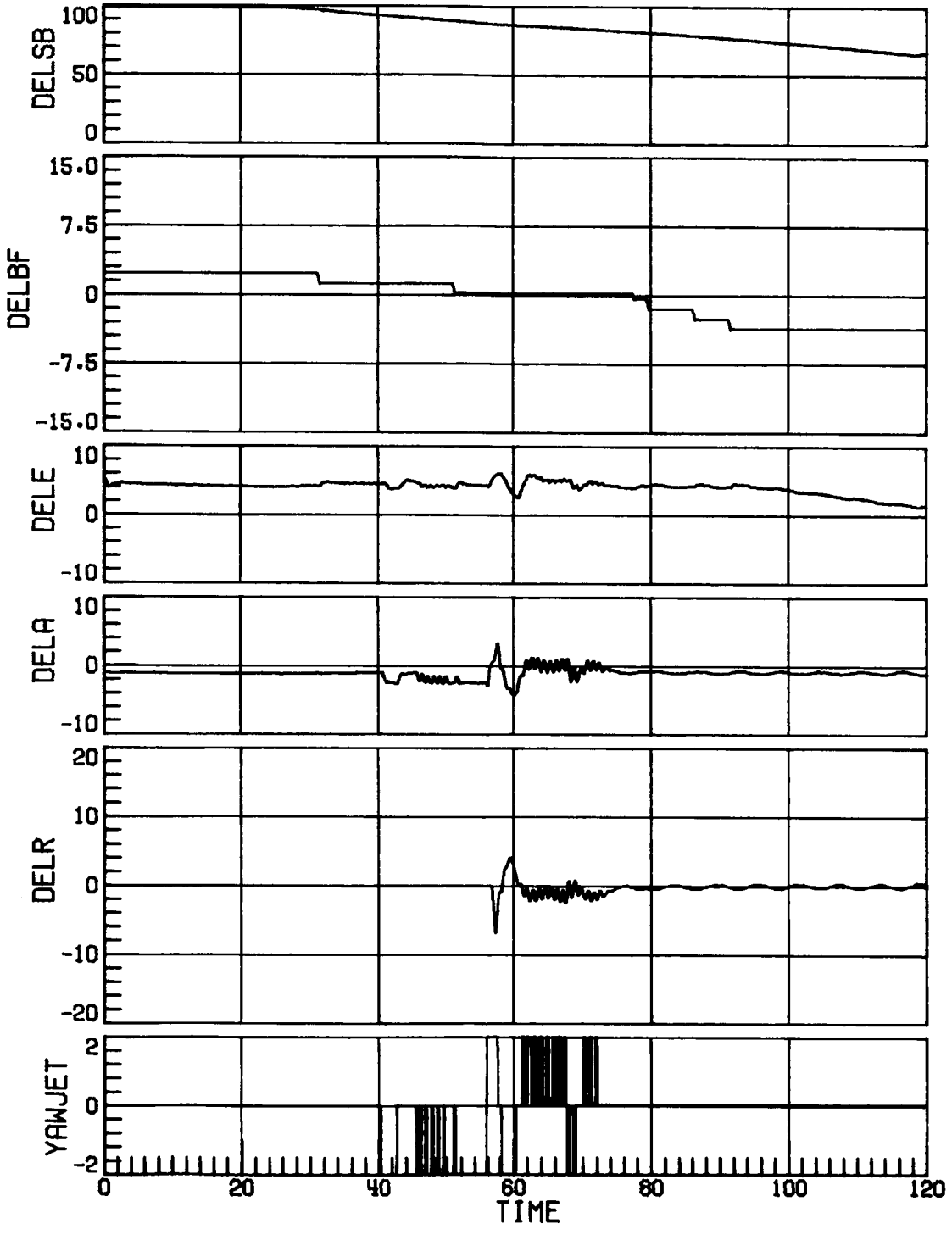

(a) Concluded.
Figure 8. Continued.

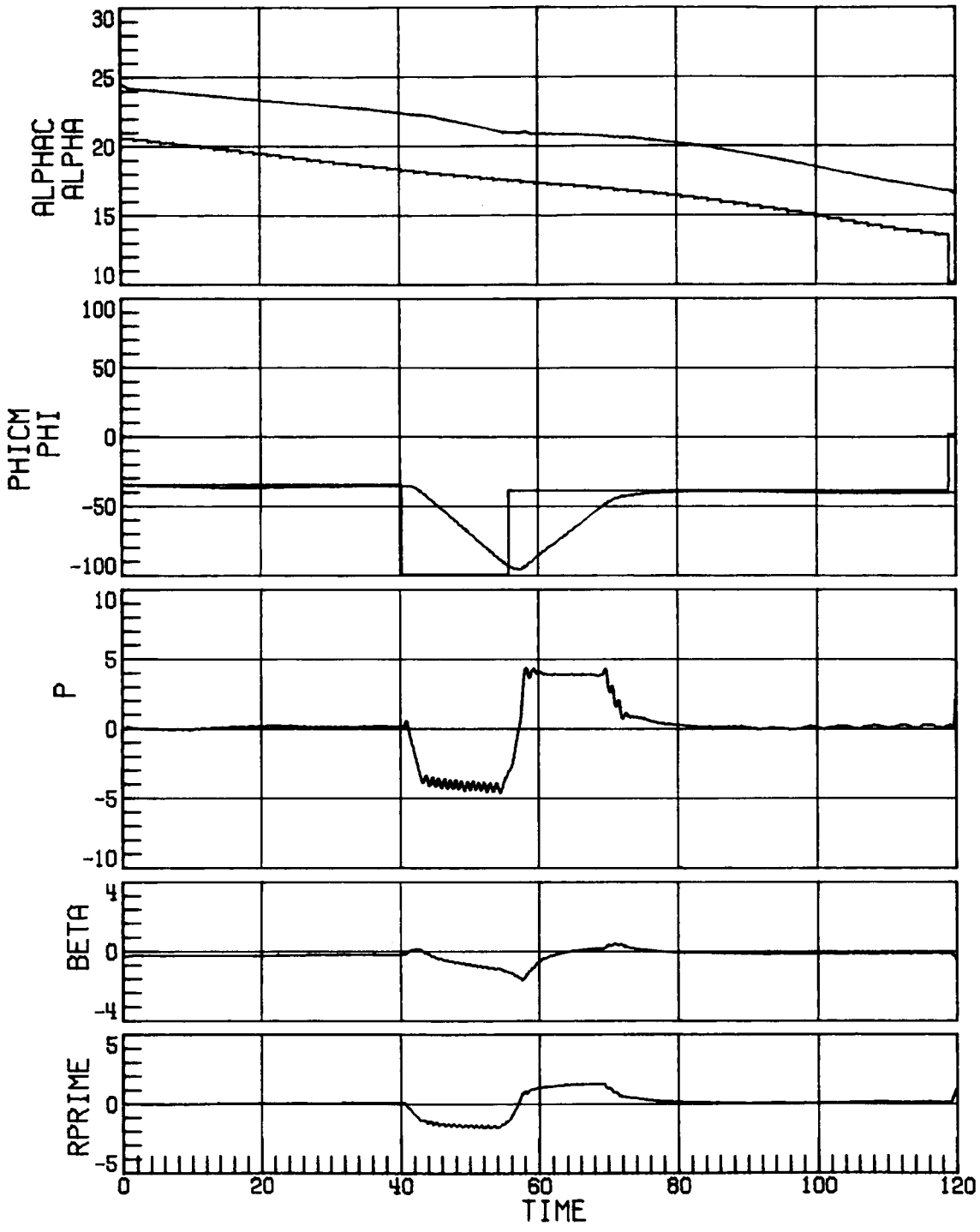

(b) Case 14.
Figure 8. Continued.

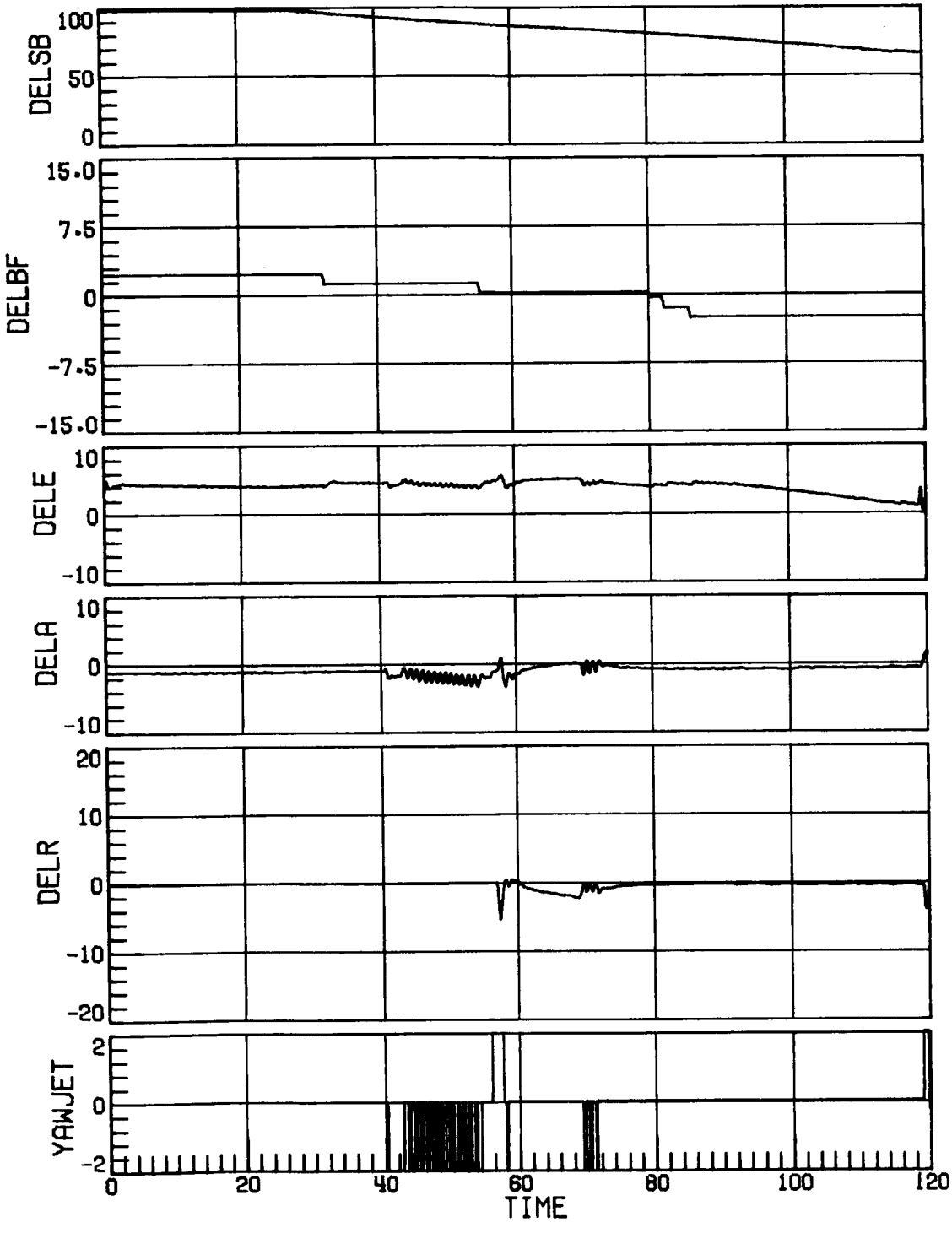

(b) Concluded.
Figure 8. Concluded.

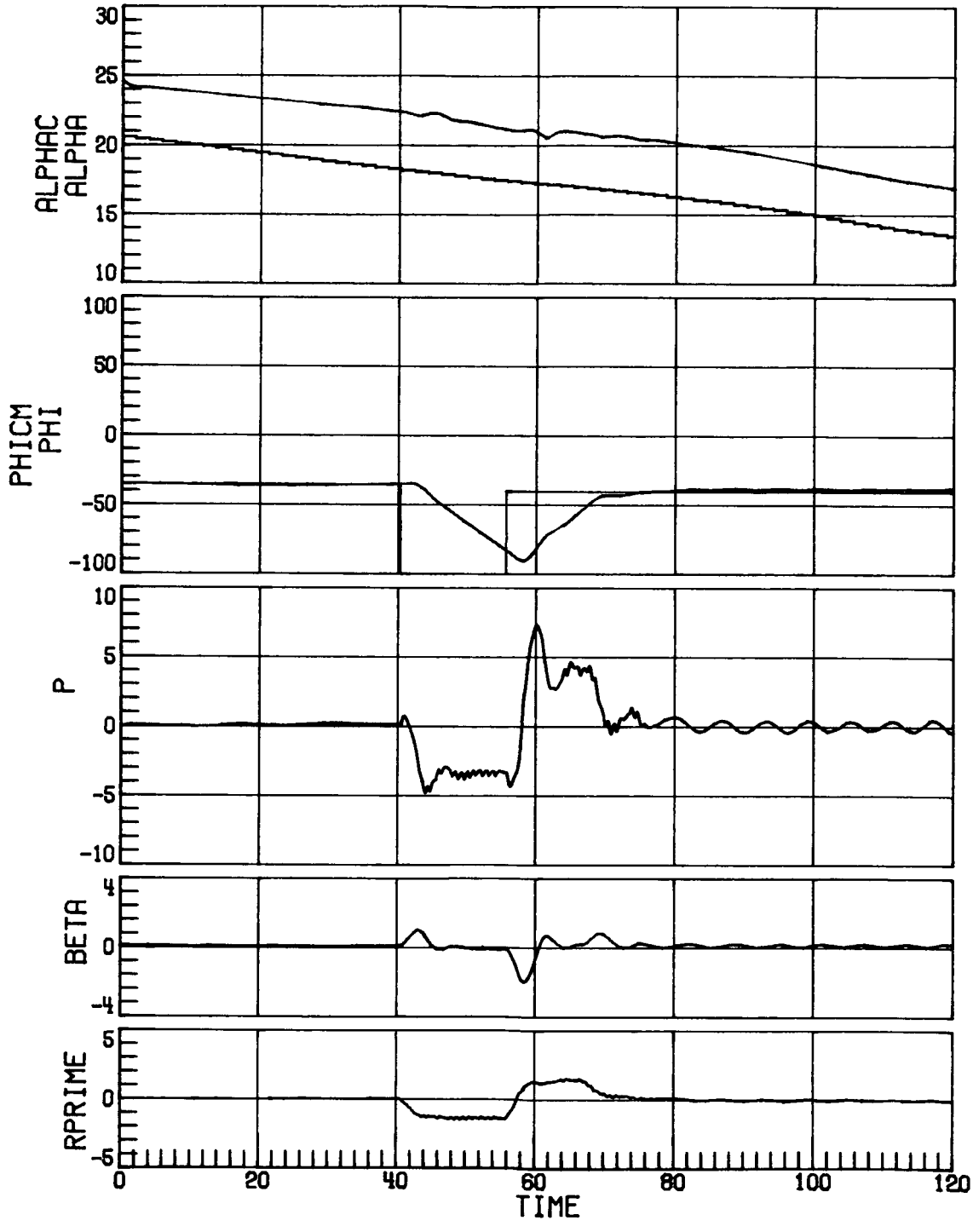

(a) RCS uncertainty set 1.

Figure 9. Time-history response for case 3 at Mach 4.6 with indicated α 4° low and increased rudder effectiveness. Time in seconds.

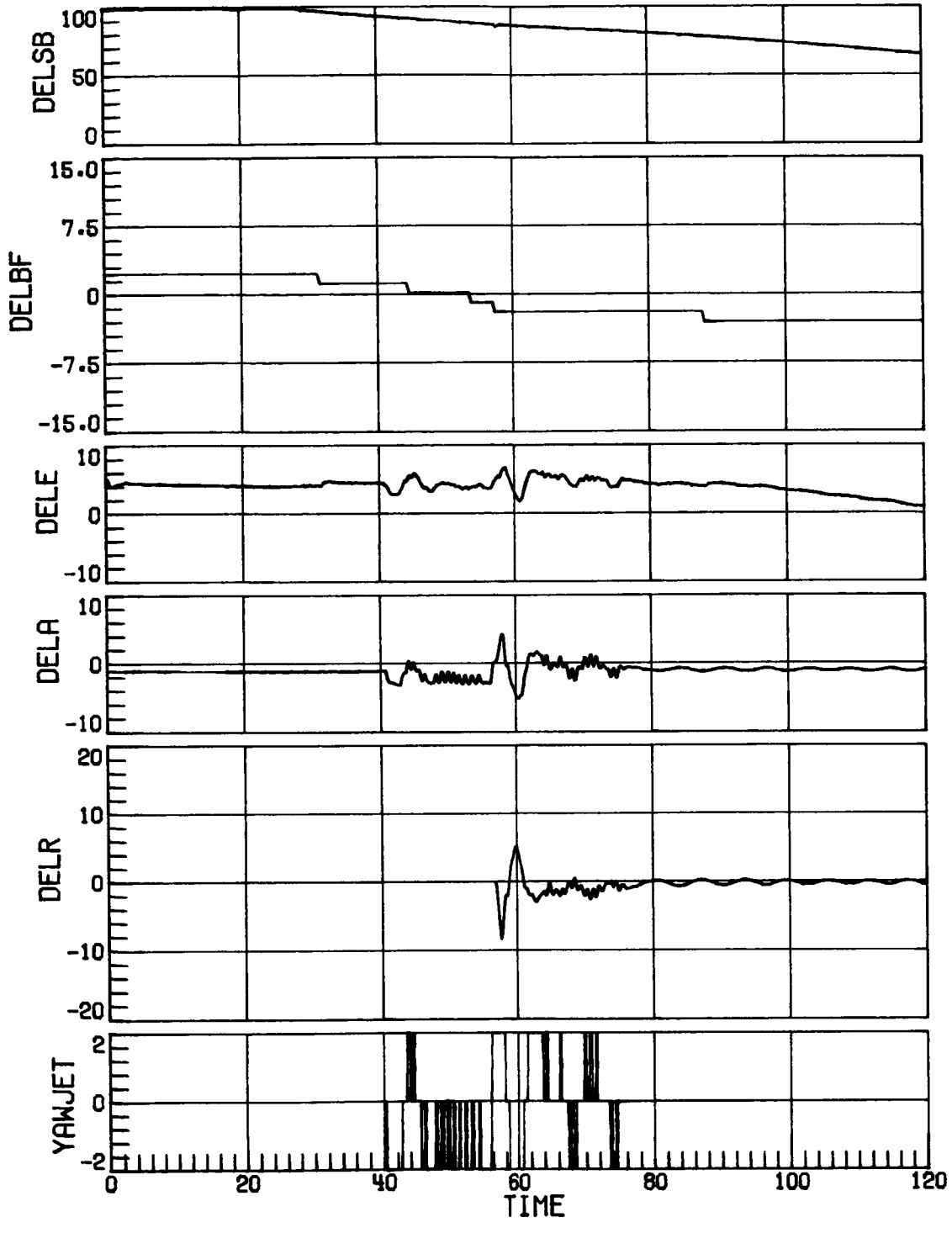

(a) Concluded.
Figure 9. Continued.

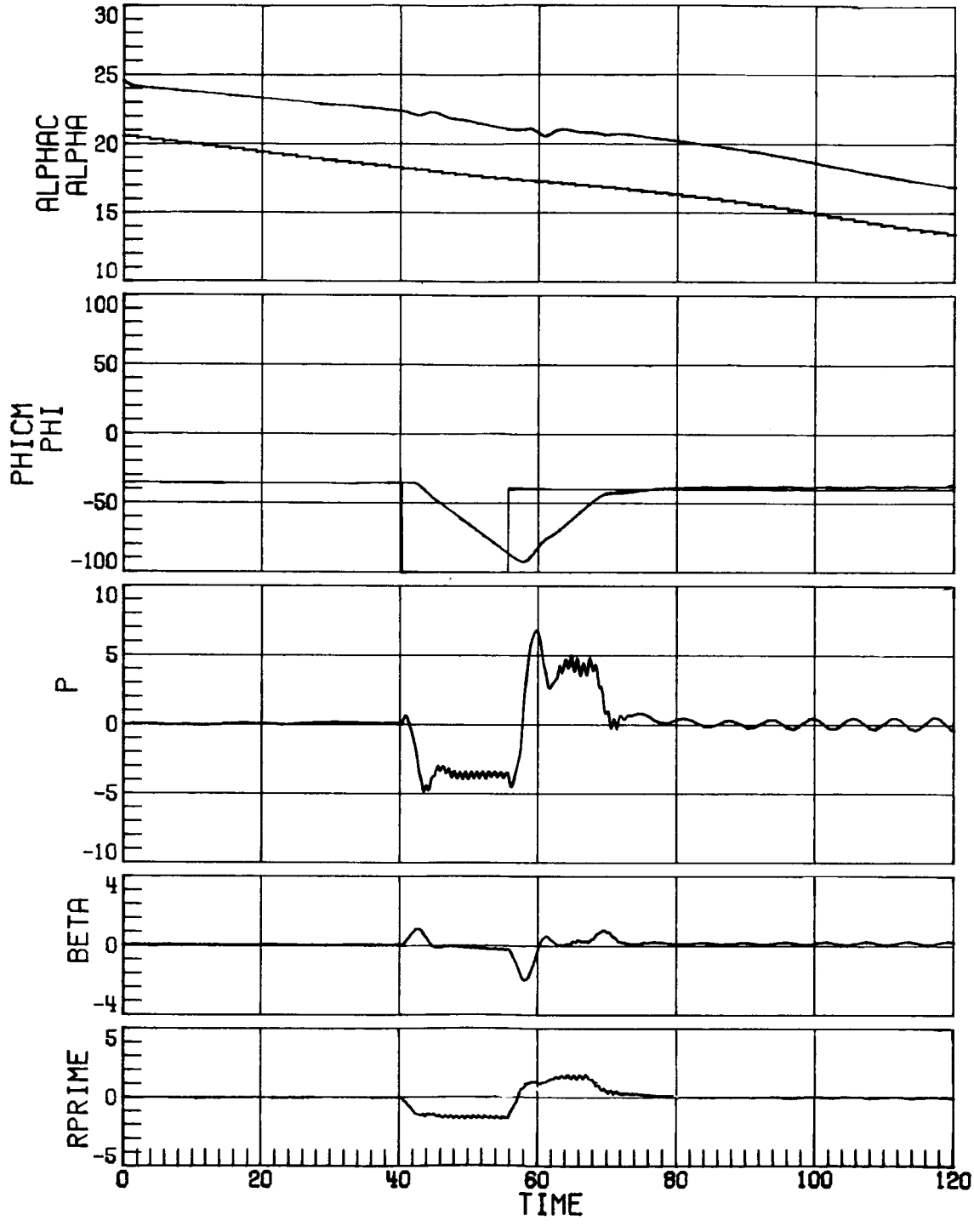

(b) RCS uncertainty set 3.
Figure 9. Continued.

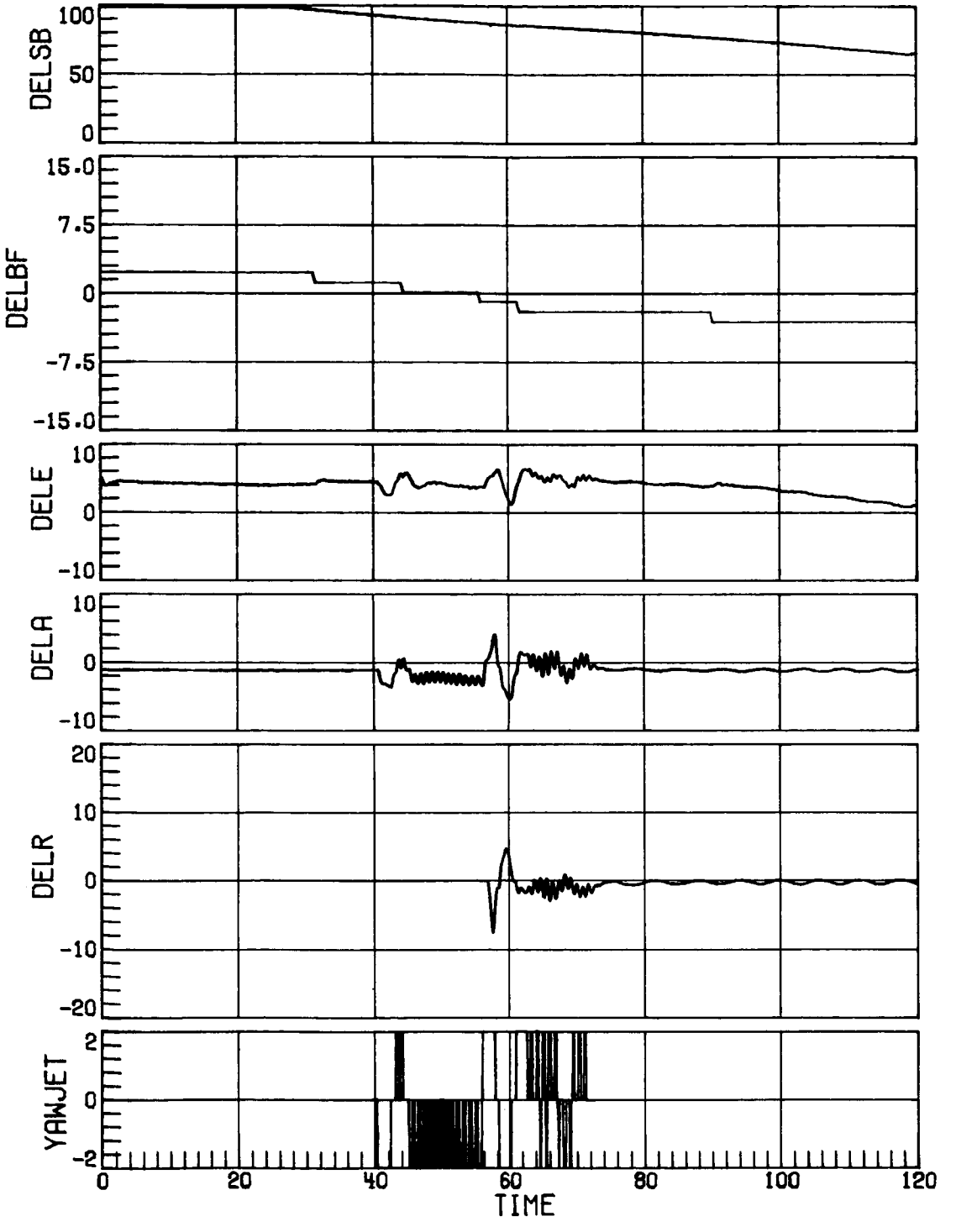

(b) Concluded.
Figure 9. Concluded.

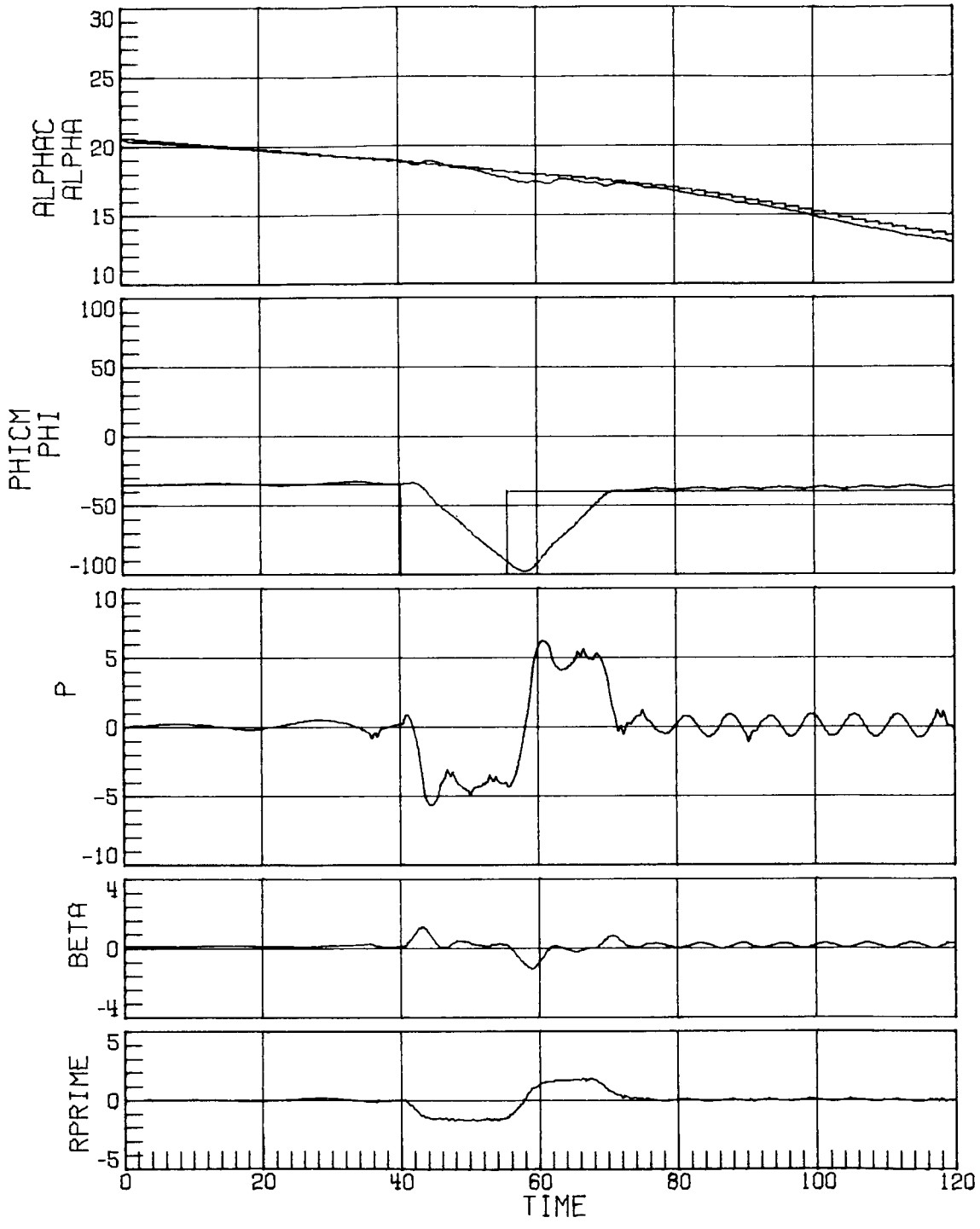

(a) Case 3; nominal α; RCS uncertainty set 1.

Figure 10. Time-history response at Mach 4.6 with increased rudder effectiveness. Time in seconds.

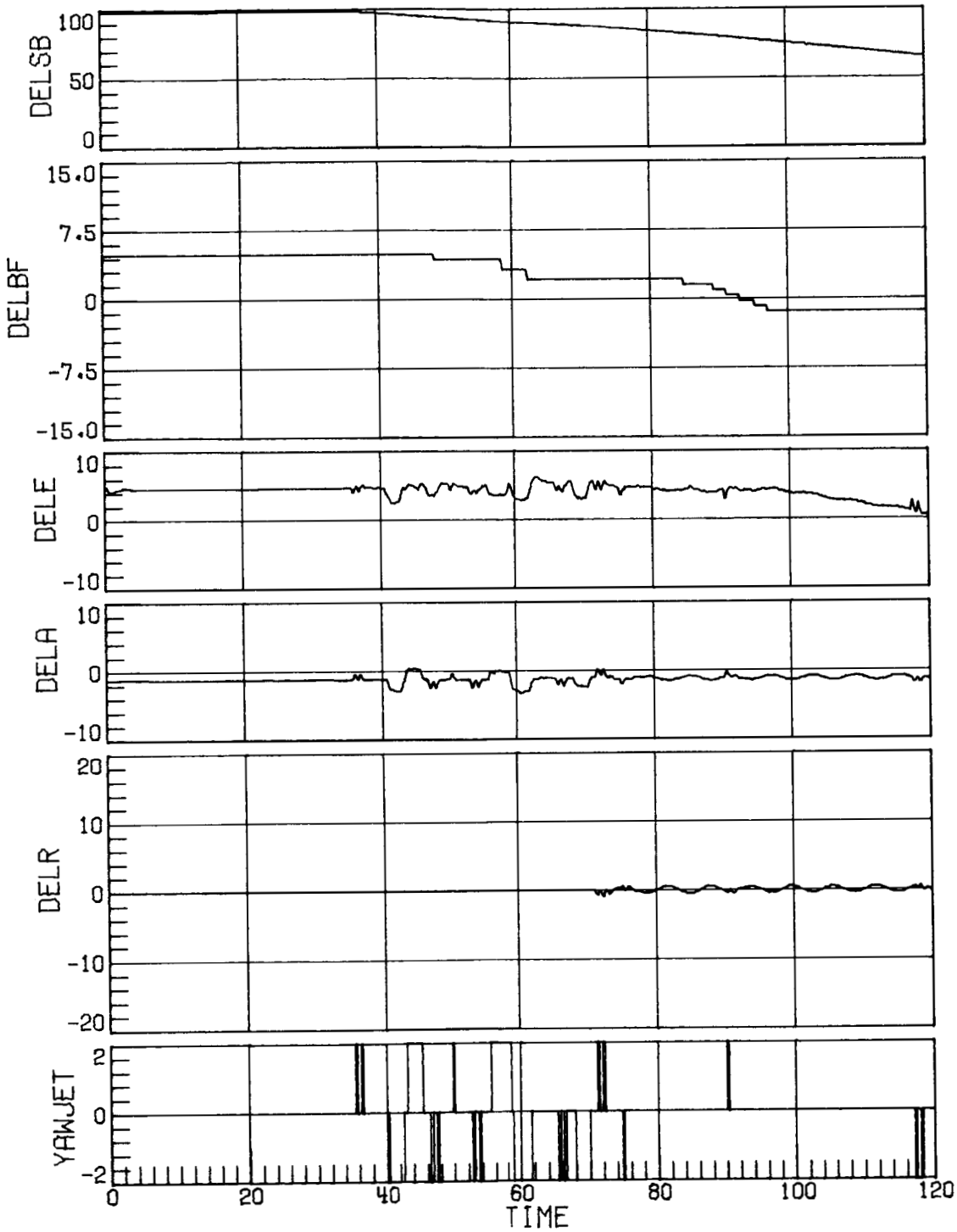

(a) Concluded.
Figure 10. Continued.

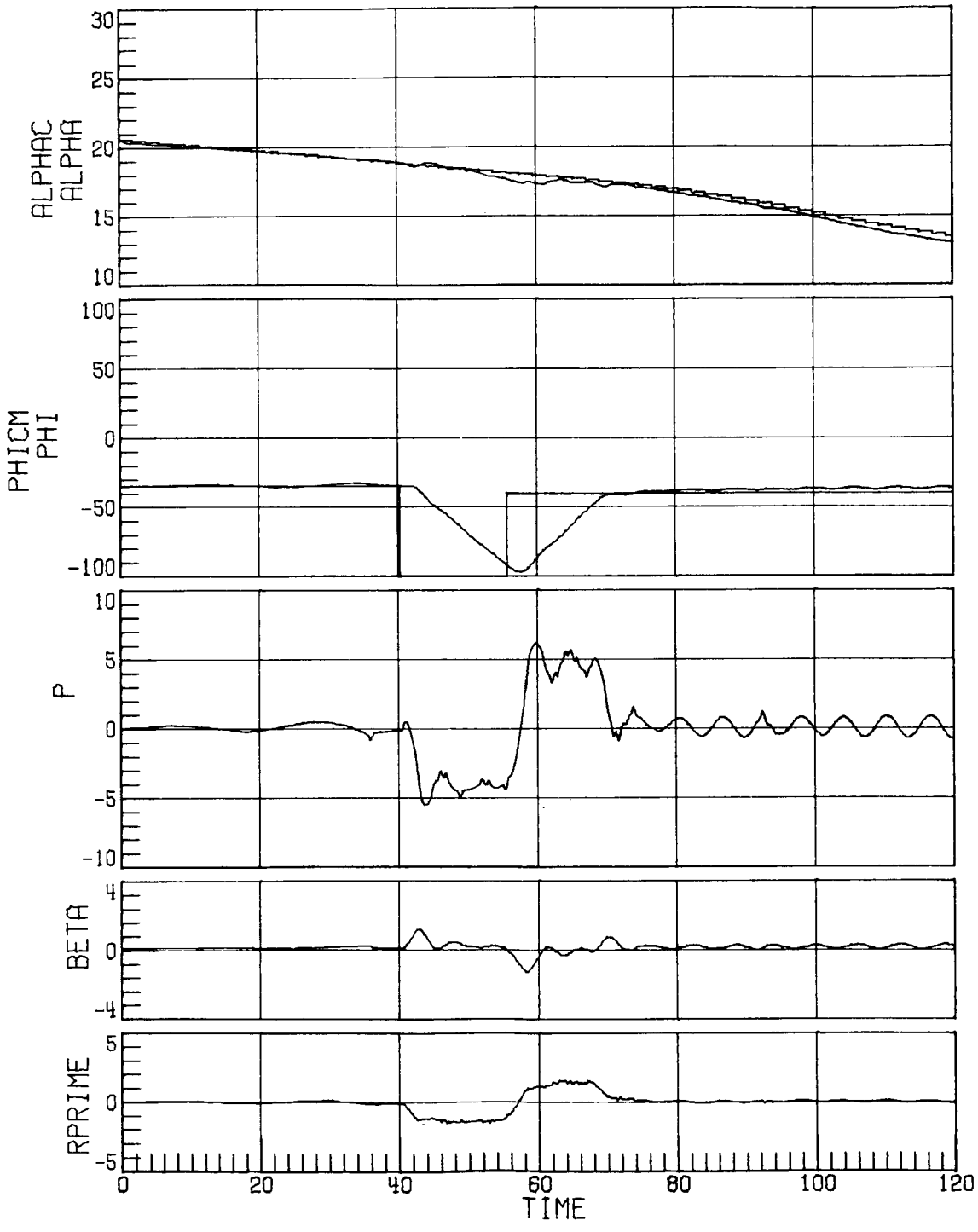

(b) Case 3; nominal α; RCS uncertainty set 3.
Figure 10. Continued.

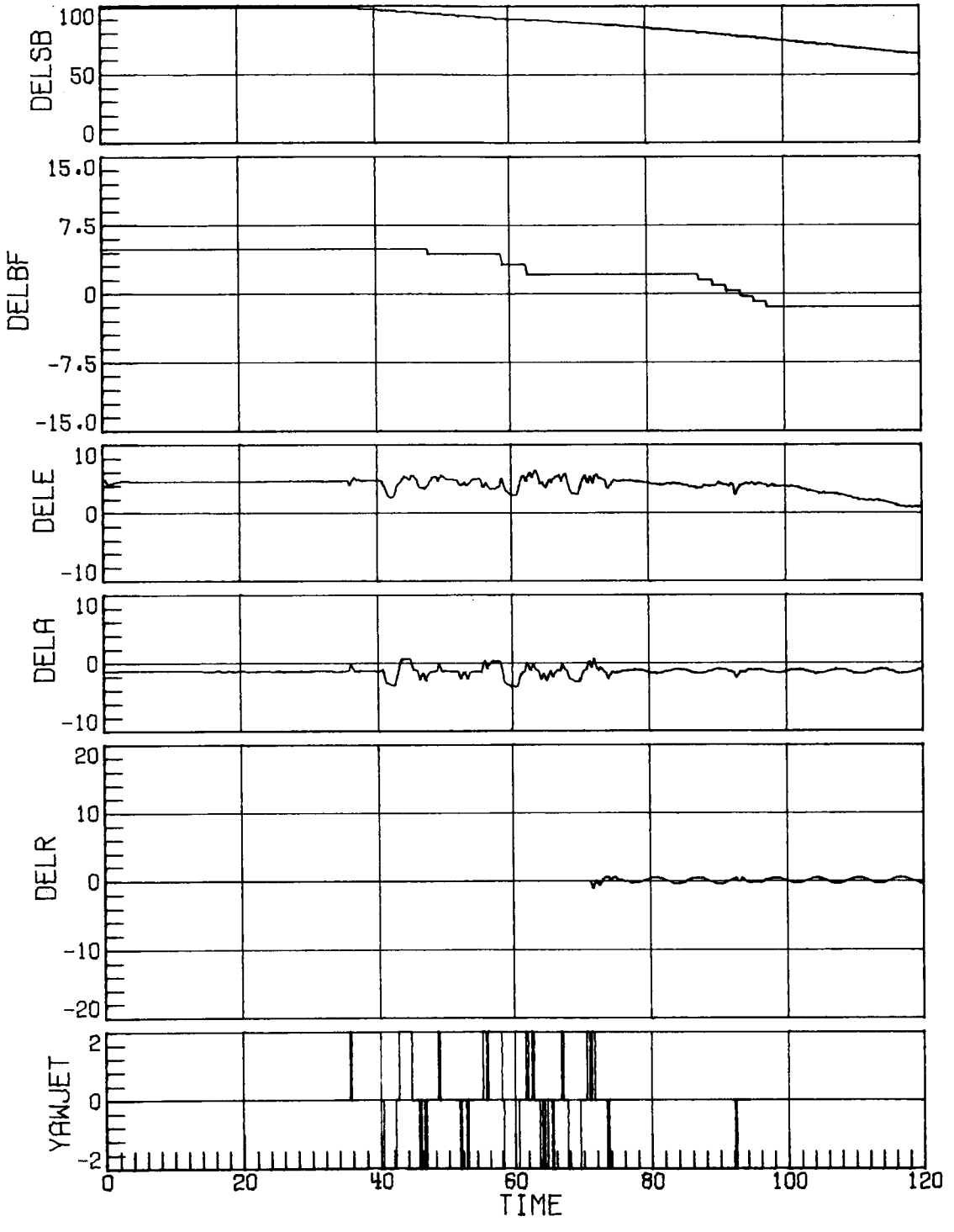

(b) Concluded.
Figure 10. Continued.

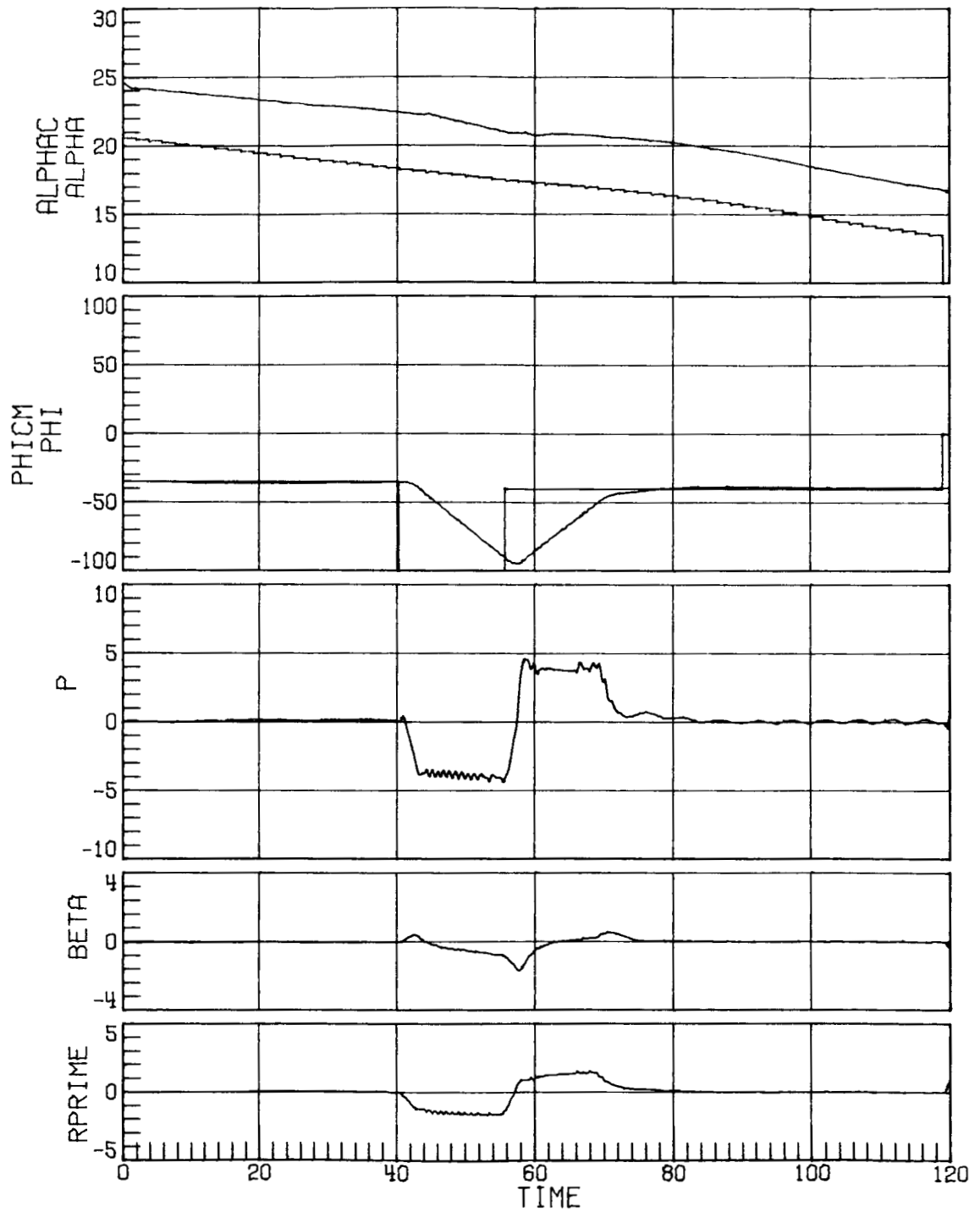

(c) Nominal aerodynamics; indicated α 4° low; nominal RCS.
Figure 10. Continued.

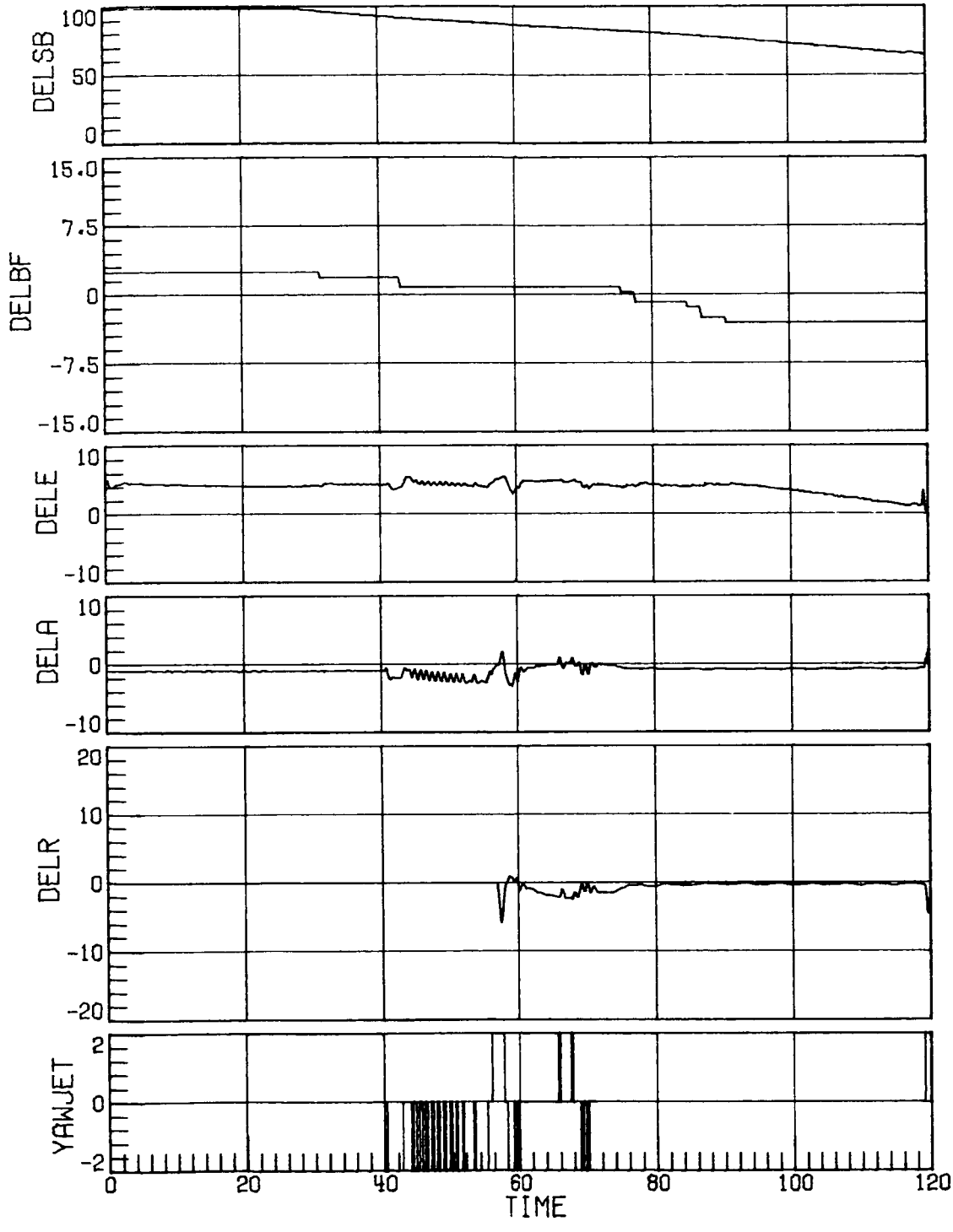

(c) Concluded.
Figure 10. Concluded.

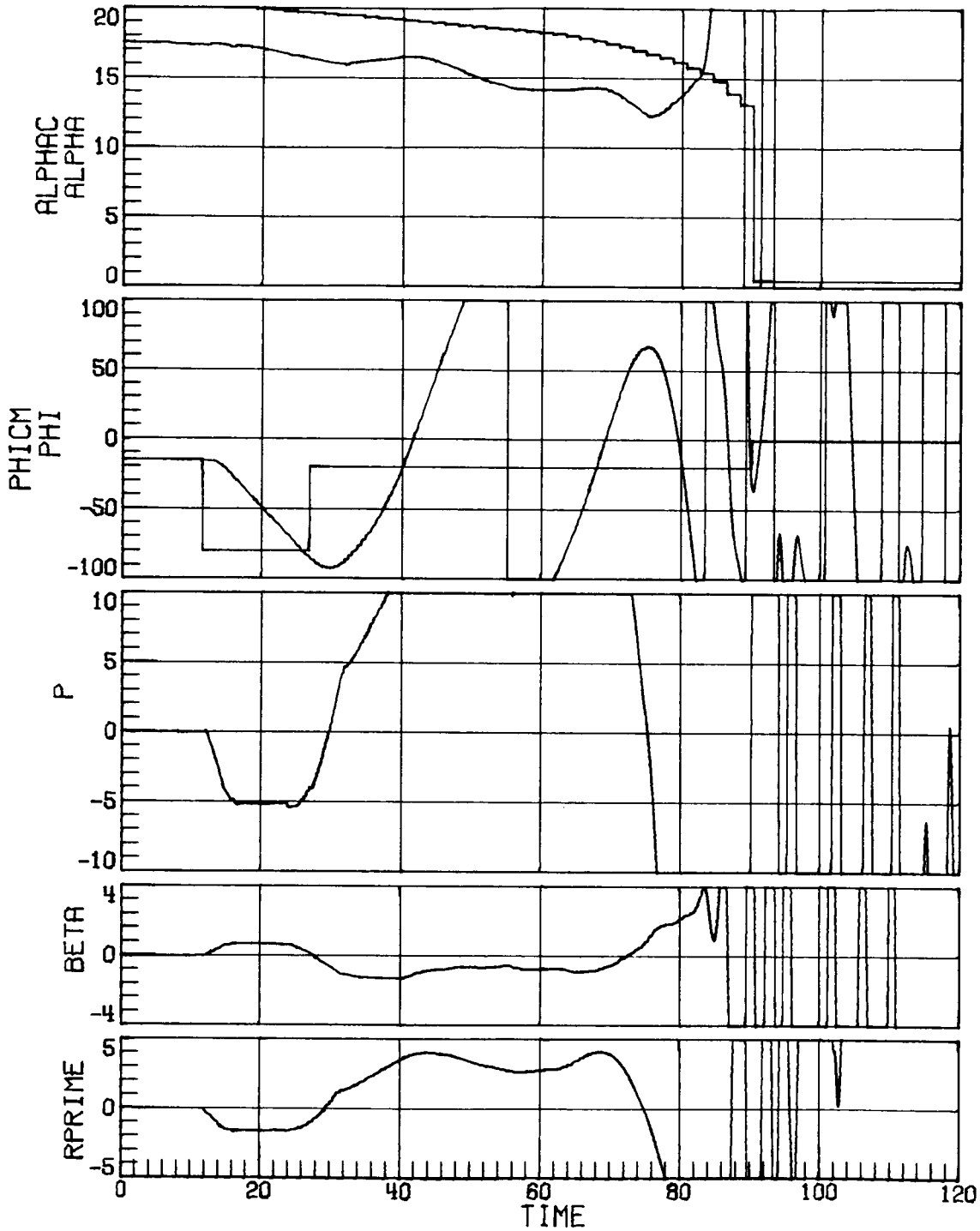

(a) Without N_Y feedback modification; indicated α 3° high.

Figure 11. Time-history response for case 11 at Mach 4.6 with decreased rudder effectiveness, RCS uncertainty set 2, decreased pitching moment, and decreased side force due to β. Time in seconds.

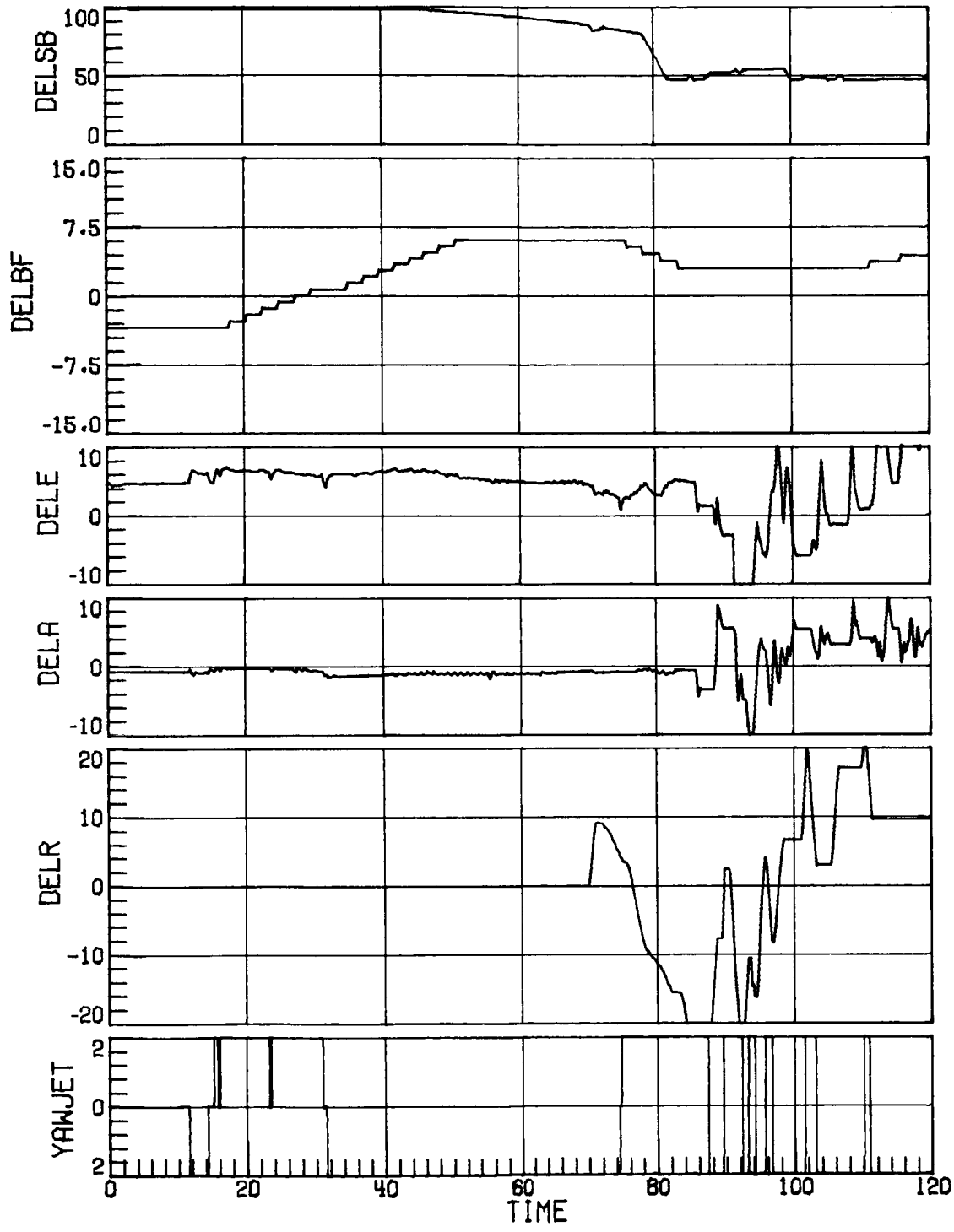

(a) Concluded.
Figure 11. Continued.

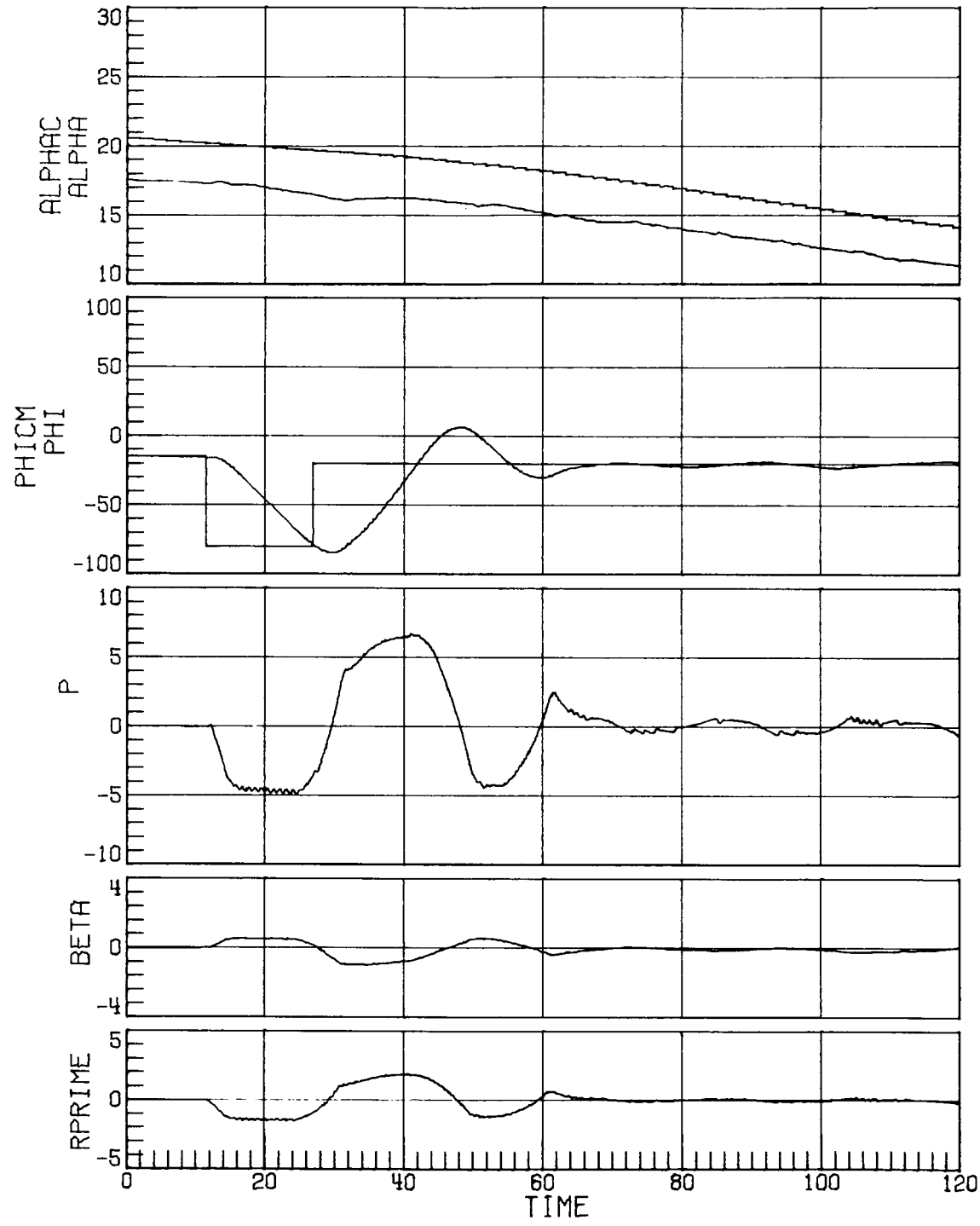

(b) With N_Y feedback modification; indicated α 3° high.
Figure 11. Continued.

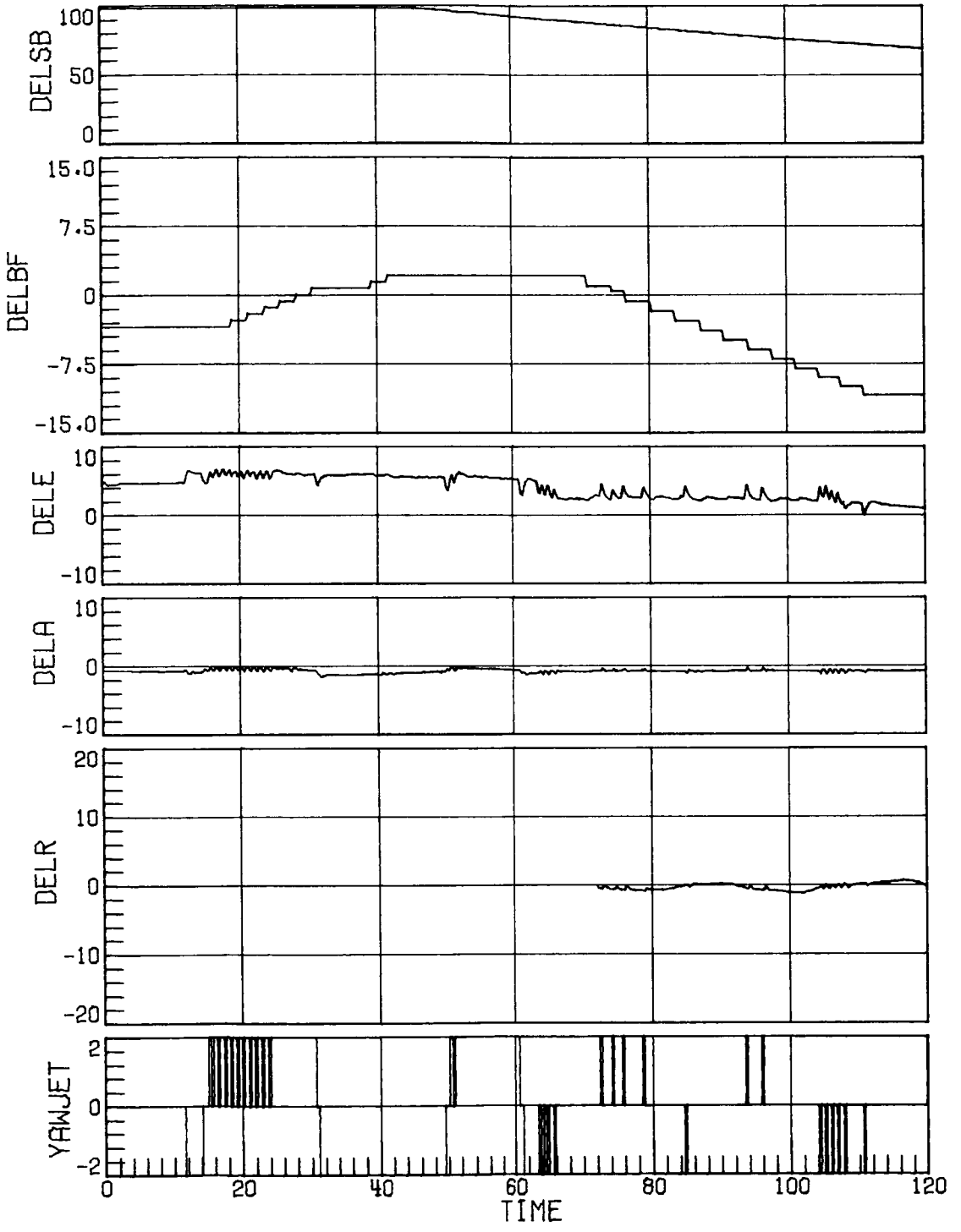

(b) Concluded.
Figure 11. Concluded.

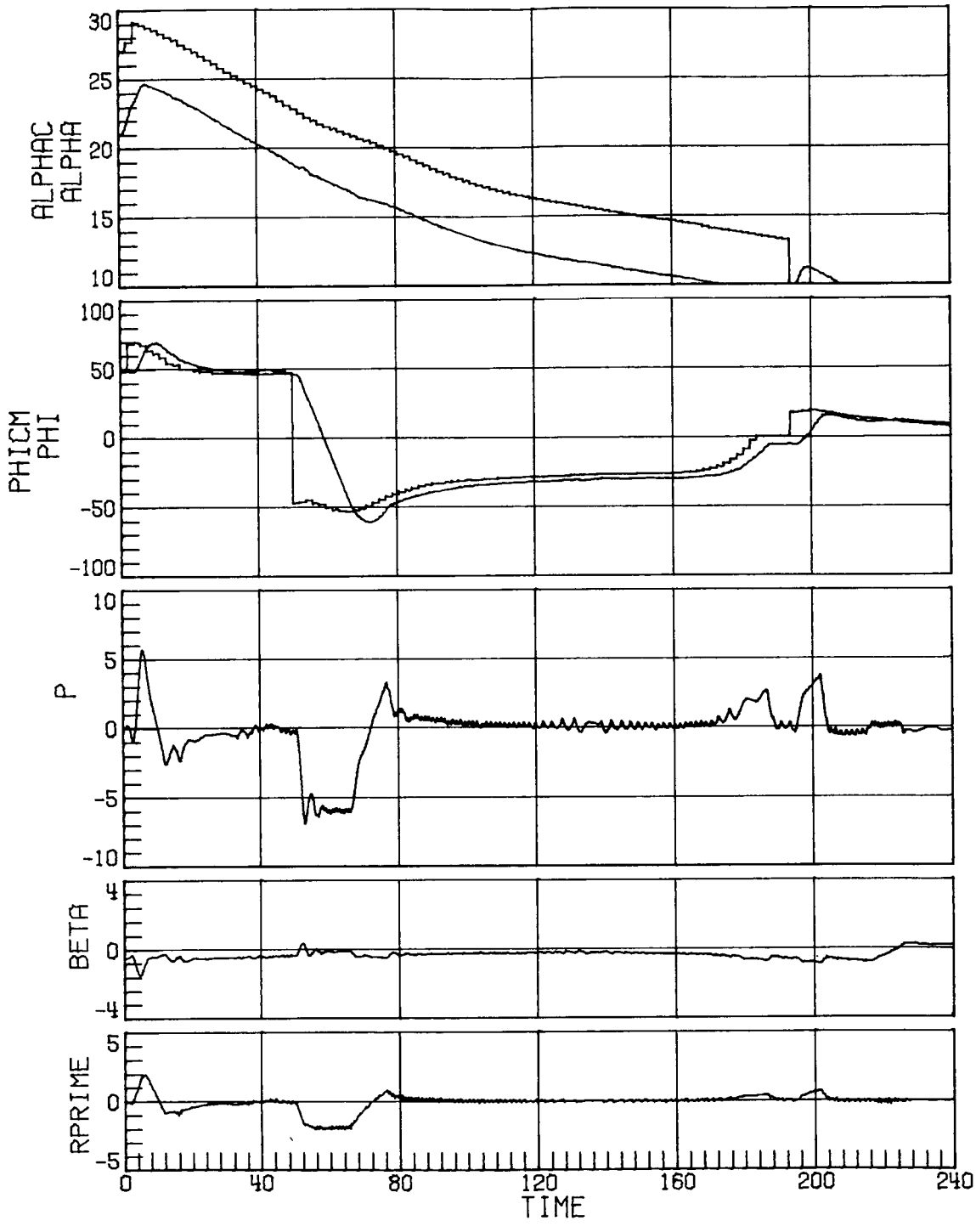

(a) Case 6.

Figure 12. Time-history response for Mach decreasing from 6.1 to 1.8 with indicated α 4° high, decreased rudder effectiveness, negative pitch uncertainty, and decreased side force due to β. Time in seconds.

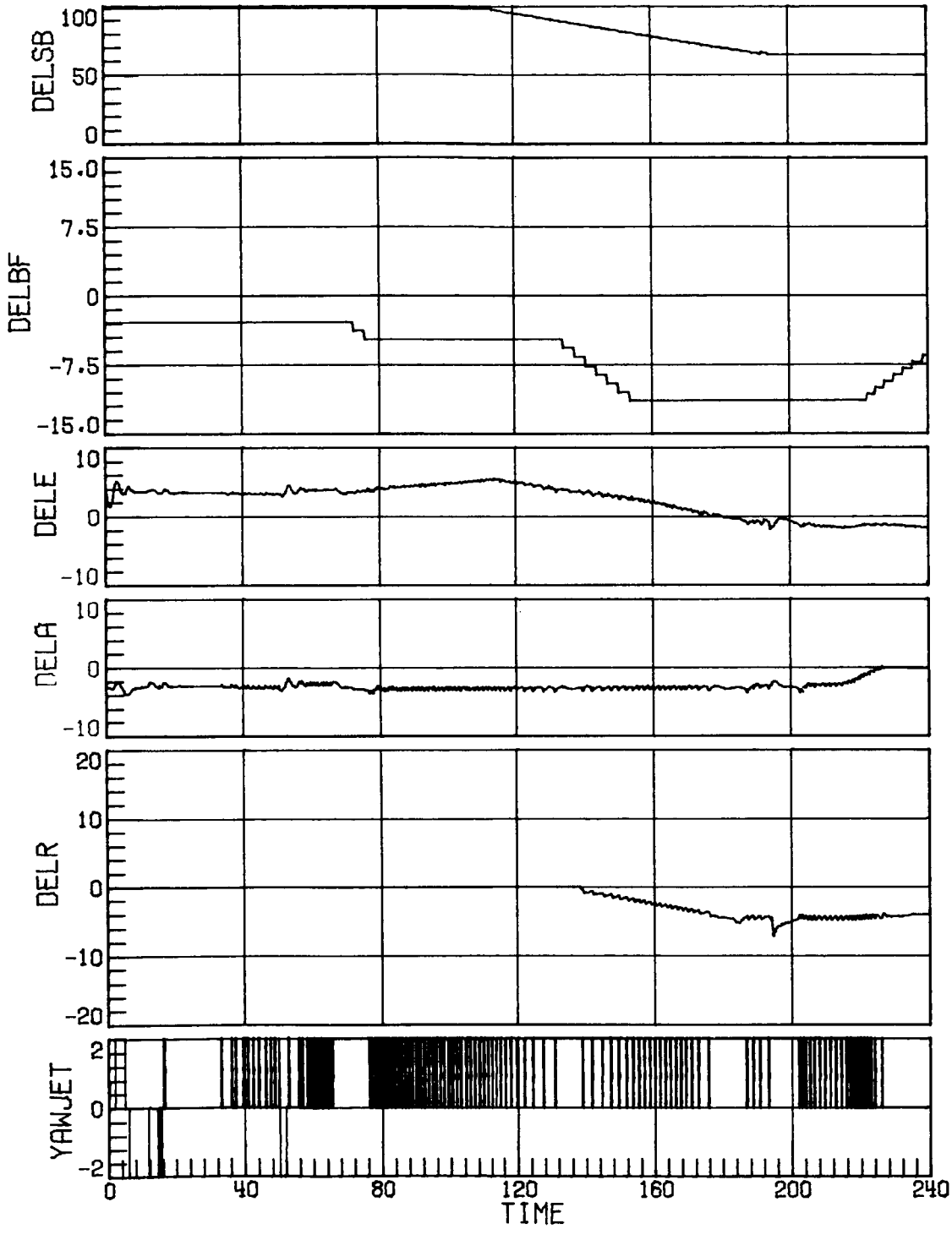

(a) Concluded.
Figure 12. Continued.

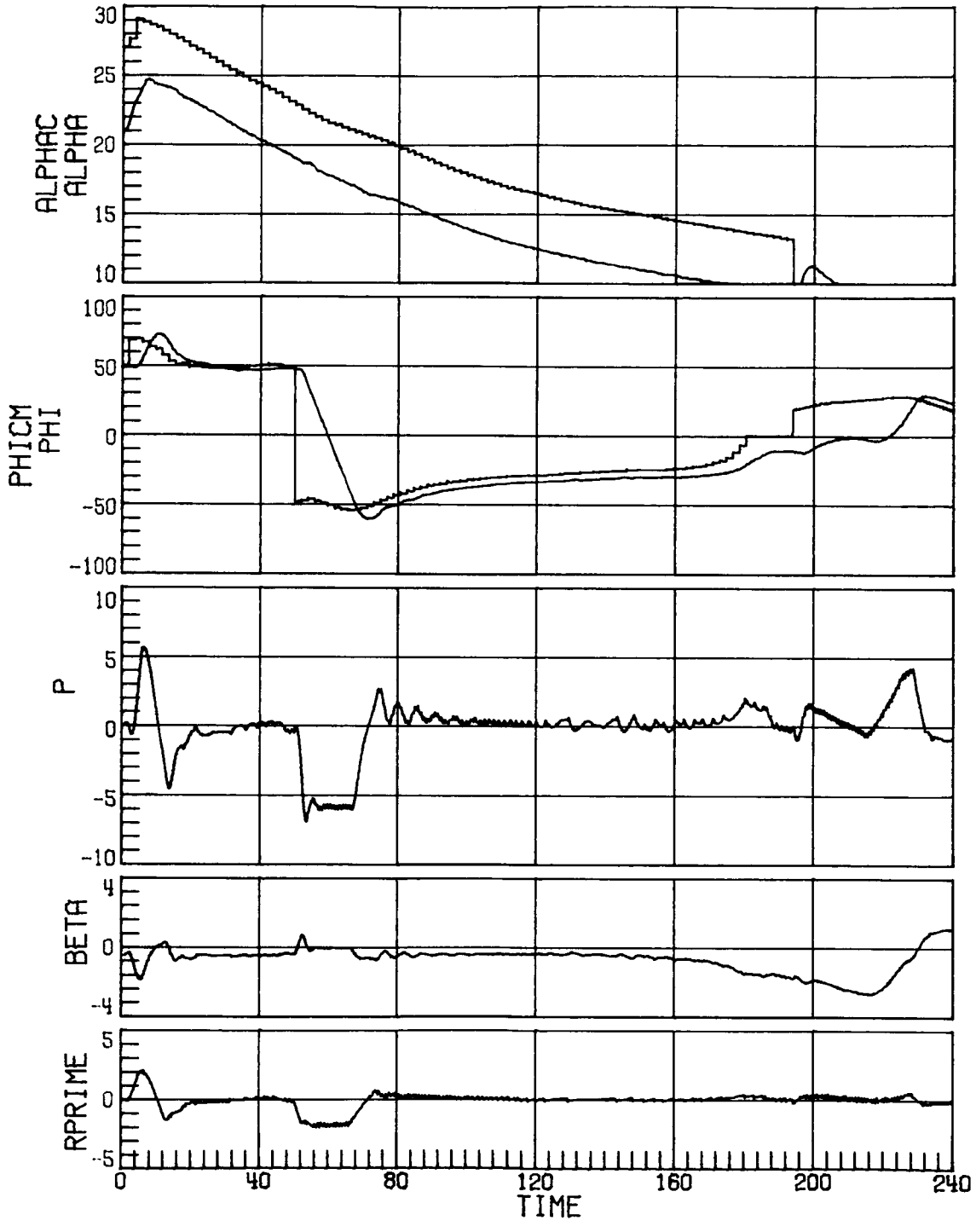

(b) Case 8.
Figure 12. Continued.

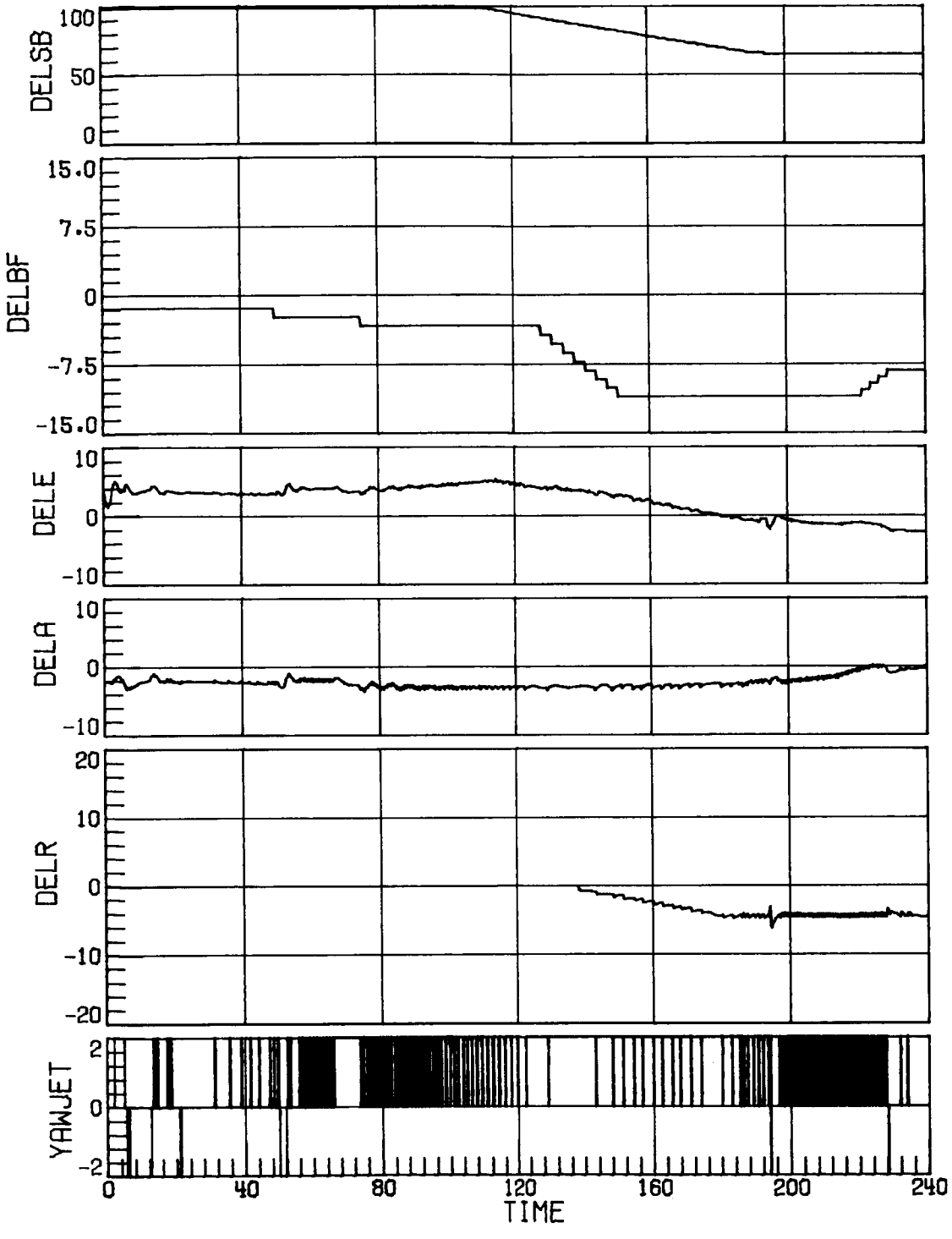

(b) Concluded.
Figure 12. Concluded.

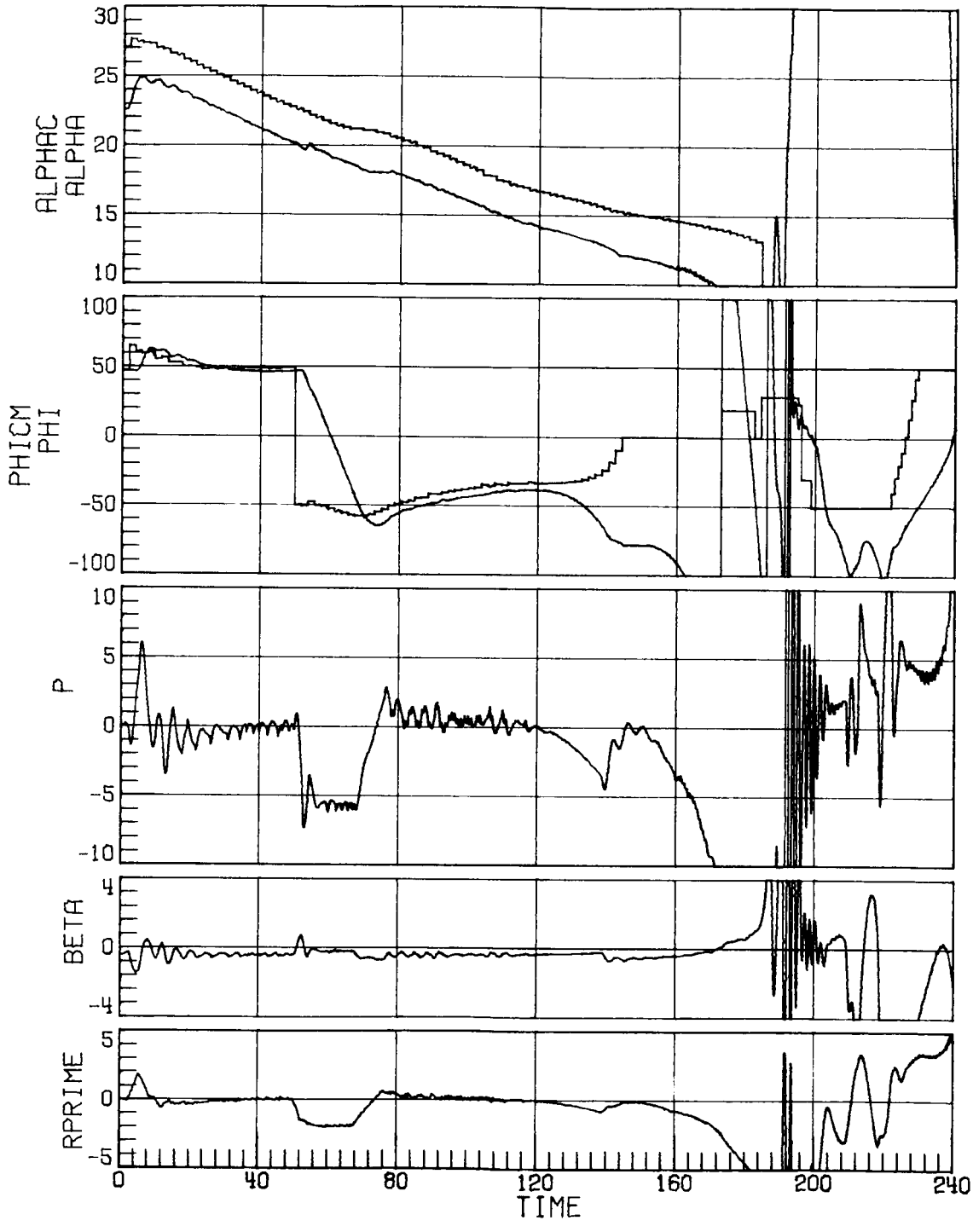

(a) Case 6; indicated α 2.5° high; two yaw jets.

Figure 13. Time-history response for Mach decreasing from 6.1 to 1.8 with RCS uncertainty set 1, decreased rudder effectiveness, negative pitch uncertainties, and decreased side force due to β. Time in seconds.

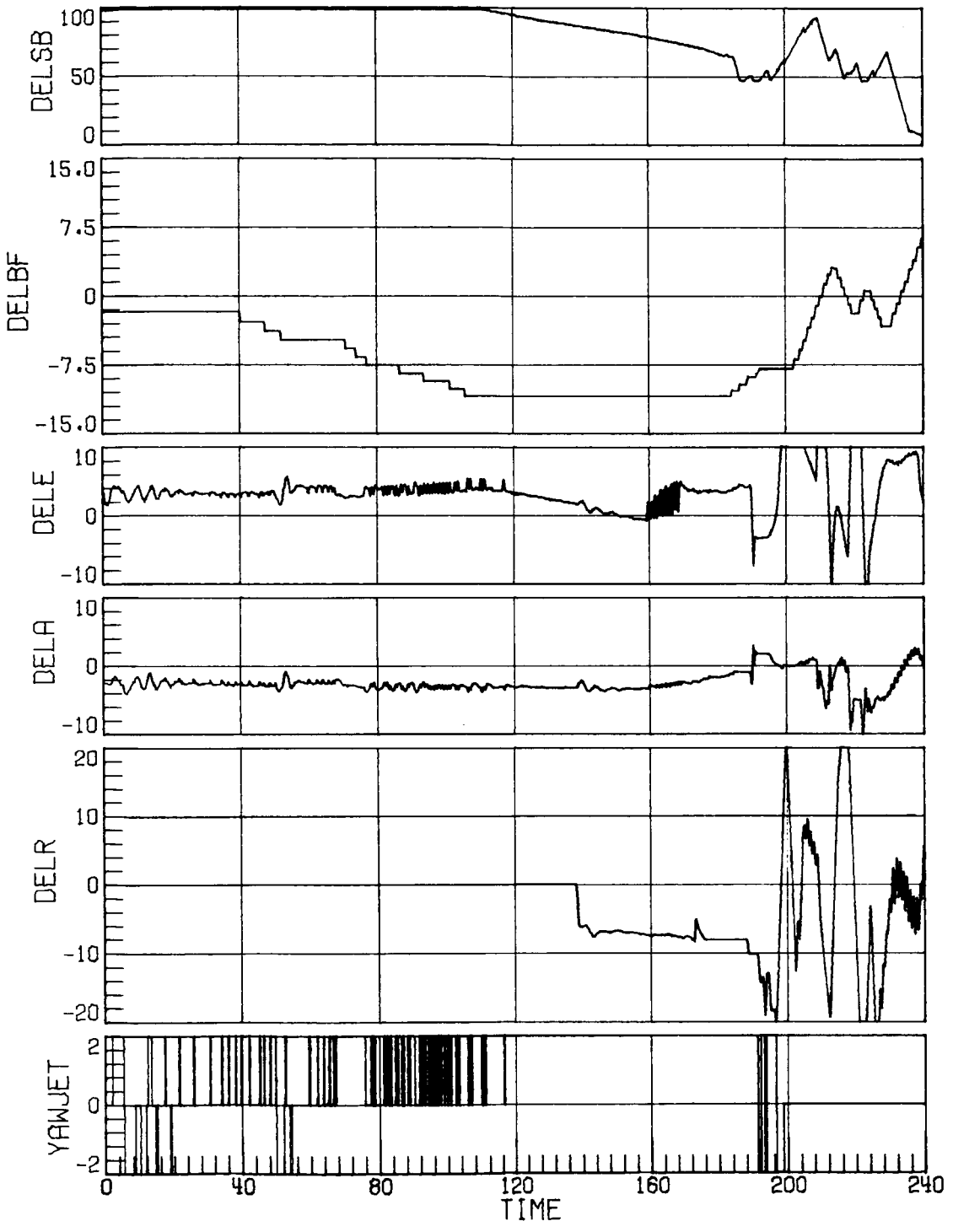

(a) Concluded.
Figure 13. Continued.

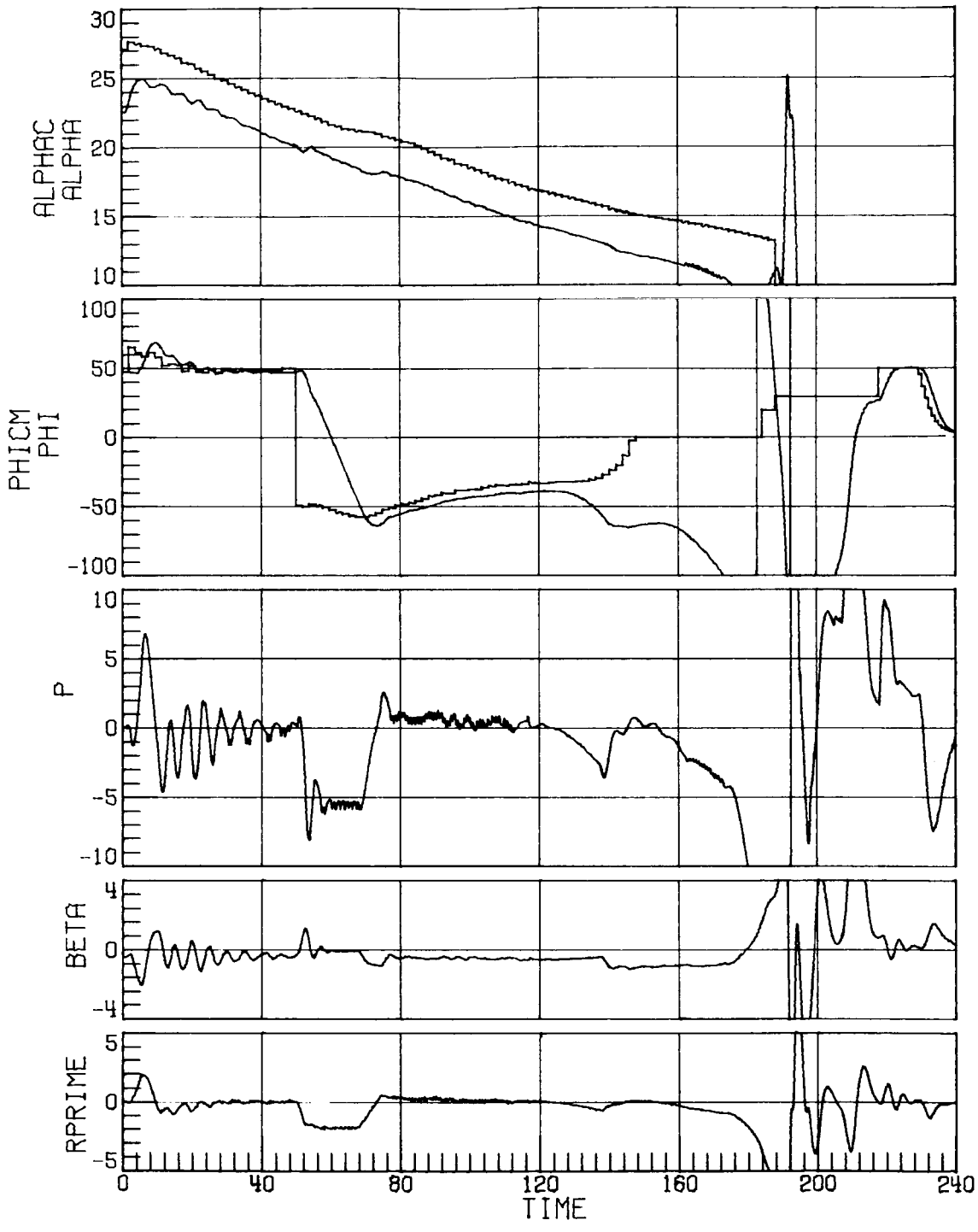

(b) Case 8; indicated α 2.5° high; two yaw jets.
Figure 13. Continued.

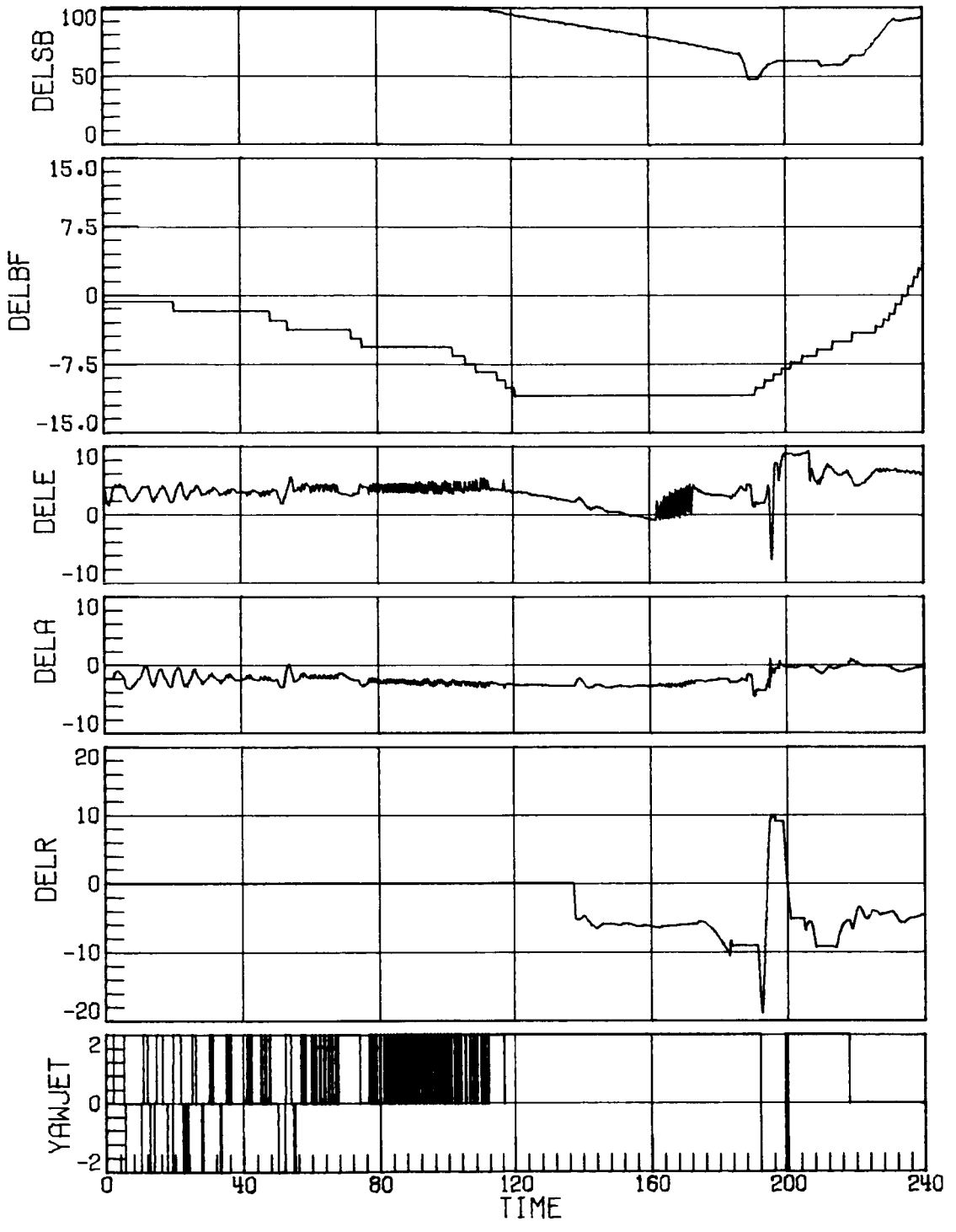

(b) Concluded.
Figure 13. Continued.

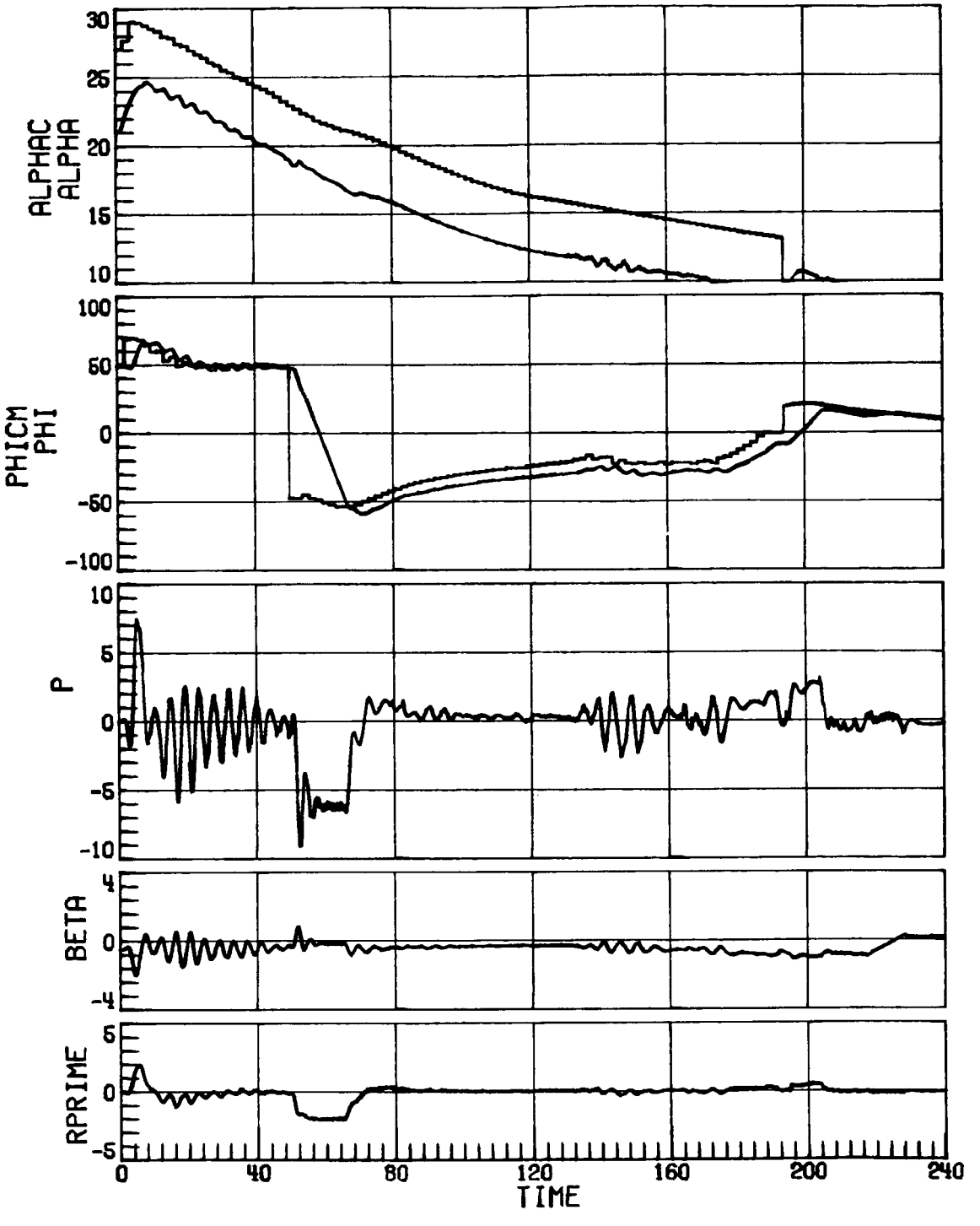

(c) Case 6; indicated α 4° high; four yaw jets.
Figure 13. Continued.

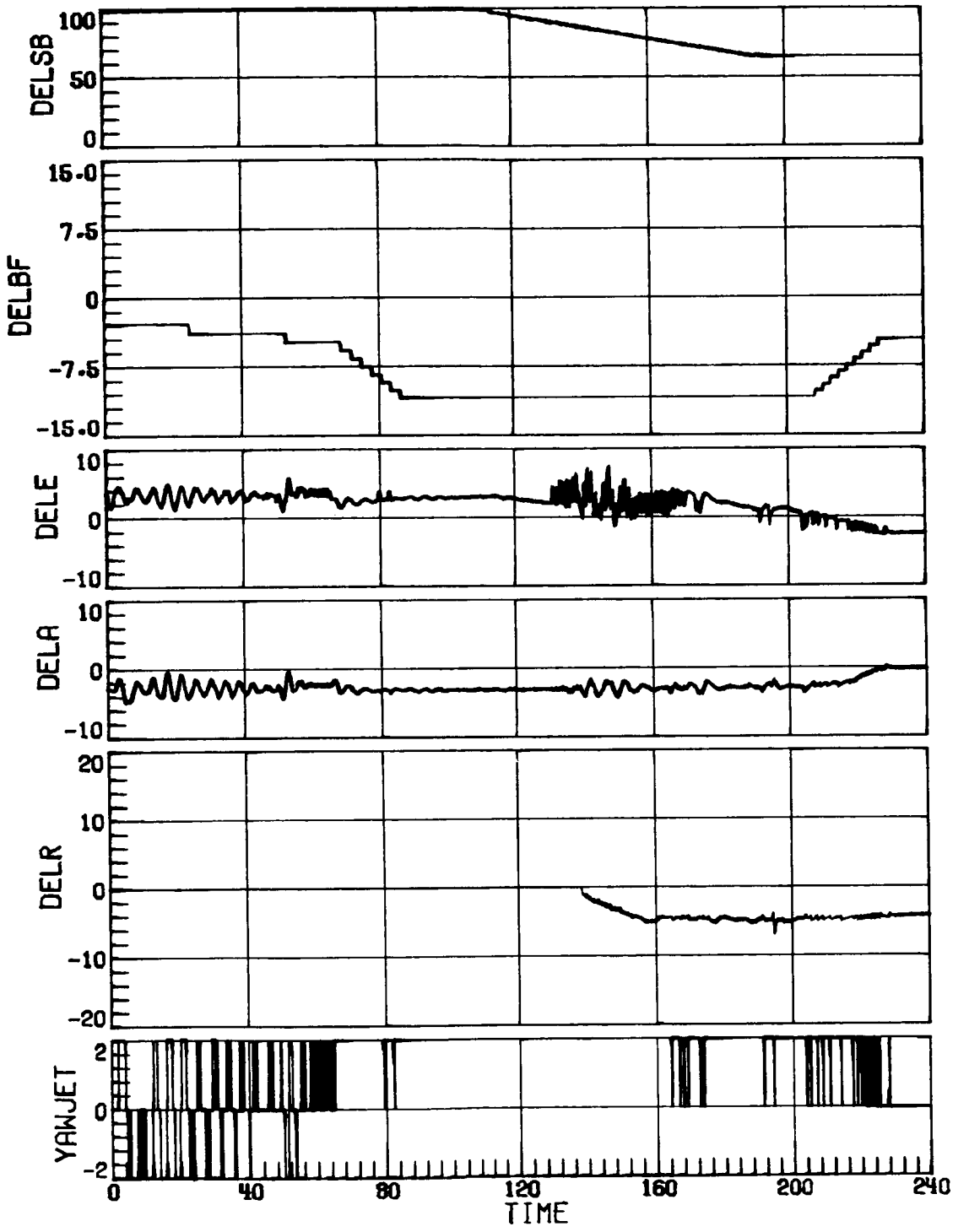

(c) Concluded.
Figure 13. Concluded.

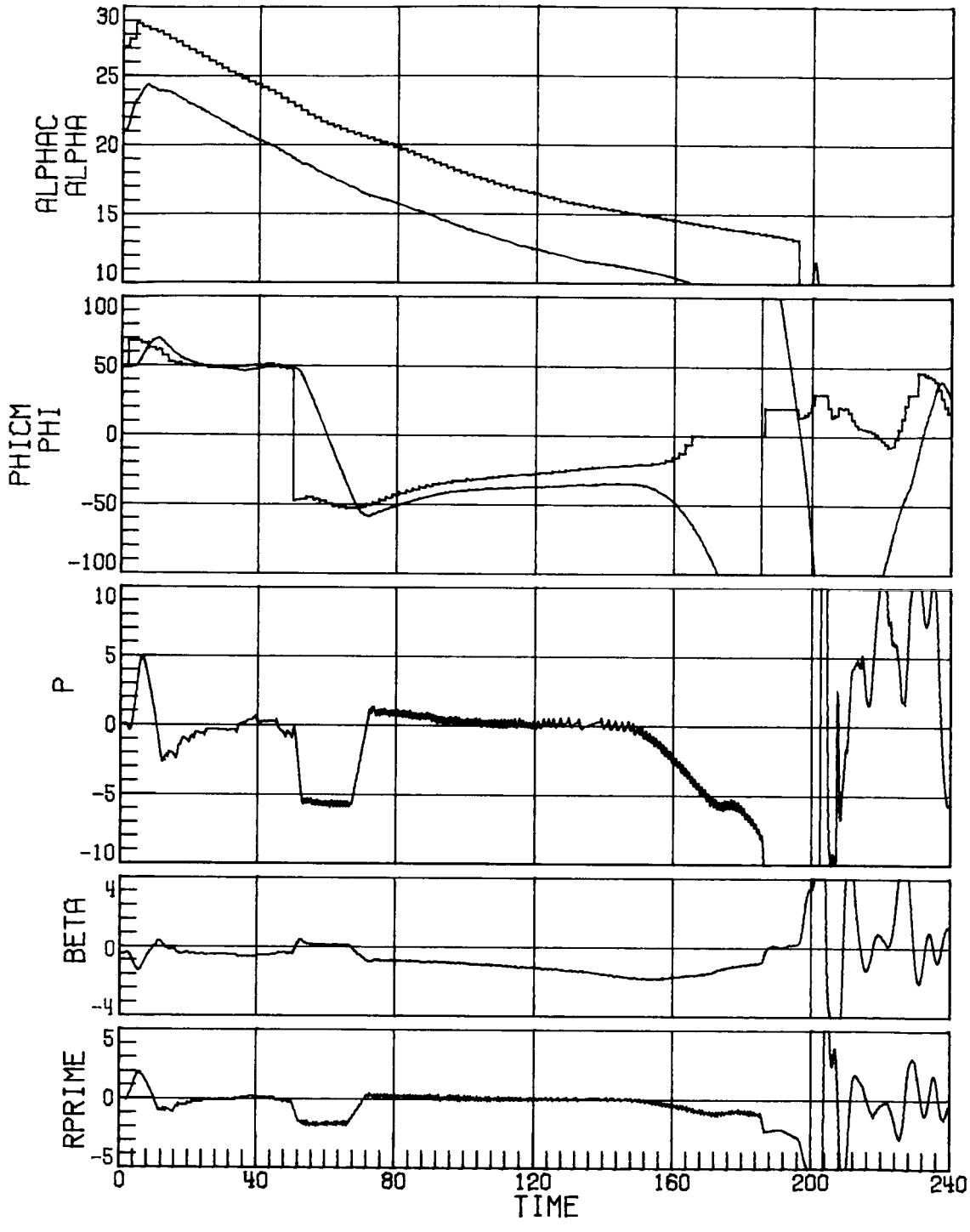

(a) Indicated α 4° high; nominal RCS; two jets.

Figure 14. Time-history response for case 16 for Mach decreasing from 6.1 to 1.8 with decreased rudder effectiveness. Time in seconds.

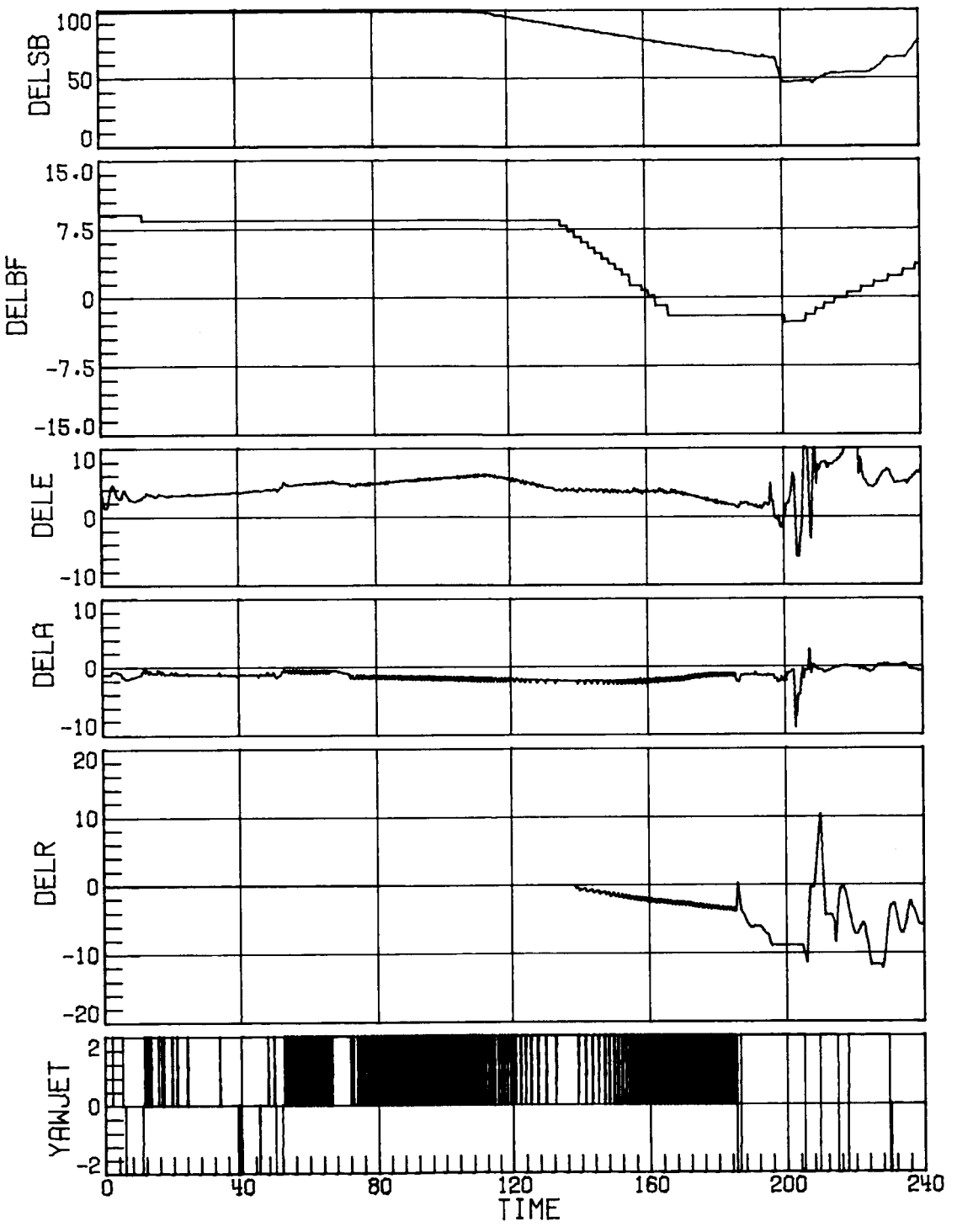

(a) Concluded.
Figure 14. Continued.

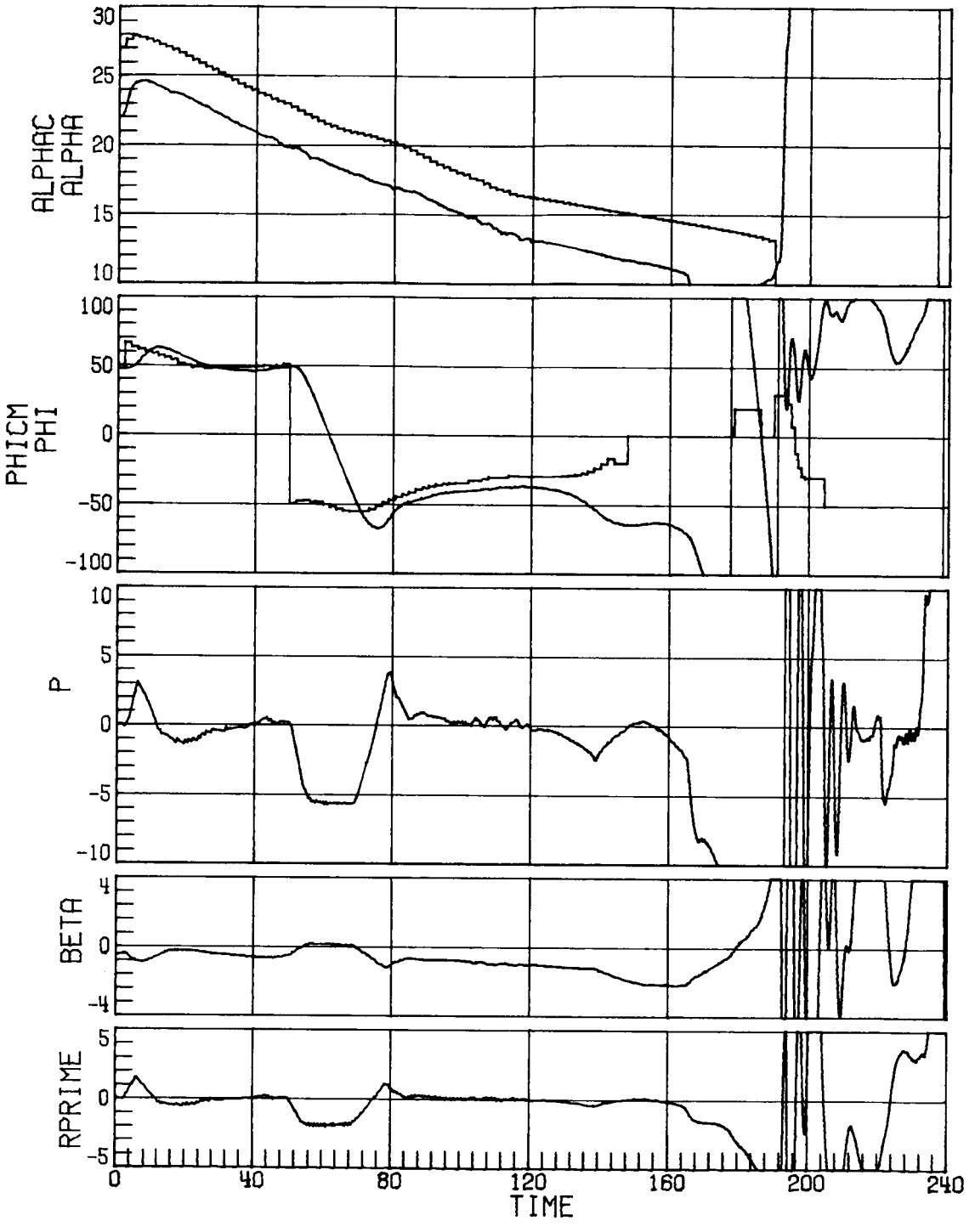

(b) Indicated α 3° high; RCS uncertainty set 2; two jets; negative pitch uncertainty; decreased side force due to β.

Figure 14. Continued.

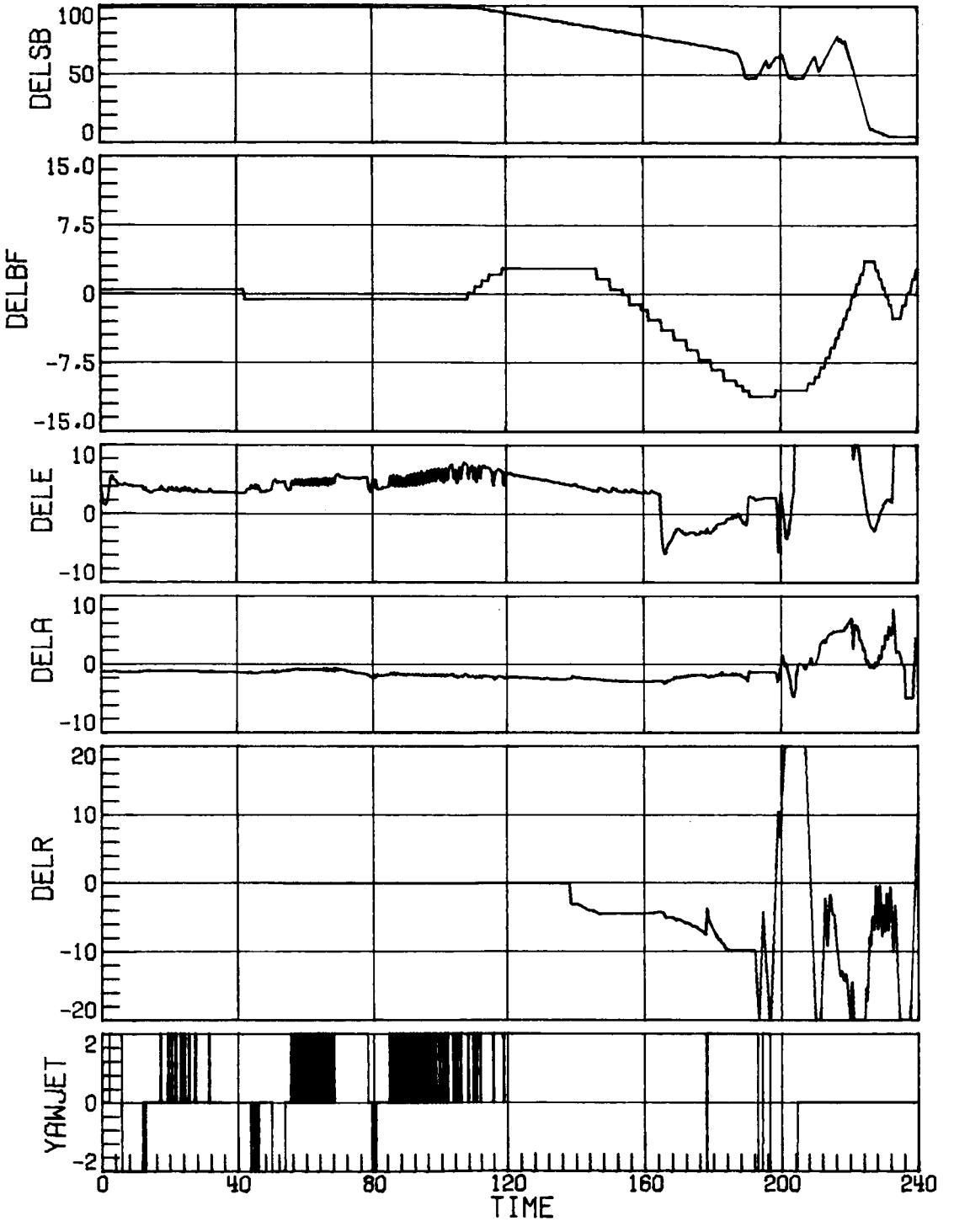

(b) Concluded.
Figure 14. Continued.

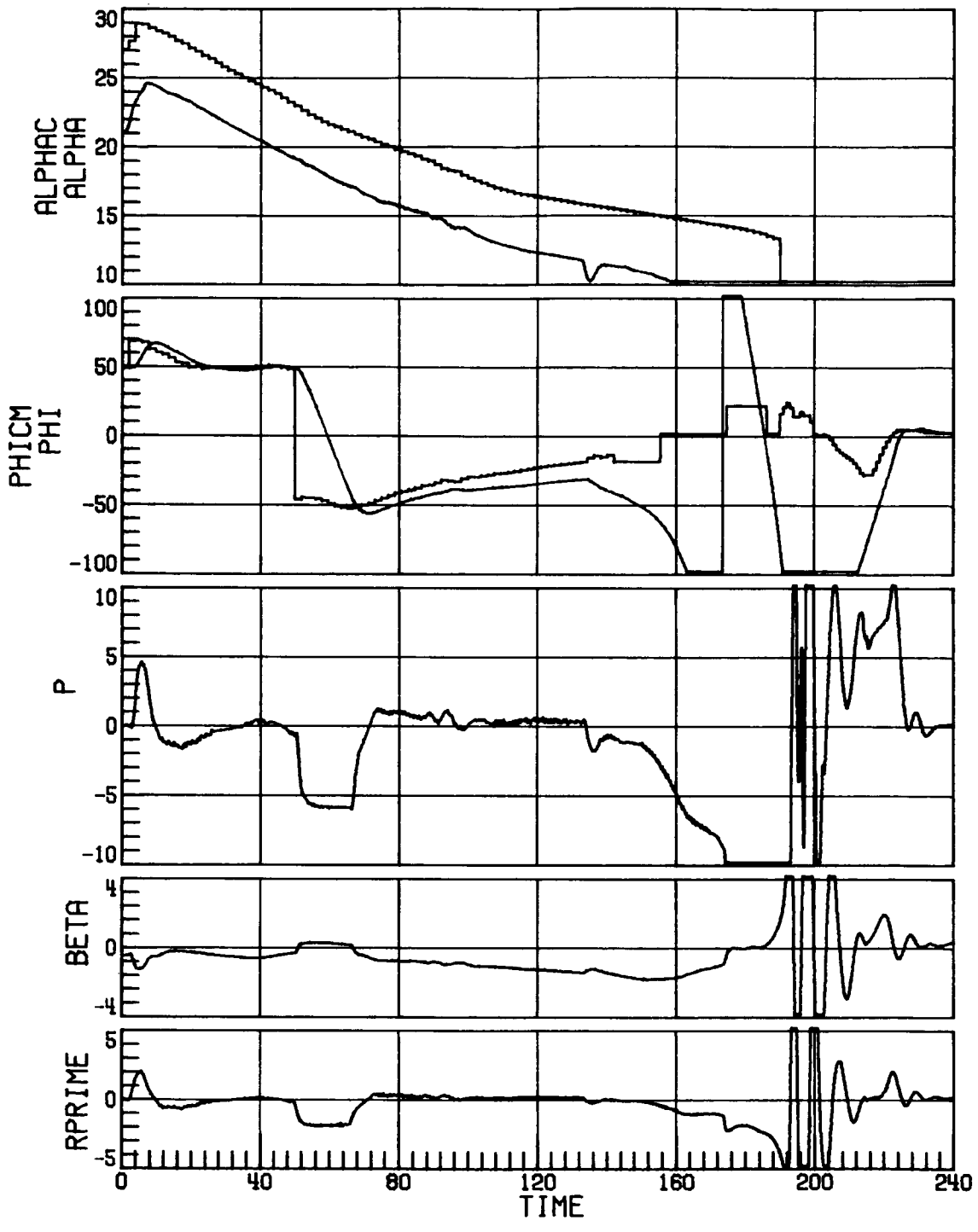

(c) Indicated α 4° high; RCS uncertainty set 2; four jets; negative pitch uncertainty; decreased side force due to β.

Figure 14. Continued

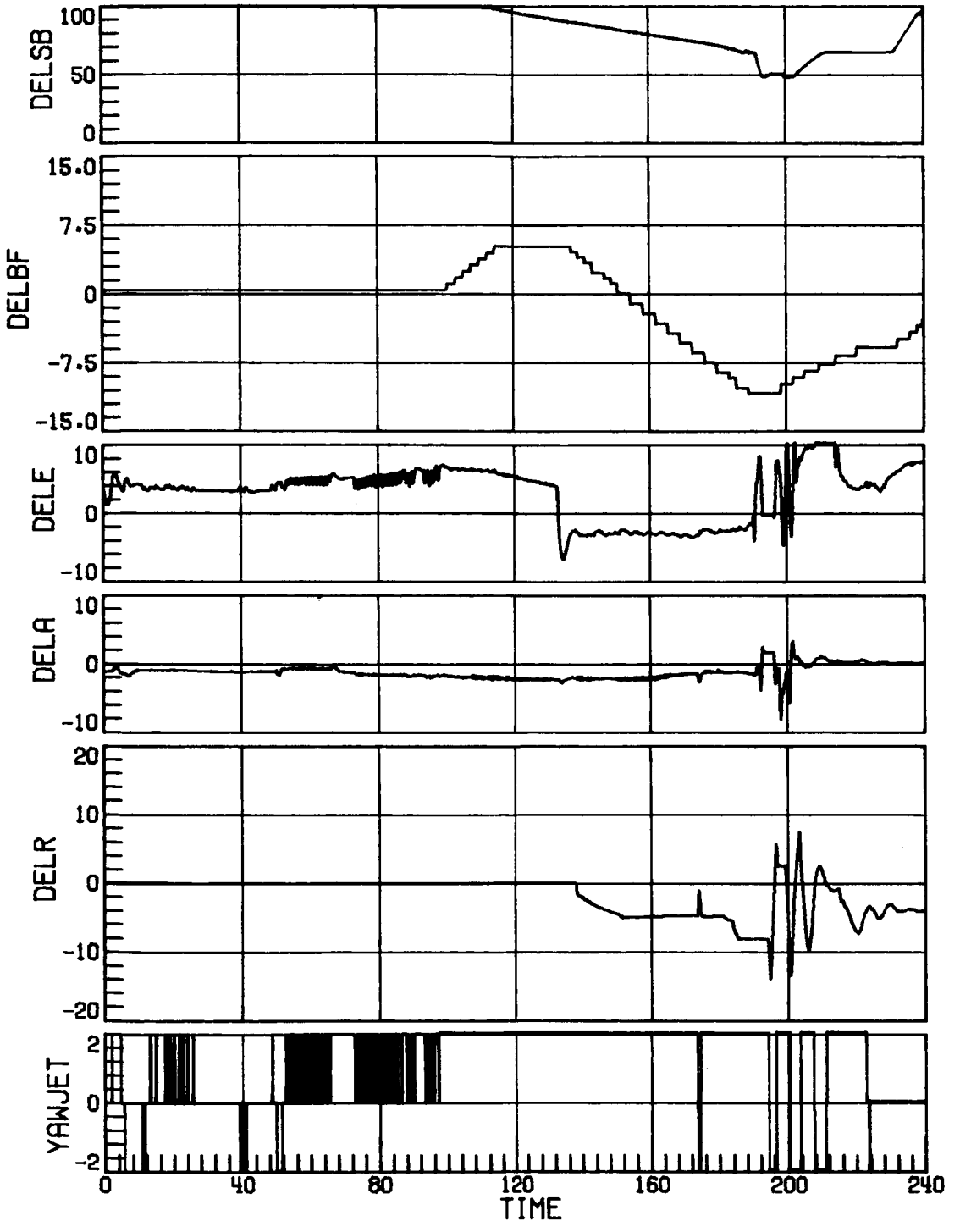

(c) Concluded.
Figure 14. Concluded.

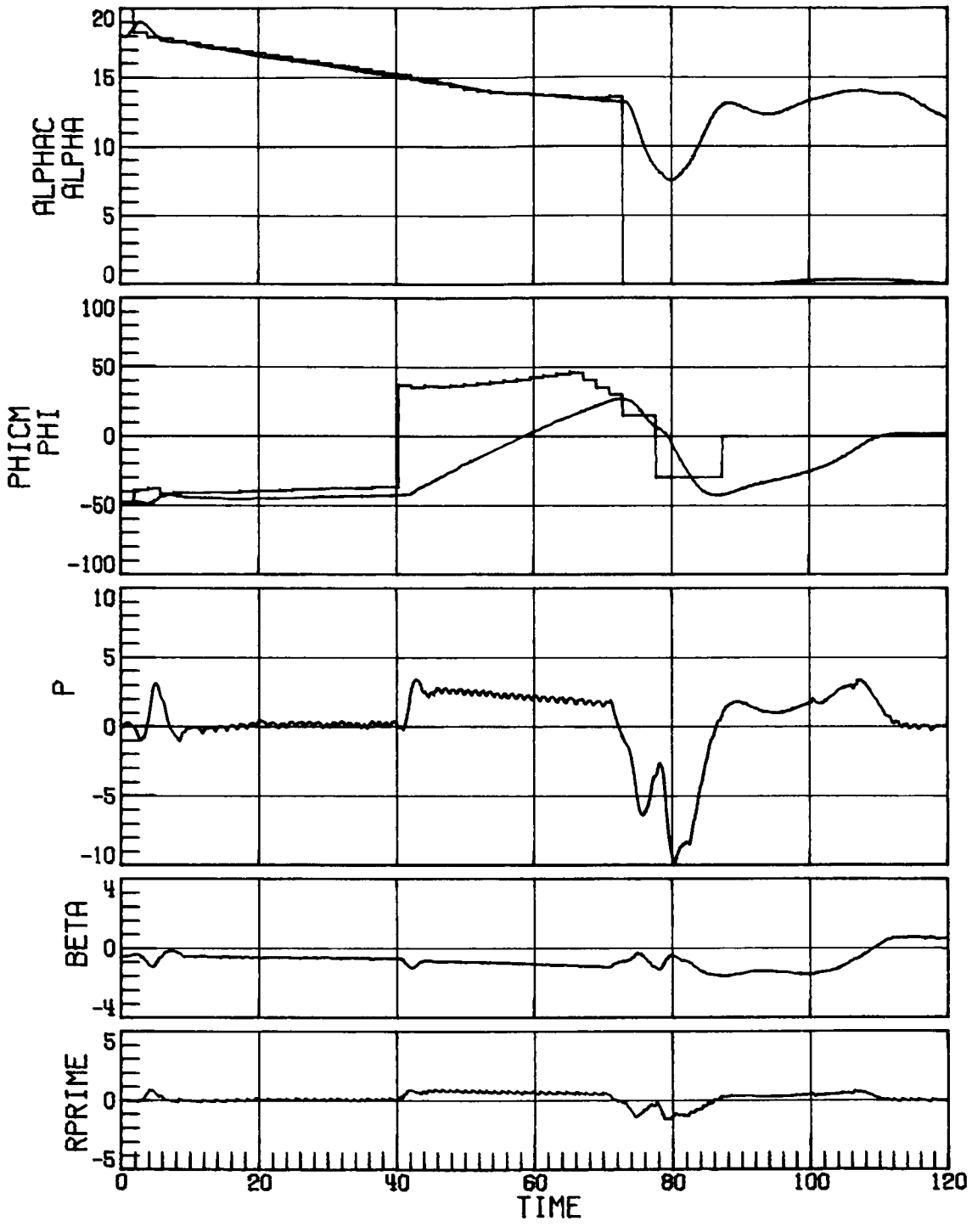

(a) Nominal side force due to β.

Figure 15. Time-history response for case 8 for Mach decreasing from 3.8 to 1.8 with decreased rudder effectiveness, nominal RCS/aerodynamic interaction, and negative pitch uncertainty. Time in seconds.

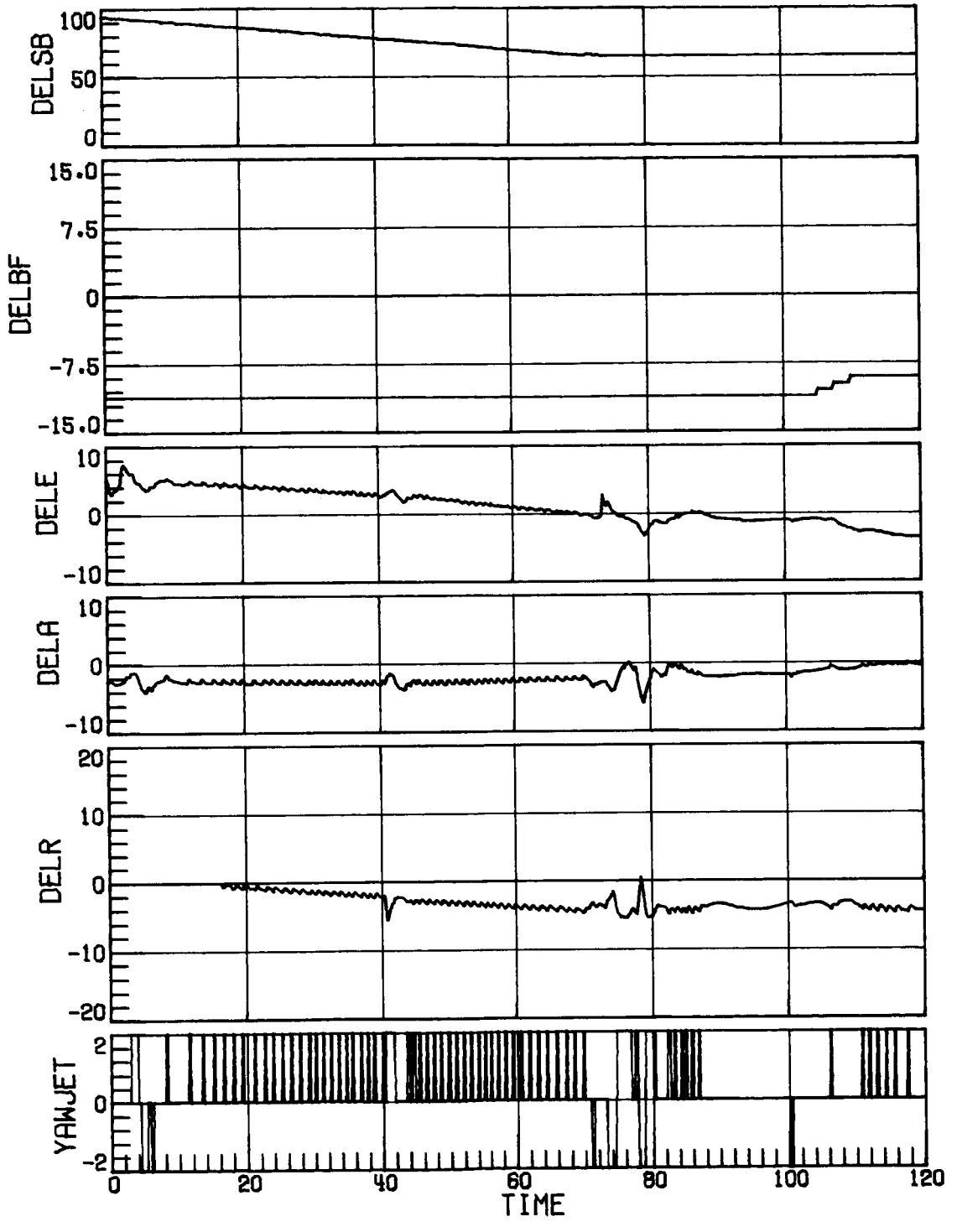

(a) Concluded.
Figure 15. Continued.

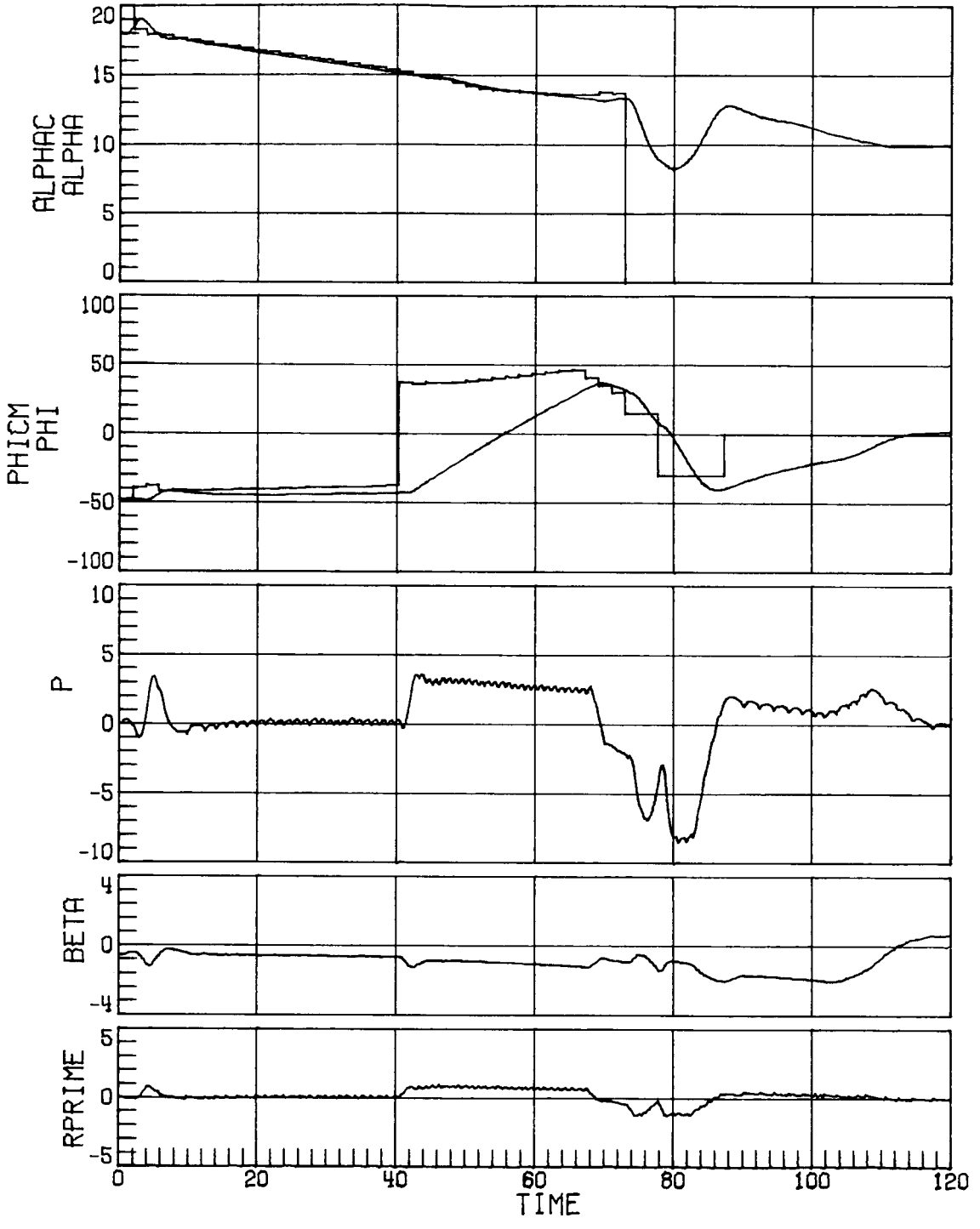

(b) Decreased side force due to β.
Figure 15. Continued.

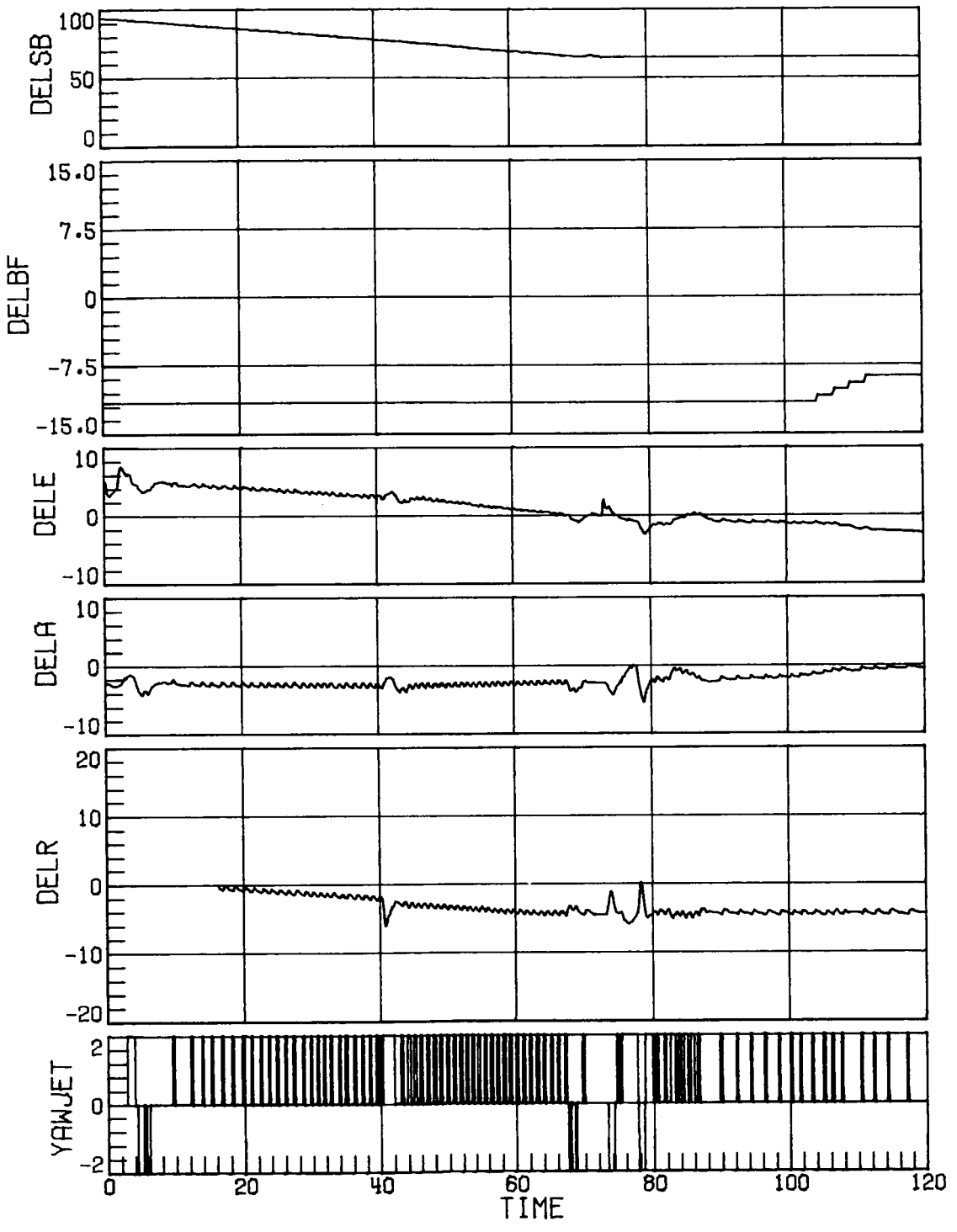

(b) Concluded.
Figure 15. Continued.

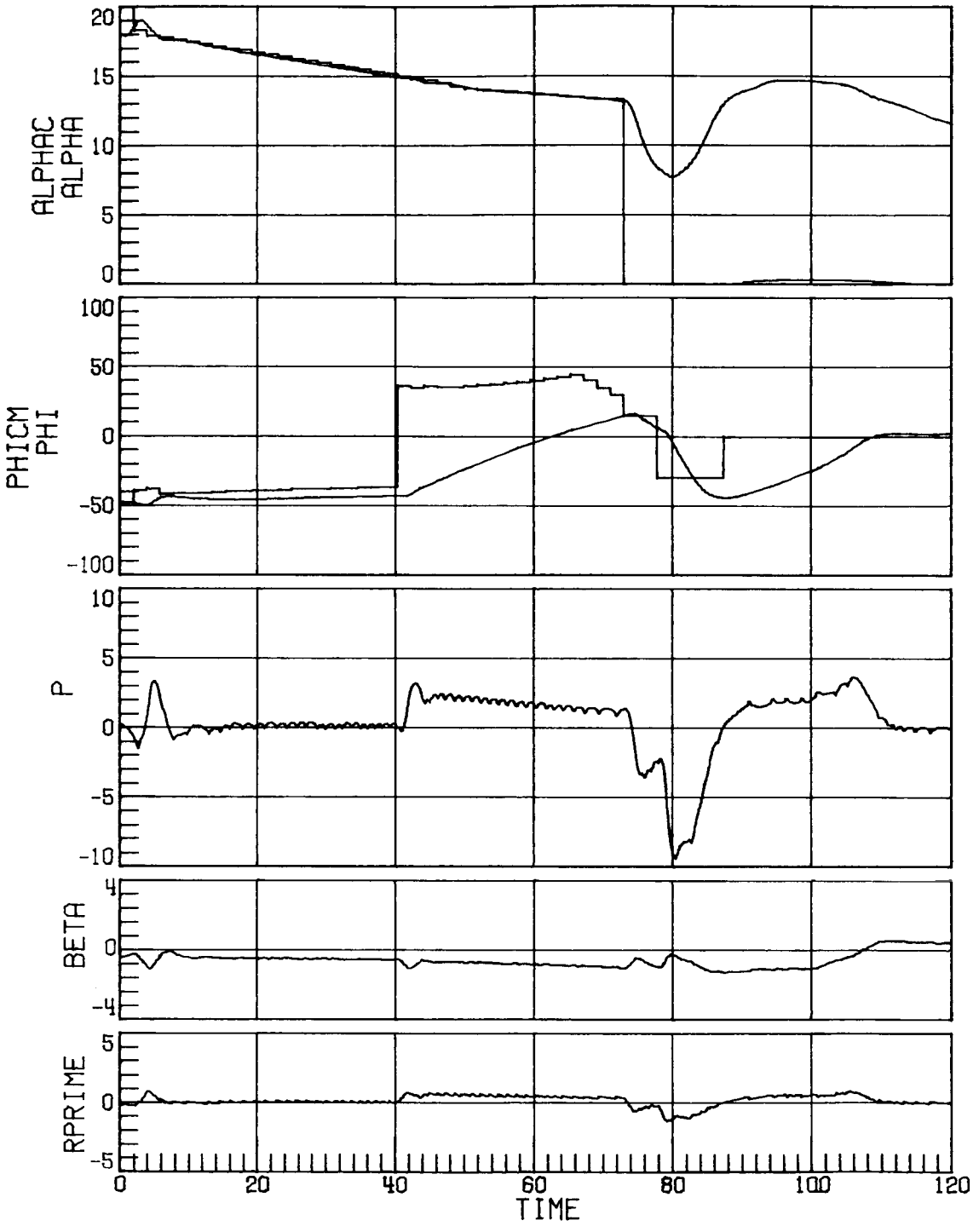

(c) Increased side force due to β.
Figure 15. Continued.

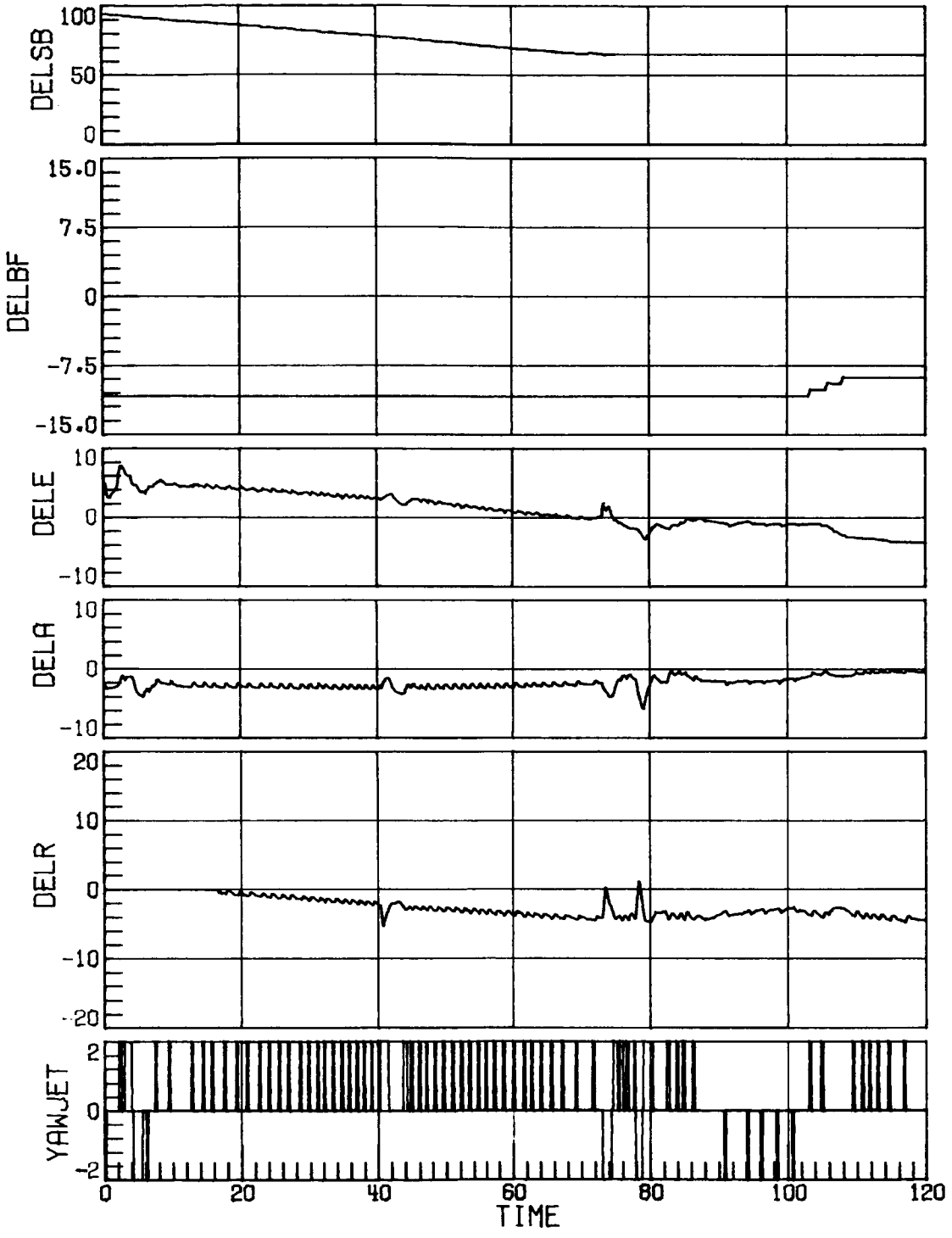

(c) Concluded.
Figure 15. Concluded.

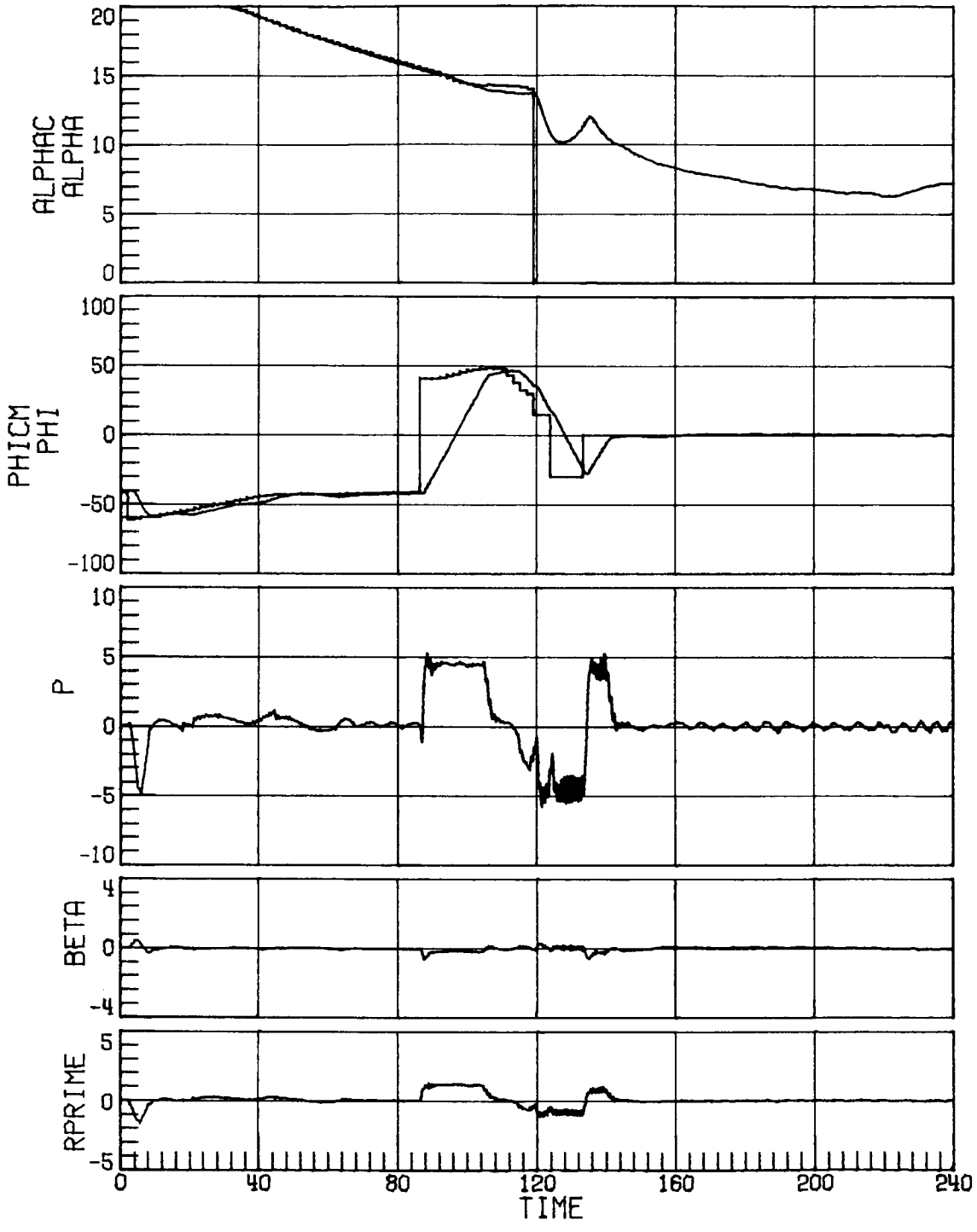

(a) Case 9.

Figure 16. Time-history response for Mach decreasing from 4.6 to 1.0 with increased rudder effectiveness, negative pitch uncertainty, and decreased side force due to β. Time in seconds.

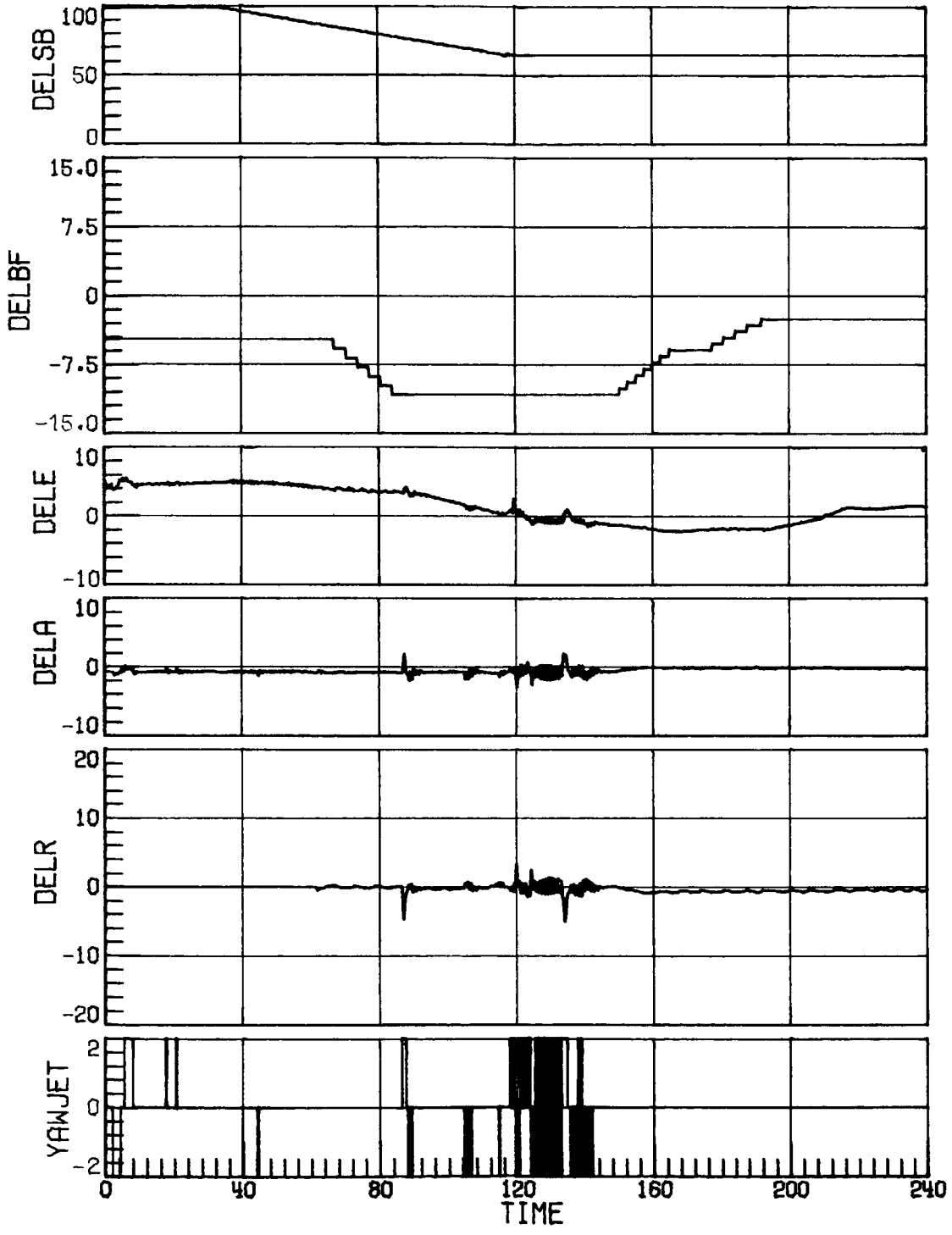

(a) Concluded.
Figure 16. Continued.

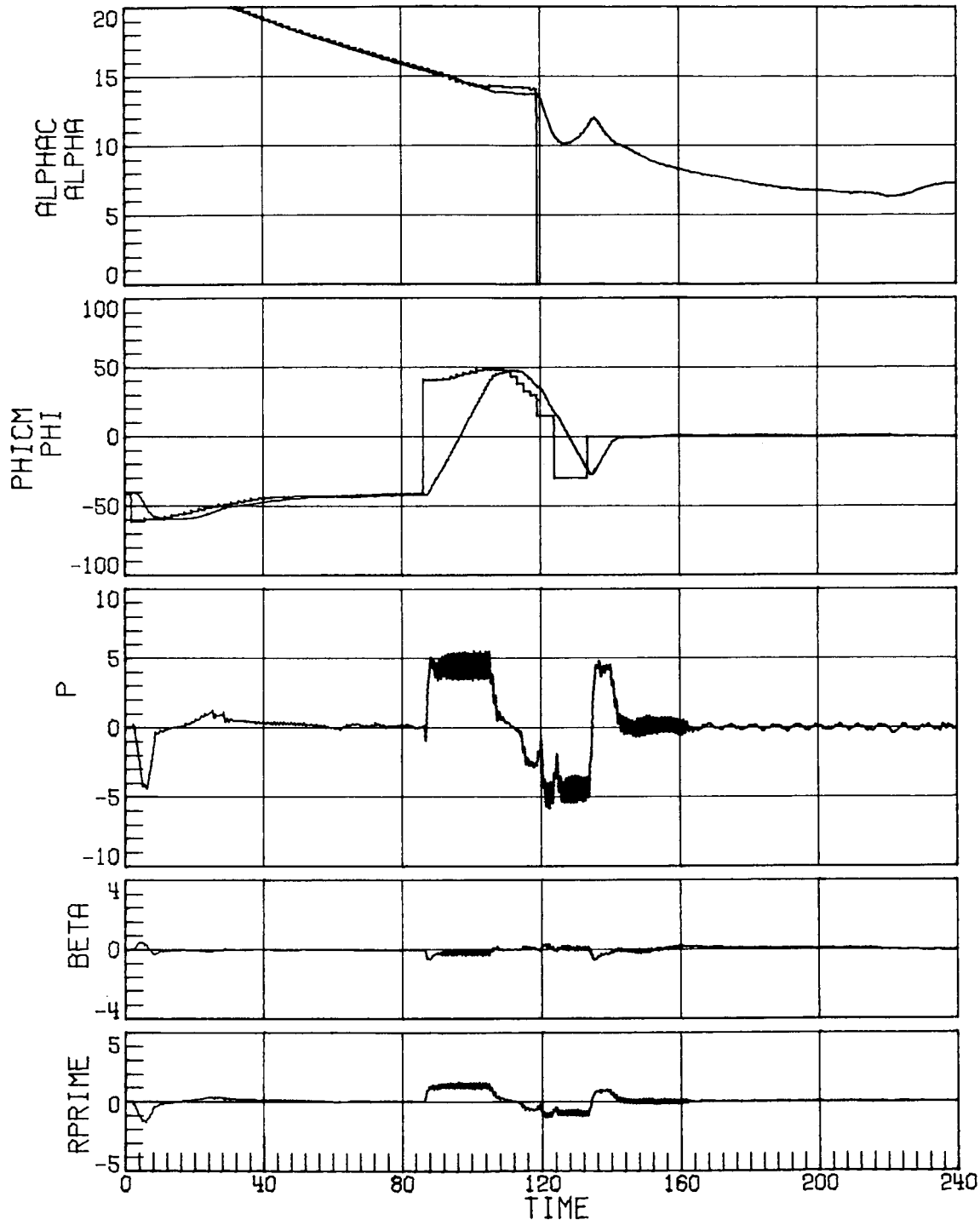

(b) Case 10.
Figure 16. Continued.

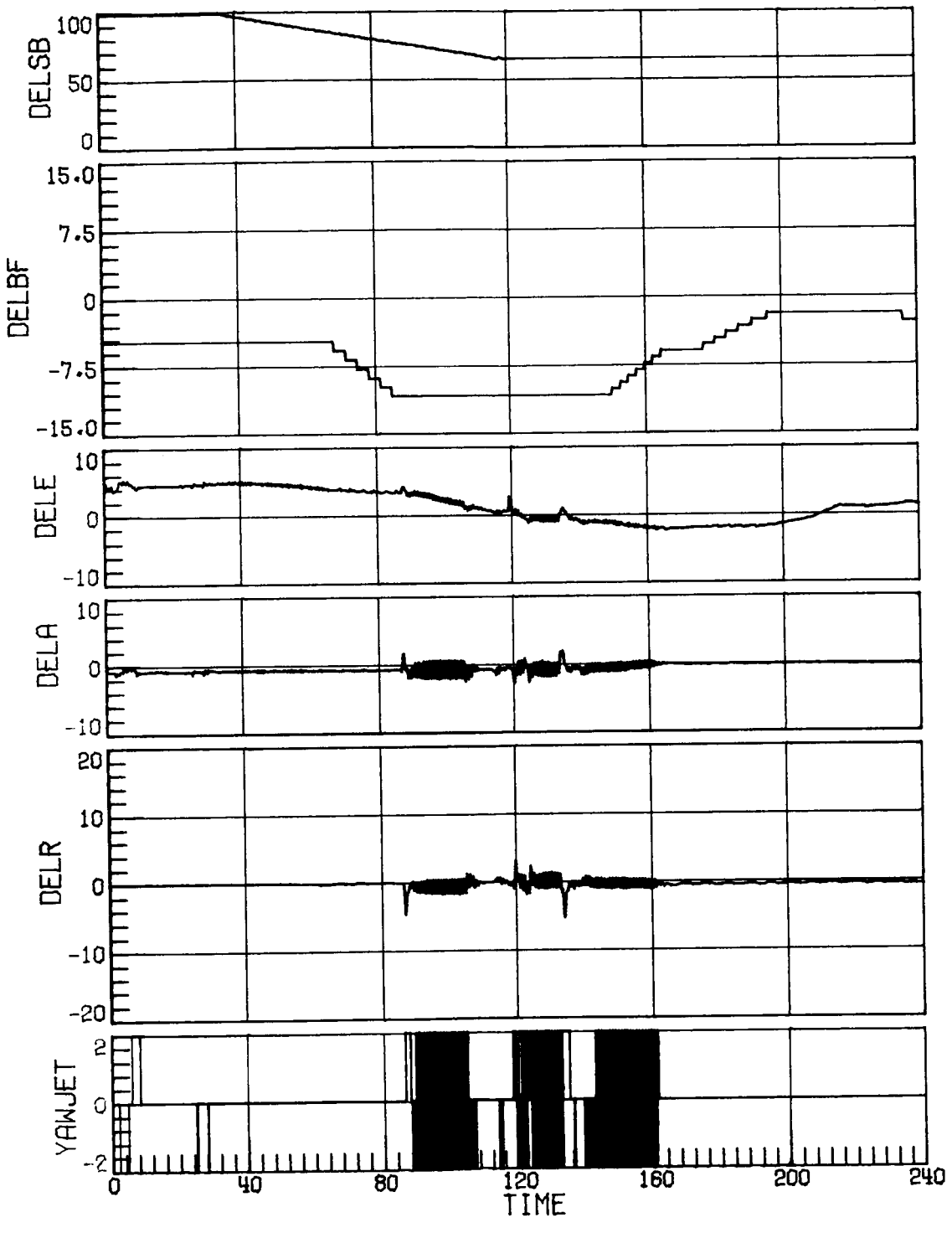

(b) Concluded.
Figure 16. Continued.

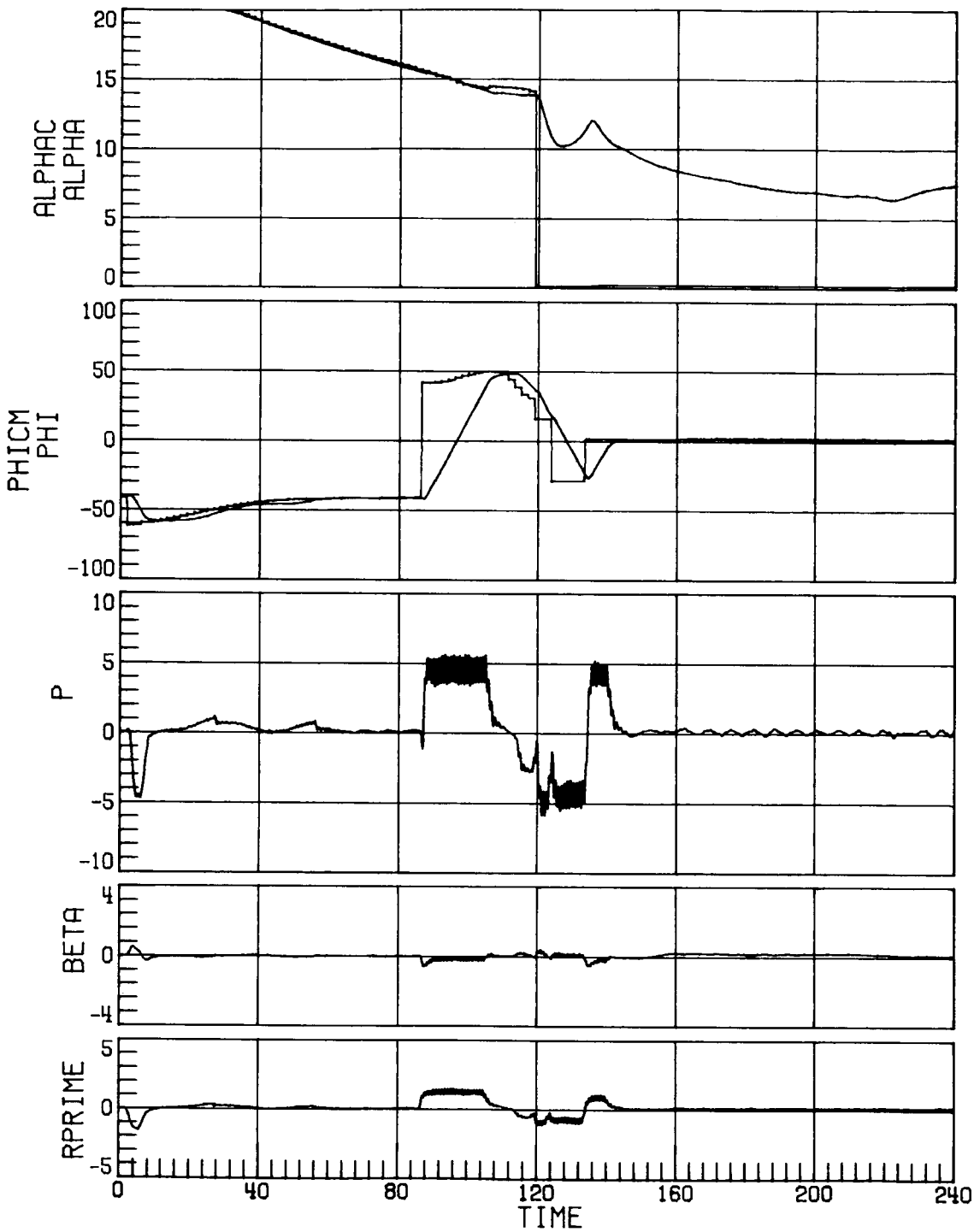

(c) Case 10; four jets.
Figure 16. Continued.

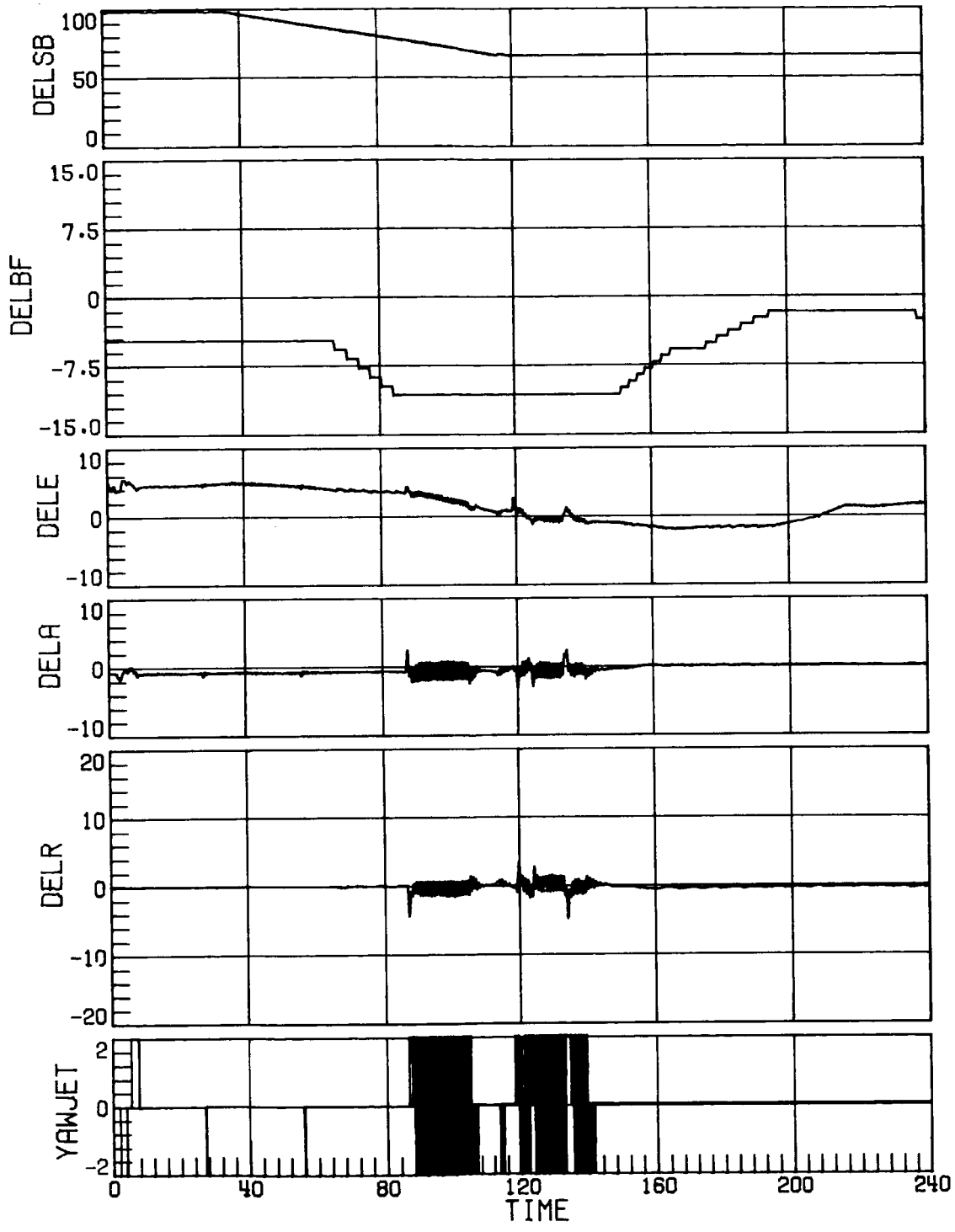

(c) Concluded.
Figure 16. Concluded.

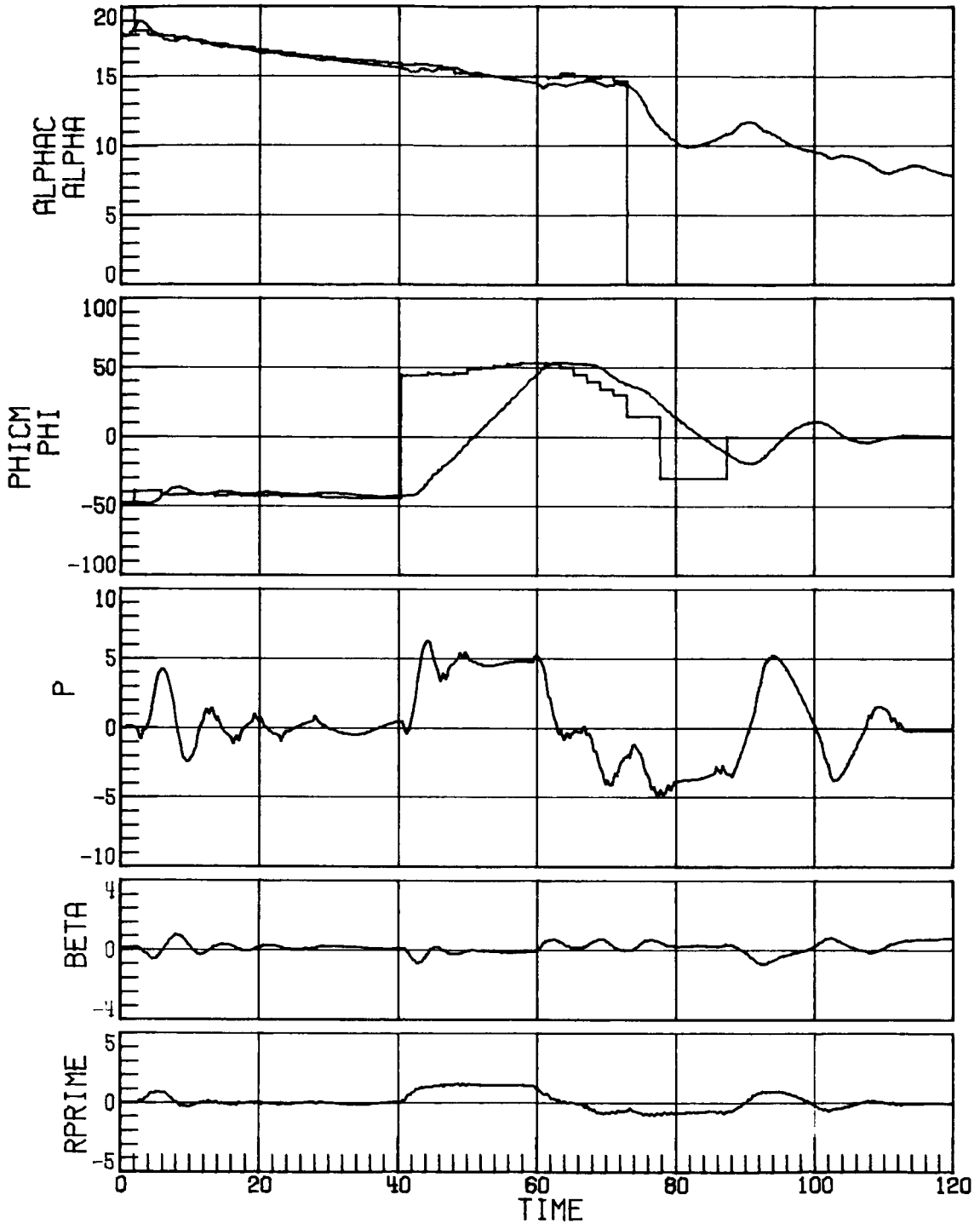

(a) Case 3; RCS uncertainty set 1.

Figure 17. Time-history response for Mach decreasing from 3.8 to 1.9 with decreased rudder effectiveness, negative pitch uncertainty, and decreased side force due to β. Time in seconds.

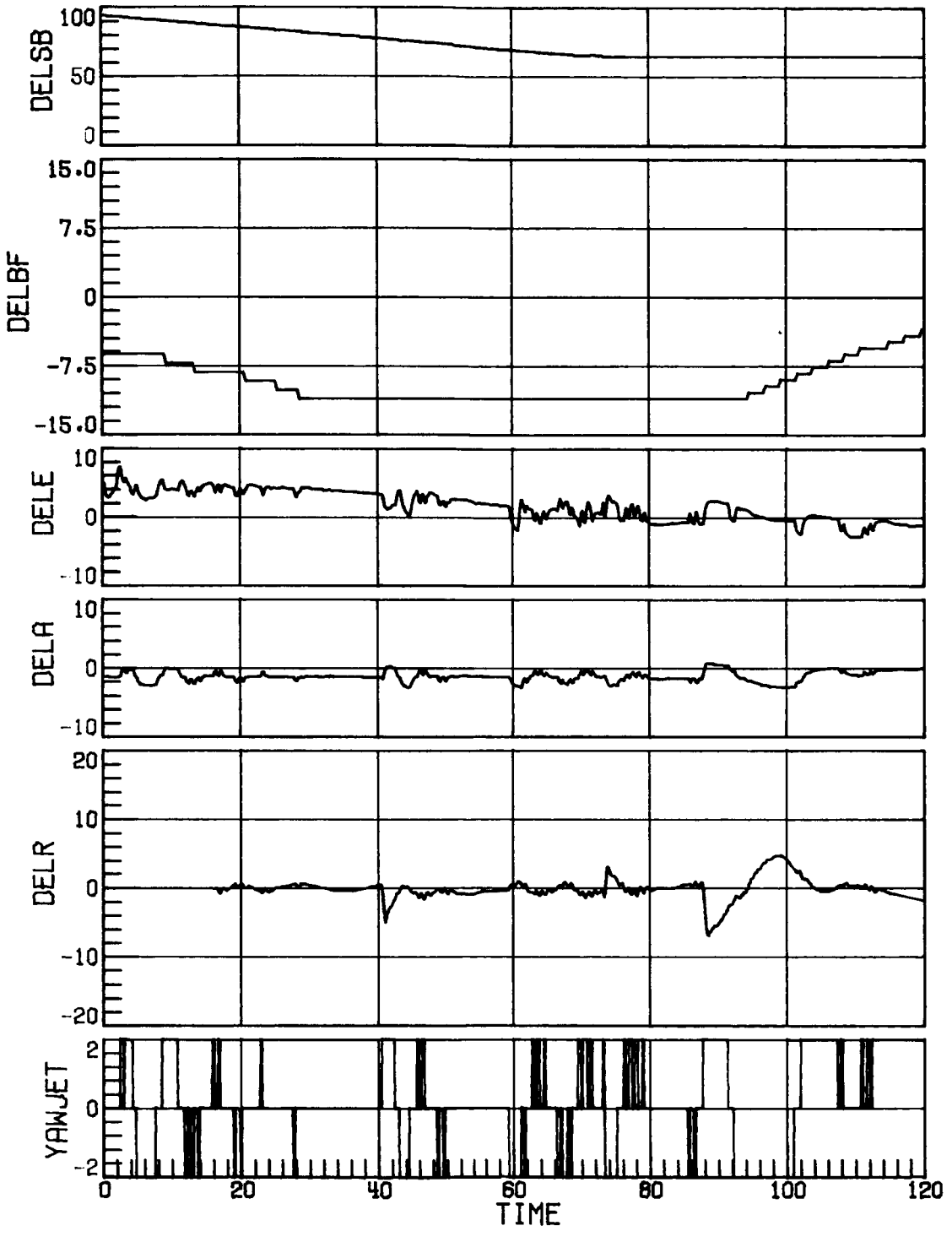

(a) Concluded.
Figure 17. Continued.

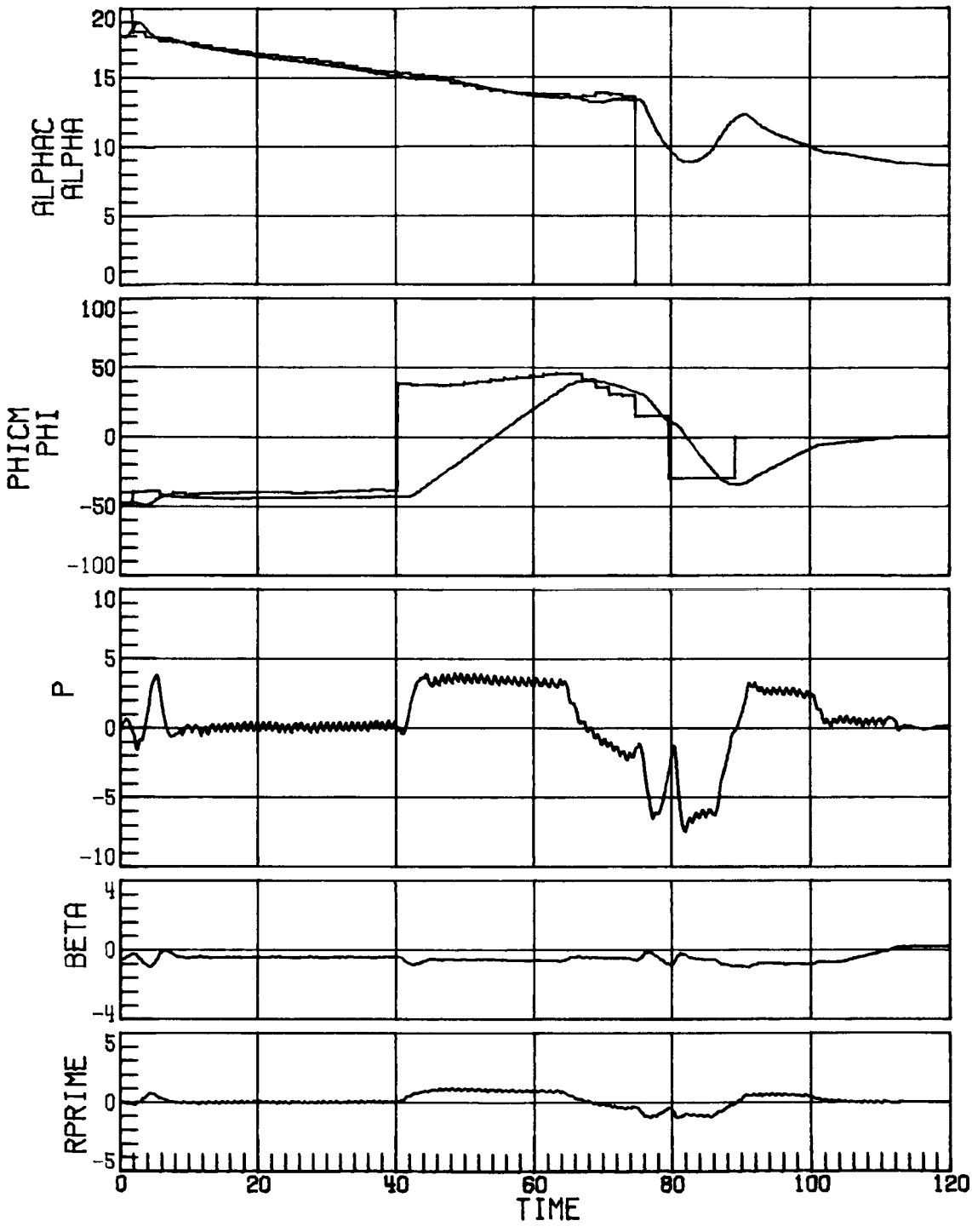

(b) Case 6; RCS uncertainty set 1.
Figure 17. Continued.

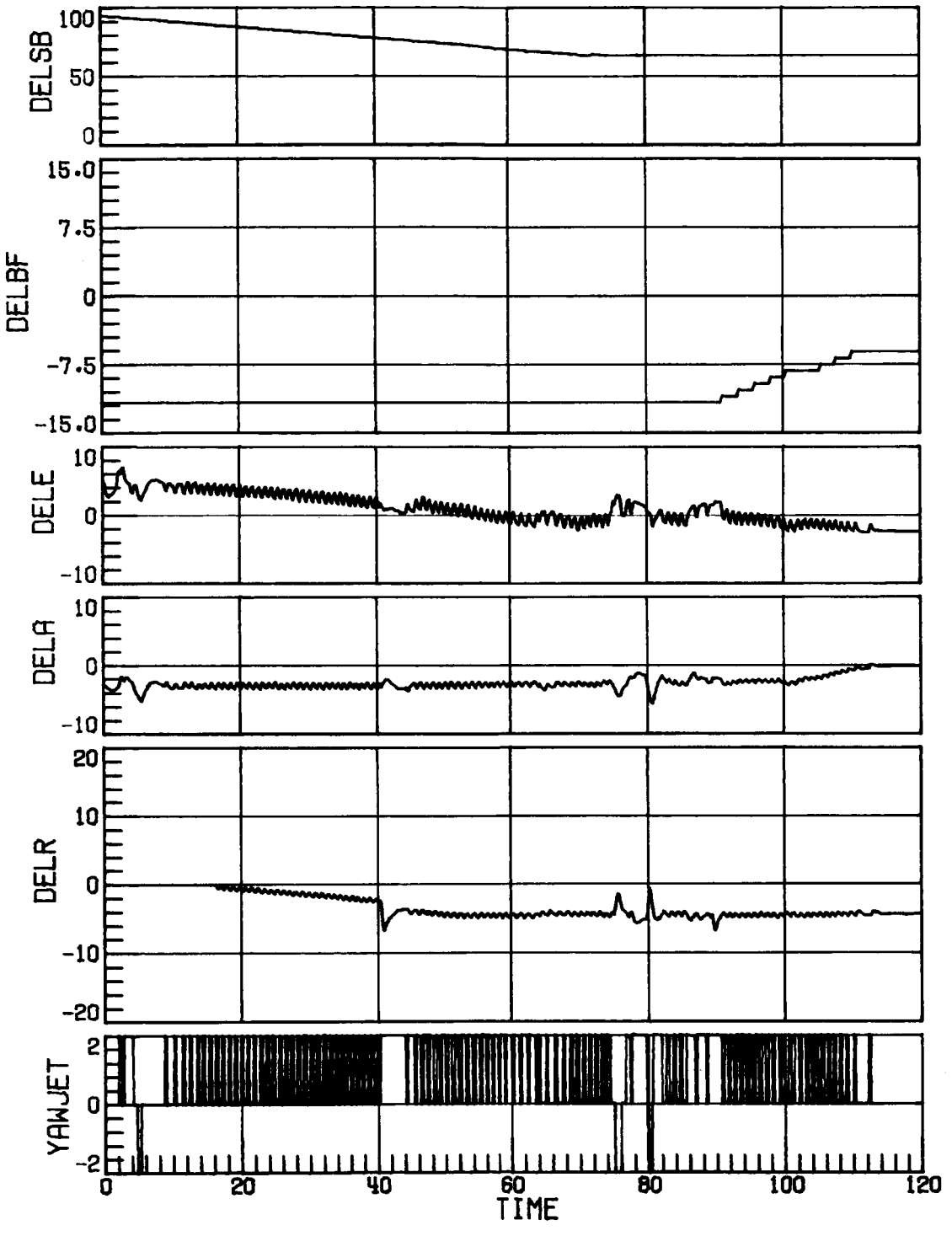

(b) Concluded.
Figure 17. Continued.

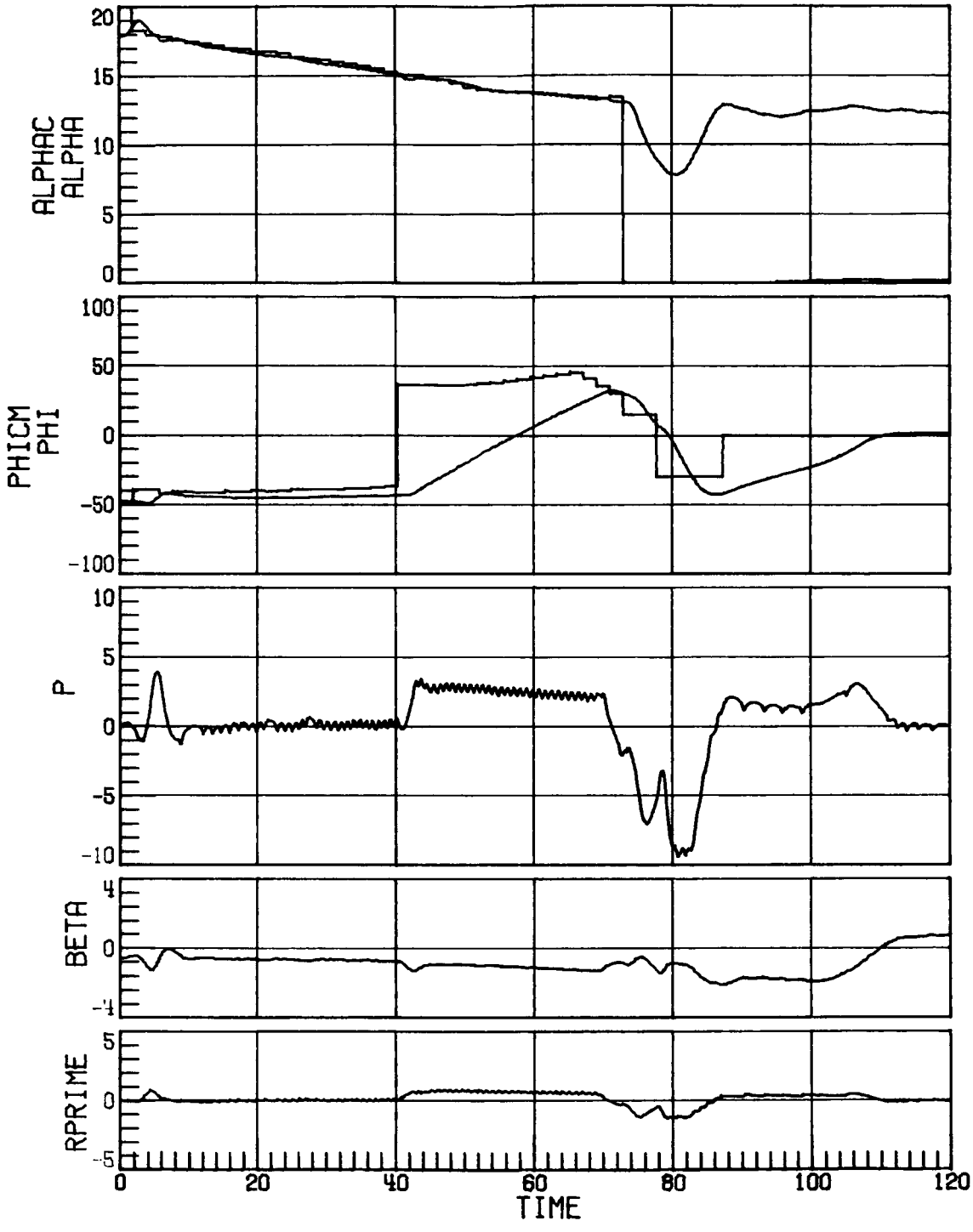

(c) Case 8; RCS uncertainty set 1.
Figure 17. Continued.

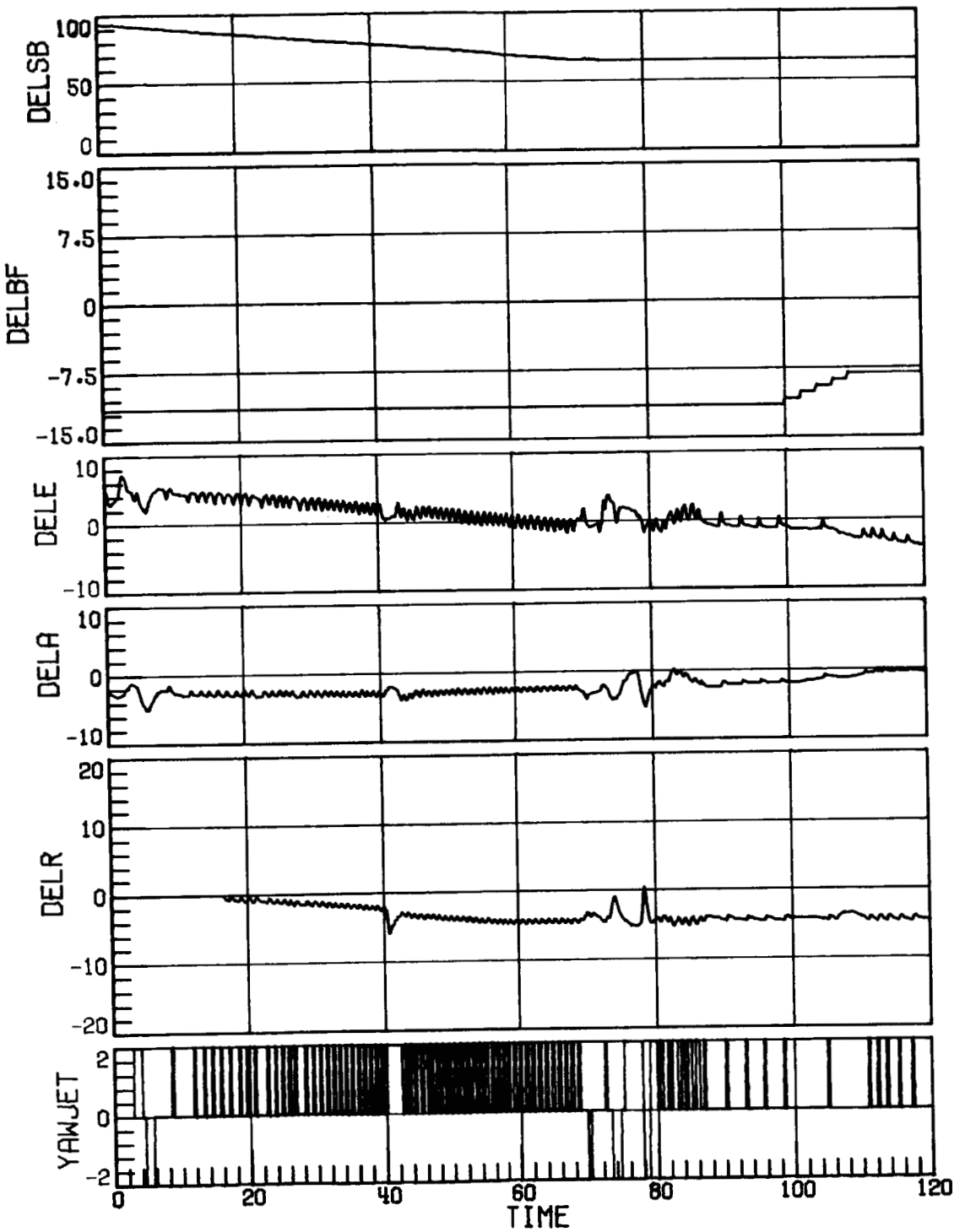

(c) Concluded.
Figure 17. Continued.

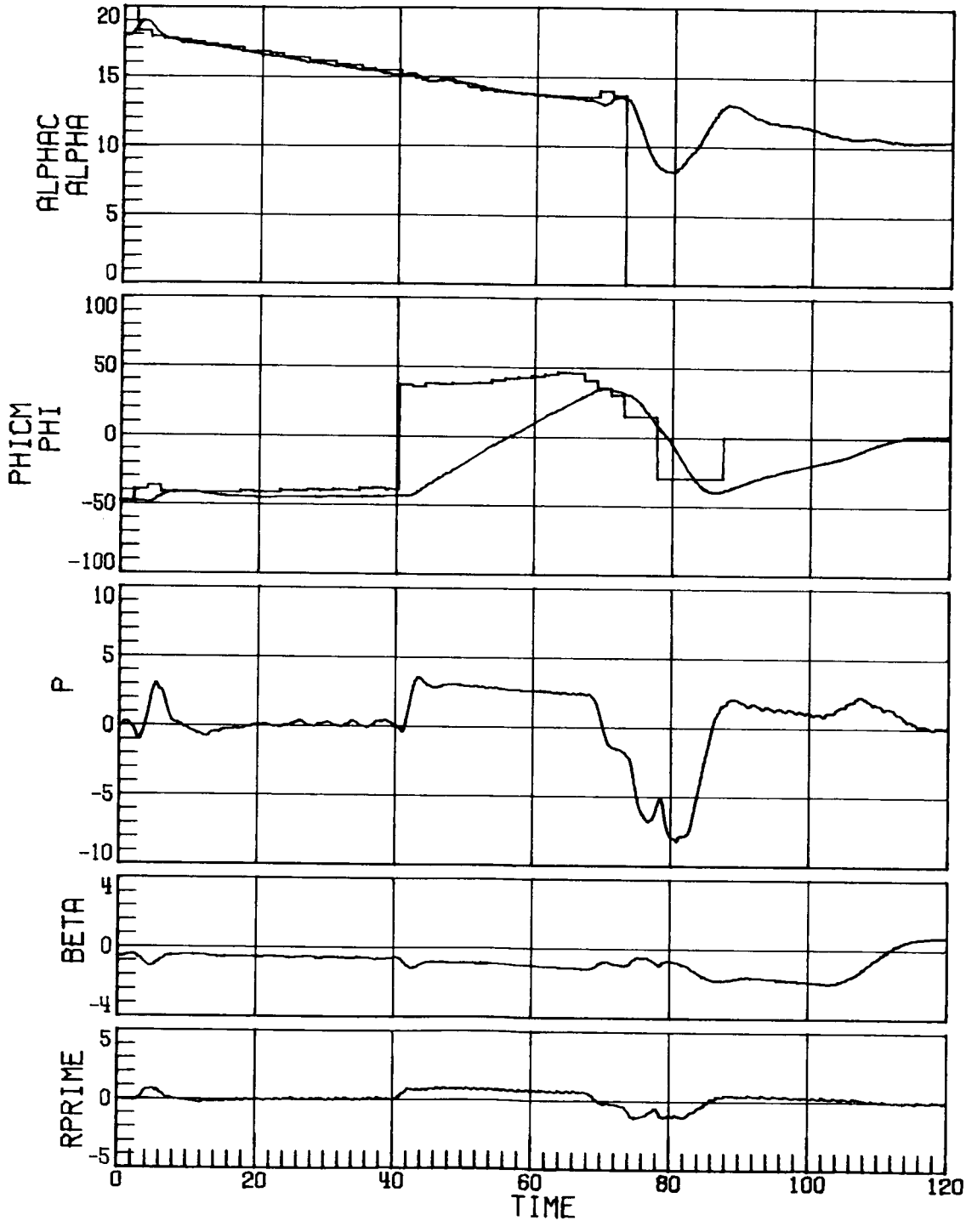

(d) Case 8; RCS uncertainty set 2.
Figure 17. Continued.

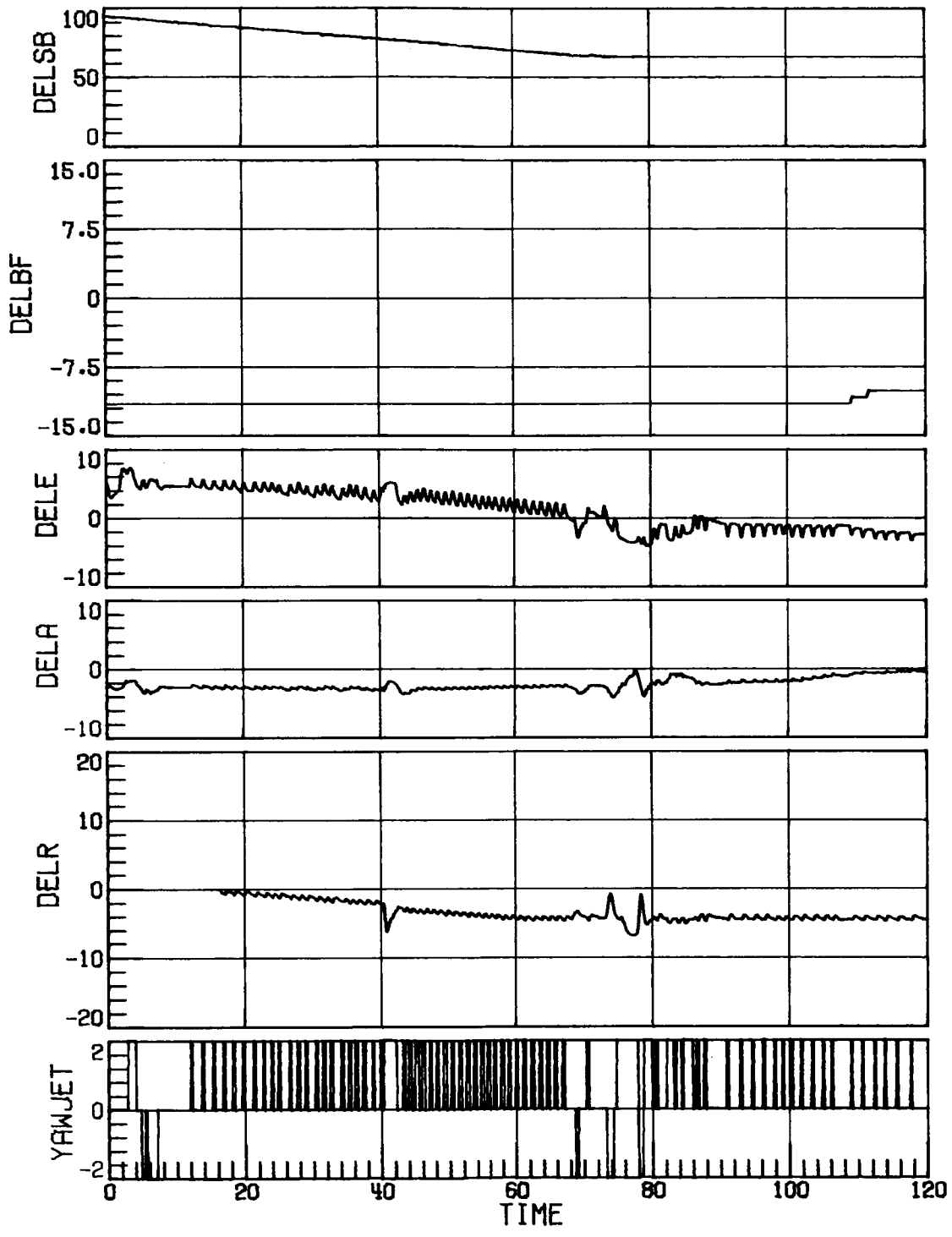

(d) Concluded.
Figure 17. Continued.

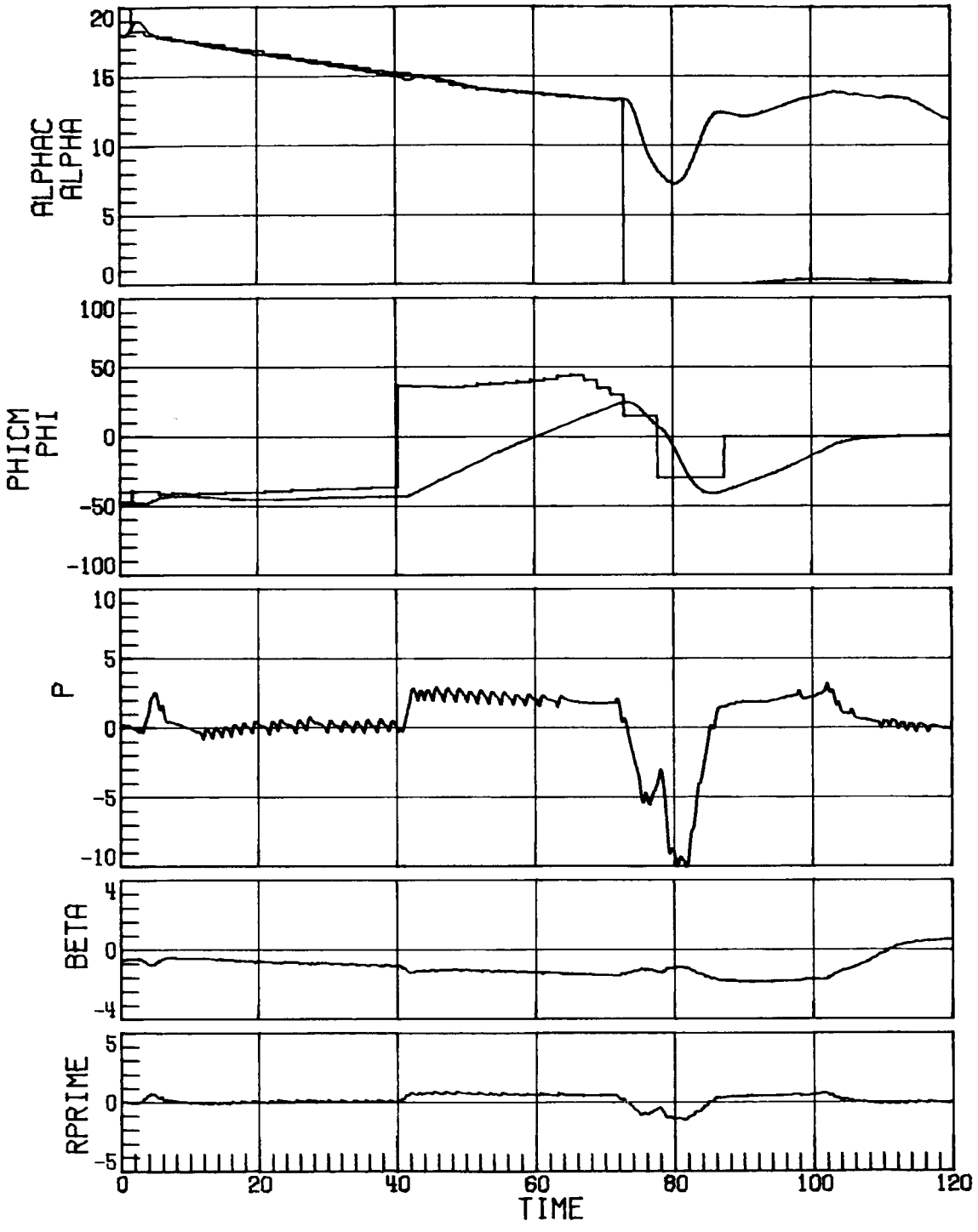

(e) Case 16; RCS uncertainty set 1.
Figure 17. Continued.

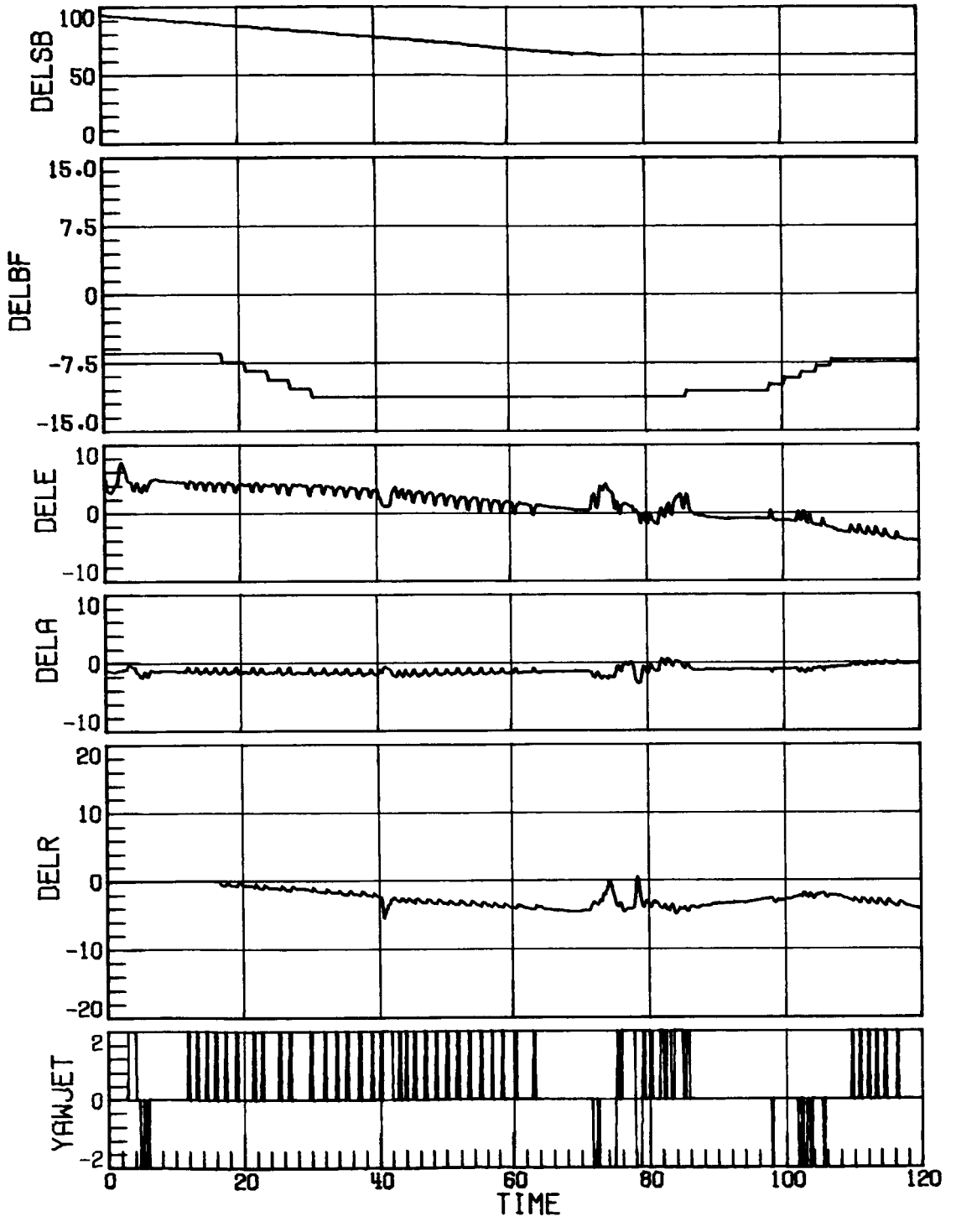

(e) Concluded.

Figure 17. Concluded.

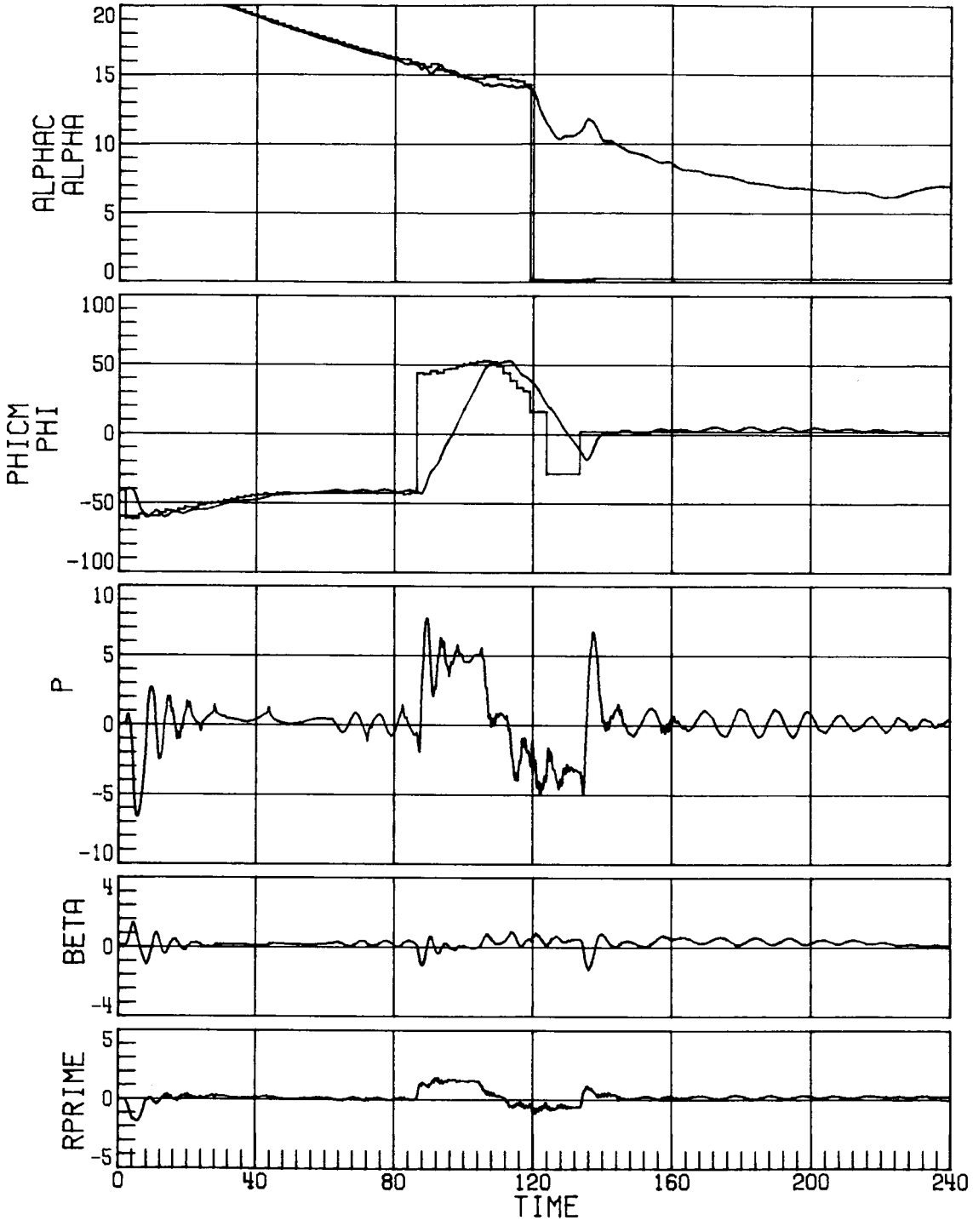

(a) Case 3; RCS uncertainty set 3.

Figure 18. Time-history response for Mach decreasing from 4.6 to 1.0 with increased rudder effectiveness, negative pitch uncertainty, and decreased side force due to β. Time in seconds.

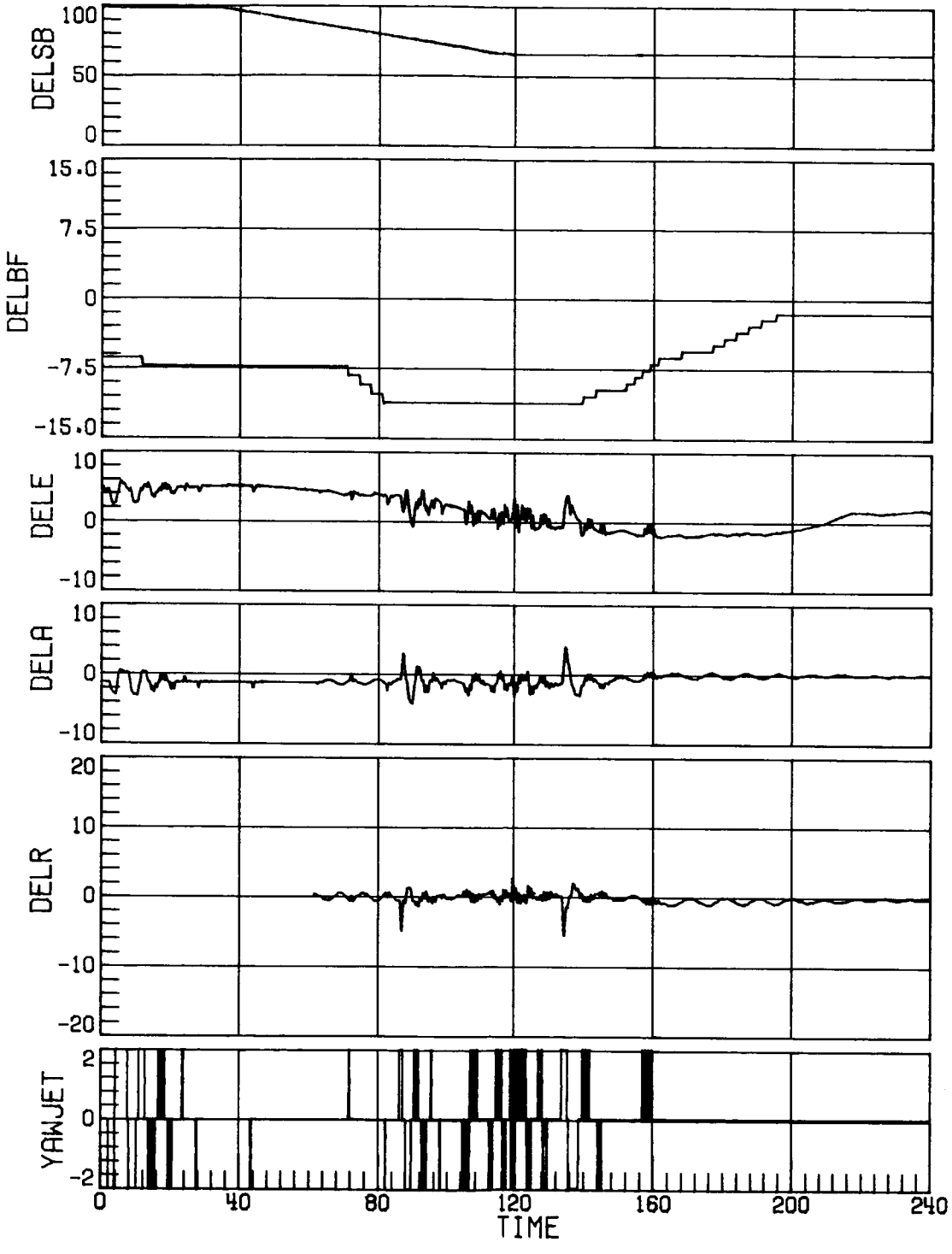

(a) Concluded.
Figure 18. Continued.

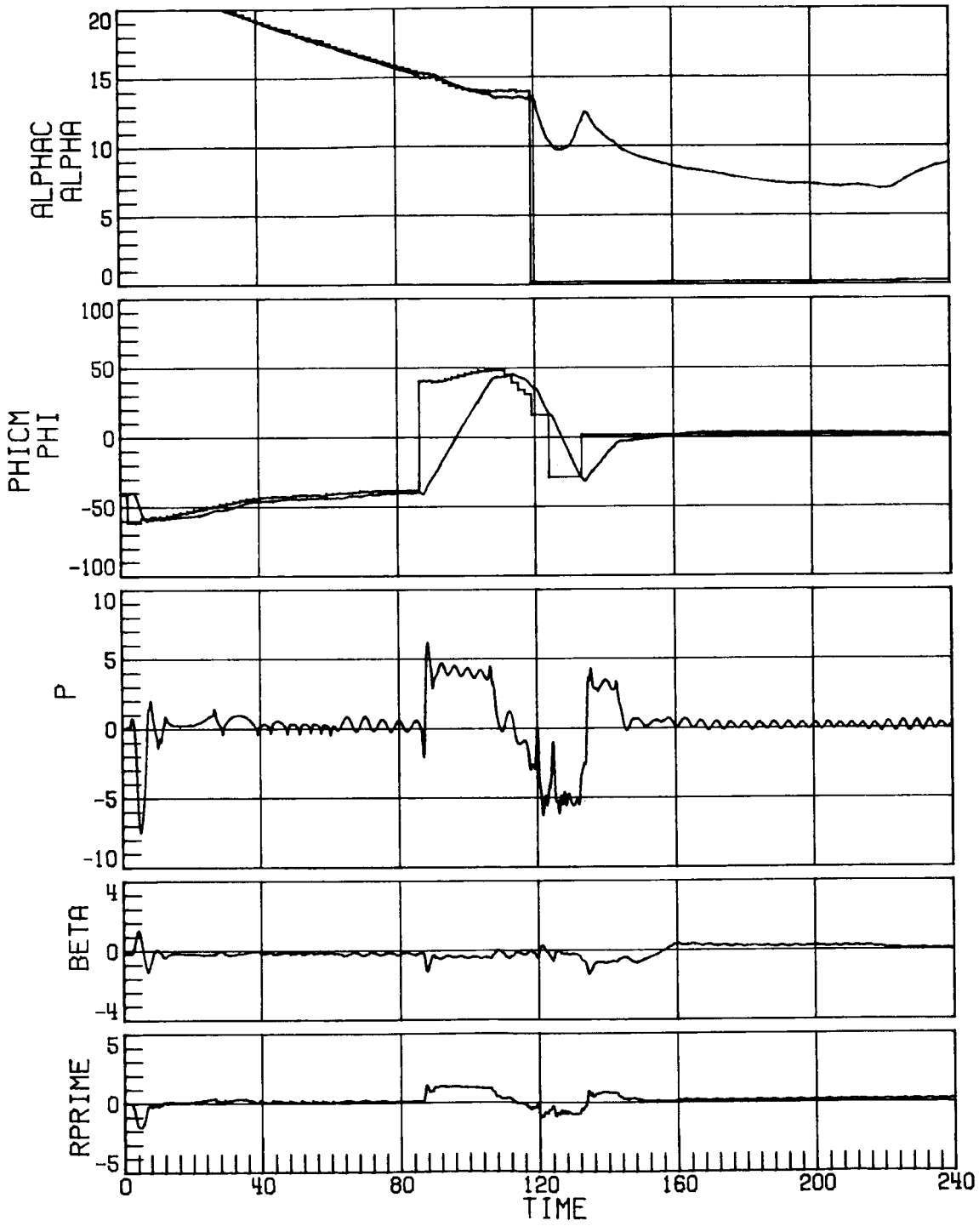

(b) Case 7; RCS uncertainty set 3.
Figure 18. Continued.

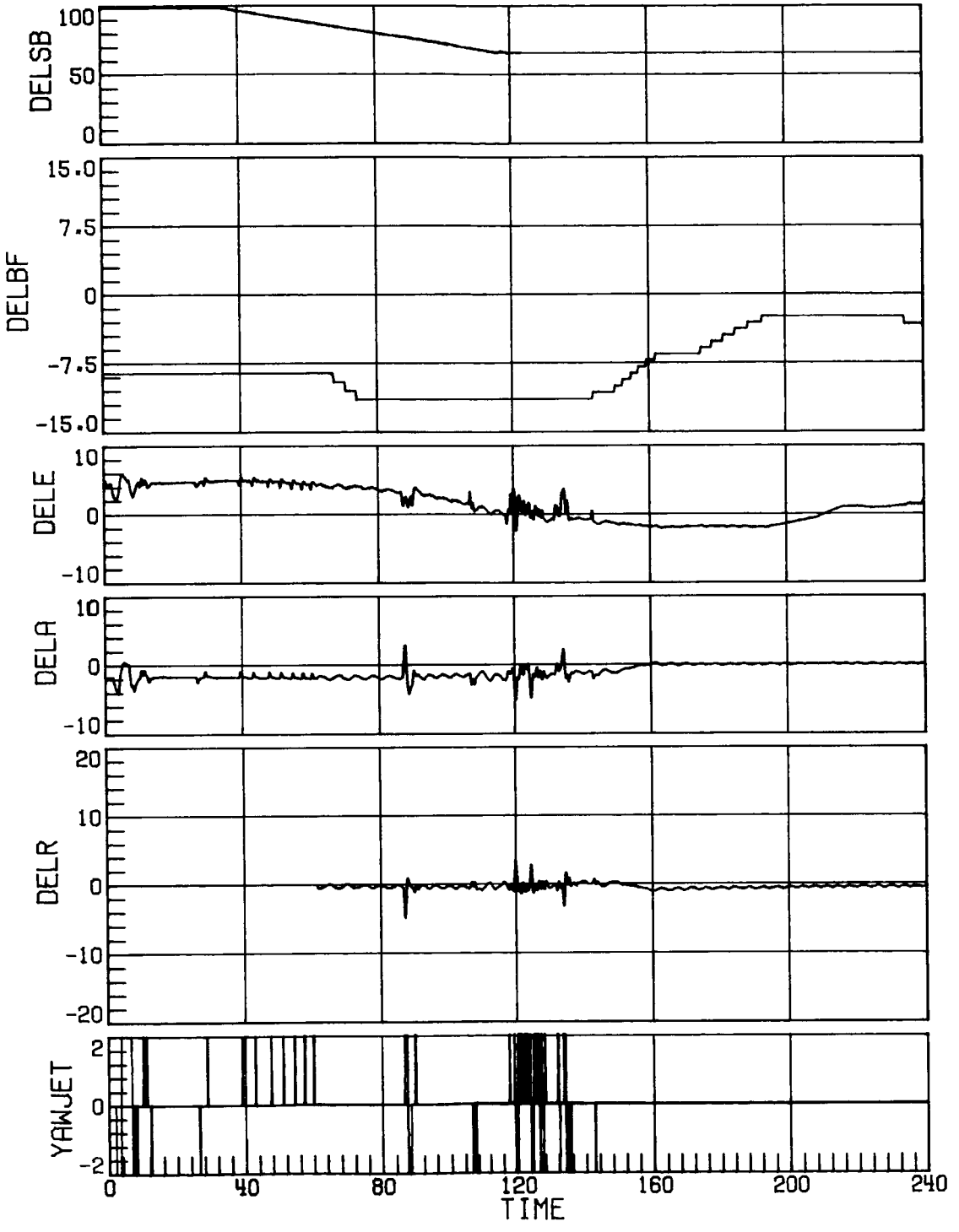

(b) Concluded.
Figure 18. Continued.

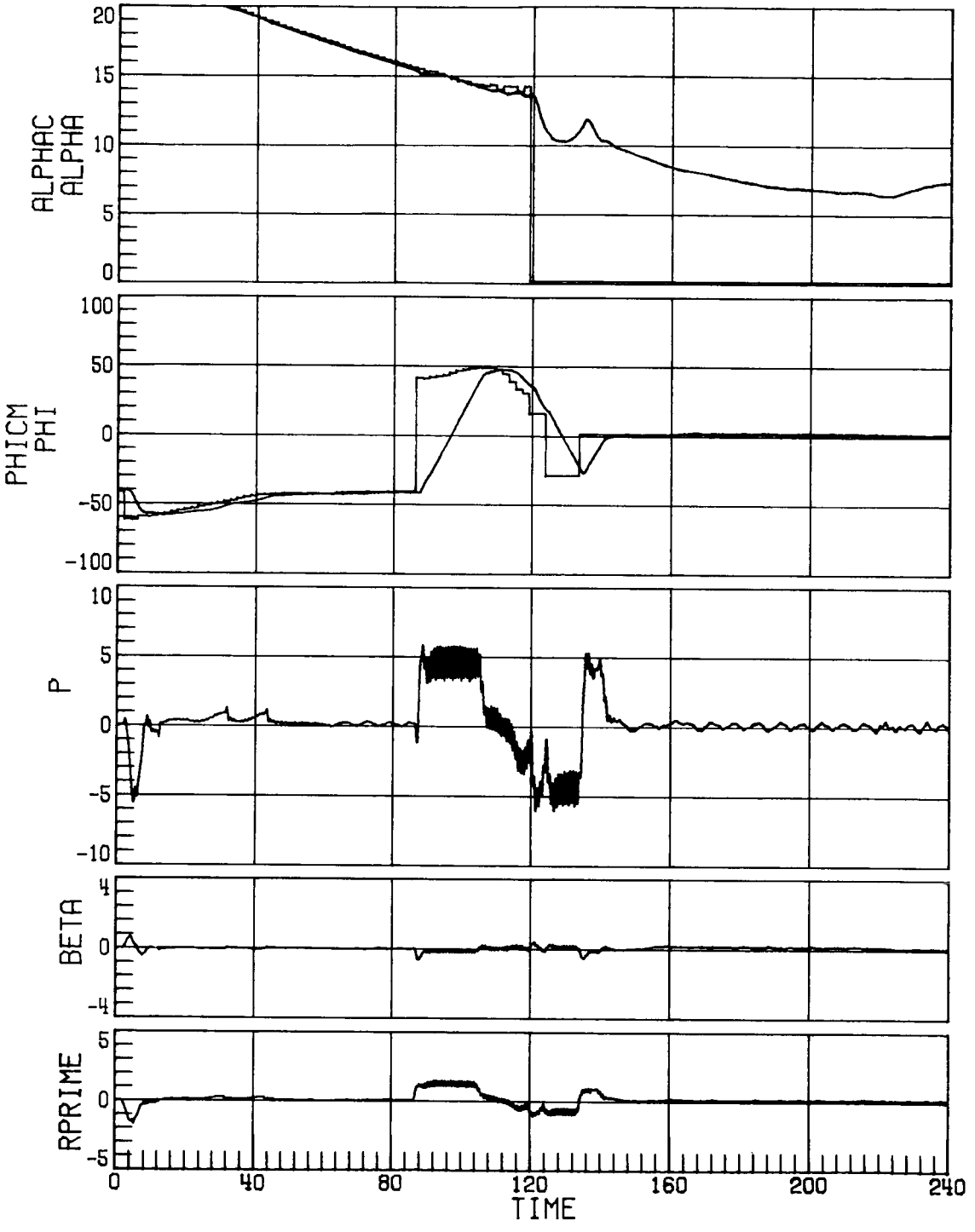

(c) Case 9; RCS uncertainty set 3.
Figure 18. Continued.

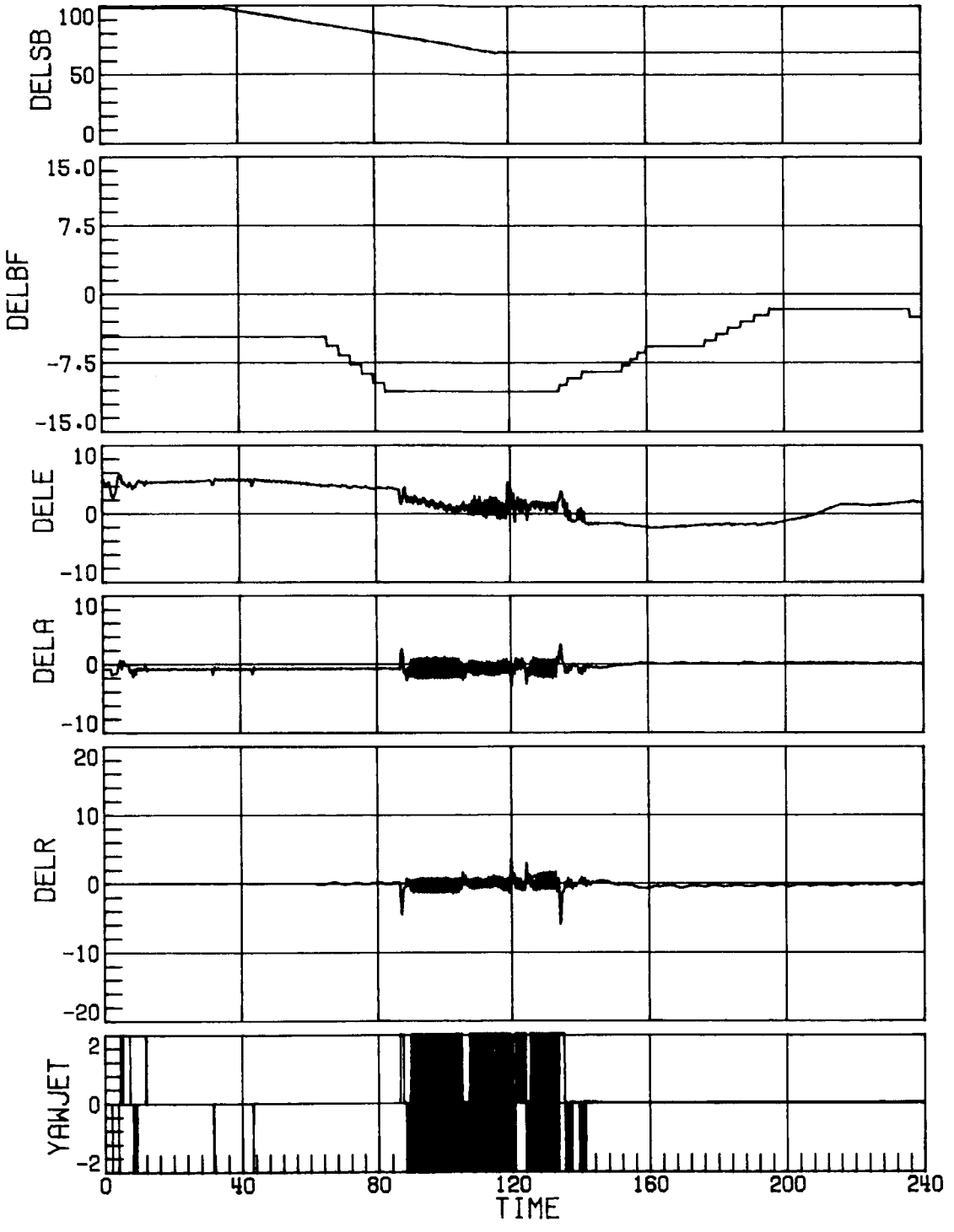

(c) Concluded.
Figure 18. Continued.

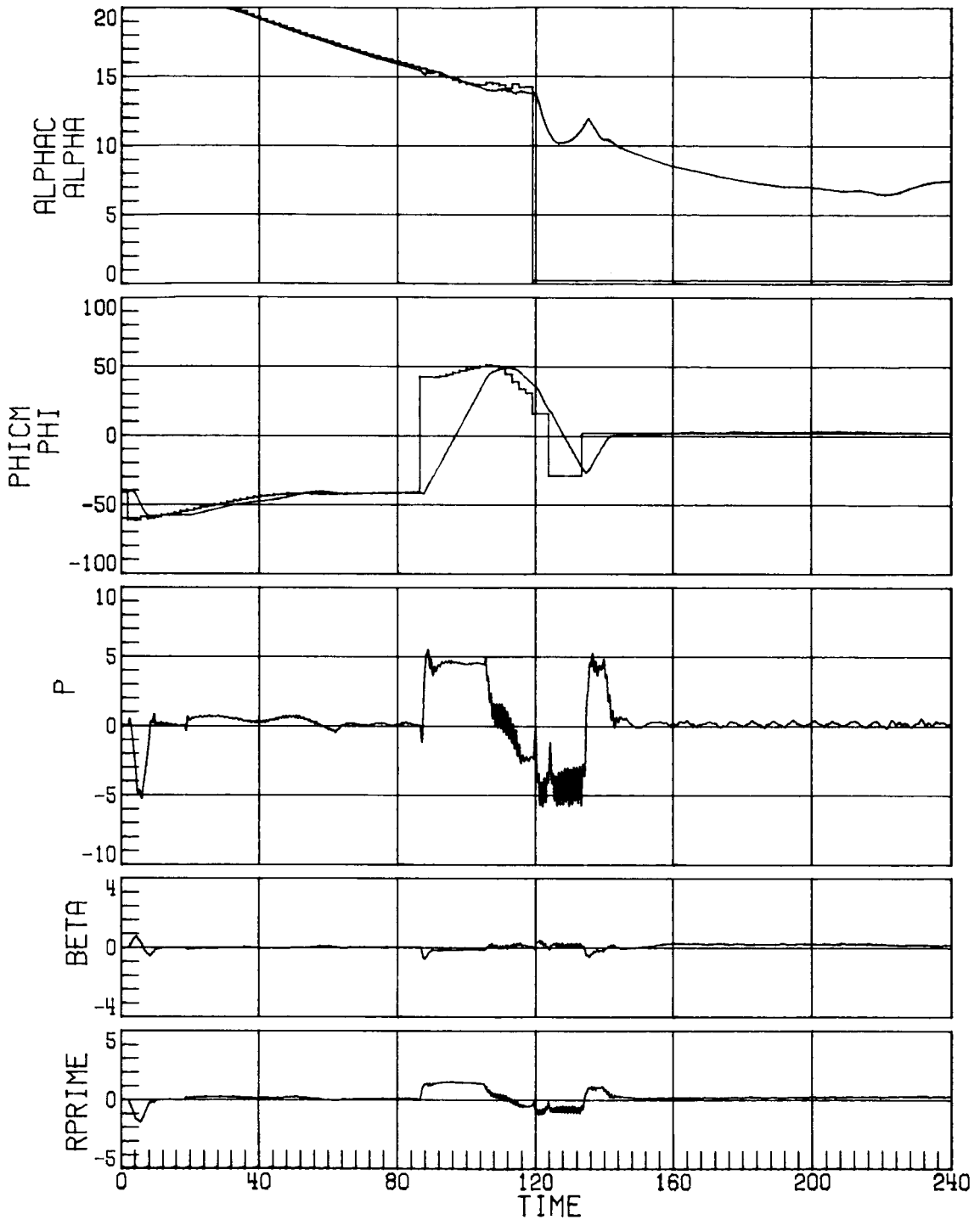

(d) Case 10; RCS uncertainty set 3.
Figure 18. Continued.

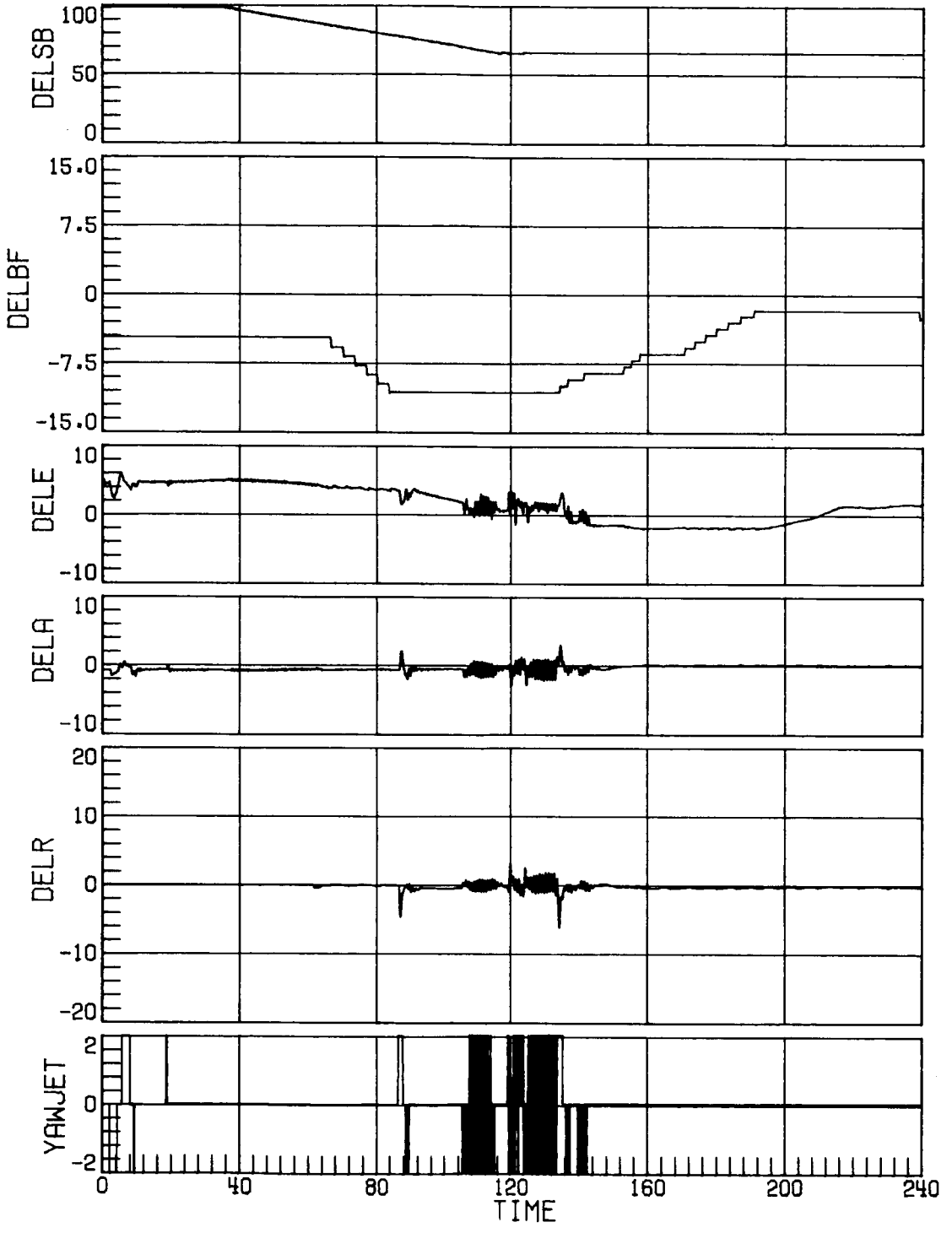

(d) Concluded.
Figure 18. Concluded.

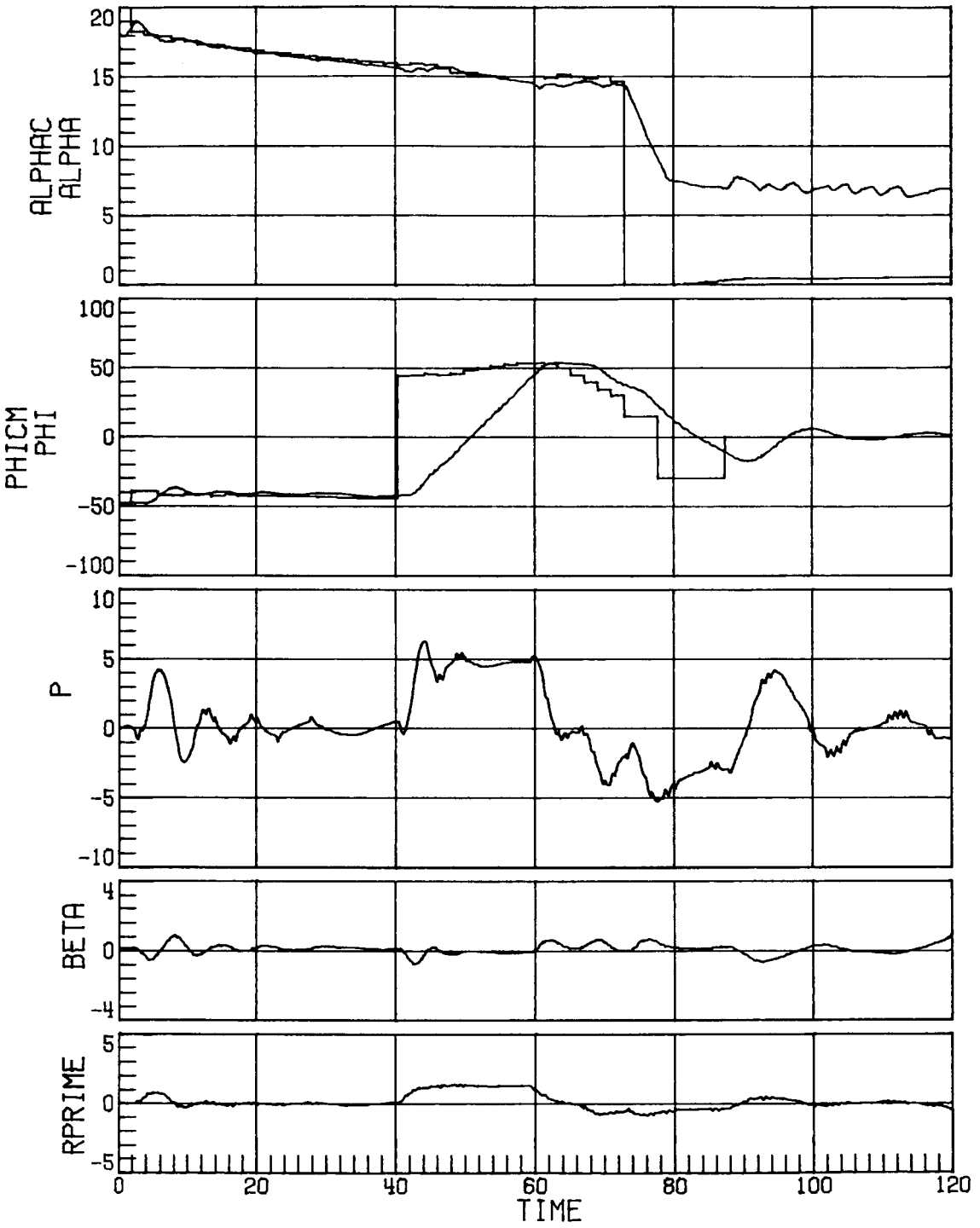

(a) Case 3; RCS uncertainty set 1.

Figure 19. Time-history response for Mach decreasing from 3.8 to 1.9 with decreased rudder effectiveness, negative pitch uncertainty, decreased side force due to β, and α 3° to 4° lower than nominal. Time in seconds.

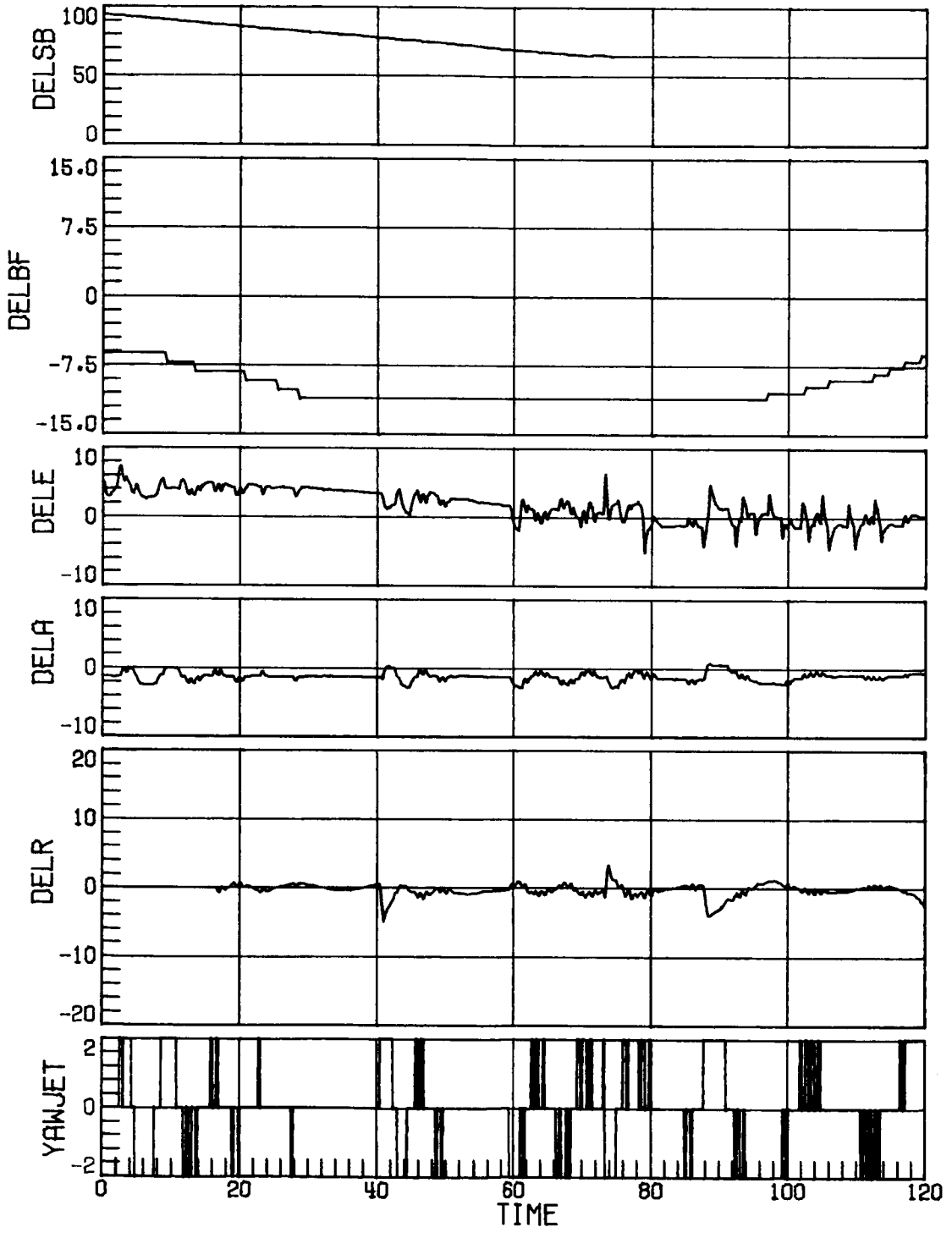

(a) Concluded.
Figure 19. Continued.

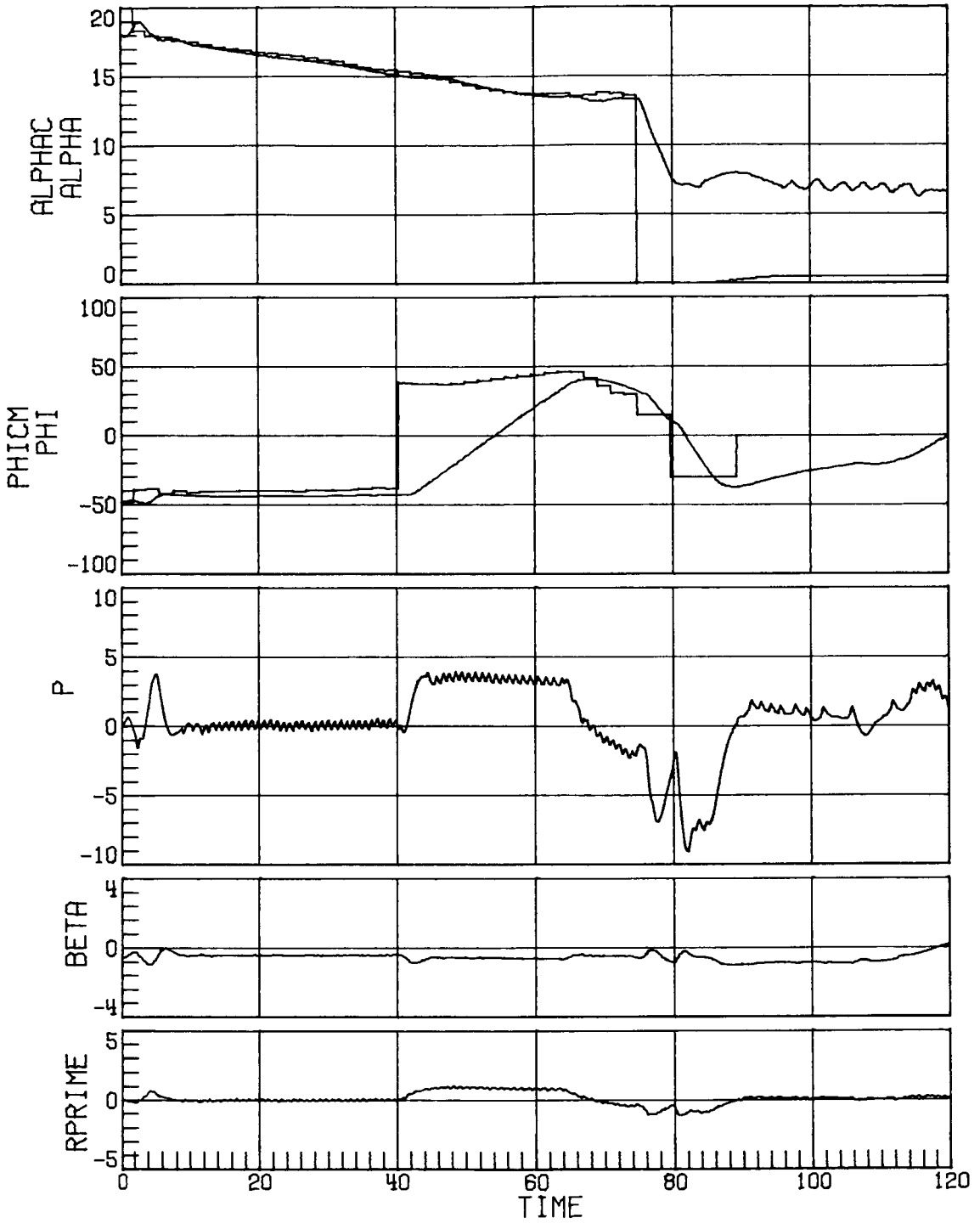

(b) Case 6; RCS uncertainty set 1.
Figure 19. Continued.

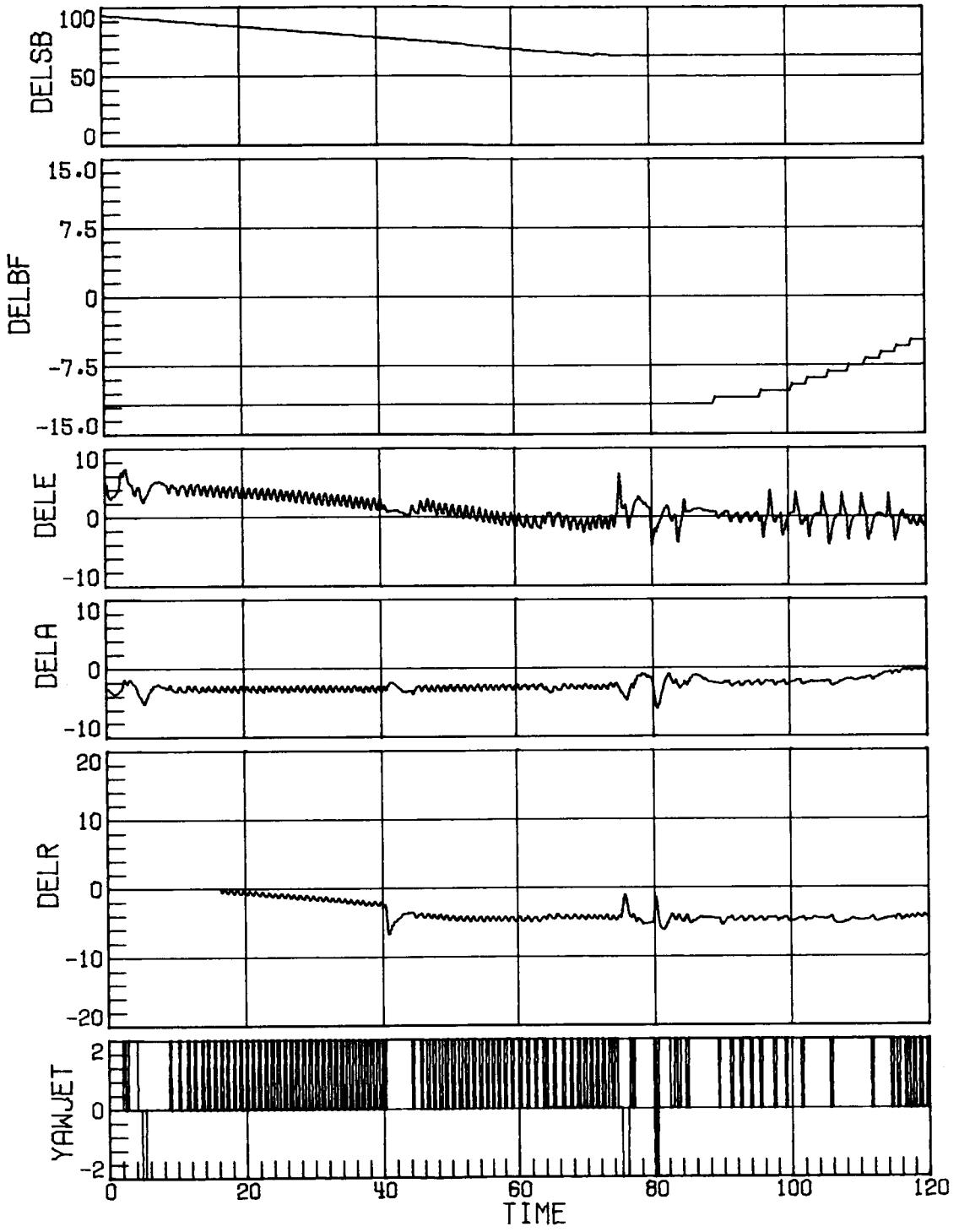

(b) Concluded.
Figure 19. Continued.

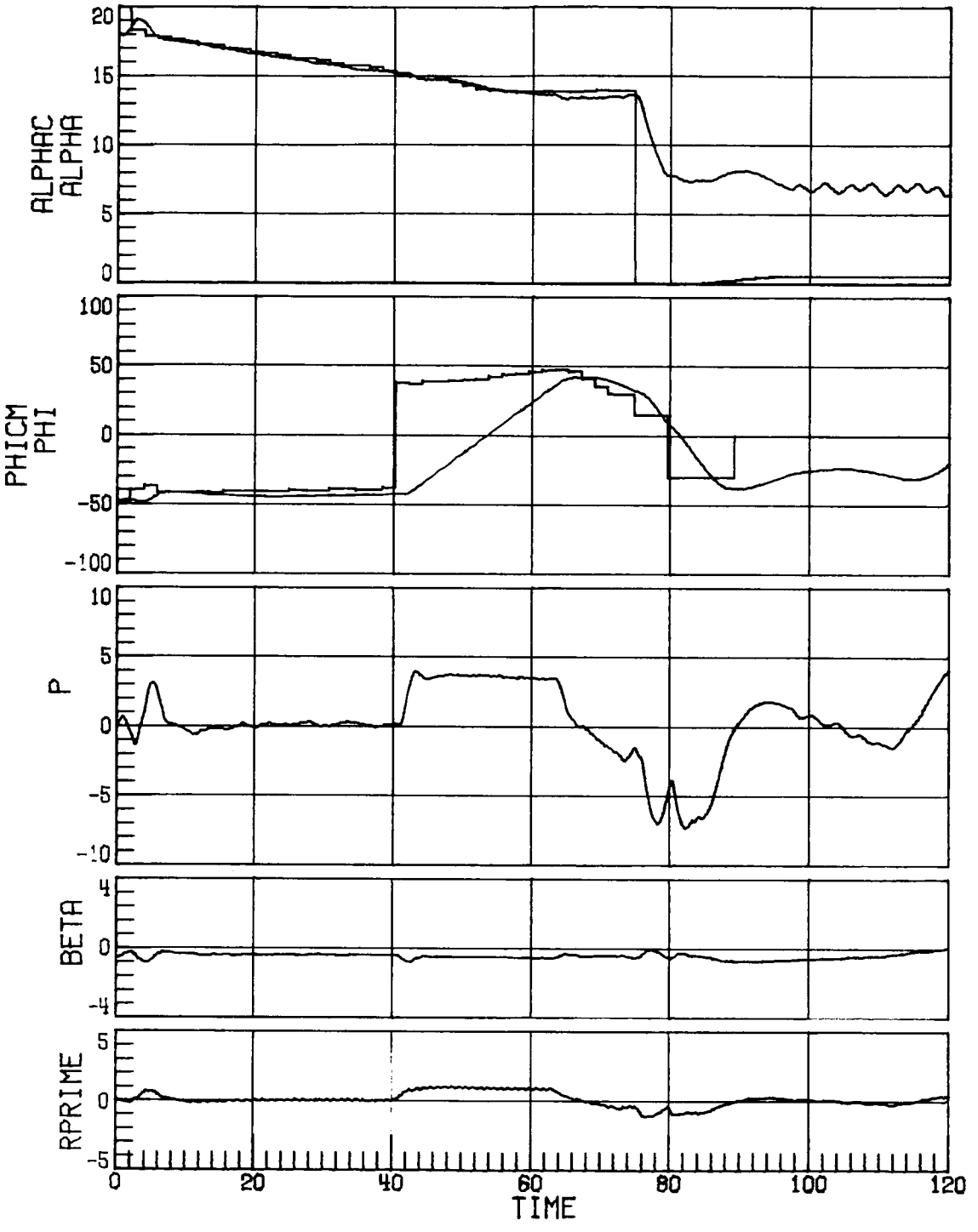

(c) Case 6; RCS uncertainty set 2.
Figure 19. Continued.

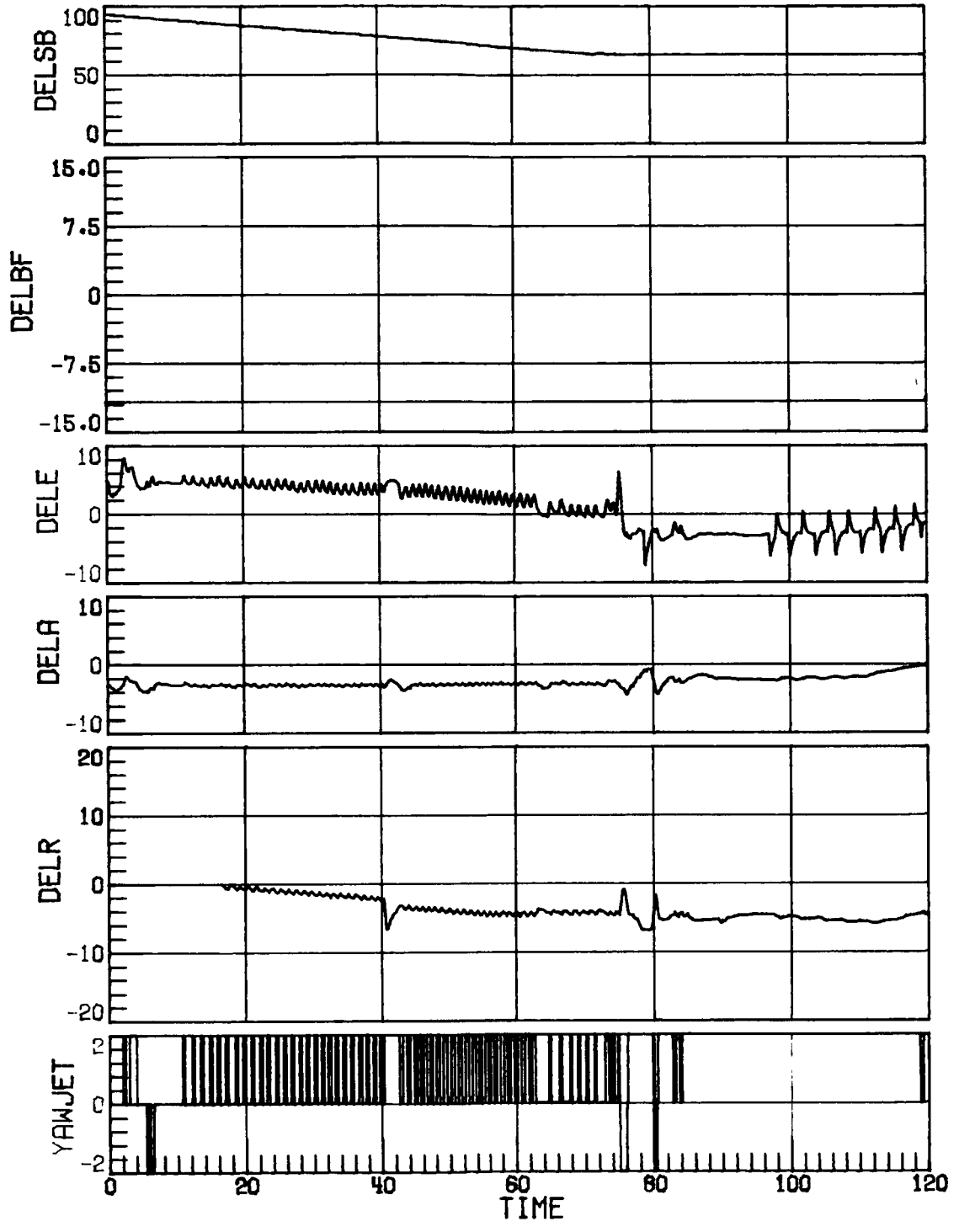

(c) Concluded.
Figure 19. Continued.

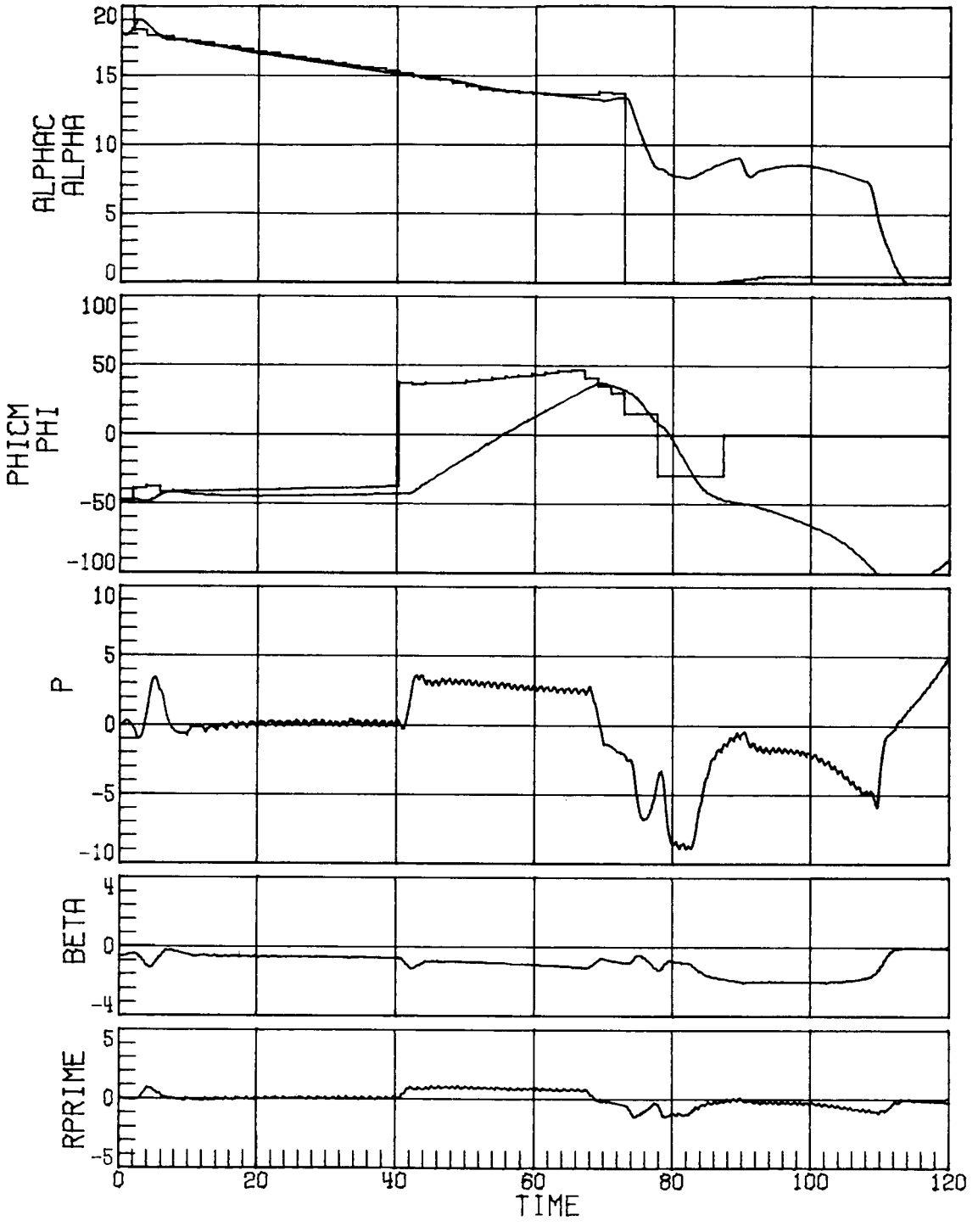

(d) Case 8; nominal RCS.
Figure 19. Continued.

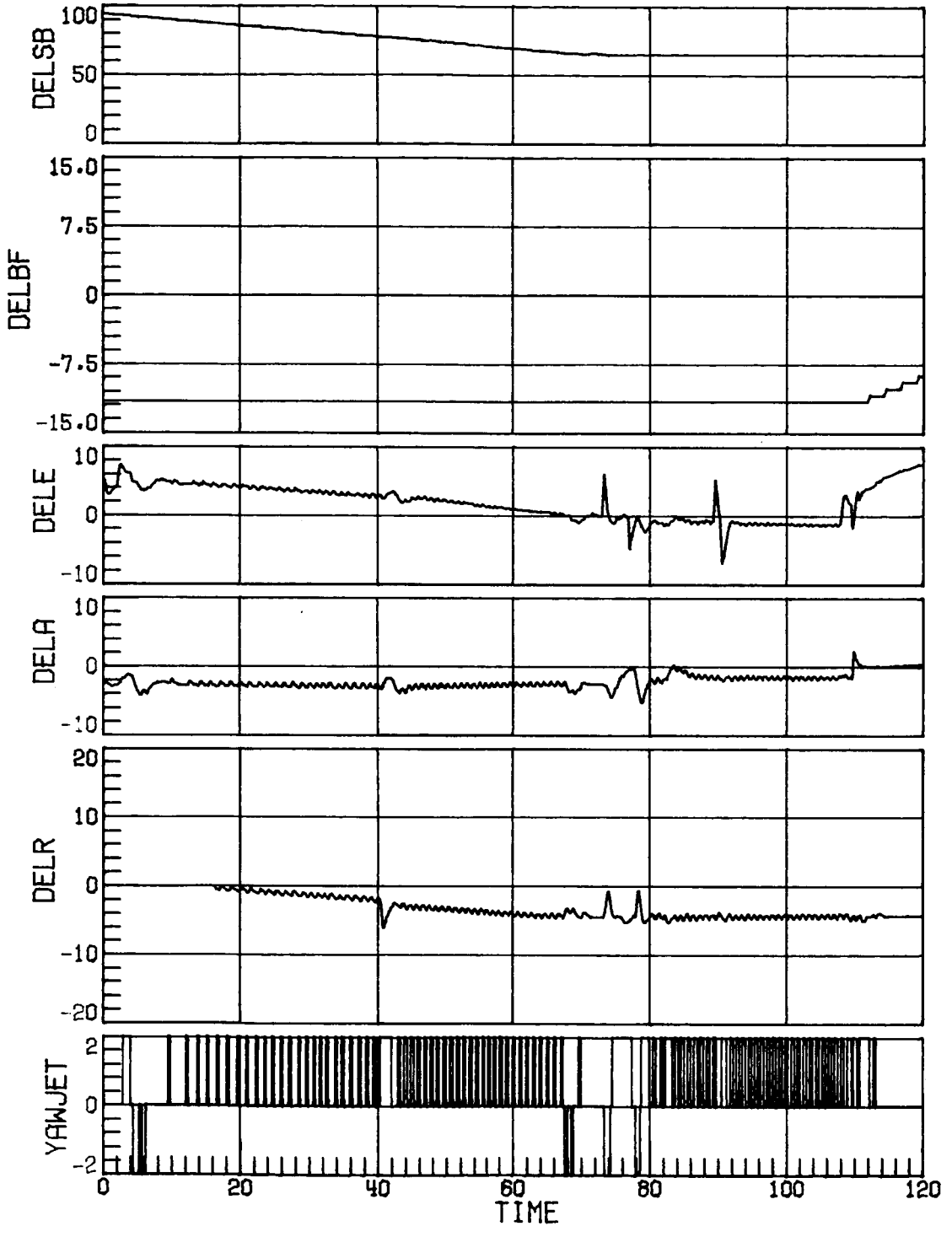

(d) Concluded.
Figure 19. Continued.

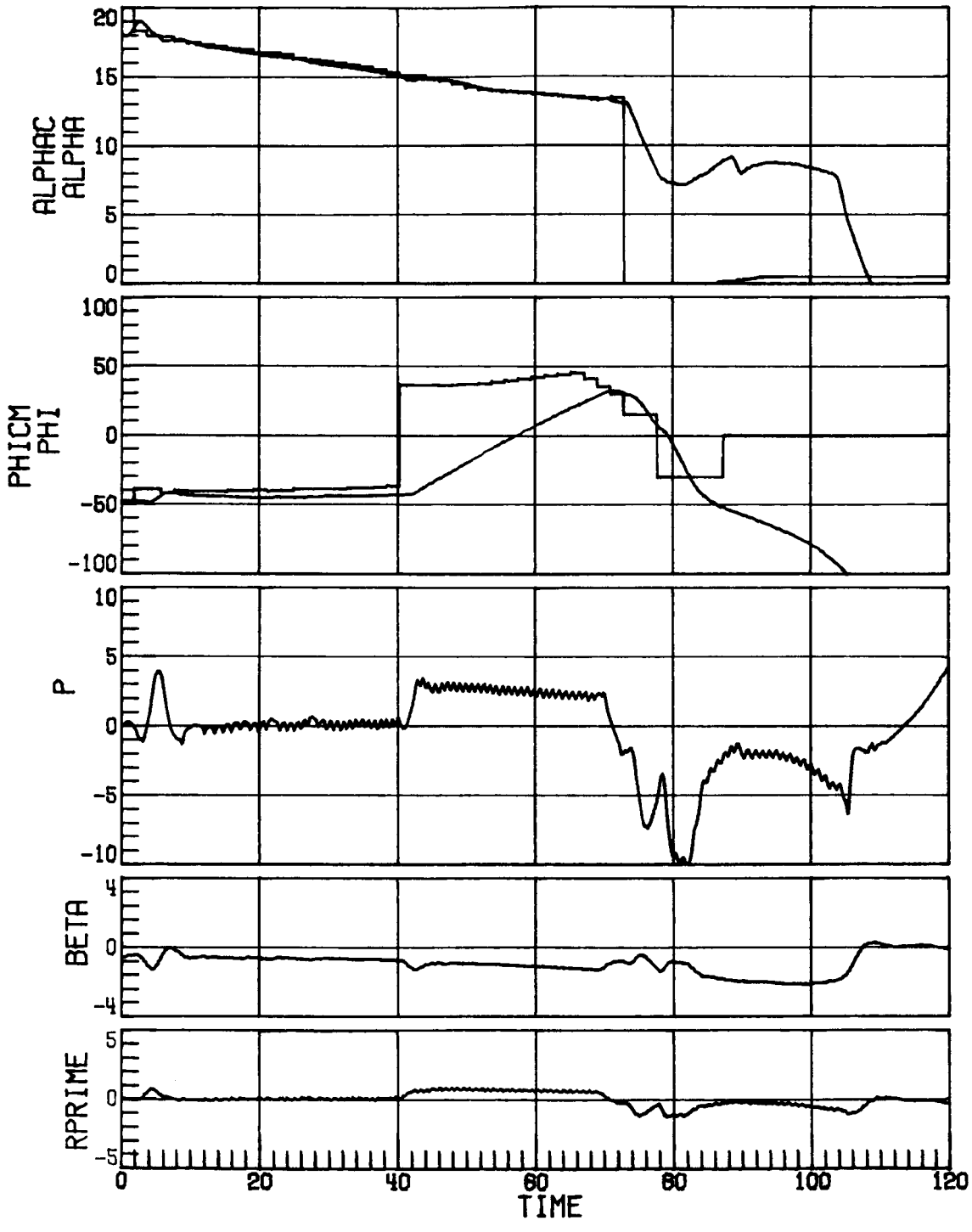

(e) Case 8; RCS uncertainty set 1.
Figure 19. Continued.

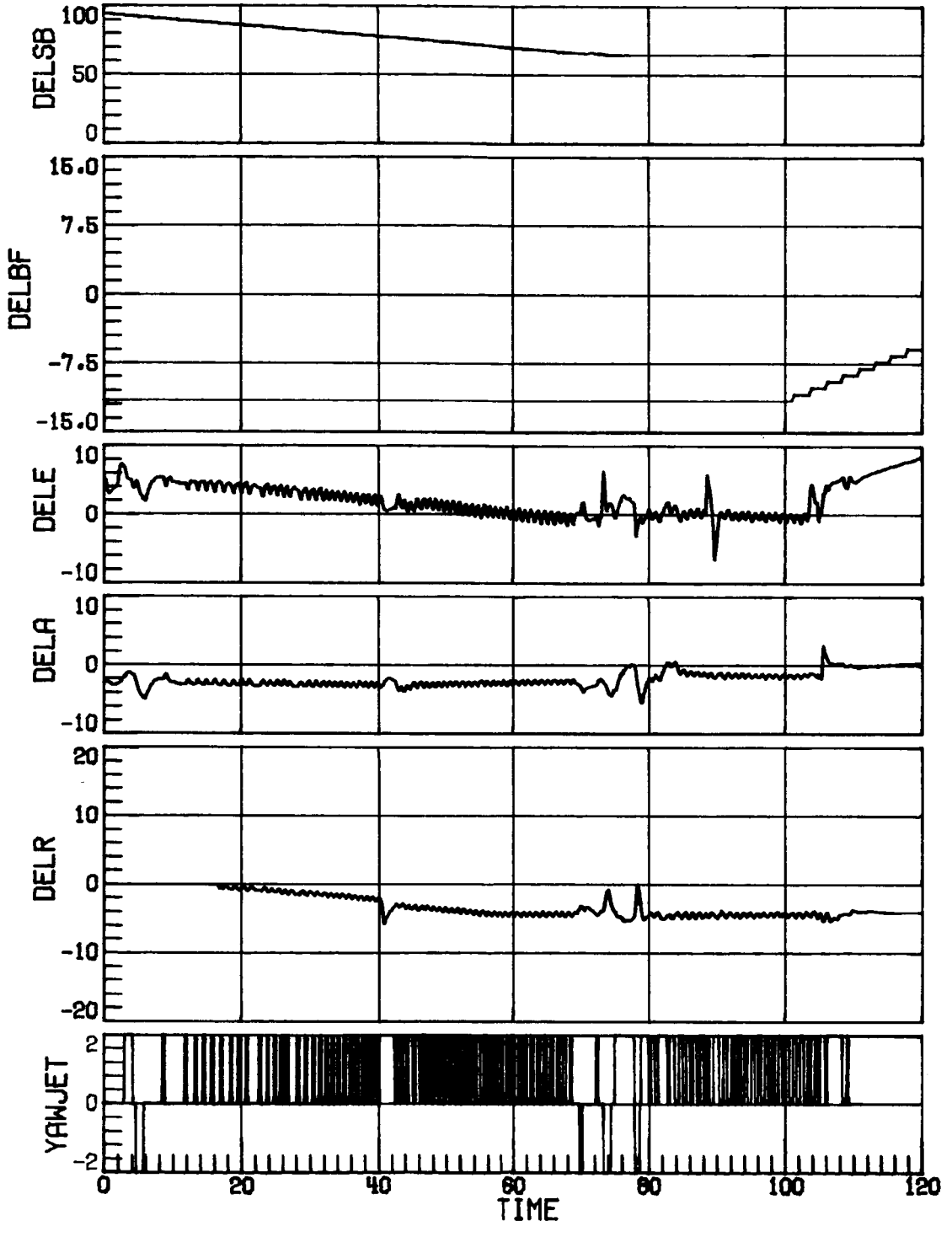

(e) Concluded.
Figure 19. Continued.

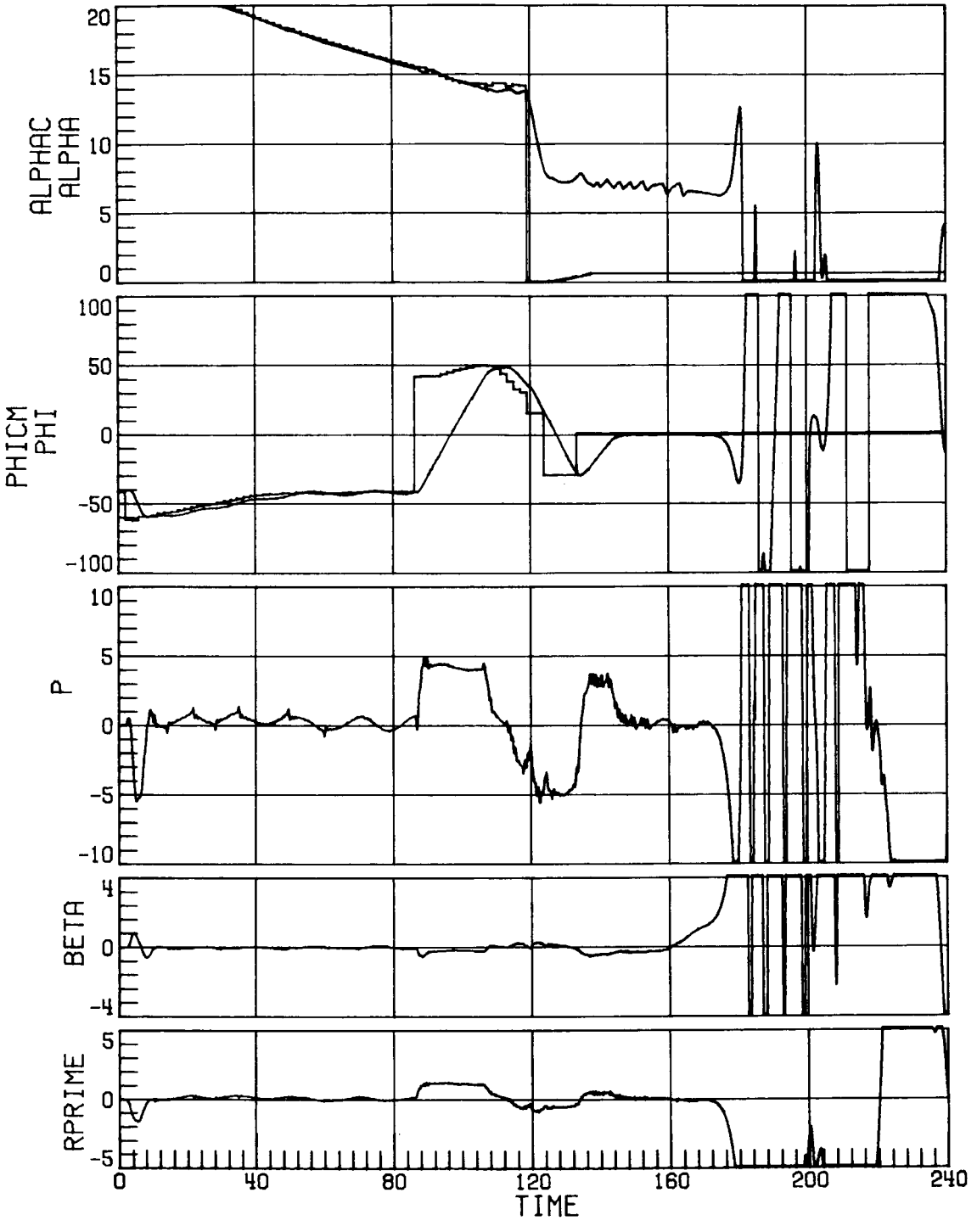

(f) Case 11; RCS uncertainty set 1; four jets operating; Mach decreasing from 4.6 to 1.8.
Figure 19. Continued.

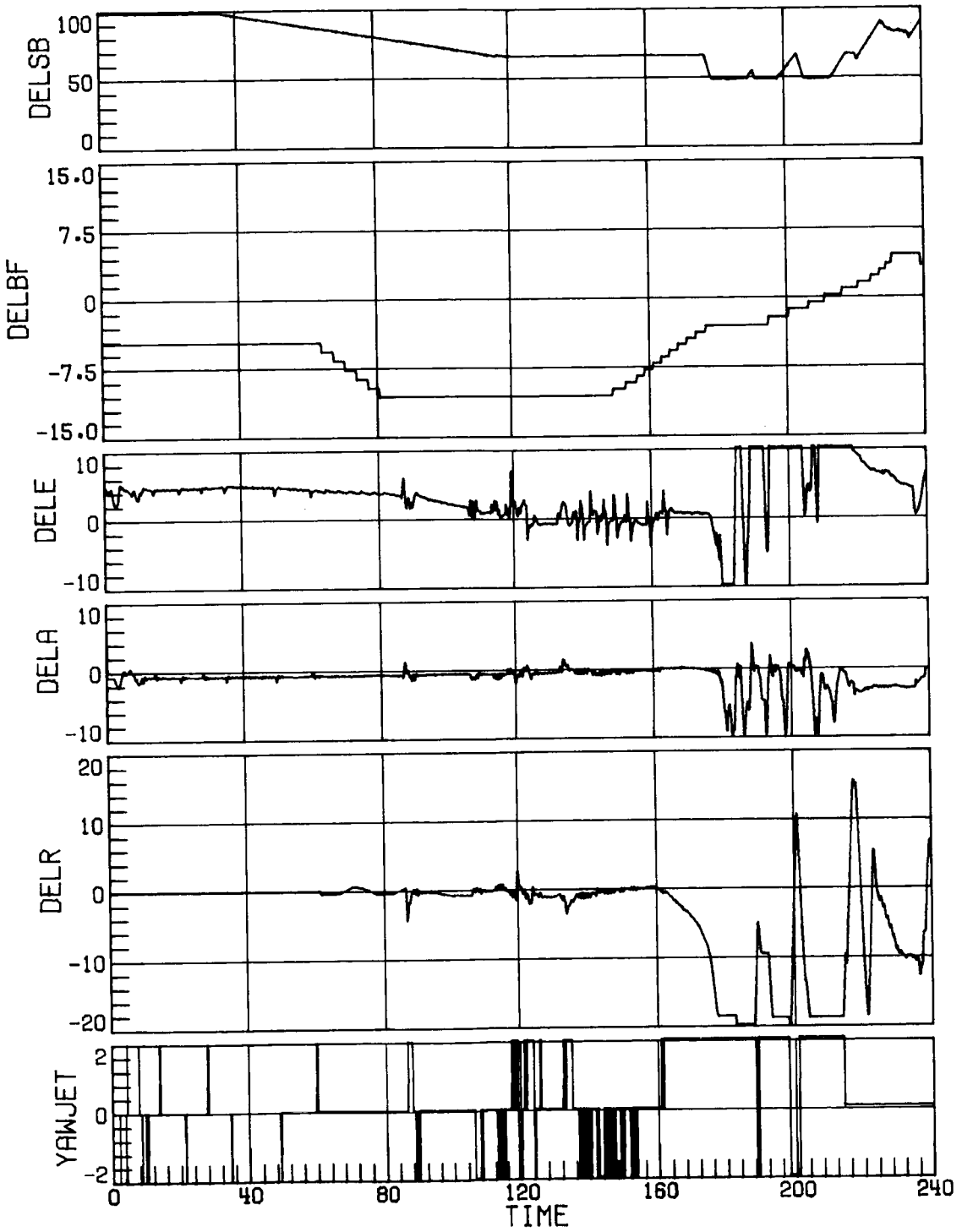

(f) Concluded.
Figure 19. Continued.

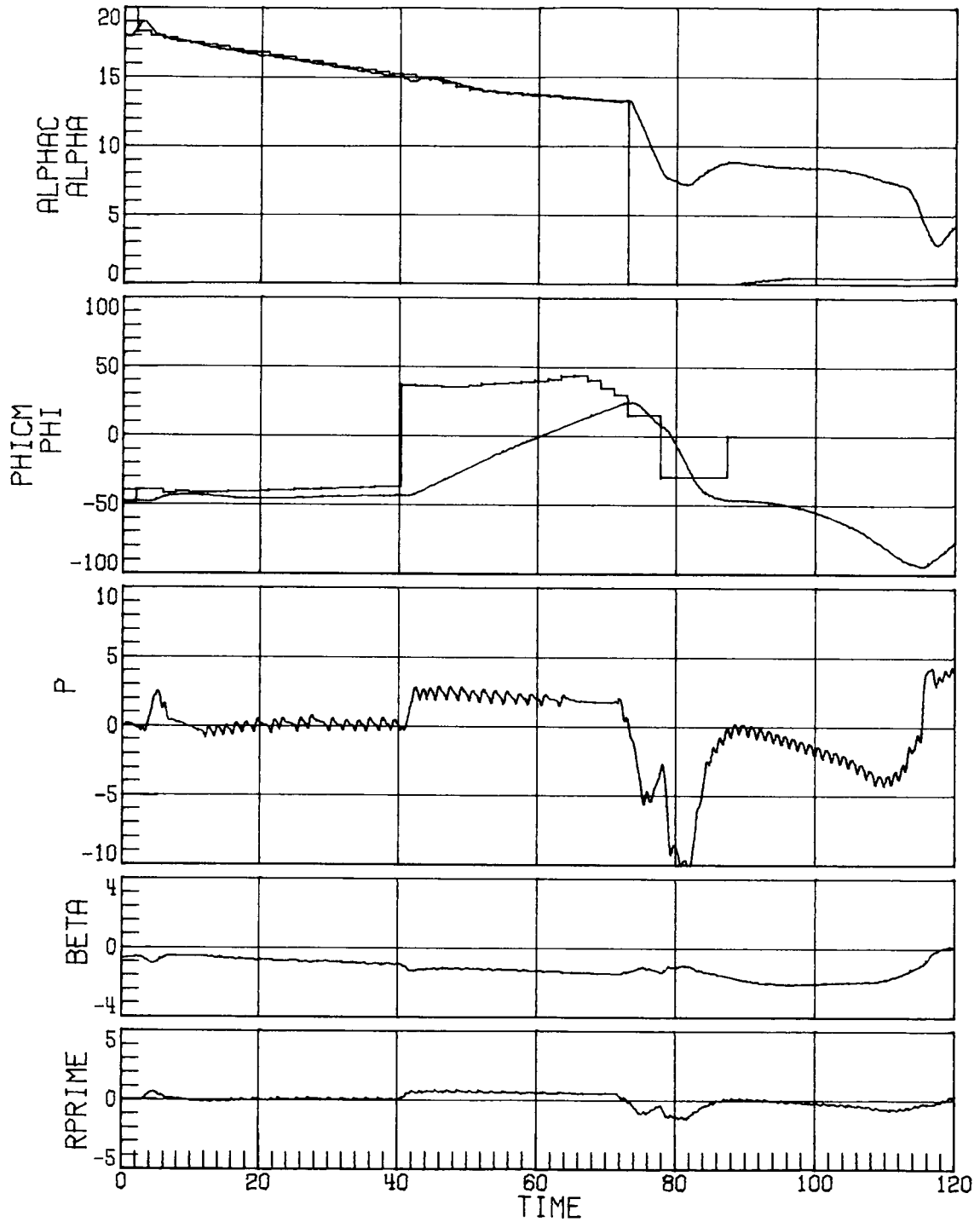

(g) Case 16; RCS uncertainty set 1.
Figure 19. Continued.

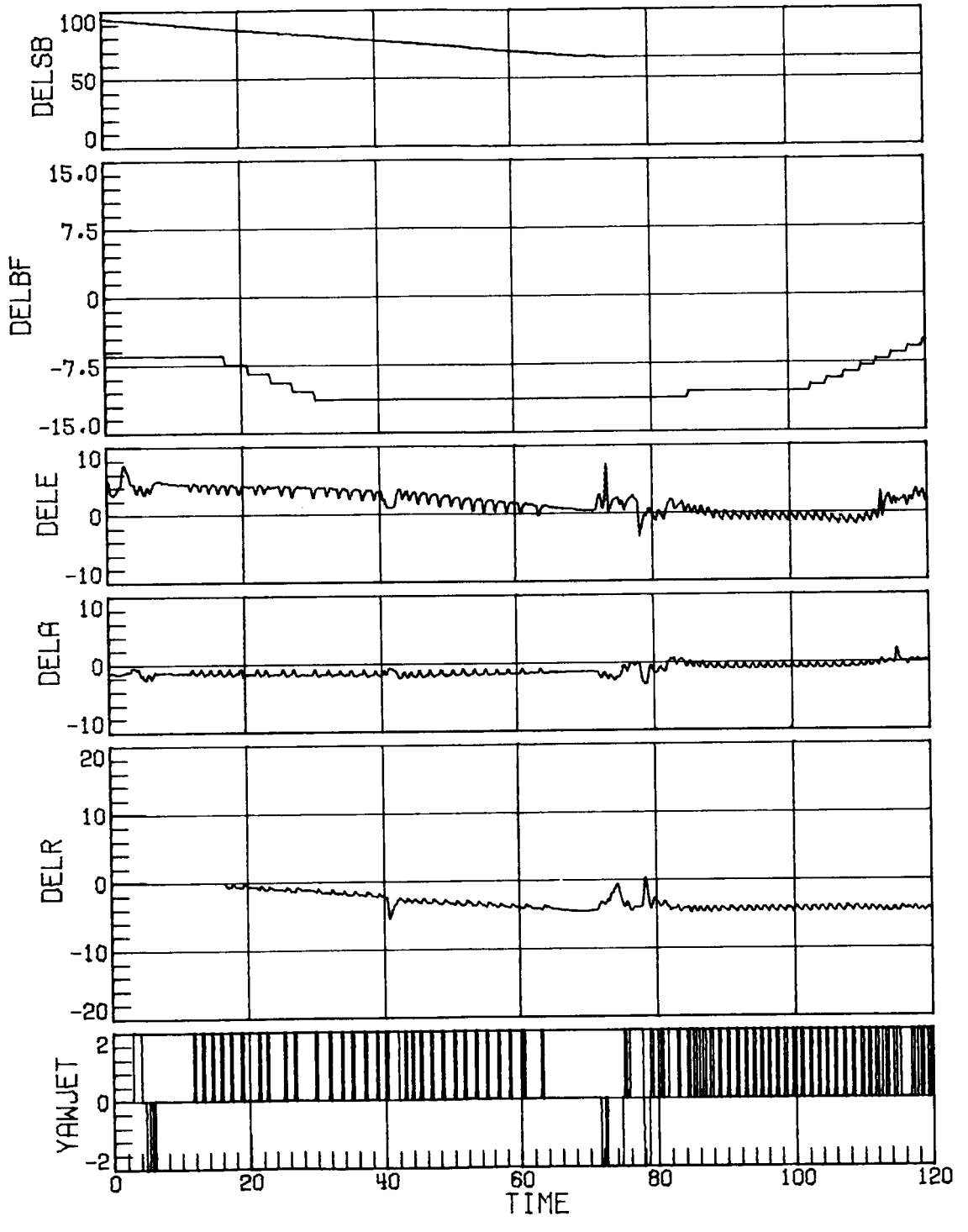

(g) Concluded.
Figure 19. Concluded.

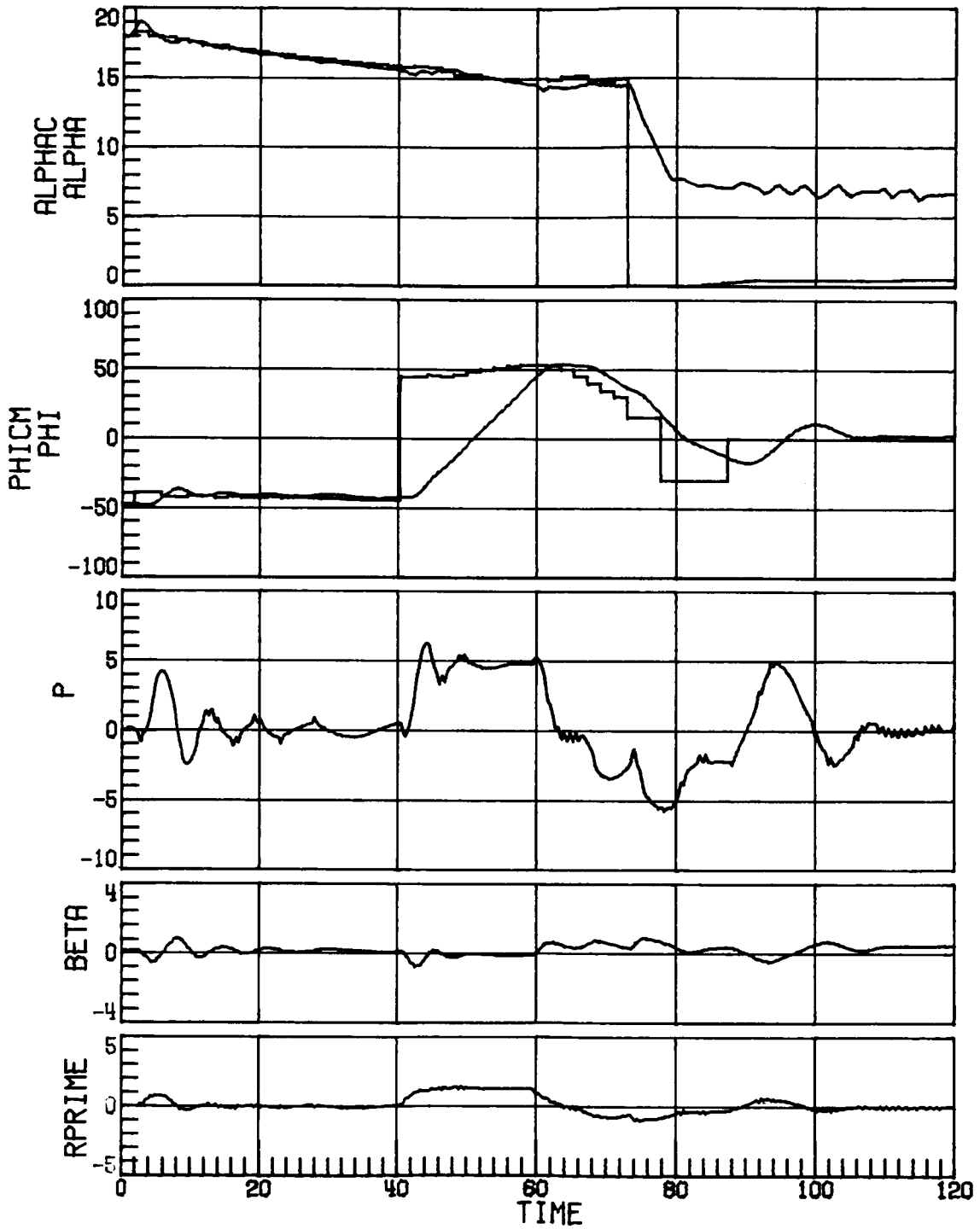

(a) Case 3; RCS uncertainty set 1.

Figure 20. Time-history response for Mach decreasing from 3.8 to 1.8 with decreased rudder effectiveness, negative pitch uncertainty, decreased side force due to β, α 3° to 4° lower than nominal, and control-system trim modifications. Time in seconds.

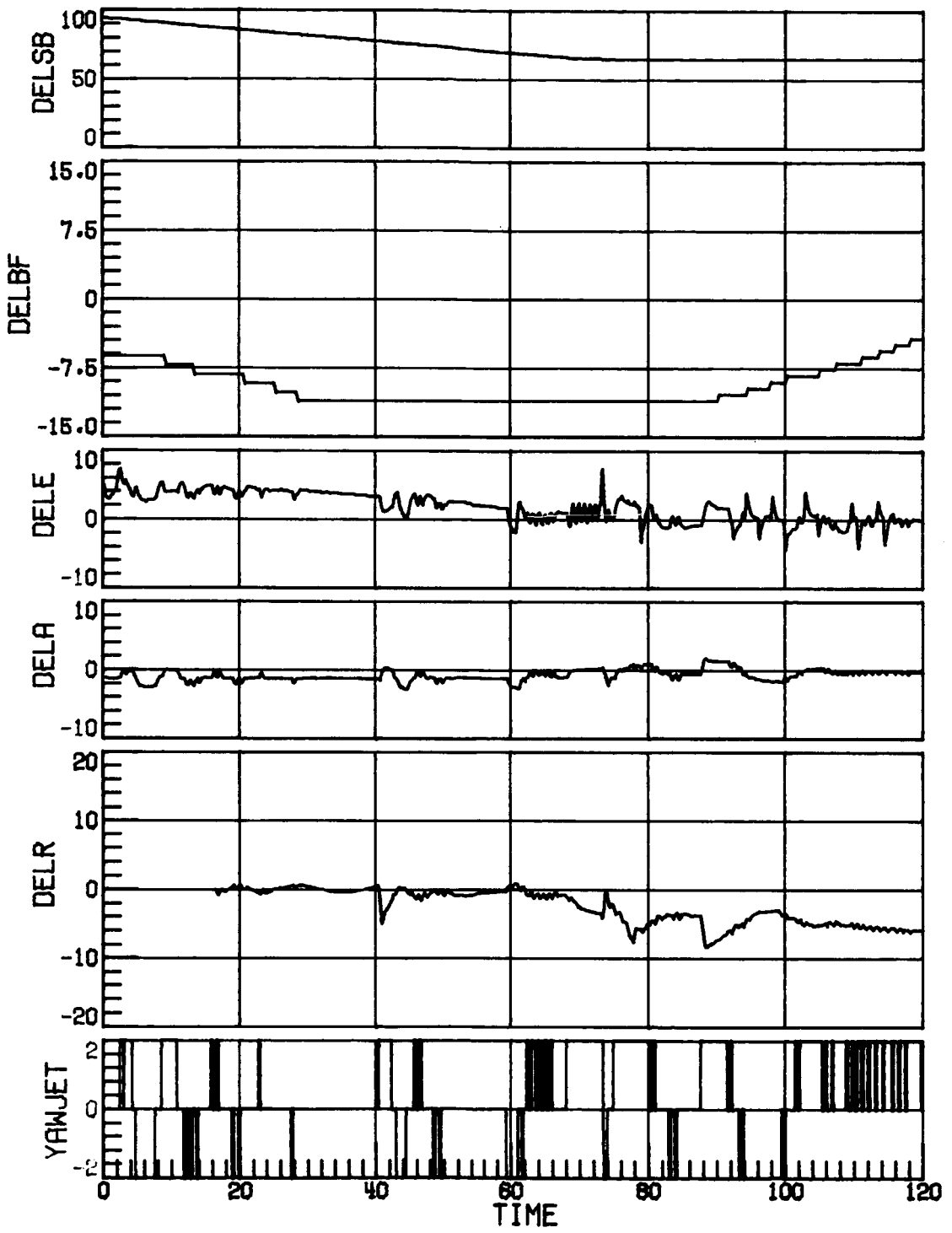

(a) Concluded.
Figure 20. Continued.

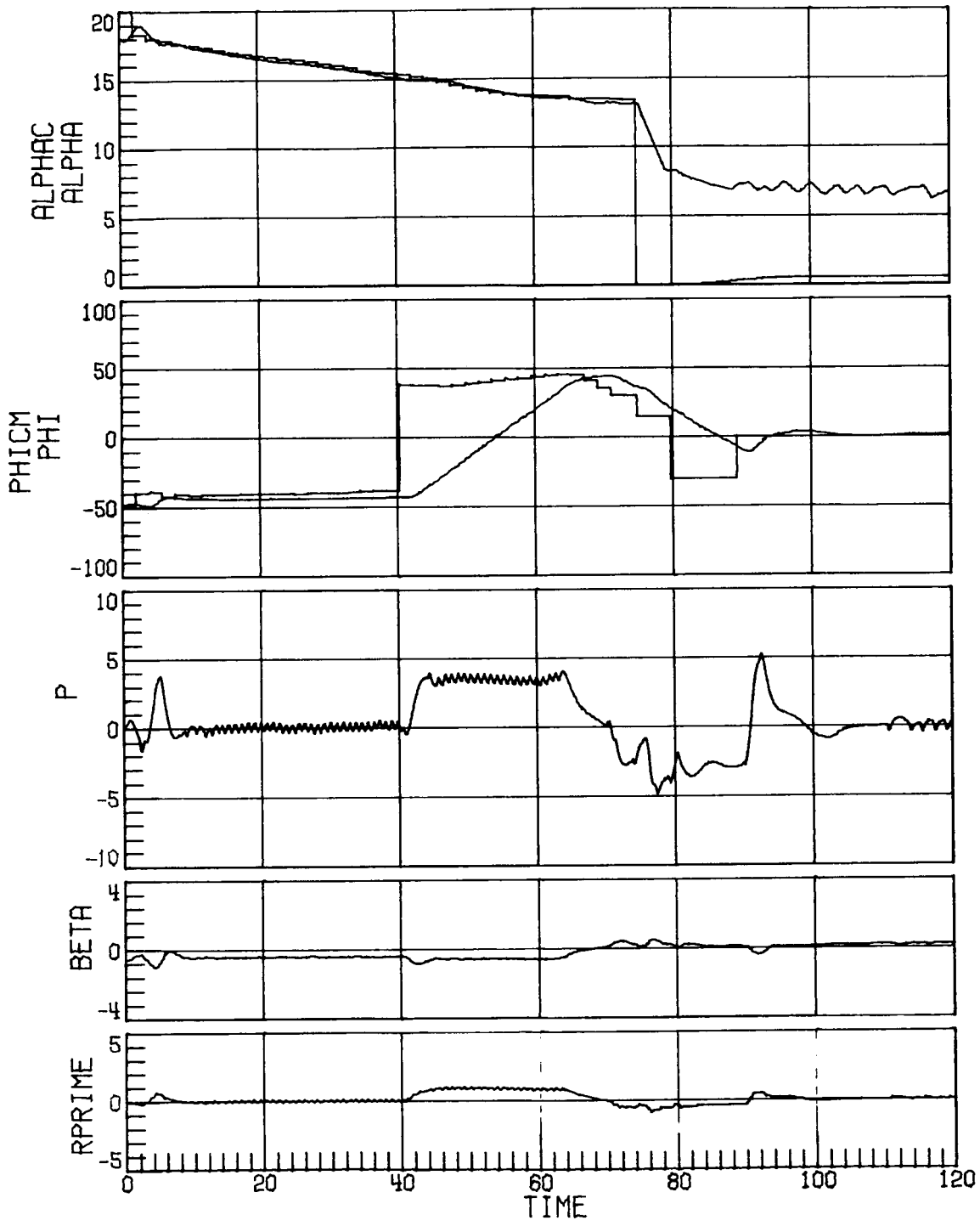

(b) Case 6; RCS uncertainty set 1.
Figure 20. Continued.

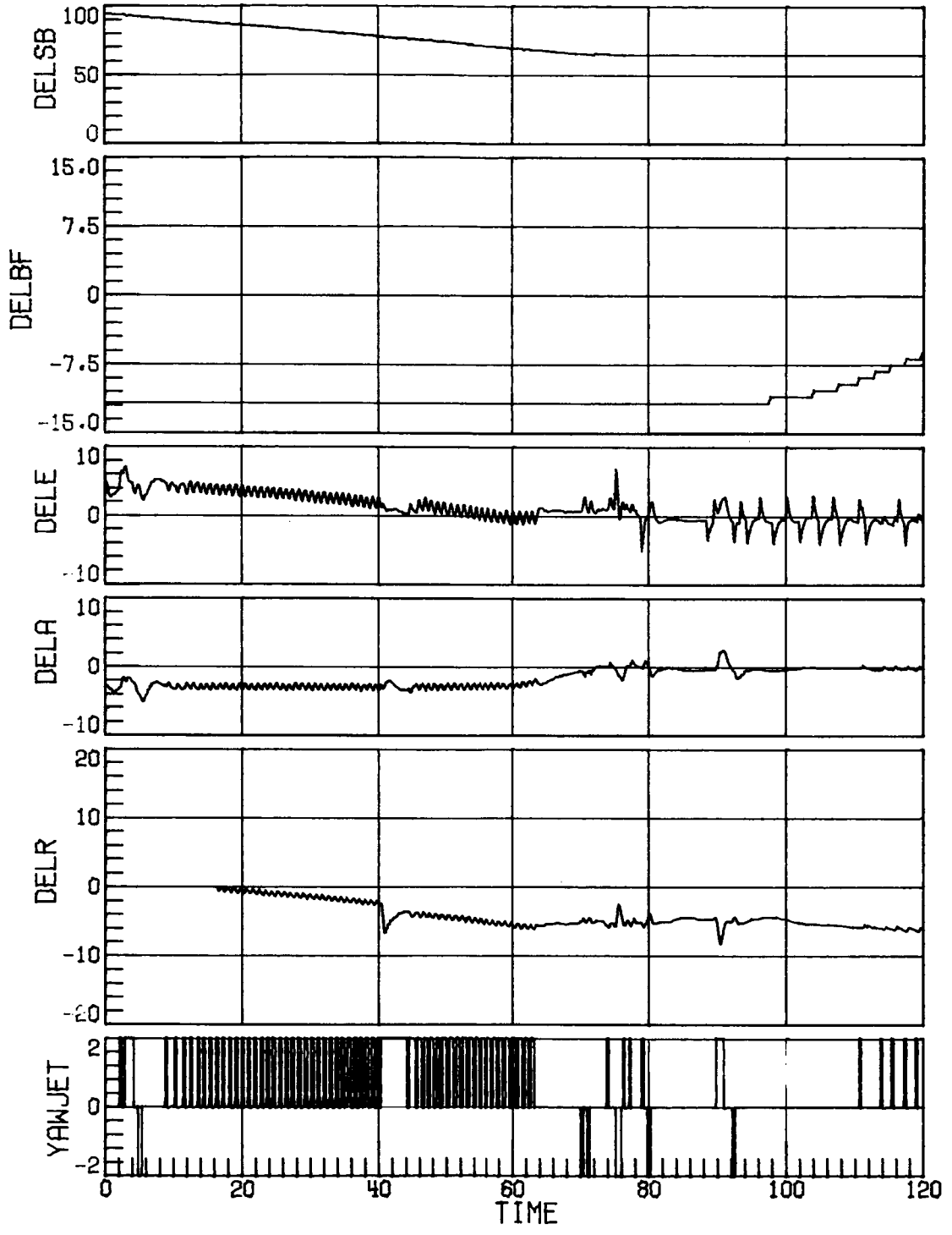

(b) Concluded.
Figure 20. Continued.

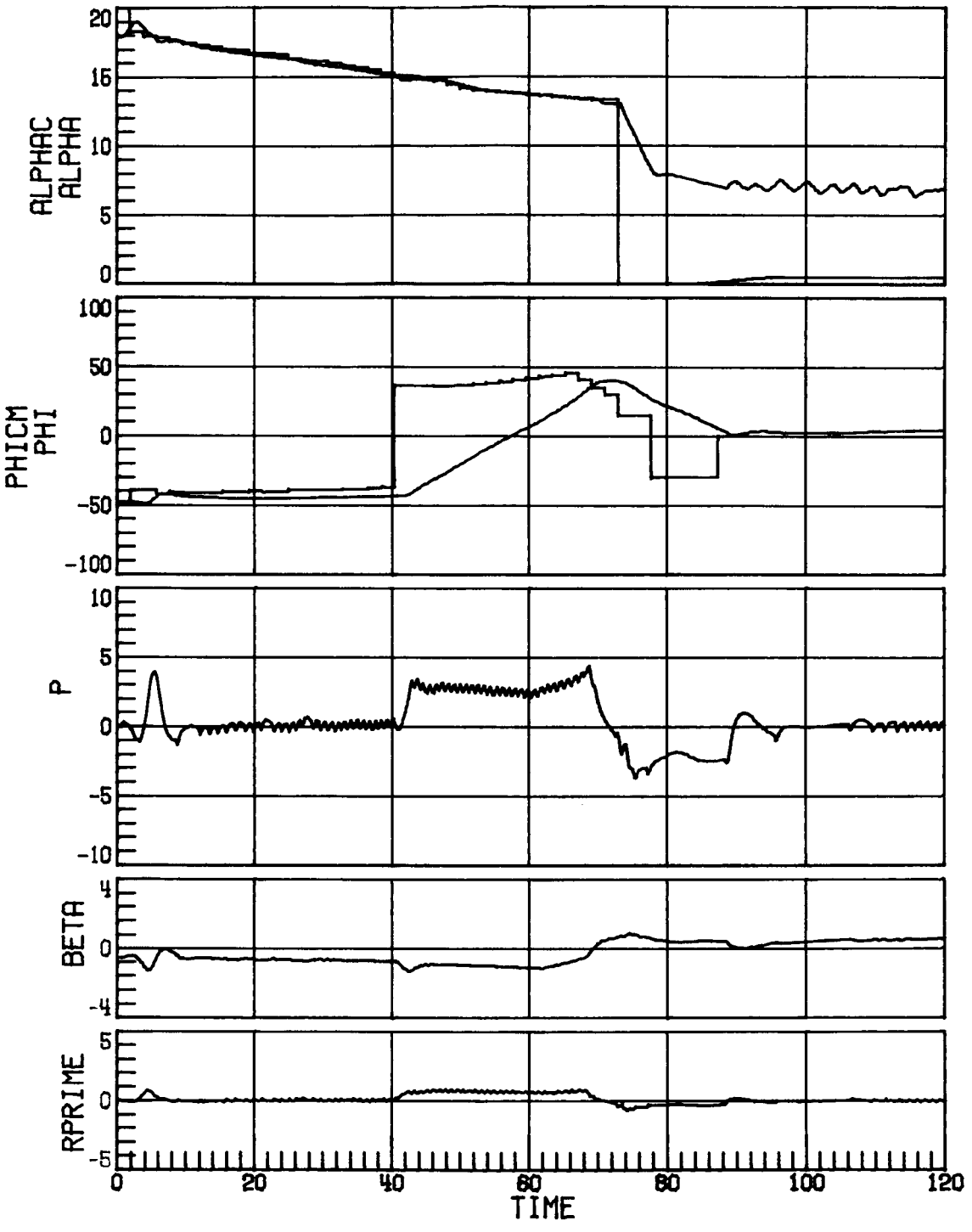

(c) Case 8; RCS uncertainty set 1.
Figure 20. Continued.

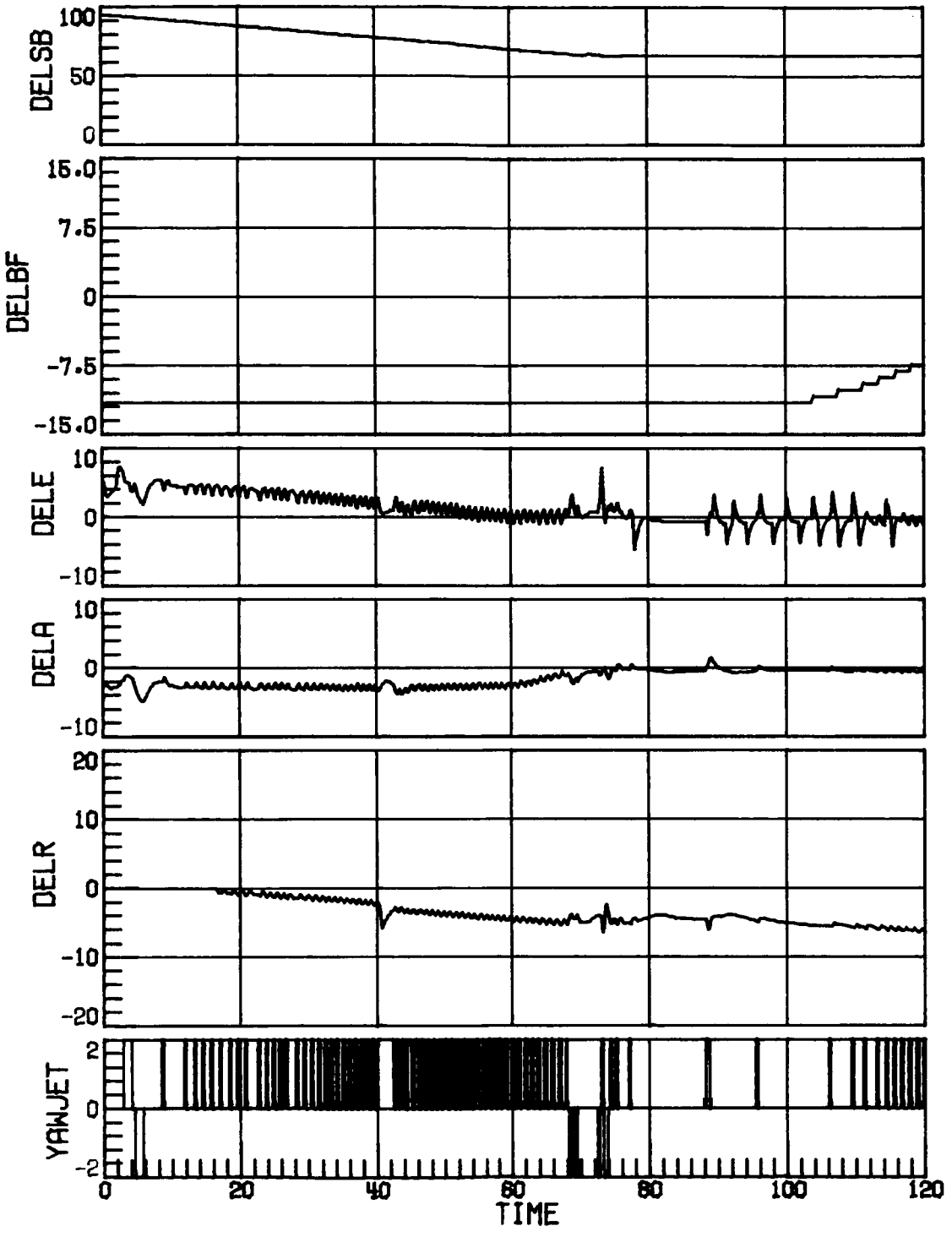

(c) Concluded.
Figure 20. Continued.

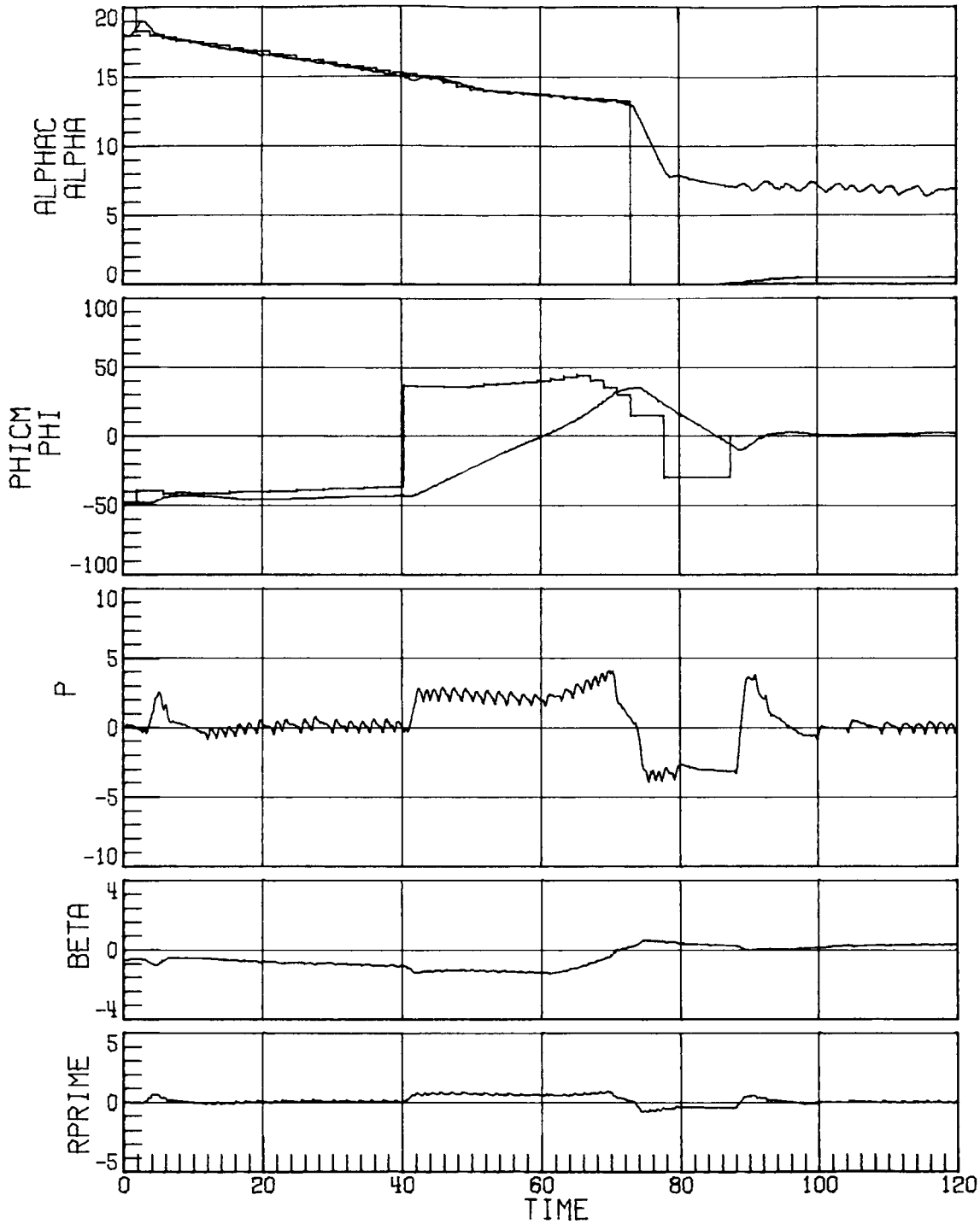

(d) Case 16; RCS uncertainty set 1.
Figure 20. Continued.

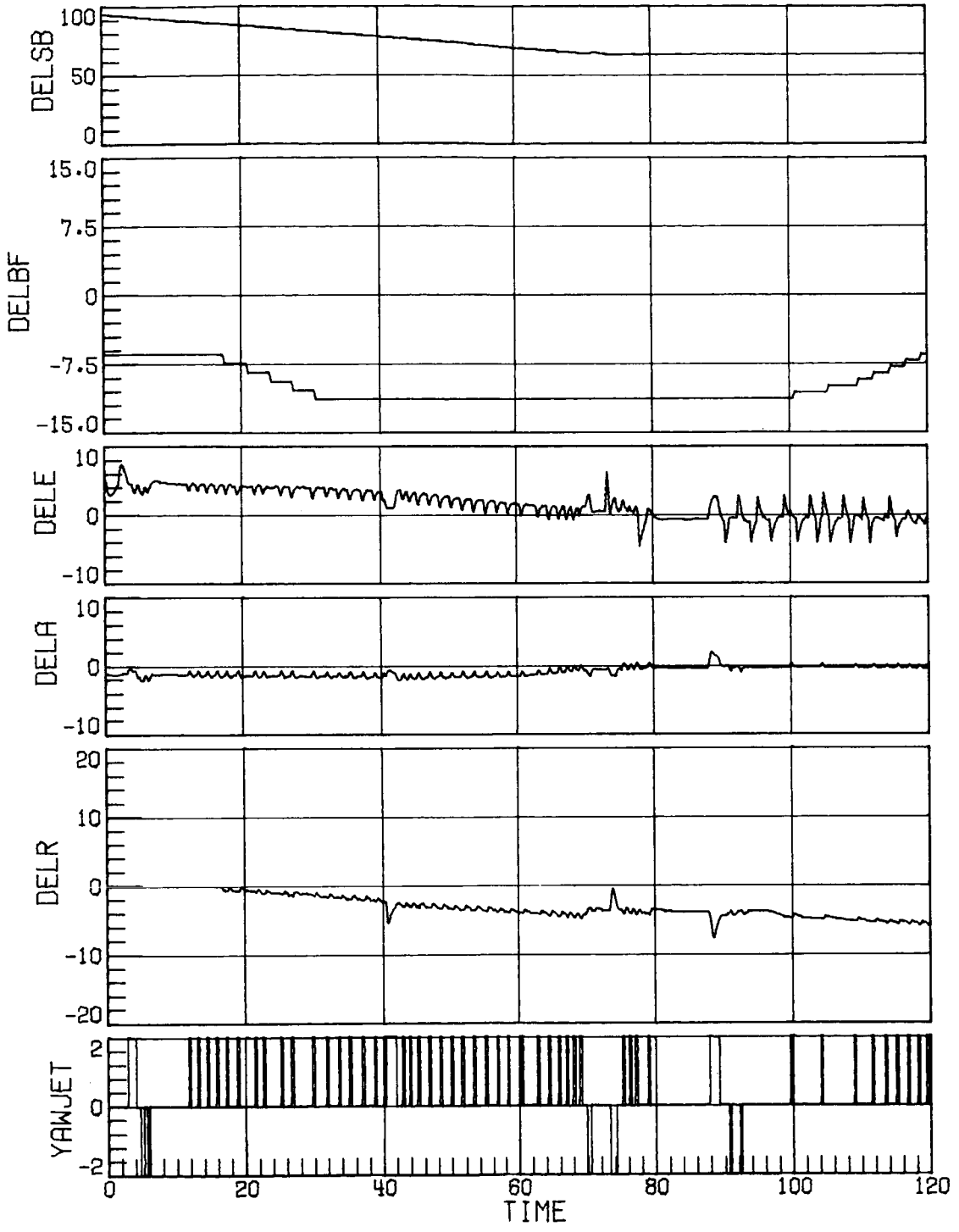

(d) Concluded.
Figure 20. Concluded.

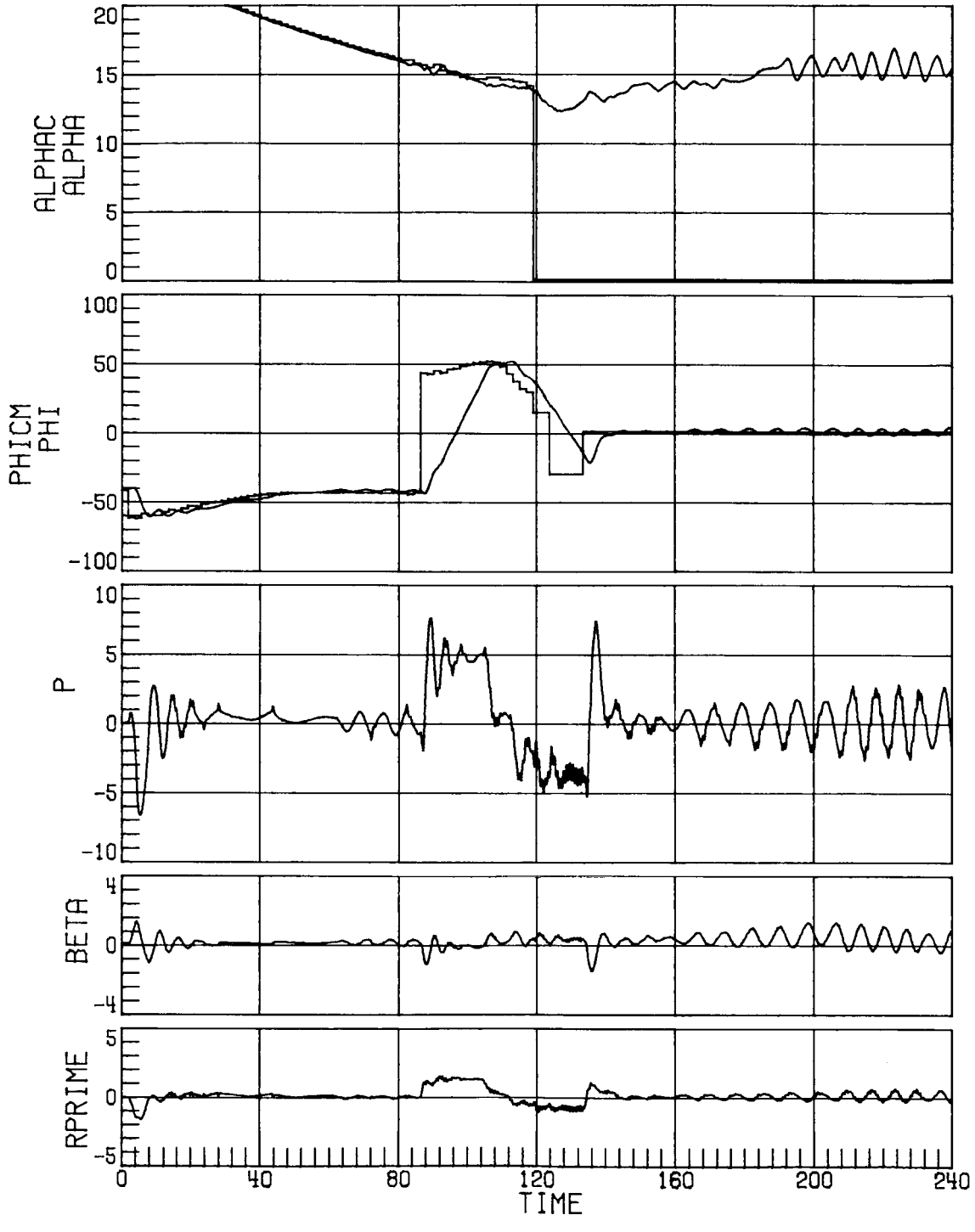

(a) Case 3; RCS uncertainty set 3.

Figure 21. Time-history response for Mach decreasing from 4.6 to 1.0 with increased rudder effectiveness, negative pitch uncertainty, decreased side force due to β, and α 3° to 7° higher than nominal. Time in seconds.

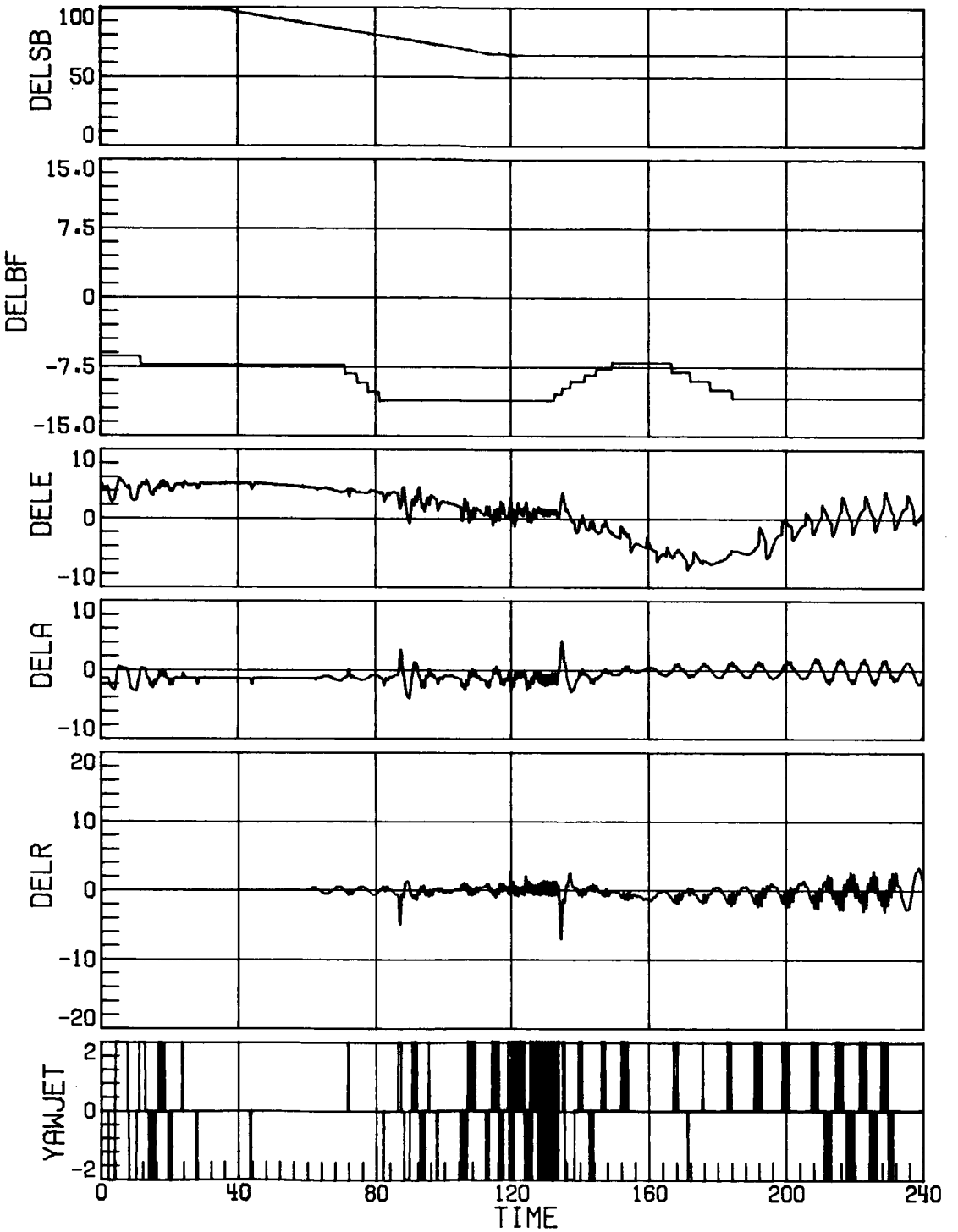

(a) Concluded.
Figure 21. Continued.

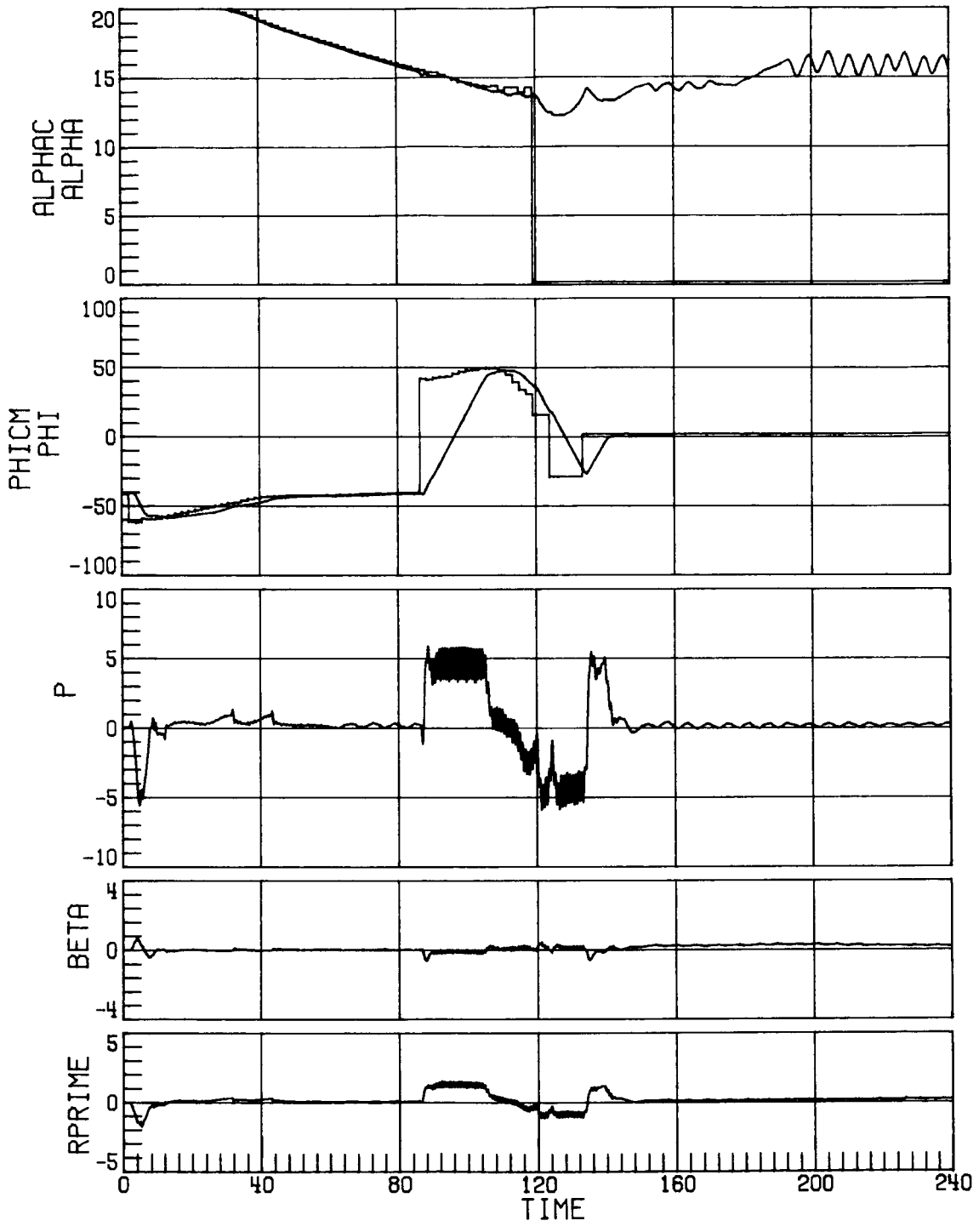

(b) Case 9; RCS uncertainty set 3.
Figure 21. Continued.

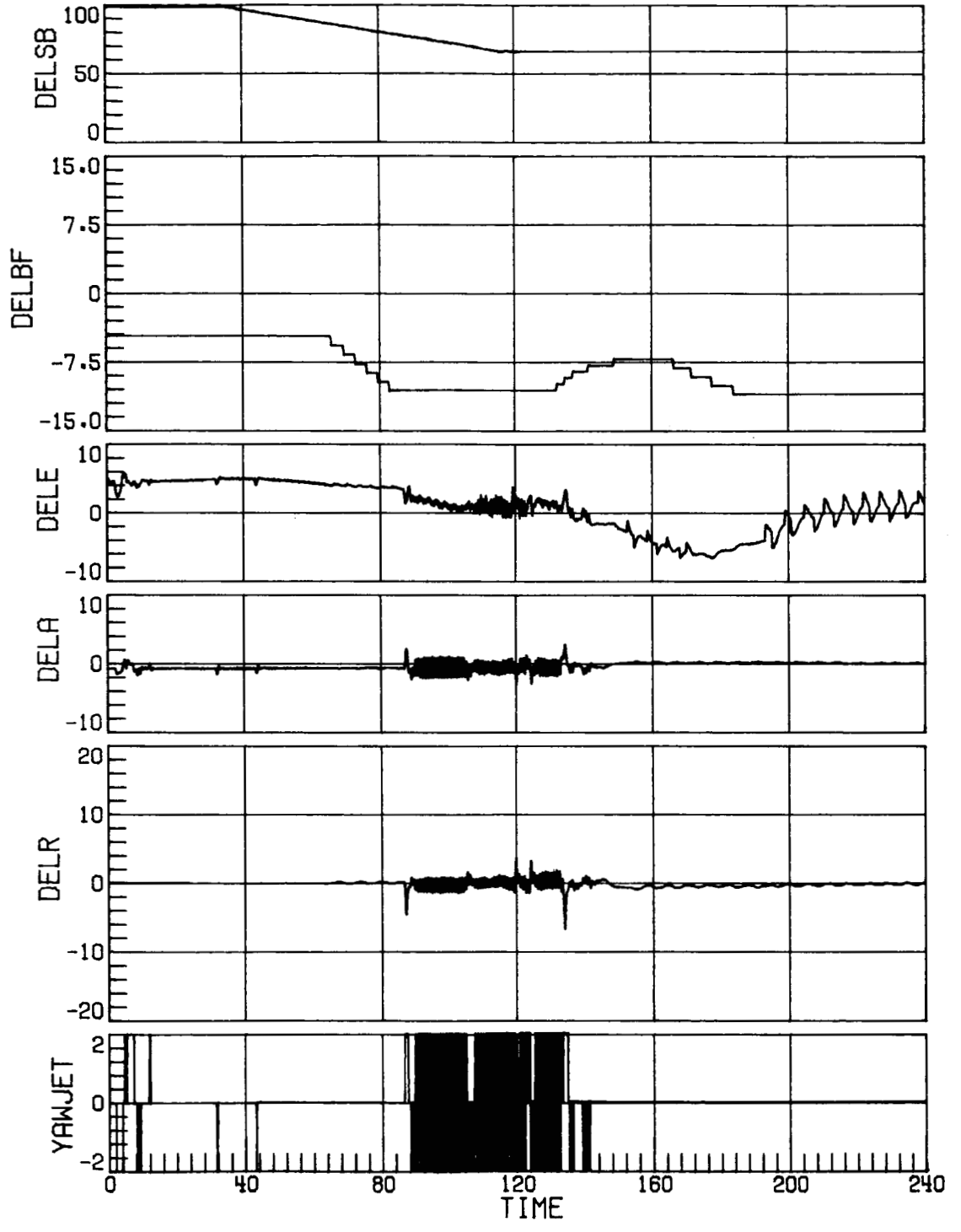

(b) Concluded.
Figure 21. Continued.

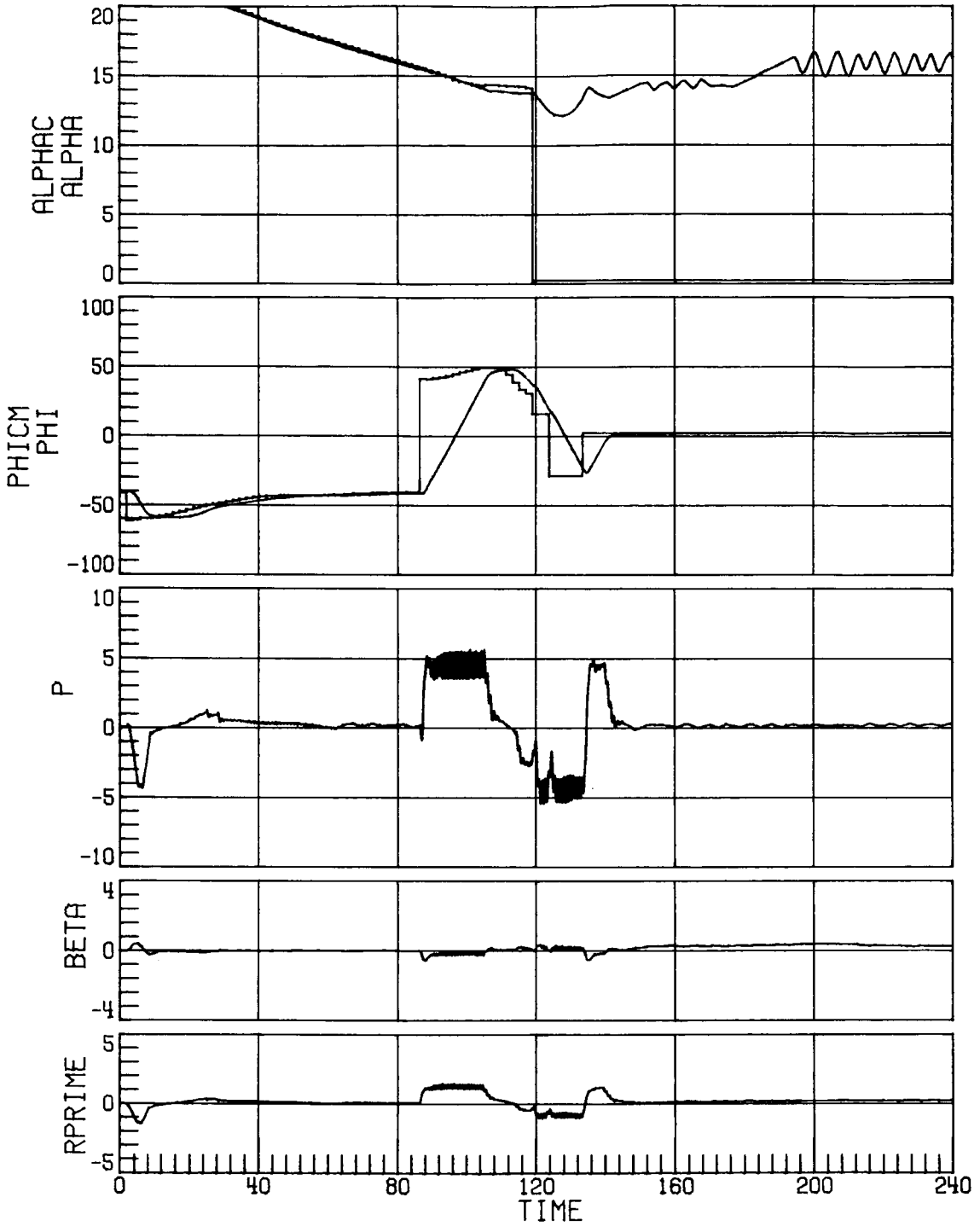

(c) Case 10; nominal RCS.
Figure 21. Continued.

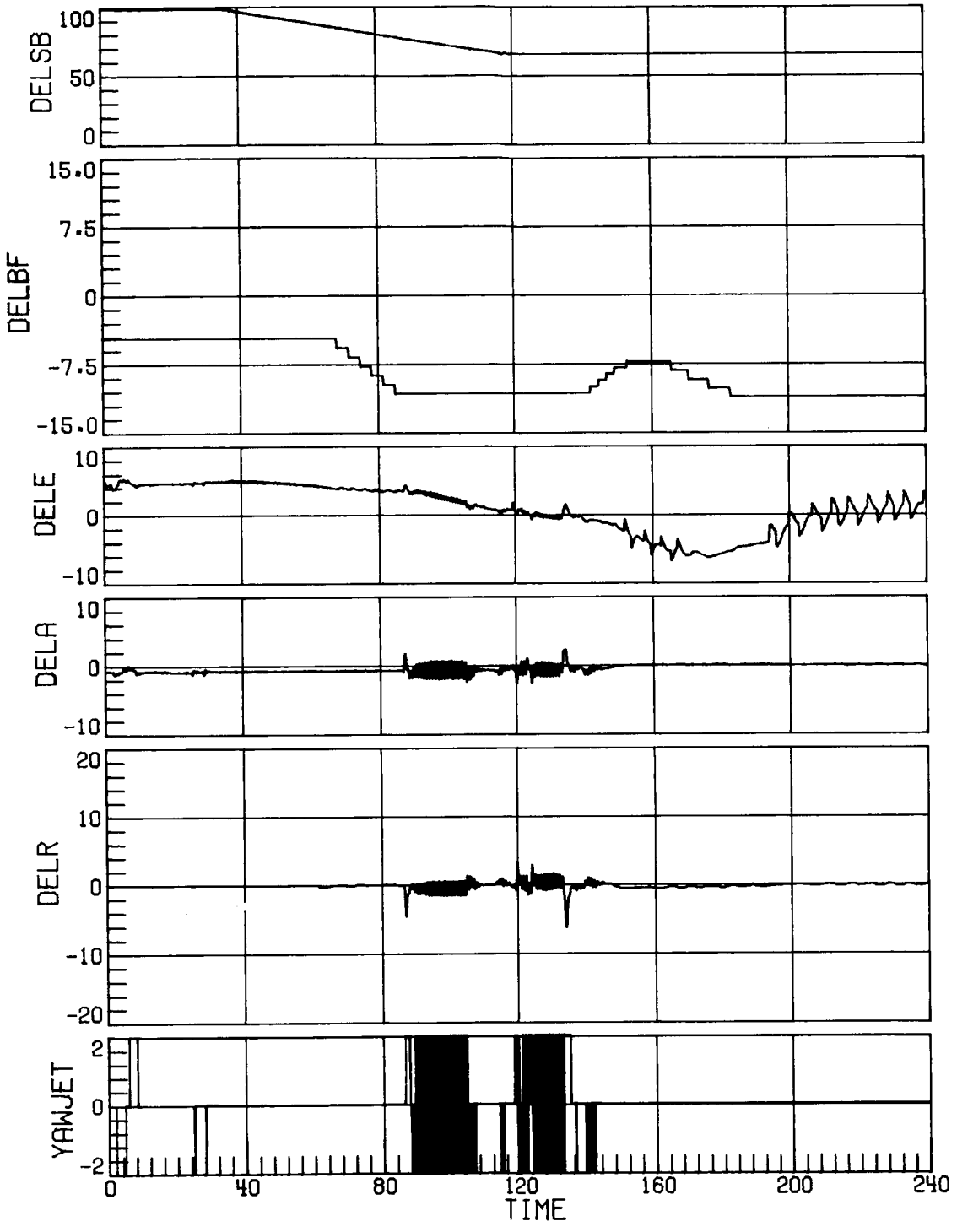

(c) Concluded.
Figure 21. Continued.

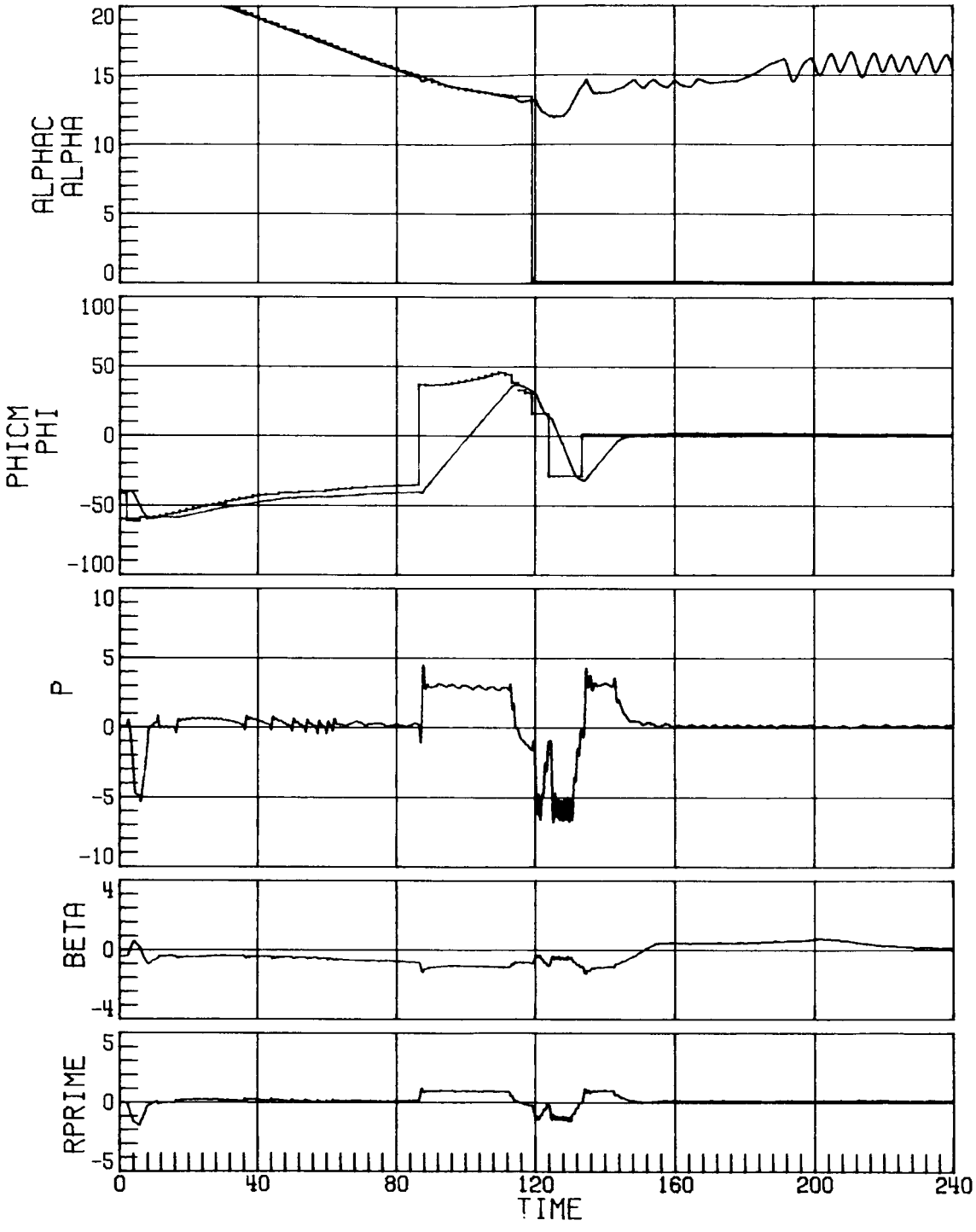

(d) Case 16; RCS uncertainty set 3.
Figure 21. Continued.

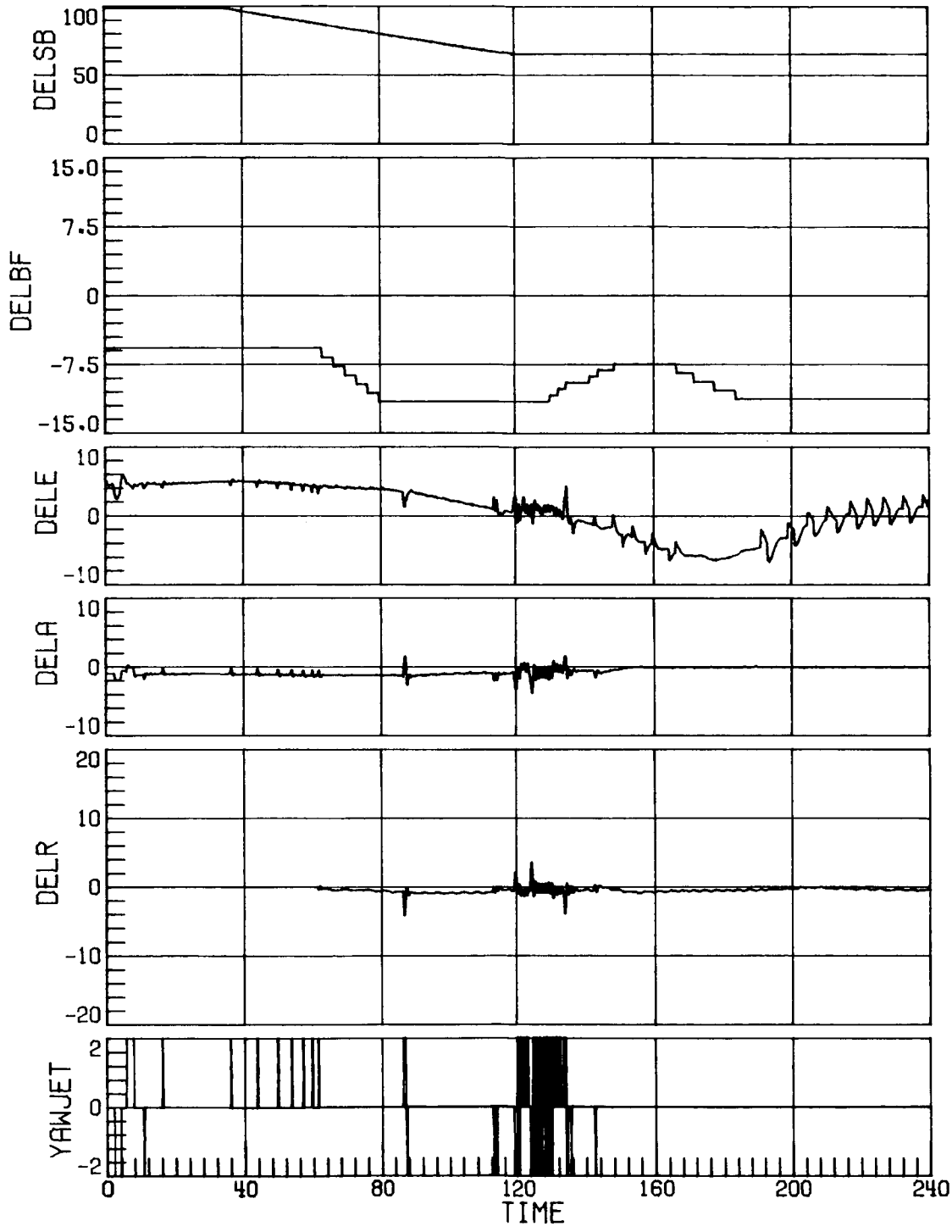

(d) Concluded.
Figure 21. Concluded.

1. Report No. NASA TP-2365	2. Government Accession No.	3. Recipient's Catalog No.
4. Title and Subtitle EFFECT OF AERODYNAMIC AND ANGLE-OF-ATTACK UNCERTAINTIES ON THE MAY 1979 ENTRY FLIGHT CONTROL SYSTEM OF THE SPACE SHUTTLE FROM MACH 8 TO 1.5		5. Report Date January 1985 6. Performing Organization Code 506-51-13-07
7. Author(s) Howard W. Stone and Richard W. Powell		8. Performing Organization Report No. L-15813 10. Work Unit No.
9. Performing Organization Name and Address NASA Langley Research Center Hampton, VA 23665		11. Contract or Grant No.
12. Sponsoring Agency Name and Address National Aeronautics and Space Administration Washington, DC 20546		13. Type of Report and Period Covered Technical Paper 14. Sponsoring Agency Code
15. Supplementary Notes		

16. Abstract

A six-degree-of-freedom simulation analysis has been performed for the Space Shuttle Orbiter during entry from Mach 8 to Mach 1.5 with realistic off-nominal conditions by using the flight control systems defined by the Shuttle contractor in May 1979. The off-nominal conditions included aerodynamic uncertainties in extrapolating from wind-tunnel-derived characteristics to full-scale flight characteristics, uncertainties in the estimates of the reaction-control-system interaction with the Orbiter aerodynamics, an error in deriving the angle of attack from onboard instrumentation, the failure of two of the four reaction-control-system thrusters on each side, and a lateral center-of-gravity offset coupled with vehicle and flow asymmetries.

With combinations of the above off-nominal conditions, the flight control system performed satisfactorily with a few exceptions. At low-hypersonic speeds, a few cases exhibited unacceptable performances when errors in deriving the angle of attack from the onboard instrumentation were modeled. The Orbiter was unable to maintain lateral trim for some cases between Mach 5 and Mach 2 and exhibited limit-cycle tendencies or residual roll oscillations between Mach 3 and Mach 1. Piloting techniques and changes in some gains and switching times in the flight control system were suggested to help alleviate these problems.

17. Key Words (Suggested by Author(s))	18. Distribution Statement
Flight control Entry Space Shuttle	Unclassified—Unlimited Subject Category 16

19. Security Classif. (of this report)	20. Security Classif. (of this page)	21. No. of Pages	22. Price
Unclassified	Unclassified	136	A07

For sale by the National Technical Information Service, Springfield, Virginia 22161

NASA-Langley, 1985